The Role of Precursor Chemistry in the Nucleation and Growth of Zinc Pnictide Based Semiconductor Quantum Dots

Benjamin Andrew Glassy

A dissertation

submitted in partial fulfillment of the

requirements for the degree of

Doctor of Philosophy

University of Washington

2017

Reading Committee:

Brandi M. Cossairt, Chair

Daniel R. Gamelin

Dennis M. Heinekey

Program Authorized to Offer Degree:

Chemistry

University of Washington

Abstract

The Role of Precursor Chemistry in the Nucleation and Growth of Zinc Pnictide Based Semiconductor Quantum Dots

Benjamin Andrew Glassy

Chair of the Supervisory Committee:

Assistant Professor Brandi M. Cossairt

Department of Chemistry

Interest in the synthesis of colloidal semiconductor nanocrystals has boomed over the last thirty years. This is, in part, due to the tunable optoelectronic properties of these colloids, which stems from the quantum confinement effect where the electronic structure evolves as a function of crystal volume. The other promising attribute of these colloidal semiconductors is their ability to be prepared and processed in solution, allowing device fabrication under ambient conditions and enabling deposition onto a wide variety of substrates. Most research to date has focused on synthesizing materials in the II-VI, IV-VI, and III-V families.

The II-V class of semiconductors, including Zn_3P_2, Cd_3P_2, Zn_3As_2, and Cd_3As_2, have not been given much attention from the colloidal nanocrystal community despite their enormous promise for light harvesting applications. These four semiconductors have bulk band gaps ranging

between 1.5 eV (Zn_3P_2) and 0 eV (Cd_3As_2). They are also completely soluble within each other, meaning an alloy of any composition is achievable and thus the bulk band gap is completely tunable over this 1.5 eV range. As a result, these semiconductors may offer advantages for a wide variety of light absorbing applications including the high earth abundance of zinc and phosphorus for cost effective light absorbing layers in solar cells, or less toxic alternatives to cadmium mercury telluride alloys for IR light detection applications. This thesis dissertation describes our efforts to elucidate and exploit novel precursor chemistry for the synthesis of Zn_3P_2, larger Zn_3P_2, and alloys of composition $(Cd_yZn_{1-y})_3As_2$.

Chapter 1 serves as an introduction into the synthesis of II-V colloidal nanocrystals as well as describing typical synthetic challenges and structural differences among the products that result from the various methodologies. Chapter 2 describes a novel synthesis of 3 nm Zn_3P_2 nanocrystals that utilizes an activated intermediate, $[Zn_5(O_2CR)_6(Et)_4]$, to promote reactivity with $P(SiMe_3)_3$. A novel P-Zn containing species then forms in a rate-limiting step prior to the nucleation and growth of the 3 nm Zn_3P_2 quantum dots. Chapter 3 will describe efforts to grow larger Zn_3P_2 particles from 3 nm seeds, which led to the identification of a different P-Zn containing intermediate with lower relative reactivity that afforded access to either bulk zinc phosphide or large 5 nm particles depending on the supporting ligands present. This chapter will also discuss the structural evolution that occurs as the particles grow from 3 to 5 nm in diameter. Chapter 4 discusses an extension of these synthetic methods for the synthesis of $(Cd_yZn_{1-y})_3As_2$ alloys. Lastly, Appendix B serves as a reference towards the synthesis of a family of arylsilylphosphines with varying electron withdrawing or electron donating groups in the para position of the aryl rings to serve as a library of potential phosphide precursors where the electronics of the P-Si bonds could be toggled.

Table of Contents

List of Figures

List of Schemes

List of Tables

Acknowledgments

This thesis is the culmination of roughly 22 years of formal education. I could not have completed this journey without the help of so many amazing people, especially as I focused my education from general knowledge to inorganic chemistry.

I want to thank my undergraduate advisor, Professor Catherine J. Page, for her enthusiasm towards chemistry and giving me a chance to try out research in the summer of 2009, which spurred my passion for research, and more specifically chemistry. When I had started out my undergraduate career I really did not know what I wanted to do besides pursue some sort of science. During my three years of research in the Page lab I got to spend a lot of time with graduate students both at the University of Oregon as well as Oregon State University. This exposure really drove me to want to pursue a Ph.D. in inorganic chemistry.

I truly do not know where I would be today if it were not for my advisor, Professor Brandi Cossairt. Without even meeting me in person she gave me a chance to join her lab the summer before I started in the graduate program at the University of Washington. Before joining the Cossairt lab I had little to no experience with inorganic synthesis or even air-free techniques. That summer I got a crash course in air-free synthetic inorganic chemistry from Brandi. I owe all of my training to her. Throughout my time at the University of Washington, her door was always open and she was always happy and willing to help. She is always happy to talk about research and to help me get through various hurdles. Her favorite phrase, which really helped shape me as a scientist was, “just think about it.” This inspired me to really take the time to critically think about what the data was telling me and formulate further experiments to solve a problem at hand. Being one of her first students allowed me to really design and shape my own projects. Brandi

has always been extremely supportive and gave me the independence to play around with various projects until I found something I really enjoyed doing. She also set up a very positive and supportive lab culture where we, as the Cossairt Lab, would also do a lot of fun group outings outside of research, from snowshoeing on Mt. Rainier to scavenger hunts in Ballard. This helped foster a community of support and camaraderie.

I would also like to thank all the members of the Cossairt lab that I have gotten to know over the past five years. It was truly an honor to work alongside such bright and talented individuals. Thank you all for being such supportive, helpful, and fun co-workers! I will truly miss you all. Also, thank you to all of the students and post docs I have interacted with over the years, for always providing knowledge, support, and laughter!

Throughout these past five years, I have had such positive interactions with a multitude of support staff, staff scientists, and maintenance employees, all of whom were necessary for my successful tenure at University of Washington. They were always willing to take time to answer any questions I had with regards to paperwork, instrumentation, potential analytical techniques, equipment malfunctions, and so much more.

I would like to thank my committee members, Brandi, Daniel, Mike, David, Hugh, and Vince, for all of their time spent on my various exams and for the thoughtful discussions, suggestions, and insight provided. They have all had a positive impact on my time here at the University of Washington and have all helped to shape me as a scientist and individual.

I would like to deeply thank my family for their tireless love, always believing in me, and constant support. My parents and sister have always encouraged me to follow my dreams and I know they will be there for me no matter what. They have and continue to serve as inspirations and great role models for me as I continue on my career path. My parents, even though they are a

Huskie and a Cougar, were happy with me going down to the University of Oregon to be a Duck. My family has always been there with me as my biggest supporters, and they have made me who I am today. There are not enough words to describe how thankful I am to my wife, Anita. She has always been there for me when times were both easy and hard. She always has, and continues to be such a great listener as I describe any issues I am facing or as I practice a presentation. She has been a constant source of support and motivation and has always made me feel like I can accomplish anything. She has also been supportive of my hobby to care for and tirelessly fawn over our two salt-water fish tanks—which have served as a great distraction for me when I don't want to think about chemistry. Anita, I truly love you.

Lastly, to all those scientists who are coming after me: remember, if you are ever having trouble interpreting some data, take a pause, and, "just think about it."

Chapter 1. II_3V_2 (II: Zn, Cd; V: P, As) Semiconductors: From Bulk Solids to Colloidal Nanocrystals

1.1 Introduction

The synthesis of colloidal nanocrystals has progressed dramatically since the landmark contribution from Murray, Norris and Bawendi on the preparation of cadmium chalcogenide quantum dots.[1] Several recent reviews are available discussing the synthesis of II-VI, III-V, IV-VI, and ternary and quaternary chalcogenide nanocrystals.[2-7] While these reports offer a detailed reference on comparisons between different synthetic methods to access these classes of semiconductors, similar accounts for II-V semiconductors are lacking.[8-9] This review seeks to highlight the progress that has been made in both the synthesis and characterization of colloidal II-V semiconductors with an emphasis on structural differences that arise as a function of crystal size, as well as detailing potential avenues of research still needed to generate high quality II-V nanocrystals for translation to a variety of light utilizing applications.

The II-V semiconductors Zn_3P_2 (1.5 eV), Zn_3As_2 (1 eV), Cd_3P_2 (0.5 eV), and Cd_3As_2 (0 eV)[10] are attractive candidates for use in a wide variety of light utilizing applications given their band gaps span the visible through the infra-red, as well as their ability to form alloys of all compositions.[11-14] These remarkable materials are characterized by a complex crystalline structure with unit cells of 40 or 160 atoms (Figure 1.1).[15]

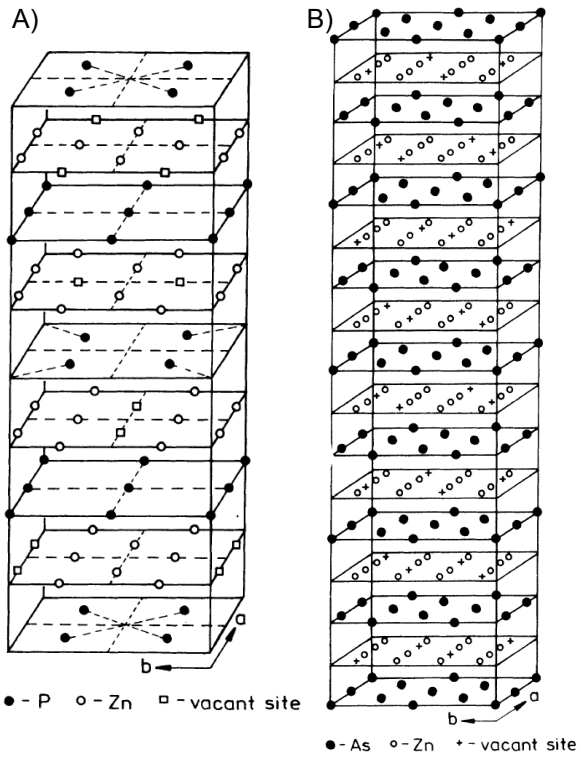

Figure 1.1. Representative unit cells of II_3V_2 metal phosphides (A) and arsenides (B). Reprinted with permission from Ref.[15] Copyright 1994 American Physical Society.

The two unit cells shown above, characteristic of the phosphides and arsenides, respectively, differ only by how the cation vacancies are arranged.[15] Given the complexity of the defect structure of these materials, debate over their precise crystalline structure is ongoing with reports of the metal arsenides crystallizing in both unit cells (Figure 1.2).[16] Regardless of the vacancy structure, the effect of crystal domain size on the presentation of these tetragonal lattices is certain to add an additional level of complexity that will impact our interpretation of the structures of these semiconductors on the nanometer length scale. This concept will be explored further in later sections of this review.

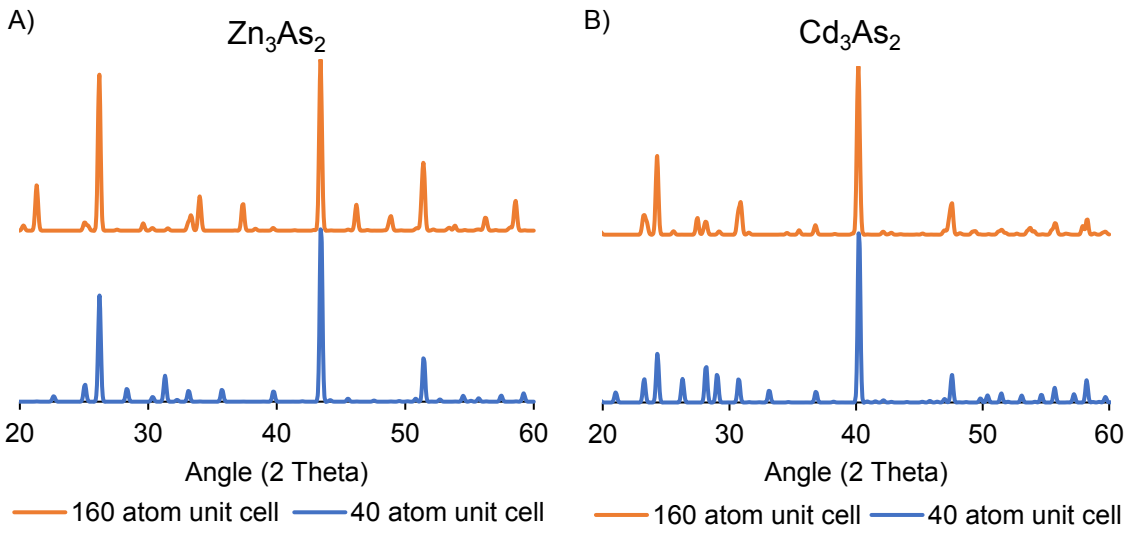

Figure 1.2. A) Bulk PXRD patterns of Zn_3As_2 characterized by the 160-atom unit cell (PDF 01-089-6345) and the 40-atom unit cell (PDF 01-089-3431). B) Bulk PXRD patterns of Cd_3As_2 characterized by the 160-atom unit cell (PDF 44-818) and the 40-atom unit cell (PDF 73-809).

The bulk electronic structure of II-V semiconductors has been studied in depth.[15, 17-31] However, our understanding of the electronic structure of these materials depends on our ability to assign the physical structure accurately, as demonstrated by evaluation of the computed band structure using two different approximations for the unit cells (Figure 1.3).[15] It is important to note that the tight binding sp^3 approximation (solid line) does not take into account the spin-orbit interaction or the tetragonal distortion. Notably, these calculations demonstrate that our expectation of both band curvature, and hence reduced carrier mass, and band gap depends on the structure we assign to these solids.

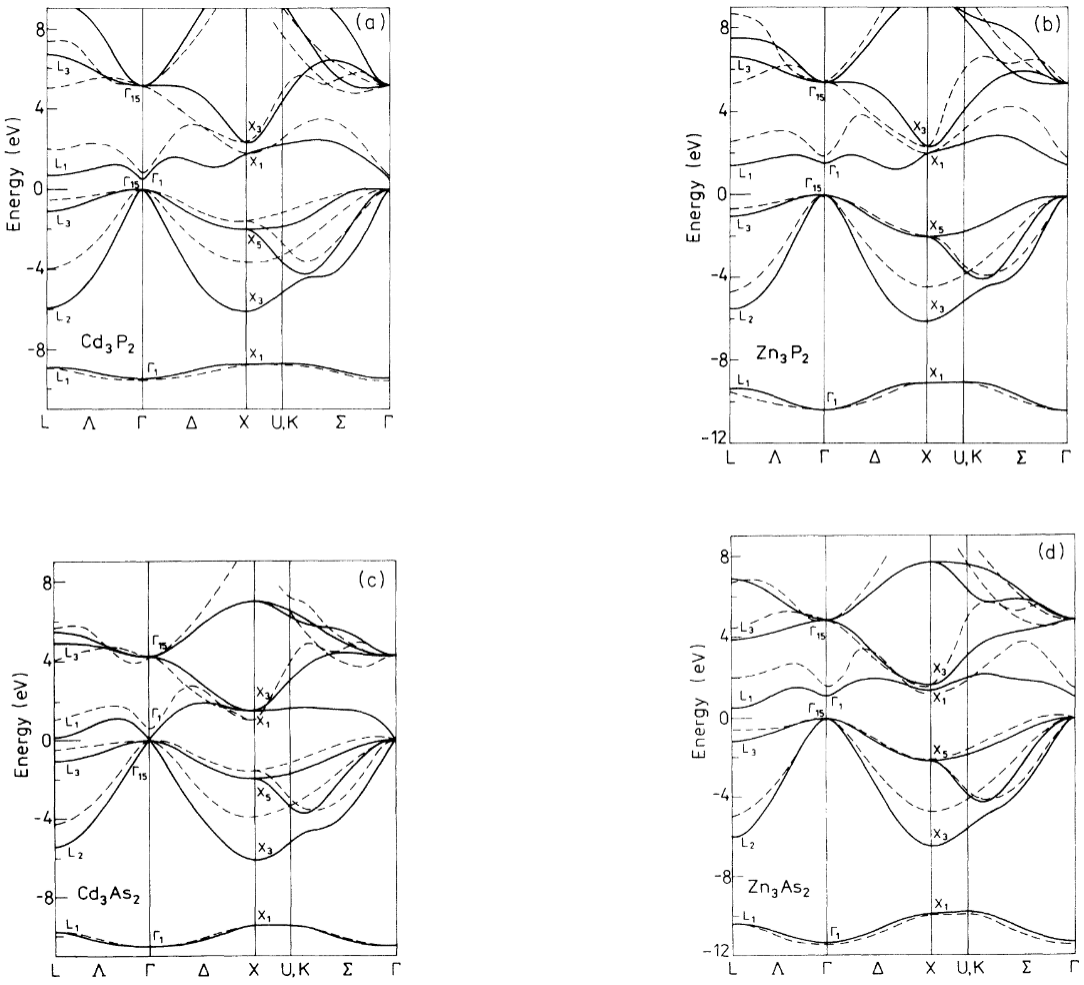

Figure 1.3. Calculated band structures derived using a tight-binding sp^3 approximation based on a zincblende structure model (solid line) and the Lin-Chung pseudopotential model (dashed line). Reprinted with permission from Ref.[15] Copyright 2016 American Physical Society.

1.2 Zn_3P_2 Nanocrystals

To date there have been 11 reports, dating back as early as 1985, on the synthesis of zinc phosphide nanocrystals (Table 1.1).[8, 32-41]

Table 1.1. Summary of Zn_3P_2 nanocrystal syntheses. Species in brackets are the active species formed *in-situ*.

P precursor	Zn precursor	Temperature (°C)	Solvent / Additive	Results
PBr_5 [$(PH)_x$]	$ZnCl_2$ [Zn^0]	200	OLA, $LiBH_4$	6 nm polydisperse crystalline particles[41]
TOP	$ZnMe_2$	I: 320, G: 350	1-ODE, TOP	9 nm crystalline nanoparticles[36]
		I:320, G: 348	1-ODE, TOP	3-7 nm crystalline nanoparticles[37]
HP^tBu_2	$ZnMe_2$	150 or 250	TOPO, TOP	4 nm particles of mixed crystallinity[33]
		167	4-ethylpyridine	4 nm particles of mixed crystallinity[33]
P_4	$ZnCl_2$ [Zn^0 NPs]	60	THF, toluene, sodium naphthalenide, TOP	1-5 nm particles, no structural data[34]
		60	THF, toluene, sodium naphthalenide, TOA	2-10 nm particles, no structural data[34]
PH_3	$Zn(ClO_4)_2$	varied	H_2O, sodium hexametaphosphate	1-2 nm particles, no structural data[32]
	$ZnEt_2$	20-80	1-ODE, TOP	5 nm particles of ambiguous crystallinity[35]
	$Zn(N(SiMe_3)_2)_2$	20-80	1-ODE, TOP	No physical characterization[35]
$P(SiMe_3)_3$	$Zn(OMe)_2$	Not Given	Not Given	4-7 nm polydisperse amorphous particles[8]
	$Zn(OCHMeCH_2NMe_2)_2$	Not Given	Not Given	2 nm polydisperse amorphous particles[8]
	$Zn(St)_2$	20-80	1-ODE, TOP	5 nm particles of ambiguous crystallinity[35]
	$ZnMe_2$	I: 20, G: 150	TOP	15 nm crystalline particles[37]
	$ZnEt_2$	300	1-ODE, HDA	3-9 nm crystalline particles[39]
	$Zn(OA)_2$, $ZnEt_2$ [$[Zn_5(OA)_6(Et)_4]$]	I: 100, G: 255-315	1-ODE	3 nm crystalline particles[38]
	$Zn(OA)_2$, $ZnEt_2$ [$[EtZnP(SiMe_3)_2]_3$]	I: 100, G: 315	1-ODE, Na(OA)	5 nm crystalline particles[40]

OLA, oleylamine; 1-ODE, 1-octadecene; TOP, trioctylphosphine; TOPO, trioctylphosphine oxide; NPs, nanoparticles; TOA, trioctylamine; St, stearate; HDA, hexadecylamine; OA, oleate; I, inject; G, grow

Syntheses of Zn_3P_2 have implemented phosphorus precursors ranging between 8 oxidation states (5+ to 3–). Early reports were only able to produce materials of low crystallinity or with limited available structural characterization. However, the electronic structure of the resulting

particles has been shown to vary considerably as a function of the synthetic conditions. The earliest report produced clusters with an excitonic transition at 300 nm, but precursor reactivity limited particle size to 1-2 nm; these particles displayed weak photoluminescence (PL), but no quantum yield (QY) was given.[32] Green and O'Brien reported a synthesis of 4 nm particles with a broad excitonic feature below 500 nm, but further analysis of these particles indicated the sample was polydisperse and had poor crystallinity. These particles displayed size tunable PLwith a reported Stokes shift of at least 0.18 eV (for 4-ethylpyridine capped QDs) or at least 0.6 eV (for TOPO capped QDs); again no QY was reported.[33] More recently there have been several reports of solution absorption data without a clear excitonic feature either indicating that these samples are perhaps no longer highly quantum confined or are characterized by broad ensemble size distributions.[35-36, 39-40] These reports either do not mention the PL, or show tunable emission with QYs below 3%. Our lab has reported the synthesis of 3 nm particles with a size dependent excitonic transition that could be tuned between 424 and 535 nm based on slight variations in particle size.[38] These particles displayed size independent PL that was attributed to recombination from a trap state to the valence band, with a QY of around 1%. A unique feature of this synthesis is the generation of metal-rich nanocrystals passivated by a shell of Z-type zinc carboxylates instead of weaker L-type ligands (neutral Lewis bases), such as trioctylphosphine or an amine, which likely influences the electronic structure of these particles and is perhaps why these particles displayed a size tunable excitonic transition.[42]

Prior to 2013, no report on the synthesis of Zn_3P_2 nanocrystals reported powder X-ray diffraction (PXRD) data.[8, 32-34] Later reports have shown some differences in the observed crystallinity of the resulting particles. Figure 1.4 shows three examples of reported PXRD data of Zn_3P_2 nanocrystals. Figure 1.4A shows a Zn_3P_2 pattern unusually similar to ZnO besides a peak at

19 2θ, which is not the typical reported pattern for bulk α-Zn_3P_2.[35] The authors report that as the synthesis progresses the intensity of this peak changes, indicating that the particles are most likely shelled by ZnO. In our report of 3 nm Zn_3P_2 quantum dots we show the PXRD data with a comparison to the 40 atom tetragonal zinc phosphide pattern (Figure 1.4B), but the intensity of the major <400> reflection is diminished, which we hypothesized could be due to the very small size of these particles as well as potential surface strain induced from the strongly binding $Zn(O_2CR)_2$ surface ligands.[38] For reference, a 1 nm diameter spherical particle has enough volume for 70% of one unit cell—however this accounts for total volume, not complete number of tetragonal cells that could fit in a sphere so the disparity is even worse. Therefore, if the particles are extremely small, it is unlikely that the PXRD pattern would match that of bulk zinc phosphide regardless of crystallinity. Lastly, many reports show a complete match between the PXRD of their nanocrystals and bulk Zn_3P_2 (Figure 1.4C). These particles are for the most part >4 nm in diameter and/or synthesized with weakly bound surface ligands.[36-37, 39-41] What these reports show is that it is possible to make structurally unambiguous zinc phosphide nanocrystals, but they must be large enough, or without strain, to not cause deviations in the structure.

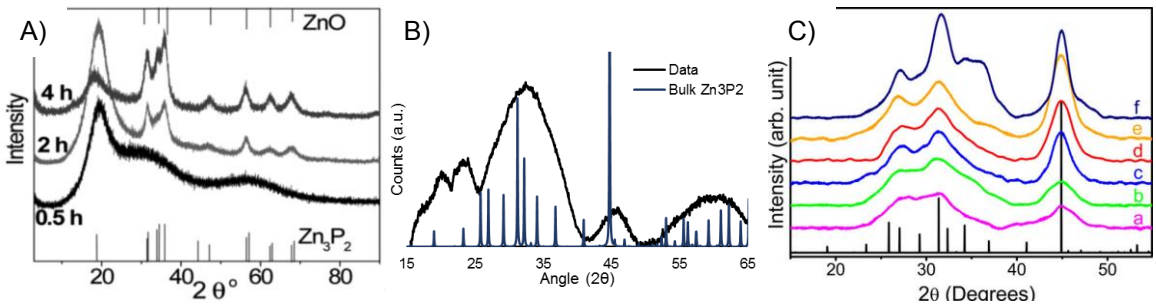

Figure 1.4. Representative PXRD data for (A) ZnO@Zn_3P_2,[35] (B) small (3 nm), strained Zn_3P_2 quantum dots,[38] and (C) Zn_3P_2 nanocrystals of varying size (5-9 nm) that match well with the bulk powder pattern.[39] (A) was reprinted with permission from Ref.[35] Copyright 2013 WILEY-VCH Verlag GmbH & Co. KGaA, Weinheim. (B) was reprinted with permission from Ref.[40] Copyright 2016 American Chemical Society. (C) was reprinted with permission from Ref.[39] Copyright 2015 American Chemical Society.

Phosphorus NMR spectroscopy, both solid and solution state, has been utilized to characterize both the final structures as well as the precursor conversion reactions involved in the synthesis of these nanocrystals. Figure 1.5 highlights examples of using ^{31}P magic angle spinning (MAS) NMR to characterize Zn_3P_2. The bulk ^{31}P MAS NMR spectrum of Zn_3P_2 has 3 distinct peaks, two of which overlap at room temperature consistent with the 40 atom tetragonal unit cell (Figure 1.5A).[43] Buriak and co-workers were able to use ^{31}P MAS NMR to characterize the amount of P(0), P(3+), and P(3–) present in their samples when TOP was used as the phosphorus source to synthesize 6.5 nm particles (Figure 1.5B) or when $P(SiMe_3)_3$ was used to synthesize 15 nm particles (Figure 1.5C).[37] What these two spectra show is that by changing the phosphorus precursor from TOP to $P(SiMe_3)_3$ the amount of oxidized phosphorus and P(0) shell observed dramatically decreased. They were also able to identify both peaks characteristic of bulk Zn_3P_2 in their samples. Our lab has shown that we can monitor the growth of 3 nm Zn_3P_2 seeds, with

observable strain in the PXRD, into larger 5 nm particles that better match both the NMR and PXRD properties of bulk zinc phosphide (Figure 1.5D).[40] This data shows that as these particles grow the phosphorus environment approaches that of the bulk structure, suggesting particles with diameters > 4 nm can support the complex defect structure of the tetragonal lattice.

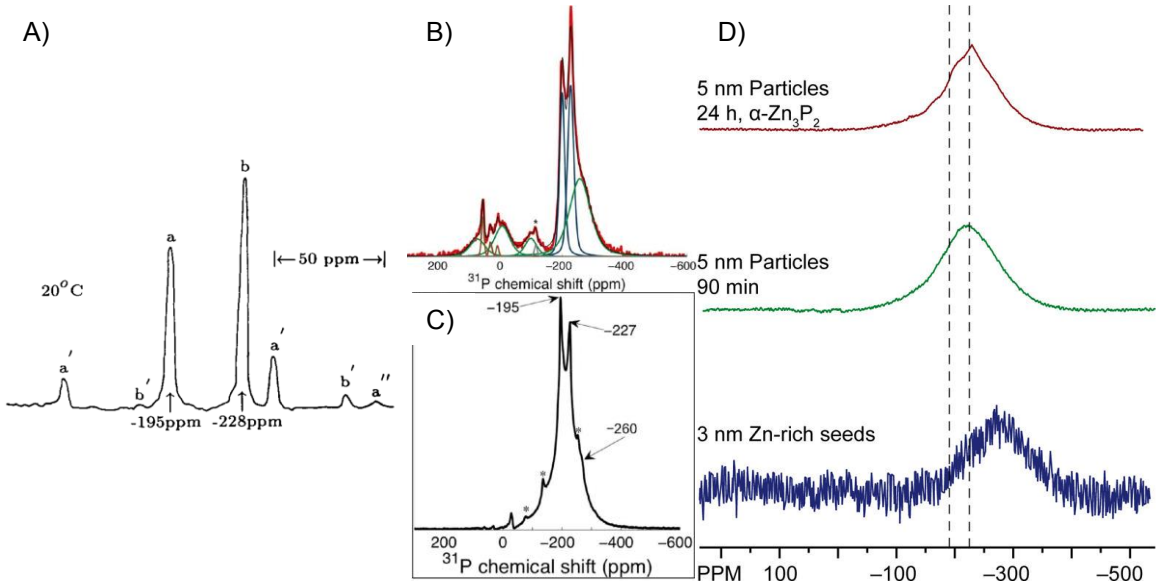

Figure 1.5. ^{31}P MAS NMR spectra of (A) bulk Zn_3P_2, spinning side bands labeled with a prime symbol,[43] (B) 6 nm particles synthesized with TOP,[37] (C) 15 nm particles synthesized with $P(SiMe_3)_3$, and (D) the growth and crystallization of particles synthesized with $P(SiMe_3)_3$ where the dashed lines represent the bulk Zn_3P_2 ^{31}P NMR spectrum.[40] (A) was reprinted from Ref.[43] Copyright 1992 with permission from Elsevier. (B) and (C) were reprinted with permission from Ref.[37] Copyright 2014 American Chemical Society. (D) was reprinted from Ref.[40] Copyright 2016 American Chemical Society.

NMR spectroscopy has not only been used to study the environment of phosphorus atoms in the core and on the surface of the synthesized particles, but also to track the precursor conversion chemistry during the synthesis (Figure 1.6).[38, 40] $P(SiMe_3)_3$ has been the most common phosphorus precursor for zinc phosphide synthesis given it is reactive, in the correct oxidization state, and is

an easily handled liquid. However, we have shown that the reactivity between $P(SiMe_3)_3$ and either alkyl zinc species or zinc carboxylates is slow.[38] The precursor reactivity can be enhanced by having both alkyl zinc and zinc carboxylates present in the reaction mixture.[38, 40] NMR spectroscopy shows the formation of two different molecular intermediates prior to the formation of Zn_3P_2 quantum dot nucleation when $P(SiMe_3)_3$, $ZnEt_2$, and $Zn(O_2CR)_2$ are combined.[37-38, 40] Depending on the ratio of zinc precursors, the speciation differs, which leads to a change in the final particle size.[40] Figure 1.6A shows that in the presence of 3:1.5 $Zn(O_2CR)_2$:$ZnEt_2$, the zinc precursors react first to form a $[Zn_5(O_2CR)_6(Et)_4]$ cluster which then rapidly reacts with $P(SiMe_3)_3$ prior to nucleation.[38, 44] Figure 1.6B shows that in a mixture of 0.2:1.5 $Zn(O_2CR)_2$:$ZnEt_2$, the Zn_5 cluster does not form and instead $[EtZnP(SiMe_3)_2]_3$ is generated, which converts at a much slower rate as compared with the phosphorus containing intermediate generated using more $Zn(O_2CR)_2$.[40, 45] These examples of NMR spectroscopic characterization serve to demonstrate the power of tracking and identifying the fate of the phosphorus atoms in these syntheses to better characterize the reaction mechanisms and to determine how the particles evolve during growth. Additionally, NMR can be used to study ligand exchange on QD surfaces to gain insight into how different ligand motifs impact the physical and electronic structure, of which there is a single report by Buriak and co-workers specifically examining particles ligated with TOP, will be an invaluable step forward in expanding the fundamental understanding of these particles.[46]

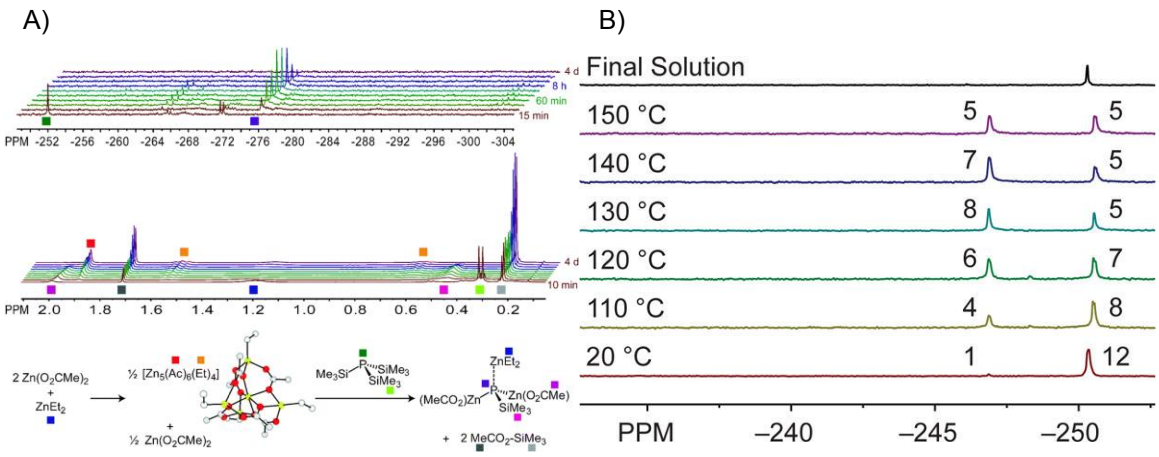

Figure 1.6. (A) ^{31}P and ^{1}H NMR spectra showing the formation of $[Zn_5(O_2CR)_6(Et)_4]$ and $(Et_2Zn)P(ZnAc)_2(SiMe_3)$ prior to 3 nm Zn_3P_2 quantum dots.[38] (B) ^{31}P NMR showing the conversion of $P(SiMe_3)_3$ (–252 ppm) into $[EtZnP(SiMe_3)_2]_3$ (–247 ppm) which could be used to either grow on Zn_3P_2 seeds or independently nucleate 5 nm particles where the numbers above the peaks represent the relative integrations of the amount of each present.[40] (A) was reproduced from Ref.[38] with permission from The Royal Society of Chemistry. (B) was reprinted with permission from Ref.[40] Copyright 2016 American Chemical Society.

There have been several reports of bulk Zn_3P_2 utilized in heterojunction devices.[47-50] However, there is only one report on the use of colloidal nanocrystals being used in such a device[36] and two reports demonstrating a proof of principle experiment where Zn_3P_2 nanocrystals could be used to generate electricity from light.[35, 38] This collection demonstrates that the body of literature on colloidal zinc phosphide has primarily focused on designing the synthesis and understanding the structure and properties of the resulting particles instead of their translation to practical device application.

1.3 Cd_3P_2 Nanocrystals

The development of cadmium phosphide nanocrystals has followed a similar trajectory to Zn_3P_2 and also dates back to 1985 (Table 1.2).[32, 51-64]

Table 1.2. Summary of Cd_3P_2 nanocrystal syntheses. Species in [ ] are the active species formed *in-situ*.

P Precursor	Cd Precursor	Temperature (°C)	Solvent / Additive	Results
TOP [Na_3P]	$CdCl_2$	250	DMF, TOP	20-30 nm crystalline (hexagonal) particles[57]
	$Cd(Ac)_2$	250	DMF, TOP	20-30 nm crystalline (hexagonal) particles[57]
$[MeCdP^tBu_2]_3$	$[MeCdP^tBu_2]_3$	90-250	TOPO, TOP	5 nm particles matched to Cd_3P_2 by TEM and IR[54]
		167	4-ethylpyridine	4 nm particles, no PXRD observed[55]
$Cd[P(SiMe_3)_2]_2$	$Cd[P(SiMe_3)_2]_2$	20	methanol	Amorphous material, no size reported[51]
$Cd[P(SiPh_3)_2]_2$	$Cd[P(SiPh_3)_2]_2$	I: 20 G: 60	toluene or pyridine, methanol	3-4 nm particles of low crystallinity[52]
Cd_3P_2 MSCs	Cd_3P_2 MSCs + HOA	150, 180	1-ODE, TOP, OLA	2 nm crystalline particles[63]
InP MSCs	$Cd(O_2CR)_2$	20	toluene and MeCN	Small MSCs[64]
PH_3	$Cd(ClO_4)_2$	varied	H_2O, sodium hexametaphosphate	1-4 nm particles (estimate), no structural data reported[32]
	$Cd(O_2CCH_2CH_3)_2$	20	n-propanol, MMA, TEA	2.7 nm crystalline (ED, not shown) particles*[53]
	CdO [$Cd(OA)_2$]	120-250	1-ODE	2-6.5 nm crystalline (cubic, Cd_6P_7) particles[61]
	CdO [$Cd(OA)_2$ + HOA]	120	1-ODE	Small MSCs[63]
$P(SiMe_3)_3$	$Cd(Ac)_2$ [Cd(Ac)(OA)]	I: 40, G: 240	1-ODE	Small MSCs, PXRD did not resemble 3D structure[56]
	CdO [$Cd(OA)_2$]	25-150	1-ODE, TOP, OLA	3.5-4.5 nm crystalline (cubic) particles[58]
	CdO [$Cd(OA)_2$ + HOA]	I: 230, G: 250	1-ODE	1.6-12 nm crystalline (2 peaks in the PXRD) particles[59]
		I: 210, G: RT	1-ODE	3nm crystalline (tetragonal) particles[62]
	$Cd(O_2CCH_3)_2(OAm)_x$	30	toluene	4-7 nm crystalline (2 peaks in the PXRD) particles[60]

TOP, trioctylphosphine; Ac, O_2CCH_3; TOPO, trioctylphosphine oxide; MSCs, magic-sized clusters; HOA, oleic acid; 1-ODE, 1-octadecene; OLA, oleylamine; MMA, methyl methacrylate; TEA, triethylamine; ED, electron diffraction; OA, oleate; OAm, octylamine; I, inject; G, grow

*Report mentions additional reaction parameter which yielded nanoparticles, but no specific details are given

Synthesis of cadmium phosphide has been accomplished with phosphorus precursors ranging between 6 oxidization states (3+ to 3–). Sodium was necessary to reduce trioctylphosphine (P in the 3+ oxidization state) to an active P^{3-} source.[57] For the use of cadmium diorganophosphide precursors (P in the 1+ oxidization state), it was found that the organic groups on the phosphorus must have β-hydrogens in order to yield Cd_3P_2 rather metallic cadmium.[55] It was found that it was possible to form Cd_3P_2 nanoparticles using cadmium disilylphosphido dimers (P in the 3– oxidization state) through an alcoholysis mechanism.[51-52] Notably, the analogous zinc dimers could not be used in the synthesis Zn_3P_2.[51] Additional studies have reported making varying sizes of nanoparticles using PH_3 or $P(SiMe_3)_3$ (both with P in the 3– oxidization state) with a metal carboxylate (either cadmium acetate or cadmium oleate).[32, 53, 56, 58-62, 65] While using alkyl zinc reagents is common in the zinc phosphide literature, there have been no literature reports using $CdMe_2$ as the cadmium precursor towards Cd_3P_2 nanocrystals.

Cadmium phosphide magic sized clusters (MSCs) have also been synthesized and examined as single source precursors for Cd_3P_2 nanocrystal synthesis.[63] These clusters were first synthesized and studied by Wang *et al*.,[56] and have also been accessed through cation exchange starting from InP MSCs.[64] While cadmium phosphide MSCs were first isolated and characterized in 2009, it was not until 2014 that their use as a single-source precursor towards the synthesis of cadmium phosphide nanoparticles was demonstrated.[63] MSCs of Cd_3P_2 have also been identified in the early time points of a synthesis of cadmium phosphide nanoparticles suggesting that the MSCs may be intermediates that build up in concentration during the synthesis of Cd_3P_2 under select conditions.[7, 61]

Similar to what has been seen for zinc phosphide, there has been a range of PXRD data reported for Cd_3P_2 nanocrystals (Figure 1.7). Structure types assigned by PXRD have included

hexagonal, cubic (Cd_6P_7), and tetragonal. Among the reports suggesting a tetragonal structure, data have varied in terms of agreement with the bulk pattern, again likely because of the small crystal size and the presence of strain leading to deviations from the bulk 40 atom unit cell. This discrepancy appears to be consistent with the reported ^{31}P MAS NMR data showing the lack of agreement compared to the bulk spectrum.

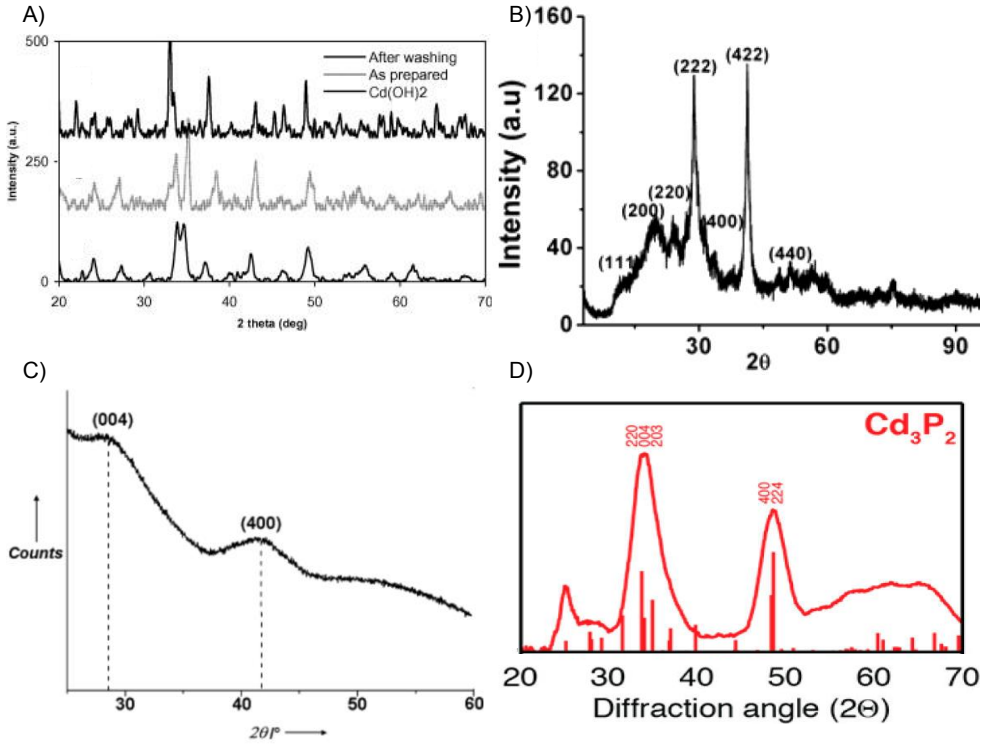

Figure 1.7. Representative experimental PXRD of Cd_3P_2 nanocrystals that are reported to be the (A) hexagonal unit cell,[57] (B) cubic unit cell,[58] (C) partial tetragonal unit cell,[60] and (D) complete tetragonal unit cell. Note that the data in (D) was collected using cobalt, not copper, as the X-ray source.[62] (A) was reprinted from Ref.[57] Copyright 2009 with permission from Elsevier. (B) was reprinted with permission from Ref.[58] Copyright 2010 American Chemical Society. (C) was reprinted with permission from Ref.[60] Copyright 2012 WILEY-VCH Verlag GmbH & Co. KGaA, Weinheim. (D) was reprinted with permission from Ref.[62] Copyright 2012 American Chemical Society.

The ^{31}P MAS NMR spectrum of bulk Cd_3P_2 has three peaks at –140, –162, and –178 ppm which is expected for a tetragonal unit cell.[43] The MSCs isolated by Yu and co-workers were characterized by a singlet at –366.3 ppm in the ^{31}P NMR spectrum.[56] This indicates the structure of these clusters is very different from that of bulk Cd_3P_2. Reports of ^{31}P MAS NMR spectra of crystalline Cd_3P_2 nanoparticles show a ^{31}P chemical shift at –227 ppm (–240 ppm in solution)[52] or –263 ppm.[60] This discrepancy in peak position could either be due to a difference in crystal phase, chemical environment, or due to quantum confinement.[66] Unlike Zn_3P_2, there have been no reports of cadmium phosphide nanocrystals with a ^{31}P MAS NMR pattern matching that of the bulk tetragonal material.

Even though the structure of Cd_3P_2 nanocrystals deviate from the bulk, their electronic structure is extremely well behaved. Photoluminescence quantum yields have been reported to be as high as 70%[59] and when shelled with ZnS, Ojo *et al*. have reported air stable quantum yields of approximately 50%.[60] Not only have very high quantum yields been reported, but the size dependent PL maximum can be tuned to cover the entire visible and NIR range (450-1500 nm, Figure 1.8).[59] Kietzmann *et al.* showed that small cadmium phosphide QDs attached to TiO_2 particles through wet chemical routes were able to inject excited electrons with a time constant less than 1 picosecond.[67] With regard to device applications, Cd_3P_2 QDs have also demonstrated a photoresponse, been translated into a functional solid state LED, been successfully incorporated into a microcavity device, and encapsulated into microspheres for use in biological imaging.[58, 61, 68-69]

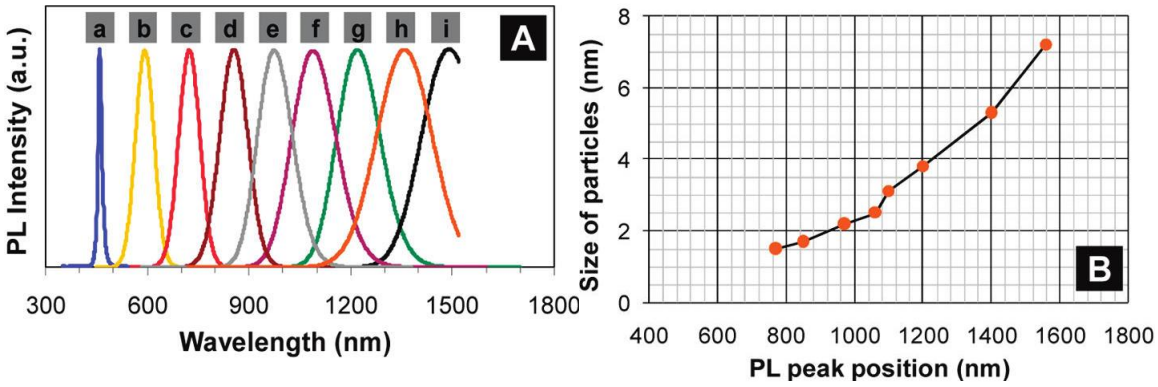

Figure 1.8. (A) Photoluminescence of particles ranging from <1.5 nm to 7.6 nm. (B) Relationship between PL peak and particle size.[59] Reprinted with permission from Ref.[59] Copyright 2010 American Chemical Society.

1.4 M_3As_2 (M: Zn, Cd) Nanocrystals

Thus far, there has only been one report on the synthesis of Zn_3As_2 QDs.[70] Our lab modified our previous procedure for the synthesis of Zn_3P_2 (*vide supra*) to obtain 3 nm zinc arsenide QDs. In this report, we were also able to access $(Cd_yZn_{1-y})_3As_2$ alloys through the replacement of $Zn(OA)_2$ with $Cd(O_2CCH_3)_2$ in the synthesis **(**Figure 1.9**)**. Evidence for alloying was provided by dramatic shifts in the excitonic transition to lower energy at a constant particle size (Figure 1.9A), and from a combination of PXRD (Figure 1.9B) and elemental analysis. The addition of cadmium into the zinc arsenide lattice enhanced the PL QY from <1% (pure zinc arsenide) up to 60% (when 25% $Cd(O_2CCH_3)_2$ was used).[70]

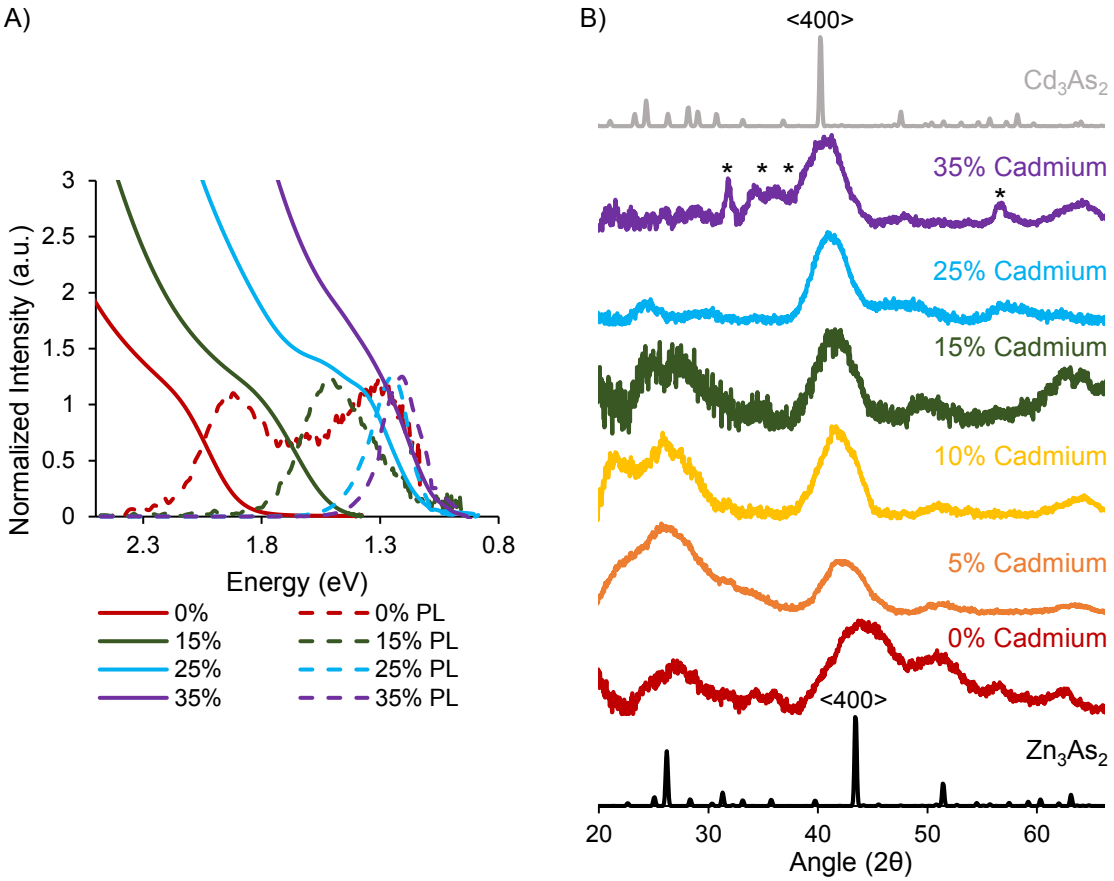

Figure 1.9. (A) UV-Vis, PL, and (B) PXRD data of the nanocrystals obtained when 0 – 35% percent of the zinc oleate was replaced with cadmium acetate compared to bulk patterns of Zn_3As_2 and Cd_3As_2 (PDF 01-089-3431 and 73-809 respectively).[70] *ZnO impurity (PDF 01-074-0534) arises from decomposition of unreacted zinc carboxylate under these conditions.[71]

Despite the dearth of synthetic methods for Zn_3As_2 nanocrystals, Cd_3As_2 has garnered more attention, most likely because of the better matched reactivites of the utulized cadmium and arsenic precursors (Table 1.3).[63, 72-76]

Table 3. Summary of Cd_3As_2 nanocrystal syntheses. Species in [ ] are the active species formed *in-situ*.

As Precursor	Cd Precursor	Temperature (°C)	Solvent / Additive	Results
$As(NMe_2)_3$	$CdCl_2$	I:130, G: 140-250	OLA, DIBAL-H (in toluene)	4.5-15 nm crystalline particles[76]
$[(Me_3Si)_2N]_2AsCl$	$Cd(Ac)_2$ [$Cd(OA)_2$ + HOA]	I: 30, G: 230	1-ODE, OLA	4 nm crystalline particles[75]
Cd_3As_2 MSCs	Cd_3As_2 MSCs + HOA	120-250	1-ODE, TOP, OLA	1-20 nm crystalline particles[63]
AsH_3	$Cd(ClO_4)_2$	varied	H_2O, sodium hexametaphosphate	Range of sizes, no PXRD or TEM reported[72]
	CdO [$Cd(OA)_2$ + HOA]	120	1-ODE	MSCs, no structural data reported[63]
	CdO [$Cd(OA)_2$]	varied	TOPO, 1-ODE	1.7-4 nm particles, no structural data reported[74]
$As(SiMe_3)_3$	$Cd(MA)_2$	175	1-ODE, TOP	2-5 nm crystalline particles[73]

OLA, oleylamine; DIBAL-H, diisobutylaluminium hydride; Ac, O_2CCH_3; OA, oleate; HOA, oleic acid; 1-ODE, 1-octadecene; MSCs, magic sized clusters; TOP, trioctylphosphine; MA, myristate; I: inject; G: grow

Given the lack of alternative commercially available arsenic precursors in the 3– oxidization state, most work has been done using AsH_3, either directly in the gas phase or synthesized *in situ* via the addition of a strong acid to bulk metal arsenide powders.[63, 72, 74] More recently, innovation in precursor chemistry has led to the successful implementation of $As(NMe_2)_3$ (a commercially available reagent with As in the 3+ oxidation state) to synthesize crystalline particles ranging from 4.5 to 15 nm in diameter.[76] Similarly, $AsCl_3$ has been used as a precursor (after chemical transformation to $[(Me_3Si)_2N]_2AsCl$) leading to 4 nm crystalline particles.[75] This chemistry only produced Cd_3As_2 when using $Cd(OA)_2$ as the source of Cd^{2+}, whereas the use of $CdCl_2$ or $Cd(O_2CCH_3)_2$ resulted in the formation of Cd^0.

Unlike the metal phosphides, there is only one procedure that utilizes the tris(trimethylsilyl) precursor to synthesize 2-5 nm crystalline particles.[73] This is most likely due to the fact that unlike

$P(SiMe_3)_3$, the arsenic analogue is not commercially available. This procedure relied on an initial rapid injection of $As(SiMe_3)_3$ into a hot solution of $Cd(OA)_2$, followed by a slow continuous injection of more $As(SiMe_3)_3$ to modulate growth. Based on calculations on the change in volume, the authors found that all subsequent growth was due to the slow addition of $As(SiMe_3)_3$ and not due to Ostwald ripening.[73] Figure 1.10 shows the wide range of excitonic absorption and PL (530 – 2000 nm) that was achieved through modulation of how much $As(SiMe_3)_3$ was added during the second injection step.[73]

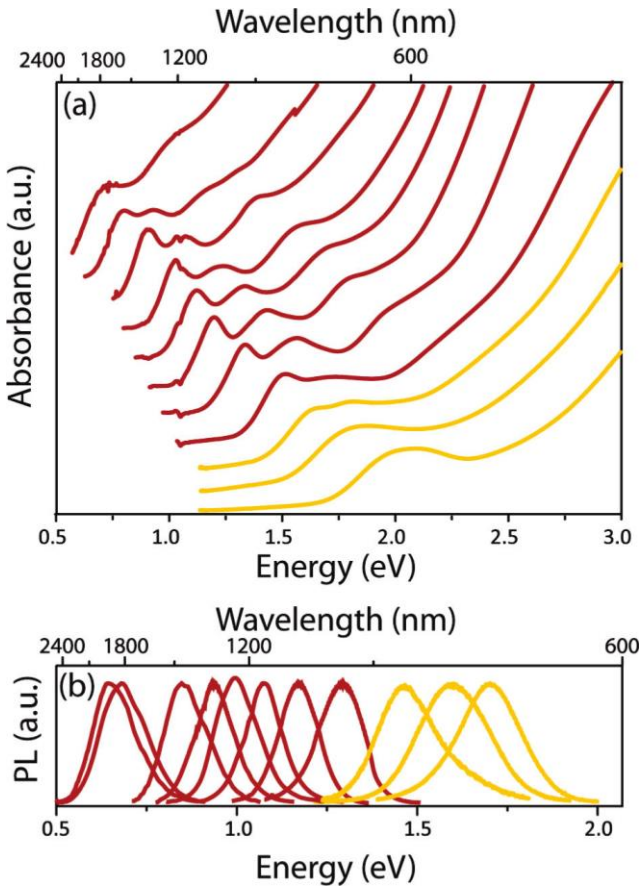

Figure 1.10. Absorption (A) and emission (B) spectra from 11 aliquots removed from a single synthesis of Cd_3As_2. Sizes range from 2 nm to 5 nm. Reprinted with permission from Ref.[73] Copyright 2011 American Chemical Society.

Based on all the reported PXRD data, there is good agreement between the structure of the nanocrystals and that of the tetragonal M_3As_2 structure. However, in terms of whether the data agree better with the 40 or 160 atom unit cell (Figure 1.2B) is a point of debate. Three reports on Cd_3As_2 compare their data to the 160 atom unit cell,[63, 73, 75] and one report compares their data to the 40 atom unit cell.[76] Our lab also found that for Zn_3As_2, our PXRD compared better to the 40 atom unit cell.[70] Given the similarity in the 40-atom and 160-atom unit cell powder patterns and given how broad the diffraction peaks are for these small nanocrystals, coalescence around a single structure type may not be possible.

Cadmium arsenide QDs are extremely luminescent with the maximum reported QY of 85% for a sample emitting at 900 nm.[73] Harris *et al.* were also able to replace $As(SiMe_3)_3$ with $P(SiMe_3)_3$ to grow a Cd_3P_2 shell on their Cd_3As_2 QDs. While this shell was able to preserve the PL in water (~1%) as well as increase the shelf-life, the authors observed shell deterioration over time.[73] Fojtik *et al.* were able to synthesize their particles in aqueous media with a QY of 10%.[72] While the optical properties of these materials are very promising, there is only one report of examining the photoresponse of a film of Cd_3As_2 on ITO in an ITO/QD/metal architecture with a 15 times current enhancement under AM1.5 illumination and a 5.0 V bias.[63] In another notable application of this material, Beberwyck and Alivisatos were able to take pre-formed Cd_3As_2 QDs and, through a cation exchange procedure, produce high quality GaAs and InAs QDs.[62]

1.5 Conclusions and Outlook

While robust syntheses of Zn_3P_2, Cd_3P_2, Zn_3As_2, and Cd_3As_2 exist to produce nanocrystals over a range of sizes, the resulting structures are poorly understood and the relationship between nanocrystal size and material structure remains underdeveloped. Given the complexity of the tetragonal unit cells of this material class, structural variations likely occur at small domain sizes as complex defect structures are unlikely to be supported. This leads to an interesting question on how the variation in physical structure may impact the electronic structure of these materials and at what crystal size these properties converge with the bulk materials. Given the somewhat limited utility of traditional X-ray diffraction analysis of these complex defective structures when small domain sizes are involved, coupling such measurements with solid-state NMR and X-ray absorption spectroscopic analysis would be beneficial. Theoretical models of structure variation as a function of crystal size would also be an excellent complement to the growing body of experimental knowledge.

In terms of synthetic strategies, there has been significant innovation in methodologies for the formation of colloidal II-V semiconductor nanocrystals that make use of phosphide and arsenide reagents that span a wide range of oxidation states. In general, synthetic strategies for the zinc-based materials are more limited than for the analogous cadmium-based materials likely due to the large disparity in reactivity between traditional zinc and cadmium precursors with conventional pnictide sources. For Zn_3P_2, Cd_3P_2, and Cd_3As_2 a range of sizes are accessible from a single synthesis: 3-9 (Zn_3P_2), 1.6-12 (Cd_3P_2), and 1-20 nm (Cd_3As_2). Interestingly the mechanism for these three reactions are notably different and no generalizable synthetic strategy has yet been devised. For Zn_3P_2, this tunable synthesis was achieved by simultaneously injecting $P(SiMe_3)_3$ and

$ZnEt_2$ into a hexadecylamine/1-ODE solution at 300 °C.[39] A range of sizes was achieved for Cd_3P_2 by varying the concentration of oleic acid used to convert CdO to $Cd(OA)_2$ followed by the injection of $P(SiMe_3)_3$ at 230 °C and heated up to 250 °C.[59] With respect to Cd_3As_2, the size range was achieved by injecting Cd_3As_2 MSCs into a mixture of 1-ODE/TOP/OLA and grown at various temperatures.[63] Preliminary work on using Cd_3P_2 MSCs with the same synthetic conditions yielded roughly 2 nm particles with little difference in diameter.[63] There have not been any reports of zinc pnictide MSCs, which could potentially serve as a valuable alternate route way to synthesize these materials *via* single-source precursors. Developing an understanding of the detailed mechanisms by which II-V nanocrystals grow and of how their defect structures evolve would likely lead to progress in the development of a generalizable synthetic strategy for II-V materials. In addition, exploration of precursor libraries that span a range of reaction rates could also aid in developing kinetically controlled crystallization strategies. Finally, gaining insight into how different ligand motifs impact the physical and electronic structure of colloidal II-V nanocrystals is an area ripe for development. Comprehension gained from such studies on synthesis, mechanism, and surface chemistry will enable the practical application of these nanocrystals in a host of optoelectronic technologies given the broad range of band gaps, from the UV down to 0 eV, spanned by this class of semiconductors.

1.6 References

1. Murray, C. B.; Norris, D. J.; Bawendi, M. G., Synthesis and characterization of nearly monodisperse CdE (E = sulfur, selenium, tellurium) semiconductor nanocrystallites. *J. Am. Chem. Soc.* **1993,** *115*, 8706-8715.

2. Rogach, A. L.; Eychmüller, A.; Hickey, S. G.; Kershaw, S. V., Infrared-Emitting Colloidal Nanocrystals: Synthesis, Assembly, Spectroscopy, and Applications. *Small* **2007,** *3*, 536-557.
3. García-Rodríguez, R.; Hendricks, M. P.; Cossairt, B. M.; Liu, H.; Owen, J. S., Conversion Reactions of Cadmium Chalcogenide Nanocrystal Precursors. *Chem. Mater.* **2013,** *25*, 1233-1249.
4. Aldakov, D.; Lefrancois, A.; Reiss, P., Ternary and quaternary metal chalcogenide nanocrystals: synthesis, properties and applications. *Journal of Materials Chemistry C* **2013,** *1*, 3756-3776.
5. Tamang, S.; Lincheneau, C.; Hermans, Y.; Jeong, S.; Reiss, P., Chemistry of InP Nanocrystal Syntheses. *Chem. Mater.* **2016,** *28*, 2491-2506.
6. Cossairt, B. M., Shining Light on Indium Phosphide Quantum Dots: Understanding the Interplay among Precursor Conversion, Nucleation, and Growth. *Chem. Mater.* **2016,** *28*, 7181-7189.
7. Friedfeld, M. R.; Stein, J. L.; Cossairt, B. M., Main-Group-Semiconductor Cluster Molecules as Synthetic Intermediates to Nanostructures. *Inorg. Chem.* **2017**.
8. Buhro, W. E., Metallo-organic routes to phosphide semiconductors. *Polyhedron* **1994,** *13*, 1131-1148.
9. Miao, S.; Eychmüller, A.; Hickey, S. G., "Artificial Supermolecule": Progress in the Study of II–V Colloidal Semiconductor Nanocrystals. In *Molecules at Work*, Wiley-VCH Verlag GmbH & Co. KGaA: 2012; pp 121-153.
10. There is debate as to whether or not Cd3As2 has an inverted band gap and is sometimes referred to as a semi-metal., There is debate as to whether or not Cd3As2 has an inverted band gap and is sometimes referred to as a semi-metal.

11. Castellion, G. A.; Beegle, L. C., The preparation and properties of Cd3As2-Zn3As2 alloys. *J. Phys. Chem. Solids* **1965,** *26*, 767-773.

12. Wagner, R.; Palik, E.; Swiggard, E., Interband Magnetoabsorption in CdxZn3-xAs2 and Cd3AsxP2-x. *J. Phys. Chem. Solids, Suppl* **1971,** *1*, 471.

13. Pawlikowski, J. M., Optical band gap of Cd3P2-Zn3P2 semiconductor solid solutions. *J. Phys. C Solid State* **1985,** *18*, 5605-5616.

14. Im, H. S.; Park, K.; Jang, D. M.; Jung, C. S.; Park, J.; Yoo, S. J.; Kim, J.-G., Zn3P2–Zn3As2 Solid Solution Nanowires. *Nano Lett.* **2015,** *15*, 990-997.

15. Sierański, K.; Szatkowski, J.; Misiewicz, J., Semiempirical Tight-Binding Band Structure of II3V2 Semiconductors: Cd3P2, Zn3P2, Cd3As2, and Zn3As2. *Phys. Rev. B* **1994,** *50*, 7331-7337.

16. Ali, M. N.; Gibson, Q.; Jeon, S.; Zhou, B. B.; Yazdani, A.; Cava, R. J., The Crystal and Electronic Structures of Cd3As2, the Three-Dimensional Electronic Analogue of Graphene. *Inorg. Chem.* **2014,** *53*, 4062-4067.

17. Pawlikowski, J. M., Band structure and properties of Zn3P2— promising new infrared material∗. *Infrared Physics* **1981,** *21*, 181-187.

18. Misiewicz, J., Optical and electrical investigations of imperfection levels in Zn3P2. *J. Phys. Chem. Solids* **1989,** *50*, 1013-1022.

19. Pawlikowski, J. M., Comments on Zn3P2 band structure. *J. Appl. Phys.* **1982,** *53*, 3639-3642.

20. Silvey, G. A., Zn3As2, A Semiconducting Intermetallic Compound. *J. Appl. Phys.* **1958,** *29*, 226-227.

21. Misiewicz, J.; Pawlikowski, J. M., Optical band-gap of Zn3As2. *Solid State Commun.* **1979,** *32*, 687-690.

22. Sujak-Cyrul, B.; Kolodka, B.; Misiewicz, J.; Pawlikowski, J. M., Intraband and interband optical transitions in Zn3AS2. *J. Phys. Chem. Solids* **1982,** *43*, 1045-1051.

23. Misiewicz, J.; Wróbel, J. M.; Jezierski, K., Interband transitions in Zn3As2. *Solid State Commun.* **1993,** *86*, 509-511.

24. Haacke, G.; Castellion, G. A., Preparation and Semiconducting Properties of Cd3P2. *J. Appl. Phys.* **1964,** *35*, 2484-2487.

25. Żdanowicz, W.; Wojakowski, A., Preparation and Semiconducting Properties of Cadmium Phosphide (Cd3P2). *Phys. Status Solidi B* **1965,** *8*, 569-575.

26. Plenkiewicz, P.; Dowgiałło-Plenkiewicz, B., Energy band structure of Cd3P2 for real D 4h15 symmetry I. Energy bands. *Phys. Status Solidi B* **1979,** *92*, 379-387.

27. Aubin, M. J.; Caron, L. G.; Jay-Gerin, J. P., Band structure of cadmium arsenide at room temperature. *Phys. Rev. B* **1977,** *15*, 3872-3878.

28. Dowgiałło-Plenkiewicz, B.; Plenkiewicz, P., Inverted band structure of Cd3As2. *Phys. Status Solidi B* **1979,** *94*, K57-K60.

29. Lin-Chung, P. J., Energy band structures of Cd3P2 and Zn3P2. *Phys. Status Solidi B* **1971,** *47*, 33-39.

30. Dowgiałło-Plenkiewicz, B.; Plenkiewicz, P., Spin–Orbit and Crystal Field Splittings of the Valence Band in II3V2 Semiconducting Compounds. *Phys. Status Solidi B* **1978,** *87*, 309-315.

31. Hupfer, A.; Hirsch, D.; Schulze, S., Photoemission on A 3IIB 2V semiconductor material. Cd3As2, Zn3As2, Cd3P2, Zn3P2 crystals and thin films. *Phys. Status Solidi B* **1989,** *152*, 505-517.

32. Weller, H.; Fojtik, A.; Henglein, A., Photochemistry of semiconductor colloids: Properties of extremely small particles of Cd3P2 and Zn3P2. *Chem. Phys. Lett.* **1985,** *117*, 485-488.

33. Green, M.; O'Brien, P., A Novel Metalorganic Route to Nanocrystallites of Zinc Phosphide. *Chem. Mater.* **2001,** *13*, 4500-4505.

34. Carenco, S.; Demange, M.; Shi, J.; Boissiere, C.; Sanchez, C.; Le Floch, P.; Mezailles, N., White phosphorus and metal nanoparticles: a versatile route to metal phosphide nanoparticles. *Chem. Commun.* **2010,** *46*, 5578-5580.

35. Miao, S.; Yang, T.; Hickey, S. G.; Lesnyak, V.; Rellinghaus, B.; Xu, J.; Eychmüller, A., Emissive ZnO@Zn3P2 Nanocrystals: Synthesis, Optical, and Optoelectrochemical Properties. *Small* **2013,** *9*, 3415-3422.

36. Luber, E. J.; Mobarok, M. H.; Buriak, J. M., Solution-Processed Zinc Phosphide (α-Zn3P2) Colloidal Semiconducting Nanocrystals for Thin Film Photovoltaic Applications. *ACS Nano* **2013,** *7*, 8136-8146.

37. Mobarok, M. H.; Luber, E. J.; Bernard, G. M.; Peng, L.; Wasylishen, R. E.; Buriak, J. M., Phase-Pure Crystalline Zinc Phosphide Nanoparticles: Synthetic Approaches and Characterization. *Chem. Mater.* **2014,** *26*, 1925-1935.

38. Glassy, B. A.; Cossairt, B. M., Ternary synthesis of colloidal Zn3P2 quantum dots. *Chem. Commun.* **2015,** *51*, 5283-5286.

39. Ho, M. Q.; Esteves, R. J. A.; Kedarnath, G.; Arachchige, I. U., Size-Dependent Optical Properties of Luminescent Zn3P2 Quantum Dots. *J. Phys. Chem. C* **2015,** *119*, 10576-10584.

40. Glassy, B. A.; Cossairt, B. M., Resolving the Chemistry of Zn3P2 Nanocrystal Growth. *Chem. Mater.* **2016,** *28*, 6374-6380.

41. Lim, T. H.; Teh, G. B.; Tilley, R. D. In *Synthesis and Characterization of Highly Crystalline Zinc Phosphide Nanoparticles*, Key Eng. Mater., Trans Tech Publ: 2016; pp 3-7.

42. Gary, D. C.; Flowers, S. E.; Kaminsky, W.; Petrone, A.; Li, X.; Cossairt, B. M., Single-Crystal and Electronic Structure of a 1.3 nm Indium Phosphide Nanocluster. *J. Am. Chem. Soc.* **2016,** *138*, 1510-1513.

43. Adolphi, N. L.; Stoddard, R. D.; Goel, S. C.; Buhro, W. E.; Gibbons, P. C.; Conradi, M. S., The 31P NMR spectra of Cd3P2 and Zn3P2. *J. Phys. Chem. Solids* **1992,** *53*, 1275-1278.

44. Orchard, K. L.; White, A. J. P.; Shaffer, M. S. P.; Williams, C. K., Pentanuclear Complexes for a Series of Alkylzinc Carboxylates. *Organometallics* **2009,** *28*, 5828-5832.

45. Rademacher, B.; Schwarz, W.; Westerhausen, M., Heteroleptische Diorganylzink‐Verbindungen mit einem Bis (trimethylsilyl) phosphanido‐Substituenten. *Z. Anorg. Allg. Chem.* **1995,** *621*, 287-300.

46. Mobarok, M. H.; Buriak, J. M., Elucidating the Surface Chemistry of Zinc Phosphide Nanoparticles Through Ligand Exchange. *Chem. Mater.* **2014,** *26*, 4653-4661.

47. Bhushan, M.; Catalano, A., Polycrystalline Zn3P2 Schottky barrier solar cells. *Appl. Phys. Lett.* **1981,** *38*, 39-41.

48. Nayar, P. S.; Catalano, A., Zinc phosphide‐zinc oxide heterojunction solar cells. *Appl. Phys. Lett.* **1981,** *39*, 105-107.

49. Kimball, G. M.; Lewis, N. S.; Atwater, H. A. In *Mg doping and alloying in Zn3P2 heterojunction solar cells*, Photovoltaic Specialists Conference (PVSC), 2010 35th IEEE, 20-25 June 2010; 2010; pp 001039-001043.

50. Yang, R.; Chueh, Y.-L.; Morber, J. R.; Snyder, R.; Chou, L.-J.; Wang, Z. L., Single-Crystalline Branched Zinc Phosphide Nanostructures: Synthesis, Properties, and Optoelectronic Devices. *Nano Lett.* **2006,** *7*, 269-275.

51. Goel, S. C.; Chiang, M. Y.; Buhro, W. E., Synthesis of homoleptic silylphosphido complexes (M[P(SiMe3)2][.mu.-P(SiMe3)2])2, where M = zinc and cadmium, and their use in metalloorganic routes to Cd3P2 and MGeP2. *J. Am. Chem. Soc.* **1990,** *112*, 5636-5637.

52. Matchett, M. A.; Viano, A. M.; Adolphi, N. L.; Stoddard, R. D.; Buhro, W. E.; Conradi, M. S.; Gibbons, P. C., Sol-gel-like route to crystalline cadmium phosphide nanoclusters. *Chem. Mater.* **1992,** *4*, 508-511.

53. Kornowski, A.; Eichberger, R.; Giersig, M.; Weller, H.; Eychmüller, A., Preparation and Photophysics of Strongly Luminescing Cd3P2 Quantum Dots. *The Journal of Physical Chemistry* **1996,** *100*, 12467-12471.

54. Green, M.; O'Brien, P., A Novel Synthesis of Cadmium Phosphide Nanoparticles Using the Single-Source Precursor [MeCdPtBu2]3. *Adv. Mater.* **1998,** *10*, 527-528.

55. Green, M.; O'Brien, P., The synthesis of cadmium phosphide nanoparticles using cadmium diorganophosphide precursors. *J. Mater. Chem.* **1999,** *9*, 243-247.

56. Wang, R.; Ratcliffe, C. I.; Wu, X.; Voznyy, O.; Tao, Y.; Yu, K., Magic-Sized Cd3P2 II−V Nanoparticles Exhibiting Bandgap Photoemission. *J. Phys. Chem. C* **2009,** *113*, 17979-17982.

57. Khanna, P. K.; Singh, N.; More, P., Synthesis and band-gap photoluminescence from cadmium phosphide nano-particles. *Current Applied Physics* **2010,** *10*, 84-88.

58. Miao, S.; Hickey, S. G.; Rellinghaus, B.; Waurisch, C.; Eychmüller, A., Synthesis and Characterization of Cadmium Phosphide Quantum Dots Emitting in the Visible Red to Near-Infrared. *J. Am. Chem. Soc.* **2010,** *132*, 5613-5615.

59. Xie, R.; Zhang, J.; Zhao, F.; Yang, W.; Peng, X., Synthesis of Monodisperse, Highly Emissive, and Size-Tunable Cd3P2 Nanocrystals. *Chem. Mater.* **2010,** *22*, 3820-3822.

60. Ojo, W.-S.; Xu, S.; Delpech, F.; Nayral, C.; Chaudret, B., Room-Temperature Synthesis of Air-Stable and Size-Tunable Luminescent ZnS-Coated Cd3P2 Nanocrystals with High Quantum Yields. *Angew. Chem. Int. Ed.* **2012,** *51*, 738-741.

61. Miao, S.; Hickey, S. G.; Waurisch, C.; Lesnyak, V.; Otto, T.; Rellinghaus, B.; Eychmüller, A., Synthesis of Monodisperse Cadmium Phosphide Nanoparticles Using ex-Situ Produced Phosphine. *ACS Nano* **2012,** *6*, 7059-7065.

62. Beberwyck, B. J.; Alivisatos, A. P., Ion Exchange Synthesis of III–V Nanocrystals. *J. Am. Chem. Soc.* **2012,** *134*, 19977-19980.

63. Li, D.; Peng, L.; Zhang, Z.; Shi, Z.; Xie, R.; Han, M.-Y.; Yang, W., Large Scale Synthesis of Air Stable Precursors for the Preparation of High Quality Metal Arsenide and Phosphide Nanocrystals as Efficient Emitters Covering the Visible to Near Infrared Region. *Chem. Mater.* **2014,** *26*, 3599-3602.

64. Stein, J. L.; Steimle, M. I.; Terban, M. W.; Petrone, A.; Billinge, S. J. L.; Li, X.; Cossairt, B. M., Cation exchange induced transformation of InP magic-sized custers. *Submitted.* **2017**.

65. Zhao, X.-G.; Shi, J.-L.; Hu, B.; Zhang, L.-X.; Hua, Z.-L., Confinement of Cd3P2 nanoparticles inside ordered pore channels in mesoporous silica. *J. Mater. Chem.* **2003,** *13*, 399-403.

66. Tomaselli, M.; Yarger, J. L.; Bruchez, M. J.; Havlin, R. H.; deGraw, D.; Pines, A.; Alivisatos, A. P., NMR study of InP quantum dots: Surface structure and size effects. *J. Chem. Phys.* **1999,** *110*, 8861-8864.

67. Kietzmann, R.; Willig, F.; Weller, H.; Vogel, R.; Nath, D. N.; Eichberger, R.; Liska, P.; Lehnert, J., Picosecond Time Resolved Electron Injection from Excited Cresyl Violet Monomers and Cd3P2 Quantum Dots into TiO2. *Molecular Crystals and Liquid Crystals* **1991,** *194*, 169-180.

68. Miao, S.; Chen, D.; Madani, A.; Jorgensen, M. R.; Bolaños Quiñones, V. A.; Ma, L.; Hickey, S. G.; Eychmüller, A.; Schmidt, O. G., Optofluidic Sensor: Evaporation Kinetics Detection of Solvents Dissolved with Cd3P2 Colloidal Quantum Dots in a Rolled-Up Microtube. *Advanced Optical Materials* **2015,** *3*, 187-193.

69. Ding, L.; He, S.; Chen, D.; Huang, M.; Xu, J.; Hickey, S. G.; Eychmuller, A.; Yu, S.-H.; Miao, S., Encapsulated Cd3P2 quantum dots emitting from the visible to the near infrared for bio-labelling applications. *CrystEngComm* **2014,** *16*, 9622-9630.

70. Glassy, B. A.; Lai, N. L.; Cossairt, B. M., Synthesis of Zn3As2 and (CdyZn1-y)3As2 colloidal quantum dots. *Submitted.* **2017**.

71. Zhao, X.; Zheng, B.; Li, C.; Gu, H., Acetate-derived ZnO ultrafine particles synthesized by spray pyrolysis. *Powder Technol.* **1998,** *100*, 20-23.

72. Fojtik, A.; Weller, H.; Henglein, A., Photochemistry of semiconductor colloids. Size quantization effects in Q-cadmium arsenide. *Chem. Phys. Lett.* **1985,** *120*, 552-554.

73. Harris, D. K.; Allen, P. M.; Han, H.-S.; Walker, B. J.; Lee, J.; Bawendi, M. G., Synthesis of Cadmium Arsenide Quantum Dots Luminescent in the Infrared. *J. Am. Chem. Soc.* **2011,** *133*, 4676-4679.

74. Huang, M.; Hickey, S. G.; Höfer, B.; Ding, F.; He, S.; Schmidt, O. G.; Eychmüller, A.; Miao, S., Band-Emission Evolutions from Magic-sized Clusters to Nanosized Quantum Dots of Cd3As2 in the Hot-Bubbling Synthesis. *J. Phys. Chem. C* **2015,** *119*, 16390-16395.

75. Das, A.; Shamirian, A.; Snee, P. T., Arsenic Silylamide: An Effective Precursor for Arsenide Semiconductor Nanocrystal Synthesis. *Chem. Mater.* **2016,** *28*, 4058-4064.

76. Srivastava, V.; Janke, E. M.; Diroll, B. T.; Schaller, R. D.; Talapin, D. V., Facile, Economic and Size-Tunable Synthesis of Metal Arsenide Nanocrystals. *Chem. Mater.* **2016,** *28*, 6797-6802.

Chapter 2. Ternary Synthesis of Colloidal Zinc Phosphide Quantum Dots

2.1 Introduction

Rising global energy demands and diminishing fossil fuel reserves necessitate innovation in alternative energy sources. Solar radiation is promising given it is environmentally benign and abundant, but the high cost of solar cell fabrication and materials, particularly high quality crystalline silicon, prevents wide-spread deployment into the power grid.[1-2] A recent cost-benefit analysis was performed on 23 semiconducting materials with electronic structures suitable for photovoltaic applications to determine possible alternatives to crystalline silicon. The study used the earth abundance of the semiconducting materials, raw material extraction costs, and theoretical efficiency of solar energy conversion based on band gap to determine their energy production potential. Of the 23 materials examined, nine were found to have the capacity to meet or exceed annual worldwide electricity consumption with a significant cost-reduction over crystalline silicon.[3] Among the most promising of these nine materials was zinc phosphide.

Zinc phosphide (Zn_3P_2) is ideally positioned as a next generation photovoltaic material as it has a direct band gap of 1.50 eV, which allows it to absorb a high percentage of the solar spectrum.[4] Zinc phosphide also has a high extinction coefficient,[5] and a long minority-carrier diffusion length (5-10 μm); properties that are desirable in efficient photovoltaic materials.[6] High-quality epitaxially grown Zn_3P_2 was first reported in 1992,[7] and heterojunction optoelectronic devices made with zinc phosphide have been fabricated, demonstrating the viability of industrial scale development of zinc phosphide semiconductor technologies.[8-11] However, for cost-effective

large-scale synthesis, solution processable device fabrication, and control over the optical and electronic band gap, a colloidal quantum dot (QD) synthesis is desirable.[12-13]

As of 2014, there have been seven accounts of colloidal syntheses of Zn_3P_2.[14-20] The earliest study showed formation of zinc phosphide clusters with a distinct lowest energy excitonic transition (LEET) at 300 nm, indicative of relatively uniform crystalline particles, with an approximated 1 nm diameter. However, larger particles could not be obtained by this method.[14] Green and O'Brien describe a synthesis that gives a broad excitonic feature below 500 nm, but analysis showed a high degree of polydispersity and a mixture of crystalline and amorphous material.[16] Recent investigations have yielded zinc phosphide with no clear excitonic features in the absorption spectra and conflicting powder diffraction data, suggesting isolation of different crystal phases of zinc phosphide with a broad size distribution and lack of quantum confinement.[18-19] These inconsistencies highlight the need for new, robust, and reproducible synthetic methods to obtain colloidal zinc phosphide quantum dots that are phase-pure, absorb in the visible region of the electromagnetic spectrum, and have low polydispersity.[21]

The reported synthetic approaches to colloidal zinc phosphide utilized a zinc precursor (zinc perchlorate,[14] zinc alkoxide,[15] zinc nanoparticles,[17] dialkylzinc,[16, 18-20] zinc stearate,[18] or zinc silylamide[18]), a phosphorus precursor (phosphine gas,[14, 18] tristrimethylsilylphosphine,[15, 18, 20] ditertbutylphosphine,[16] white phosphorus,[17] or trioctylphosphine[19-20]), and excess ligands such as hexametaphosphate,[14] pyridine,[15-16] trioctylphosphine,[16-20] or stearate.[18] This chapter discusses a novel synthesis that relies on the *in situ* generation of a highly reactive pentanuclear zinc cluster from $ZnEt_2$ and $Zn(O_2CR)_2$ (R = $(CH_2)_{12}CH_3$ [MA] or $C(CH_2)_7CH{=}CH(CH_2)_7CH_3$ [OA]) followed by its *in situ* reaction with $P(SiMe_3)_3$ to generate $(Et_2Zn)P(ZnO_2CR)_2(SiMe_3)$ prior to conversion to zinc phosphide. The molecular precursor conversion is probed using ^1H and $^{31}P\{^1H\}$ NMR

spectroscopy. Through control of the reaction temperature during nanocrystal growth, crystalline particles with clear excitonic transitions in the visible are obtained. Detailed characterization of the structure and composition of the resulting zinc-rich zinc phosphide nanocrystals by HRTEM, TEM, ICP-OES, TGA, NMR, and powder XRD are presented.

2.2 Results and Discussion

2.2.1 General Synthetic Strategy and Optical Properties of the Resulting Quantum Dots

Our strategy to avoid the difficulties in forming this covalent material was to pre-form a cluster containing Zn−P bonds, with initial focus on silylphosphine and alkylzinc reagents inspired by an unusual Zn_6P_4 cluster observed by Arno Pfitzner and co-workers.[22] Our best results were obtained by injecting a mixture of $ZnEt_2$ and $P(SiMe_3)_3$ into $Zn(O_2CR)_2$ at 100 °C followed by heating to the growth temperature (Scheme 2.1). UV-vis spectra of timed aliquots for a typical synthesis (Figure 2.1A) show the progression of the LEET as a function of temperature and time. Particles with a clear excitonic feature only formed when utilizing this heat-up method and all three precursors (Figure 2.2).

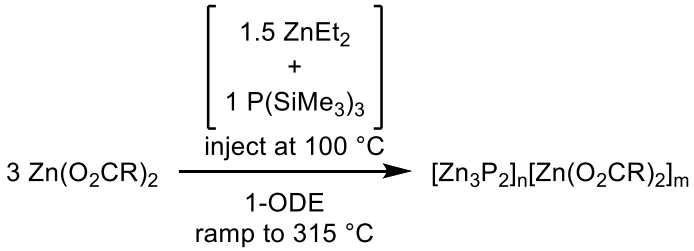

Scheme 2.1 Synthesis of zinc-rich zinc phosphide quantum dots from $ZnEt_2$, $Zn(O_2CR)_2$ where R is $(CH_2)_{12}CH_3$ or $(CH_2)_7CH{=}CH(CH_2)_7CH_3$, and $P(SiMe_3)_3$.

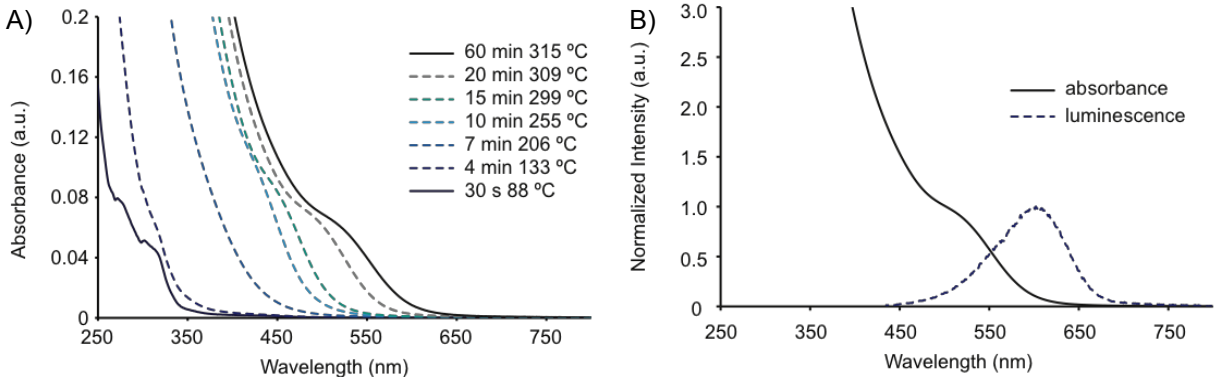

Figure 2.1. (A) UV-Vis spectra showing the temporal evolution of zinc phosphide quantum dots formed using Scheme 1. (B) Absorbance and room temperature photoluminescence of isolated zinc phosphide quantum dots.

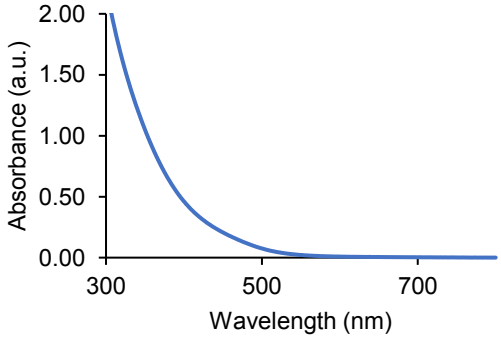

Figure 2.2. 60 minute trace for a 0.2 mmol $P(SiMe_3)_3$ reaction where $ZnEt_2$ was not used.

The position of the final LEET is dependent on the final growth temperature achieved and ranged from 424 to 535 nm, with absorption onsets extending beyond 600 nm (Figure 2.3).[23]

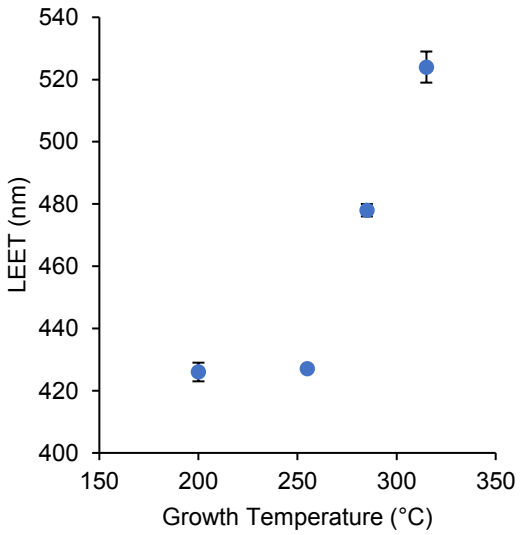

Figure 2.3. Final temperature effect on LEET for particles synthesized by Scheme 2.1 and modulating the final temperature (200-315 °C). Each synthesis used 0.2 mmol $P(SiMe_3)_3$ and was repeated three times.

Photoluminescence (PL) was observed for all samples grown to temperatures ≥ 255 °C and was red shifted from the absorbance peak by at least 0.37 eV (Figures 2.1B) and was independent of the energy of the LEET. The red shift in fluorescence and the lack of correlation of the emission profile from the absorption maxima suggests luminescence from mid-gap trap states.[18] The PL quantum yields were around 1%, typical of related metal phosphide systems.[18, 24-25]

Experiments probing the effect of concentration on the synthesis indicated that a lower total concentration dramatically increased the energy of the LEET (Figure 2.4). This is in line with classical nucleation theory whereby a greater fraction of the available monomer reserves is consumed during the nucleation event leaving less available monomers for further growth in a low total concentration scenario.[26-27]

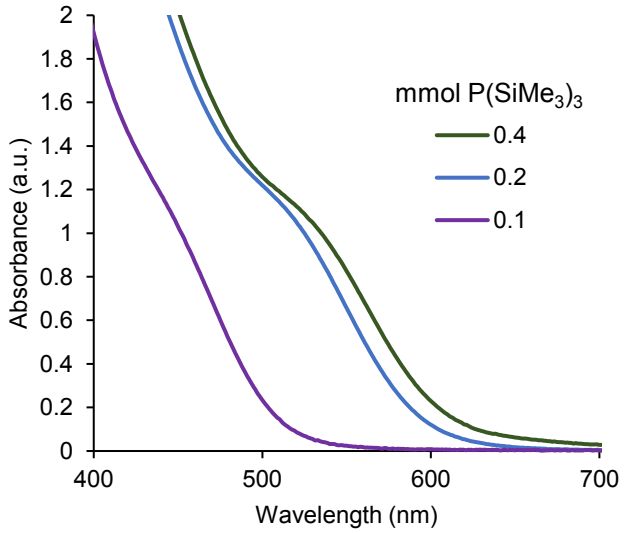

Figure 2.4. Concentration effect on absorption of particles grown to 315 °C, determined by altering the amount of reagents and keeping the total volume (8 grams of 1-ODE) the same to preserve the ramp rate.

2.2.2 Probing the Precursor Conversion with NMR Spectroscopy

NMR experiments were conducted to elucidate the mechanism of precursor conversion and to understand the synergistic role of using two different zinc precursors. A series of control experiments were first performed to determine the individual roles of each molecular precursor. When $P(SiMe_3)_3$ and $ZnEt_2$ were combined in C_6D_6 in a J-Young tube, the ^1H and $^{31}P\{^1H\}$ NMR spectra reveal no change over the course of 24 hours at room temperature. There is also no change at 80 °C over the course of one hour (Figure 2.5). These results suggest that $P(SiMe_3)_3$ does not directly react with $ZnEt_2$ under these conditions. In C_6D_6, $P(SiMe_3)_3$ and $Zn(O_2CR)_2$ react over the course of hours (half-life of 5 hours for R = CH_3) at room temperature and do not form any resolvable phosphorus containing intermediates (Figure 2.6). Zinc carboxylates and diethyl zinc,

however, are known to react to form $[Zn_5(O_2CR)_6(Et)_4]$ clusters in non-coordinating solvent, and we have identified this species in our the ^1H NMR data (Figure 2.7).[28] When $P(SiMe_3)_3$ is combined with this pre-formed zinc cluster, it reacts on the order of minutes (half-life of < 5 minutes) to form a phosphorus-containing intermediate with a chemical shift of −276 ppm (Figure 2.8).

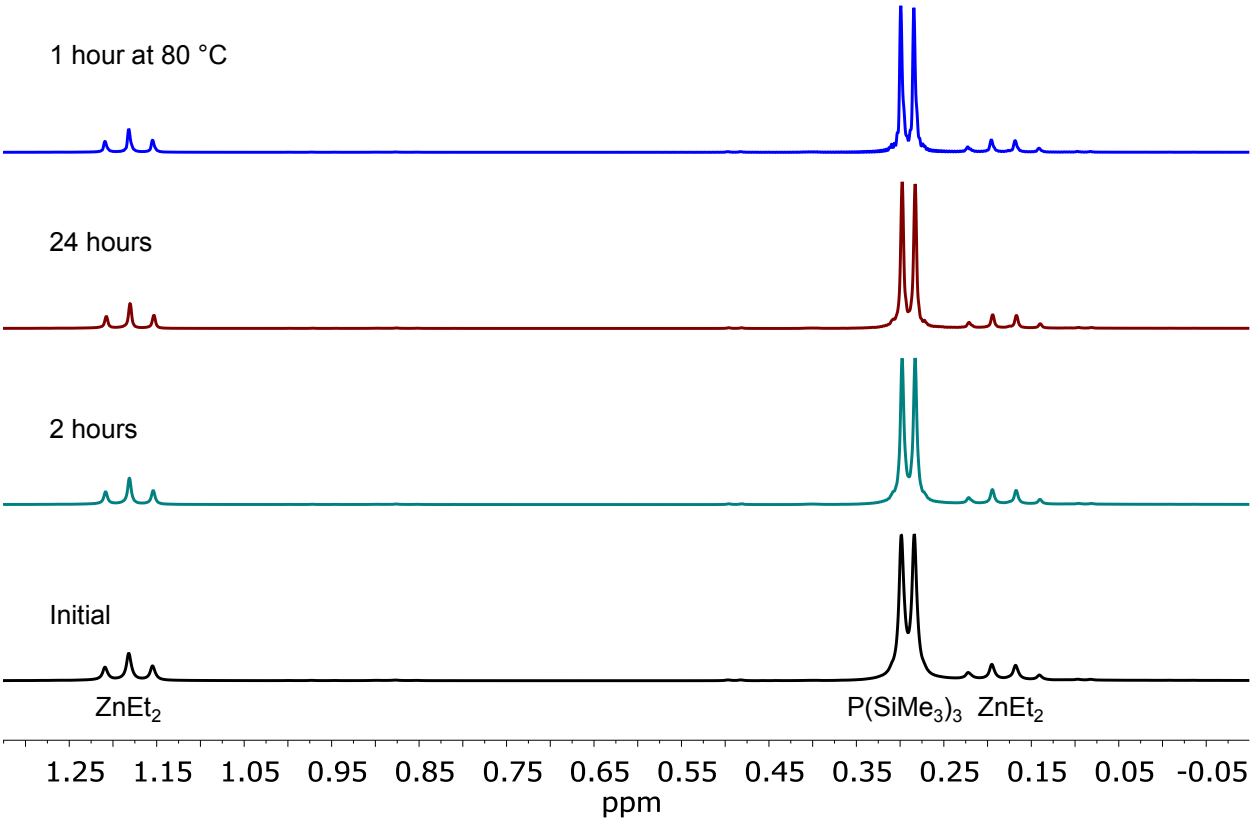

Figure 2.5. ^1H NMR spectra of a control mixing 1.5 $ZnEt_2$ and 1 $P(SiMe_3)_3$ showing no reaction between these two species in C_6D_6 at room temperature or even 80 °C. The triplet at 1.19 and quartet at 0.19 ppm are from $ZnEt_2$ and the doublet at 0.29 is from $P(SiMe_3)_3$.

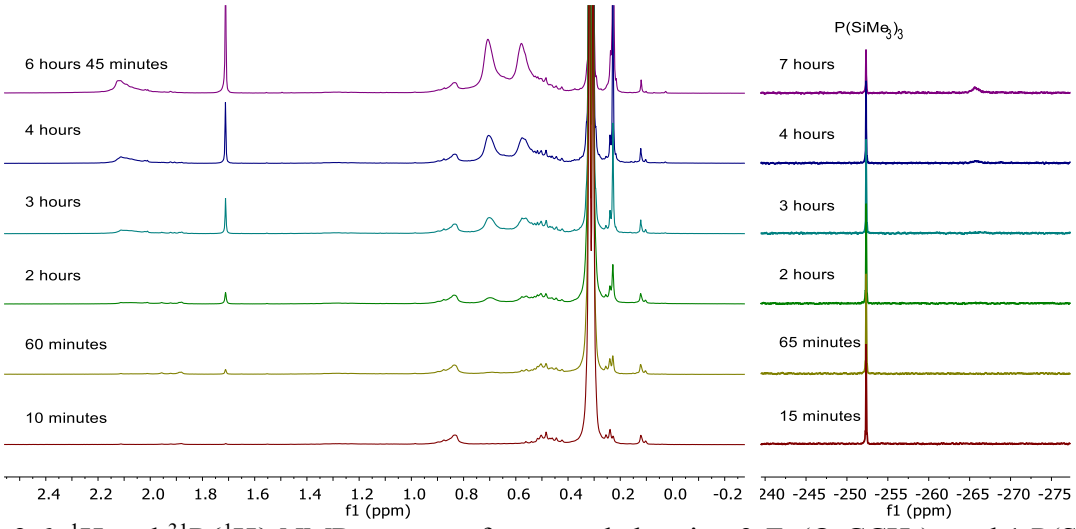

Figure 2.6. ^{1}H and $^{31}P\{^{1}H\}$ NMR spectra of a control showing 3 $Zn(O_2CCH_3)_2$ and 1 $P(SiMe_3)_3$ reacting very slowly over the course of hours. The half-life was determined to be around 5 hours.

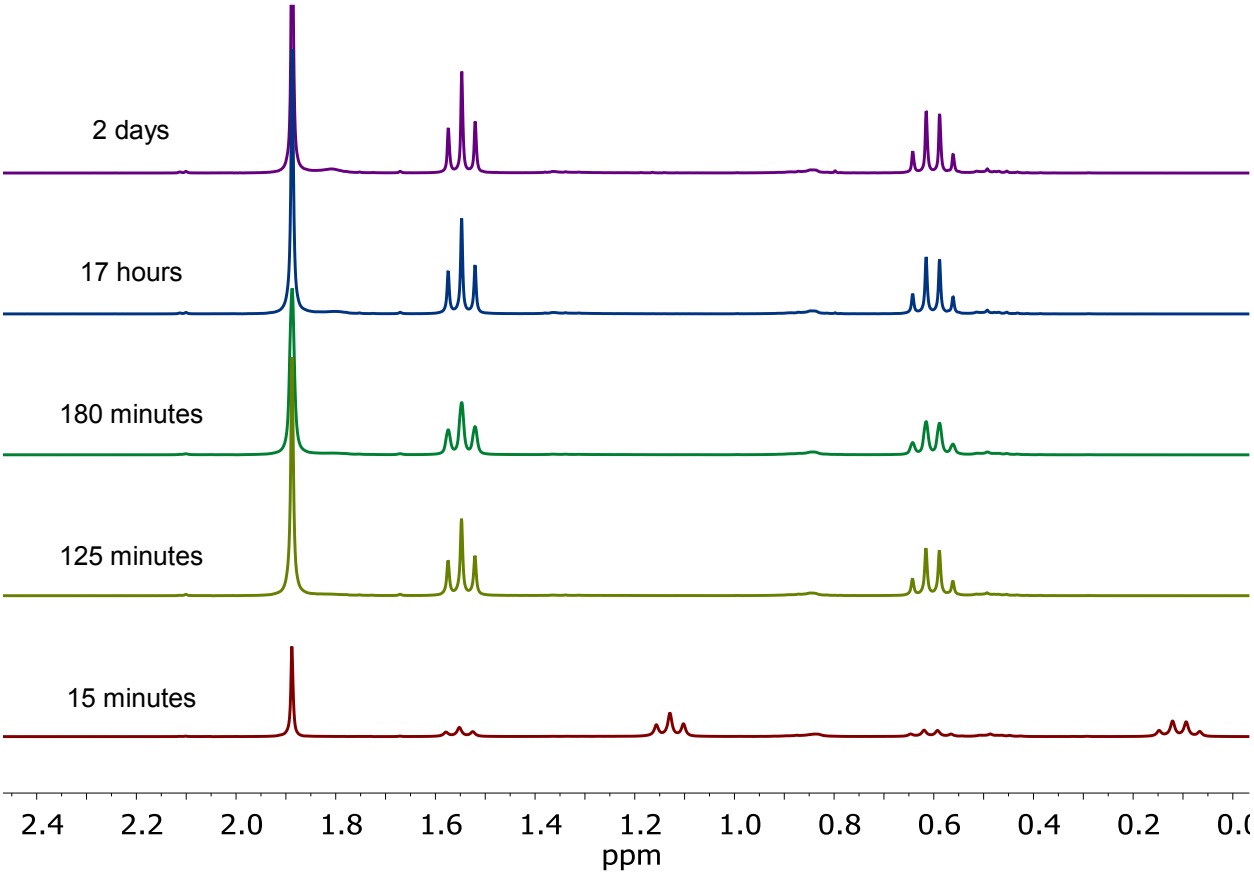

Figure 2.7. ^{1}H NMR data showing the formation of $[Zn_5(O_2CCH_3)_6(Et)_4]$ by mixing 3 $Zn(O_2CCH_3)_2$ and 1.5 $ZnEt_2$ in C_6D_6 at room temperature.

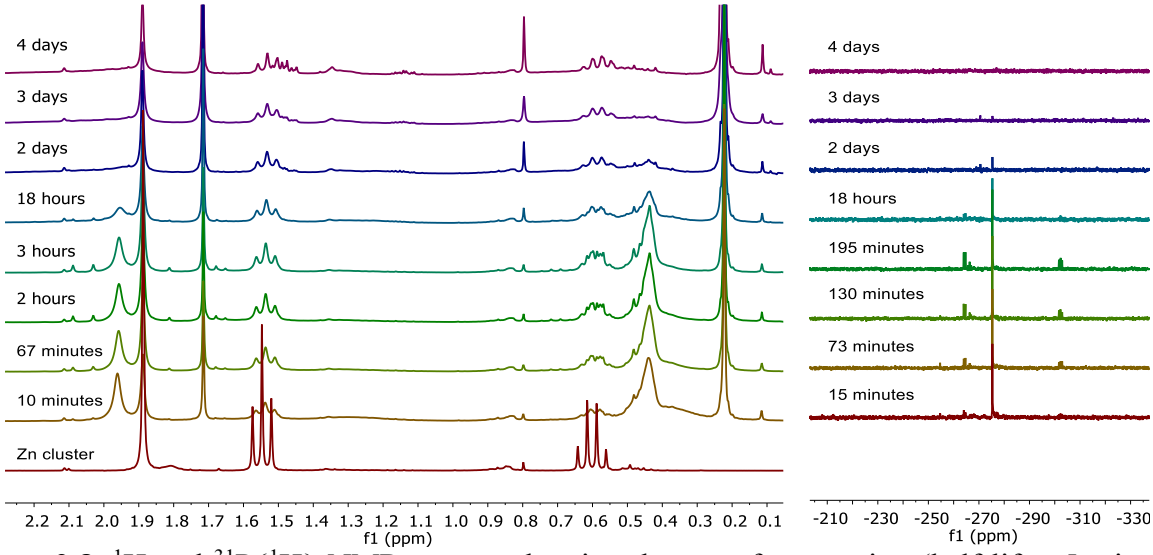

Figure 2.8. ^{1}H and $^{31}P\{^{1}H\}$ NMR spectra showing the very fast reaction (half-life <5 minutes) between $[Zn_5(O_2CCH_3)_6(Et)_4]$ and $P(SiMe_3)_3$ in C_6D_6 at room temperature.

To probe the molecular transformation of all three precursors, $Zn(MA)_3$, $P(SiMe_3)_3$, and $ZnEt_2$ were mixed in a J-Young tube at room temperature in C_6D_6 and was monitored by $^{31}P\{^{1}H\}$ and ^{1}H NMR spectroscopy. The time resolved $^{31}P\{^{1}H\}$ NMR spectra show the disappearance of the $P(SiMe_3)_3$ singlet at −252 ppm along with the concomitant appearance of a new singlet at −276 ppm, which suggests that $P(SiMe_3)_3$ is converting to a new molecular species over the period of hours at 22 °C (Figure 2.9). The ^{1}H NMR spectra are difficult to analyze due to the overlapping peaks from the myristate ligands, however the complexity of the ^{1}H NMR spectra can be significantly reduced by replacing $Zn(MA)_2$ with $Zn(O_2CCH_3)_2$.

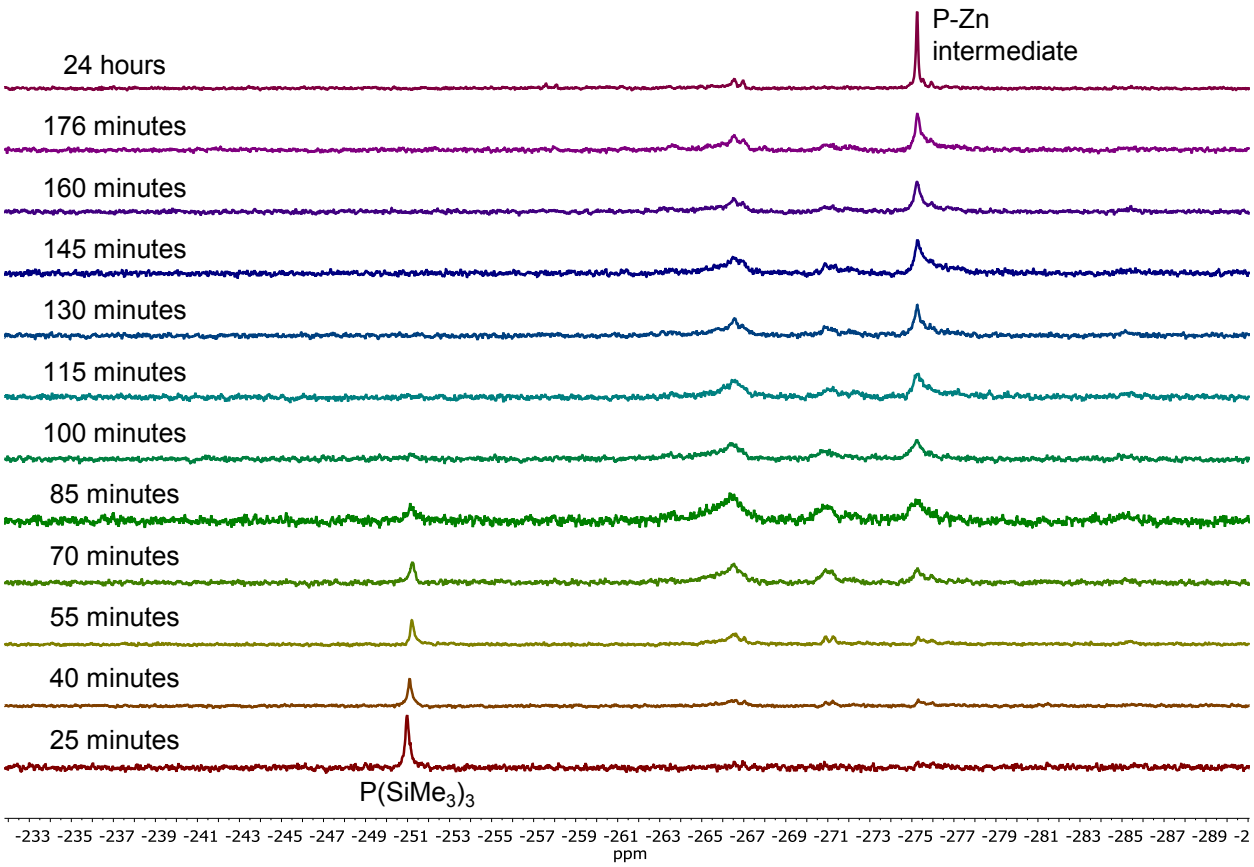

Figure 2.9. $^{31}P\{^{1}H\}$ NMR data showing the room temperature reaction between 3 $Zn(MA)_2$, 1.5 $ZnEt_2$, and $P(SiMe_3)_3$.

When $Zn(O_2CCH_3)_2$, $P(SiMe_3)_3$, and $ZnEt_2$ are combined in C_6D_6 in a J-Young NMR tube at room temperature, the reaction mixture is initially heterogeneous due to the insolubility of $Zn(O_2CCH_3)_2$ in C_6D_6, but becomes homogenous over time. The time resolved $^{31}P\{^{1}H\}$ NMR spectra show the formation and disappearance of a singlet at −276 ppm, as observed when using $Zn(MA)_2$ (Figure 2.10A). This reaction also has a corresponding resolvable ^{1}H NMR spectrum which shows the formation and disappearance of the proposed phosphorus-containing intermediate in addition to the pentanuclear $[Zn_5(O_2CCH_3)_6(Et)_4]$ cluster, and the silylacetate co-product (Figure 2.10B). Based upon the integration of a ^{1}H NMR spectrum taken two hours after all three

precursors were mixed together (Figure 2.11), we propose that the smallest unit of the long lived phosphorus containing intermediate is $(Me_3Si)P[Zn(O_2CCH_3)]_2$ with a $ZnEt_2$ group datively bound (Figure 2.10C). The assignment of P-bound $ZnEt_2$ is based on the observation of the downfield shift and broadening of free $ZnEt_2$ concomitant with the appearance of the phosphorus-containing intermediate in addition to its subsequent shift back and sharpening on loss of this intermediate. There is literature precedent for related tetrahedrally-coordinated phosphorus species displaying $^{31}P\{^1H\}$ NMR signals at −318.5[29] and −270.3[30] ppm. We were unable to isolate and purify the proposed $(Et_2Zn)P[Zn(O_2CCH_3)]_2(SiMe_3)$ species due to its limited lifetime and instability under reduced pressure.

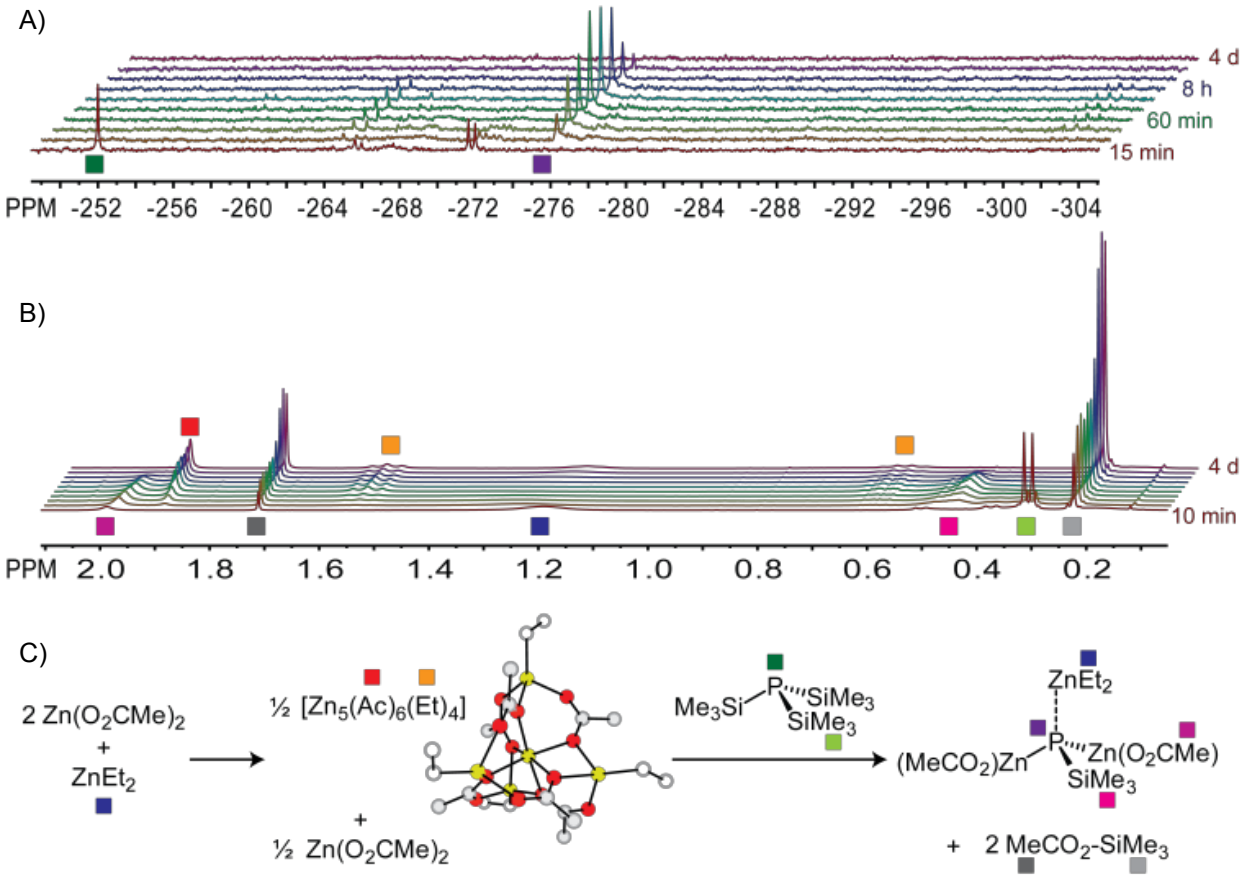

Figure 2.10. (A) $^{31}P\{^{1}H\}$ NMR spectra showing time evolution of the zinc phosphide precursor conversion reactions at 22 °C. (B) ^{1}H NMR spectra showing the corresponding time evolution of the zinc phosphide precursor conversion reactions at 22 °C. (C) Proposed scheme for the zinc phosphide precursor conversion reactions.

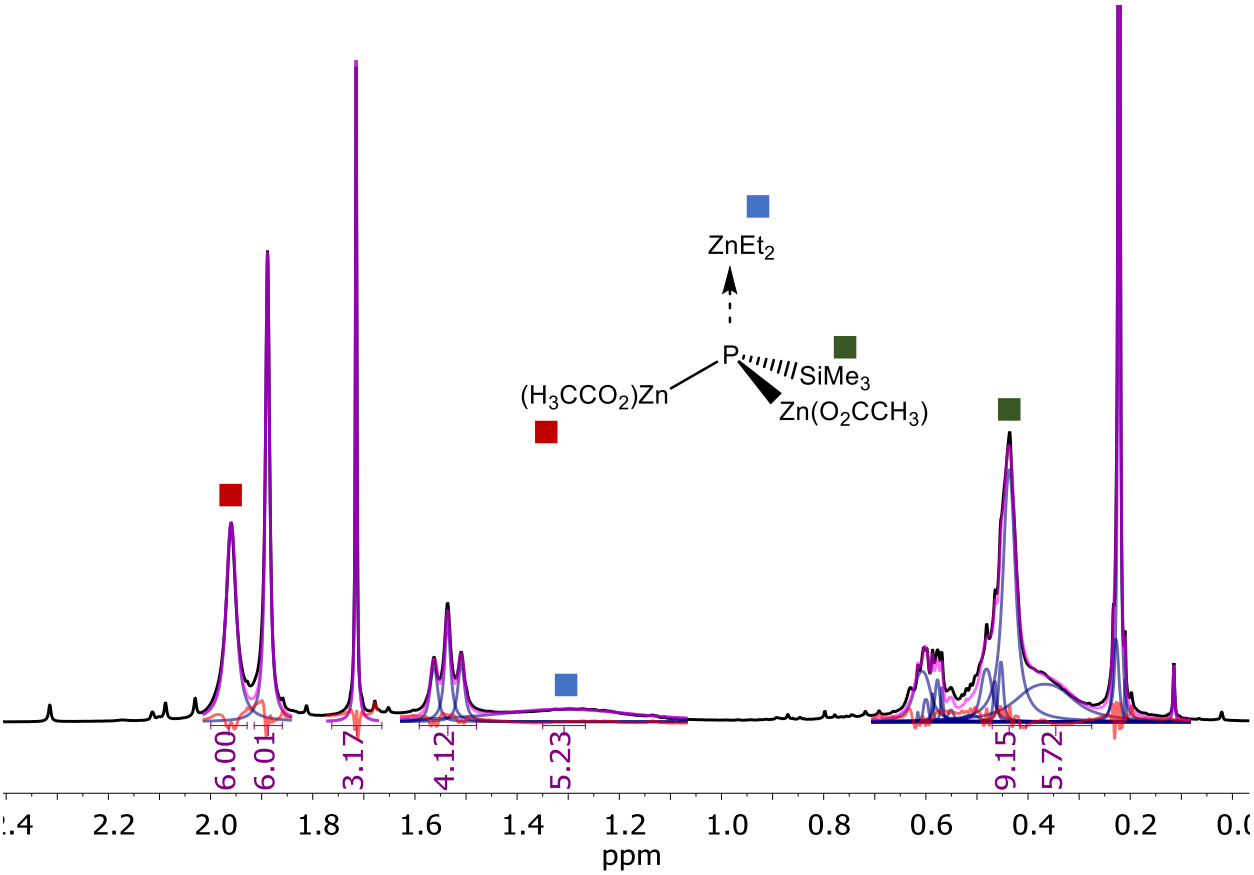

Figure 2.11. Fitting of the 125 minute time trace of the ^{1}H NMR data of the room temperature reaction between 3 $Zn(O_2CCH_3)_2$, 1.5 $ZnEt_2$, and 1 $P(SiMe_3)_3$. These integrations show the formation of our proposed intermediate.

2.2.3 Probing the Relevance of the Identified Molecular Intermediate in the Nucleation and Growth of the Zinc Phosphide QDs

The observed intermediate with a $^{31}P\{^{1}H\}$ NMR peak at −276 ppm was also implicated as the species directly responsible for the formation of QDs in a typical heat-up synthesis. This intermediate was the only molecular species containing phosphorus observed by $^{31}P\{^{1}H\}$ NMR in an aliquot taken 30 seconds post injection from a typical synthesis (Figure 2.12) and no phosphorus

containing molecular species were observed by $^{31}P\{^{1}H\}$ NMR in an aliquot taken after Zn_3P_2 QD formation. These observations indicate the loss of the intermediate observed at −276 ppm by $^{31}P\{^{1}H\}$ NMR directly correlates with the formation of QDs and is not a by-product of the reaction.

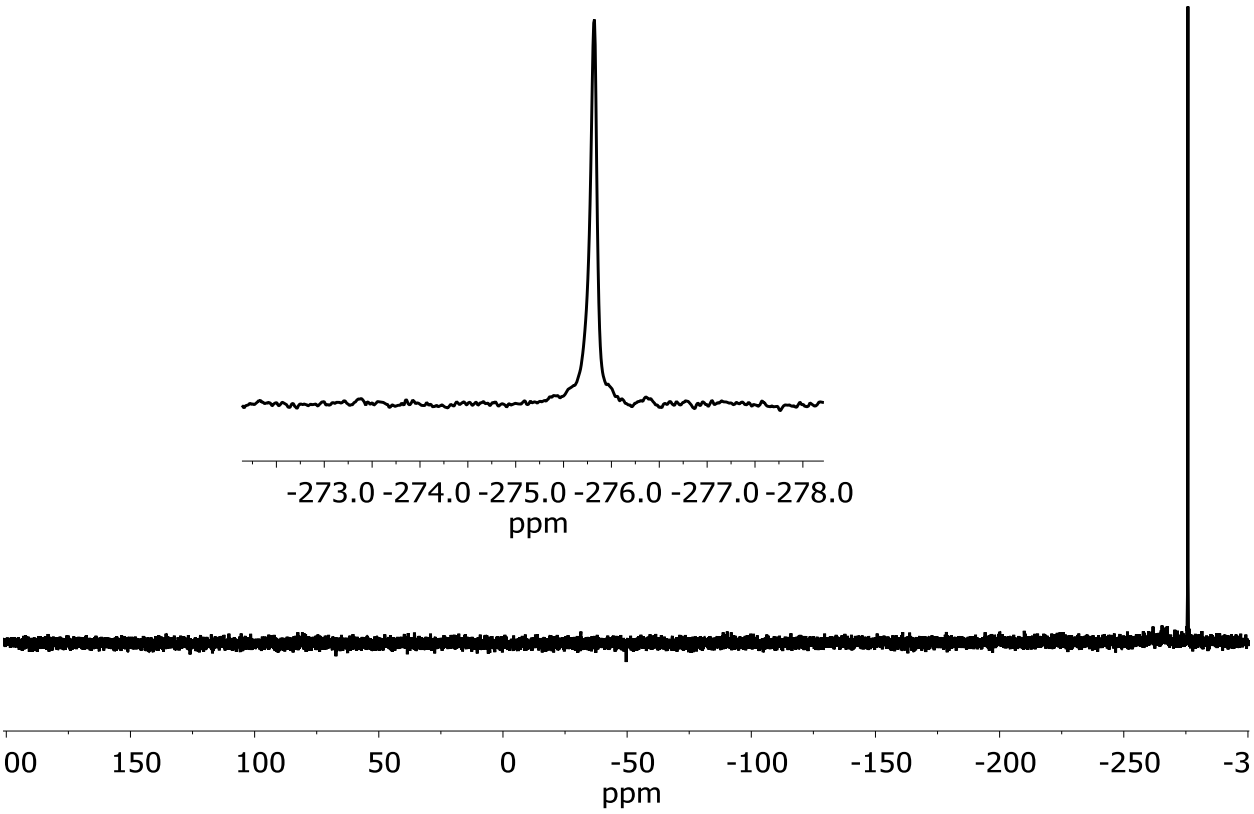

Figure 2.12. $^{31}P\{^{1}H\}$ NMR spectrum of a 30 second aliquot showing that the only molecular species present is the intermediate at –276 ppm. The inset is a close-up of the peak showing it is the only molecular species present.

To further support this hypothesis, a QD synthesis was performed in a J-Young tube to monitor the formation and disappearance of the observed molecular intermediate during QD formation. In this experiment, 3 $Zn(MA)_2$, 1.5 $ZnEt_2$, and 1 $P(SiMe_3)_3$ were mixed in 1-ODE in a J-Young tube and heated up in a sand bath and $^{31}P\{^{1}H\}$ NMR spectra were taken after the NMR

tube had been heated to various temperatures. This series of $^{31}P\{^{1}H\}$ NMR spectra show the growth of the intermediate species at −276 ppm followed by its gradual disappearance, suggesting that this species is active in QD formation and is the only long-lived phosphorous containing molecular precursor observable prior to QD formation (Figure 2.13).

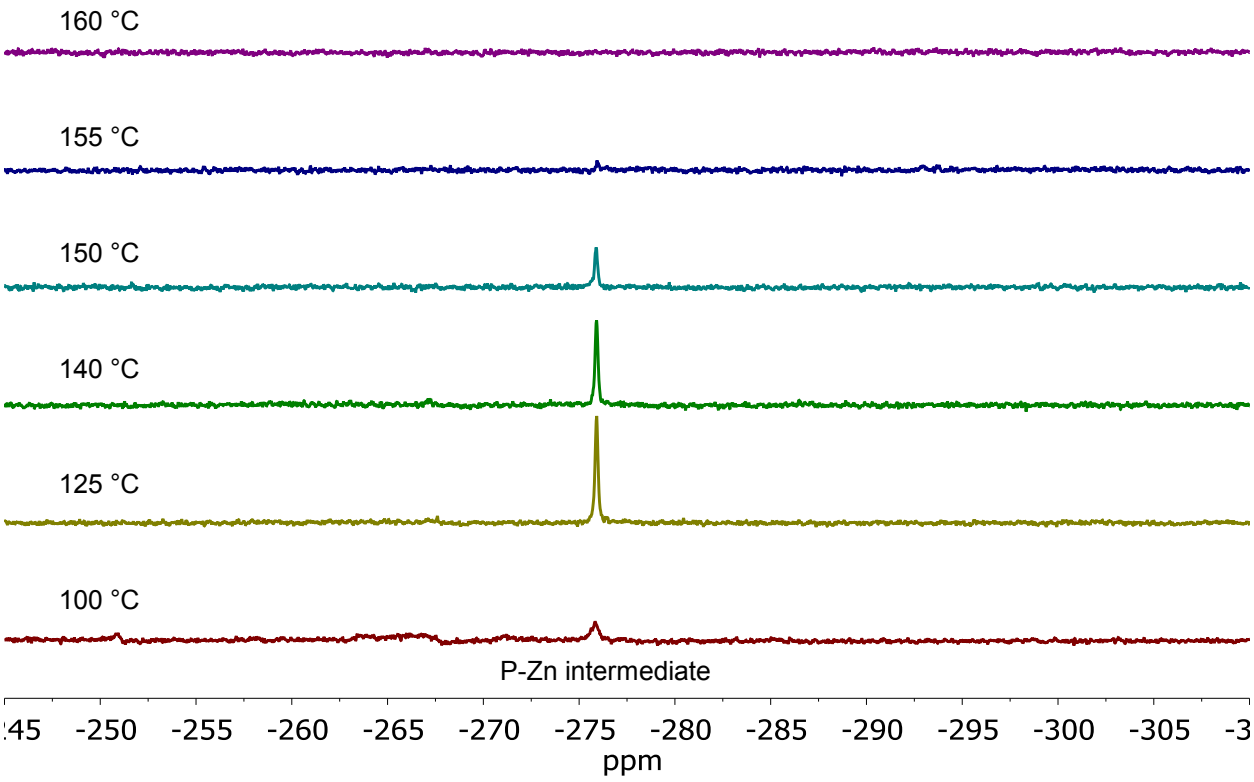

Figure 2.13. $^{31}P\{^{1}H\}$ data for a typical QD reaction performed in a J-Young NMR tube left at the labeled temperatures for 1 minute each.

Further evidence in support of this hypothesis resulted from pre-mixing all three molecular precursors ($Zn(MA)_2$, $ZnEt_2$, and $P(SiMe_3)_3$) in 3 grams of 1-ODE at room temperature until complete conversion to the molecular species with a $^{31}P\{^{1}H\}$ NMR resonance at –276 ppm was observed (8 hours). This solution, containing the pre-formed precursor, was injected into 5 grams

of 1-ODE at 100 °C and heated to 315 °C. The formation of Zn_3P_2 QDs was observed, similar to a typical synthesis in which this species was not purposely pre-formed (Figure 2.14). To corroborate our hypothesis that the pentanuclear zinc cluster (Figure 2C) forms first in a typical synthesis, a QD reaction was performed in which there was a 15 minute delay between injecting $ZnEt_2$ and $P(SiMe_3)_3$ into a $Zn(OA)_2$ solution in 1-ODE in a three neck flask prior to heating up to 315 °C (Figure 2.15). The size and spectroscopic characteristics of the particles formed in this experiment were within error of particles formed when $ZnEt_2$ and $P(SiMe_3)_3$ are introduced simultaneously.

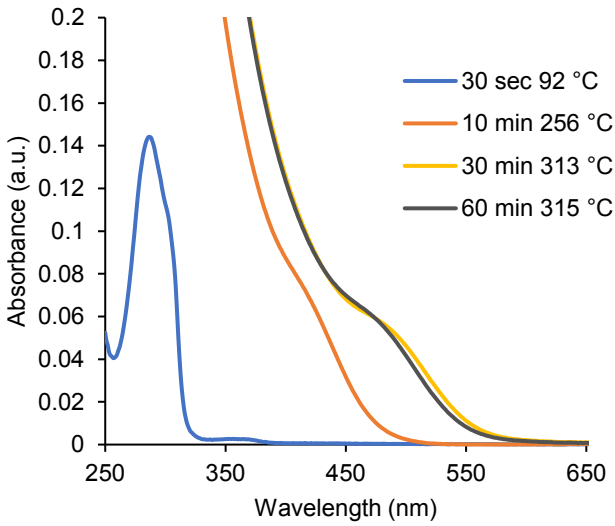

Figure 2.14. UV-Vis spectra of aliquots taken during a reaction where the 3 precursors were premixed in 3 grams of 1-ODE for 8 hours to fully form the molecular intermediate prior to injection into 5 grams of 1-ODE and heated up to 315 °C.

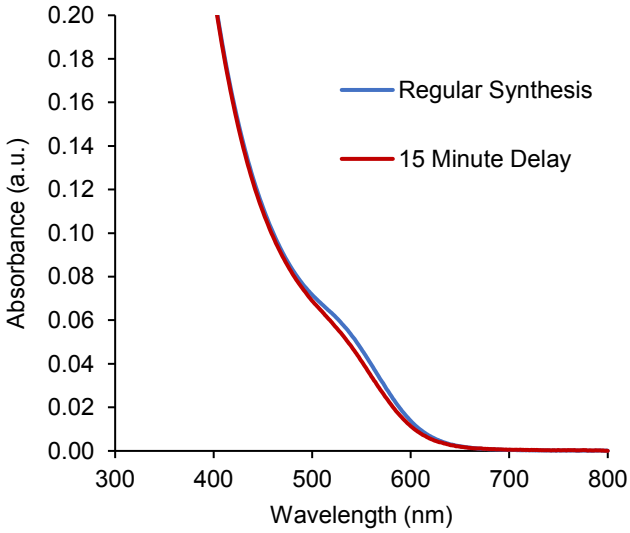

Figure 2.15. UV-Vis data showing there is no difference in adding $P(SiMe_3)_3$ and $ZnEt_2$ simultaneously versus pre-forming the pentanuclear zinc cluster $[Zn_5(O_2CCH_3)_6(Et)_4]$ prior to injecting $P(SiMe_3)_3$.

The results of these experiments are consistent with the postulate that in the ternary synthesis, a pentanuclear zinc cluster is initially formed via reaction of $Zn(O_2CR)_2$ with $ZnEt_2$. The rate of reaction between $[Zn_5(O_2CR)_6(Et)_4]$ with $P(SiMe_3)_3$ is greatly enhanced relative to $ZnEt_2$ or $Zn(O_2CR)_2$ alone, and this reaction leads to formation of the long-lived $(Et_2Zn)P(ZnO_2CR)_2(SiMe_3)$ intermediate with a ^{31}P NMR signal at −276 ppm. This species is the key molecular precursor preceding nucleation and growth of the reported Zn_3P_2 QDs.

2.2.4 Structural Characterization of the Resulting QDs

Transmission electron microscopy (TEM) images were collected to determine the average particle size of the Zn_3P_2 QDs. Quantum dots grown to 315 °C (LEET at 535 nm) had an average

diameter of 2.9 ± 0.6 nm based upon measurements made on 300 individual particles using ImageJ[31] (Figure 2.16, histogram found in Figure 2.17),[32] while quantum dots grown to 255 °C (LEET at 424 nm) had an average diameter of 2.6 ± 0.5 nm (Figure 2.18). QDs grown to the two temperatures had average particle diameters within 0.3 nm, however the energy of the LEET from the UV-vis spectra differed by 0.6 eV, indicative of a high degree of quantum confinement.

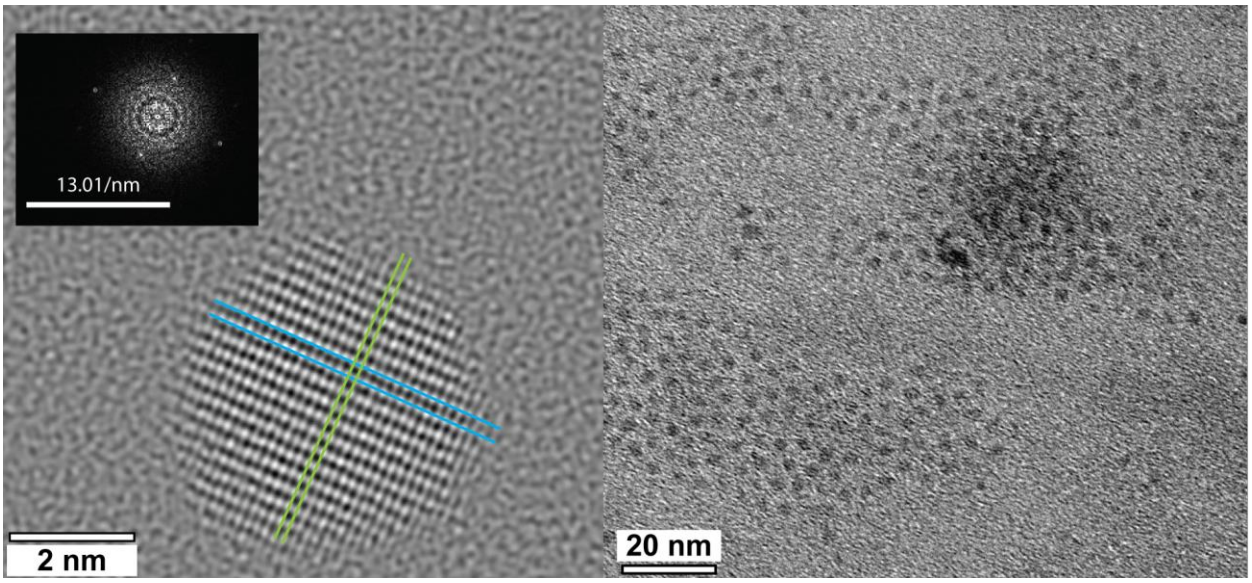

Figure 2.16. (Left) High resolution TEM image of a single zinc phosphide quantum dot with the FFT as an inset and (Right) low resolution TEM image of zinc phosphide quantum dots.

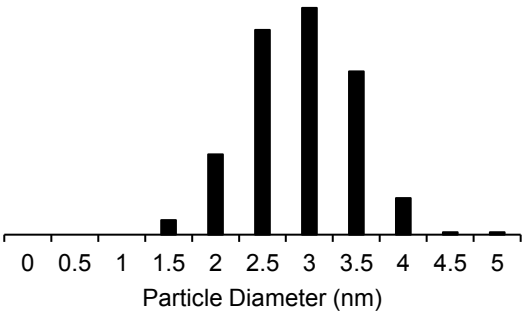

Figure 2.17. Size distribution of particles grown to 315 °C in a synthesis using 0.2 mmol of $P(SiMe_3)_3$, which were found to have an average size of 2.9 ± 0.6 nm. 300 particles were measured.

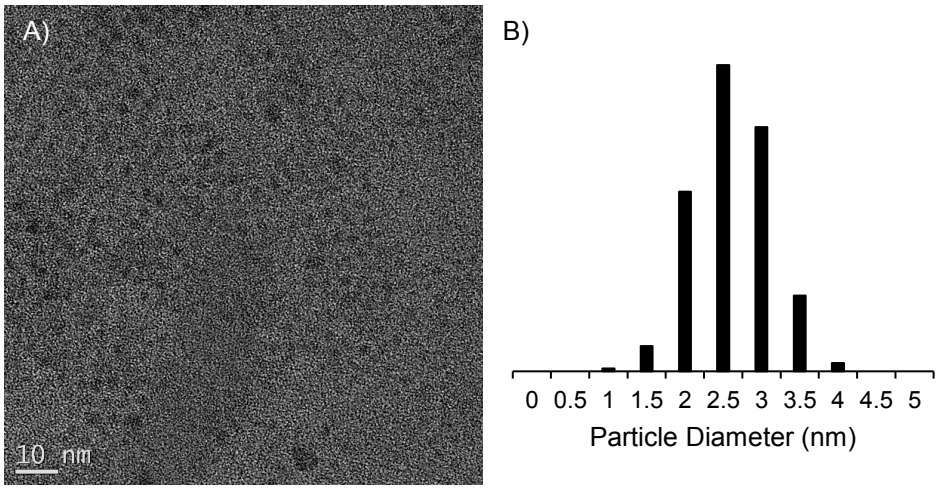

Figure 2.18. (A) TEM and (B) size distribution of particles grown to 255 °C in a synthesis using 0.2 mmol $P(SiMe_3)_3$, which were found to have an average size of 2.6 ± 0.5 nm. 300 particles were measured. The image contrast was increasing in Photoshop.

Calculation of the expected average particle size based on the energy of the LEET using the Brus equation with a range of reported reduced electron and hole masses predict this behavior, with a maximum difference in expected radius of 0.4 nm between the two samples.[33] Using the same range of electron and hole masses, the exciton Bohr radius of Zn_3P_2 was calculated to range between 3 and 7 nm.[34] This is consistent with our assignment of the Zn_3P_2 prepared here as quantum confined semiconductor nanocrystals. Particles formed without $ZnEt_2$ had an average diameter of 2.6 ± 0.5 nm (Figure 2.19), however these particles exhibit no excitonic features in the visible and the sample is likely largely amorphous (*vide infra*). High resolution TEM (HRTEM or phase-contrast TEM) was used to confirm the crystallinity and lattice spacing of QDs grown to 315 °C with all three precursors. FEI TrueImage software was used to reconstruct the exit wavefunction using a series of images taken at different focus points. Analysis of the particle shown in Figure 2.16 (left) showed lattice plane spacings of 2.6 and 1.6 Å which are consistent with the (301) and (051) planes of the tetragonal α-Zn_3P_2 phase, respectively.[35]

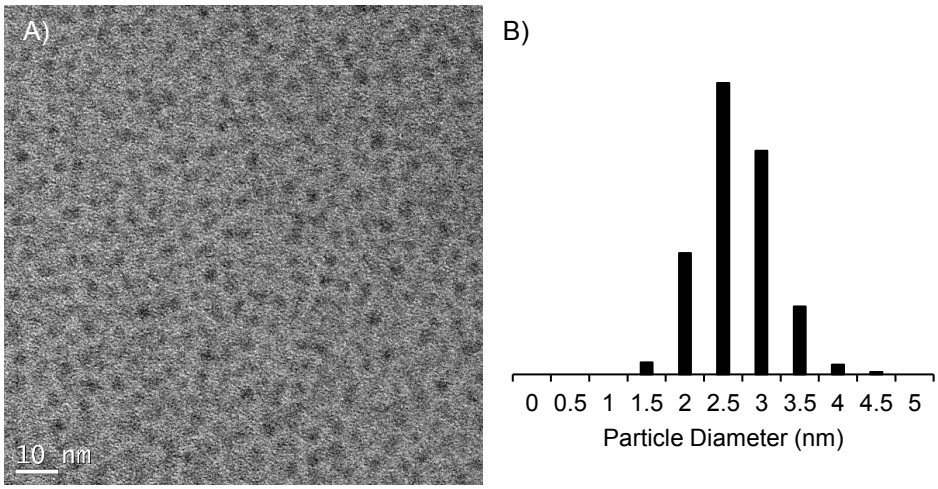

Figure 2.19. TEM and size distribution of particles synthesized with 0.6 mmol $Zn(OA)_2$ and 0.2 mmol $P(SiMe_3)_3$. The average diameter was determined to be 2.6 ± 0.5 nm. 300 particles were measured.

Air-free X-ray diffraction (XRD) was performed by sealing a solid sample of synthesized particles under a Kapton® film. The collected diffraction pattern (Figure 2.20) agrees favorably with the pattern for Zn_3P_2 (tetragonal α-Zn_3P_2; COD 1010287). Upon air oxidization, there is a change in diffraction pattern indicating these particles are air sensitive (Figure 2.21). An air-free pattern of particles synthesized without $ZnEt_2$ shows a very intense peak at 19° 2θ which could be indicative of poor crystallinity (Figure 2.22). Sherrer analysis was performed on the particles grown using all three precursors using both the peaks at 32° and 45° 2θ[36] and yielded an average particle diameter of 1.1 and 2.8 nm, the second of which is consistent with the TEM data (Figure 2.23) for a 0.4 mmol $P(SiMe_3)_3$ reaction.[37-38] The peak at 32° 2θ was analyzed assuming one reflection was the sole cause of the intensity, which may not be the case. Also, given the small particle size, the surface will have a larger impact on lattice strain which would broaden the peak width.

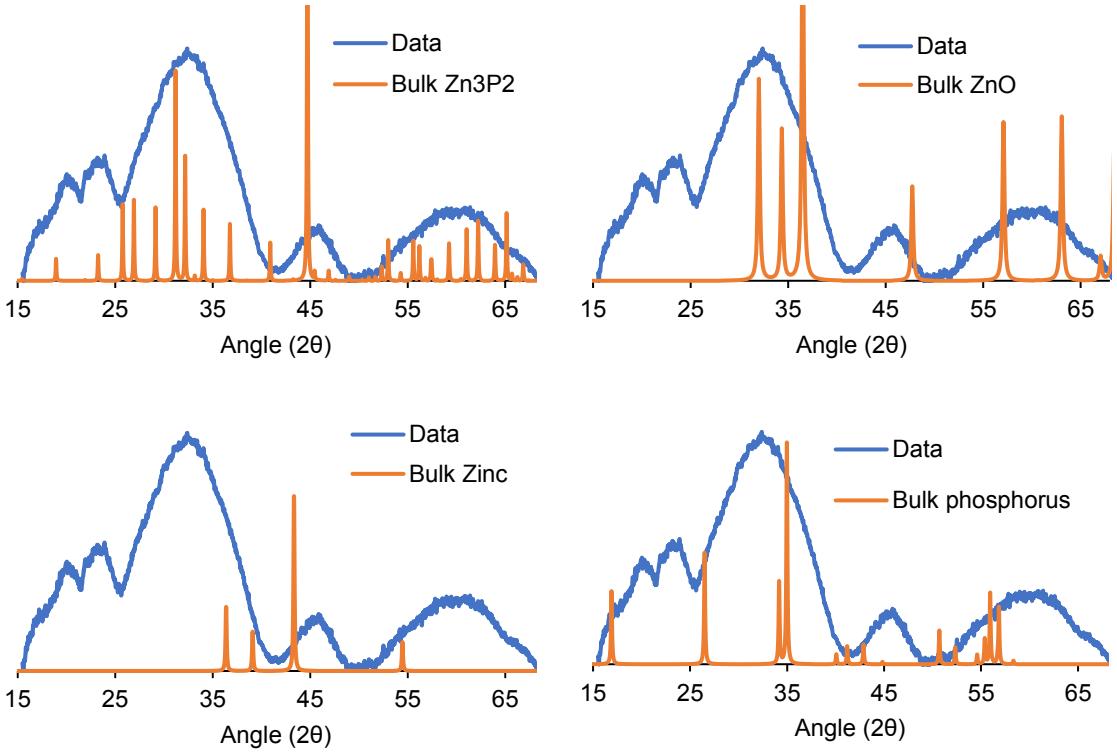

Figure 2.20. Air-free XRD data collected from a dried sample of particles synthesized using 0.4 mmol of $P(SiMe_3)_3$ and sealed under a Kapton film. The data was collected for four hours and the signal from the Kapton film was subtracted off. The data is compared to Zn_3P_2, ZnO, Zn, and P (COD 1010287, 1011258, 9012345, and 4307698).

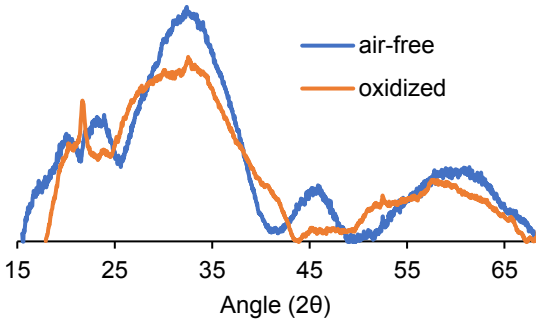

Figure 2.21. Sample used for XRD was left out in air for several weeks and was re-analyzed showing air oxidization had occurred.

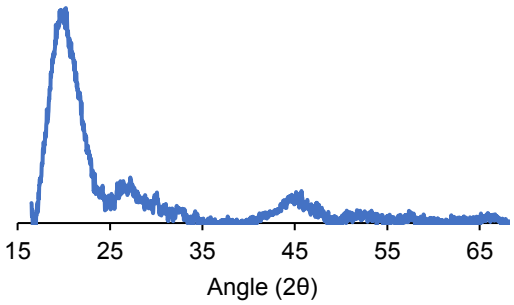

Figure 2.22. Air-free XRD of particles synthesized with 0.6 mmol $Zn(OA)_2$ and 0.2 mmol $P(SiMe_3)_3$.

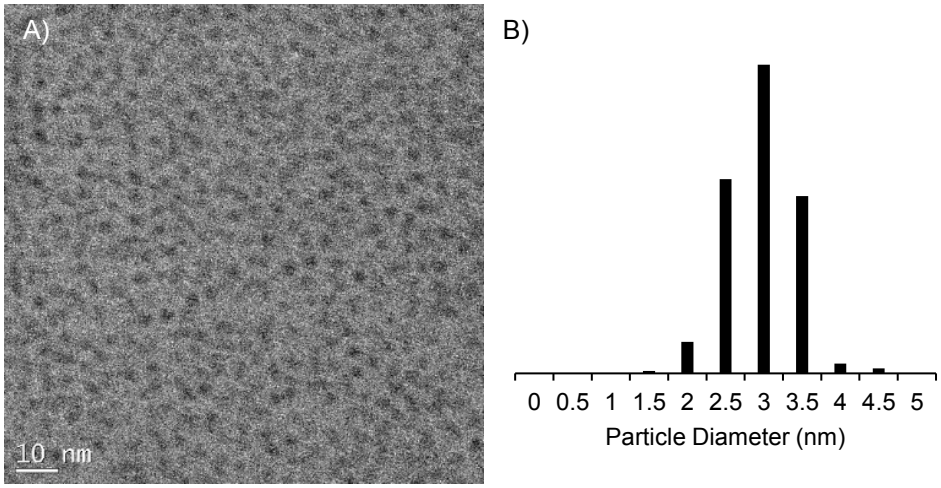

Figure 2.23. (A) TEM and (B) size distribution of particles grown to 315 ˚C in a synthesis using 0.4 mmol $P(SiMe_3)_3$, which were found to have an average size of 3.0 ± 0.5 nm. 300 particles were measured.

Due to the similarity in the solubility of the zinc phosphide QDs and zinc myristate, particles synthesized with this zinc reagent could not be separated from excess zinc myristate. Zinc phosphide QDs were therefore prepared using more soluble zinc oleate for complete excess ligand removal. ^{1}H NMR data confirmed clean isolation of zinc-rich particles capped only by oleate ligands (Figure 2.24). Particles grown to 255 °C had a zinc to phosphorus ratio of 7.6:2 and

particles grown to 315 °C had a zinc to phosphorus ratio of 5:2 as determined by inductively coupled plasma atomic emission spectroscopy (ICP-OES). Thermogravimetric analysis (TGA) was performed under nitrogen on particles grown to 315 °C, showing a single weight loss transition centered near 400 °C. Following TGA, 46% inorganic mass remained, consistent with a $Zn(O_2CR)_2$-capped zinc phosphide formulation with less than a mono-layer of zinc oxide included at the surface (Figure 2.25, see Appendix A for particle model).

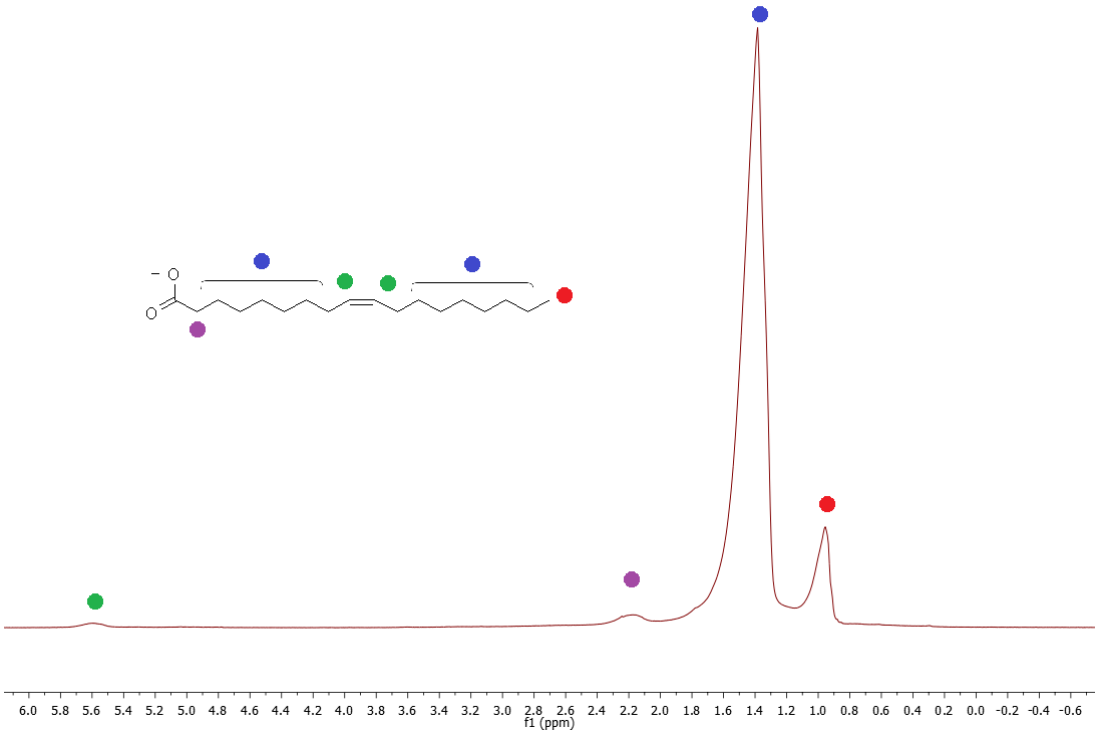

Figure 2.24. ^{1}H NMR taken on a 300 MHz spectrometer in C_6D_6 of worked up QDs showing only oleate ligands.

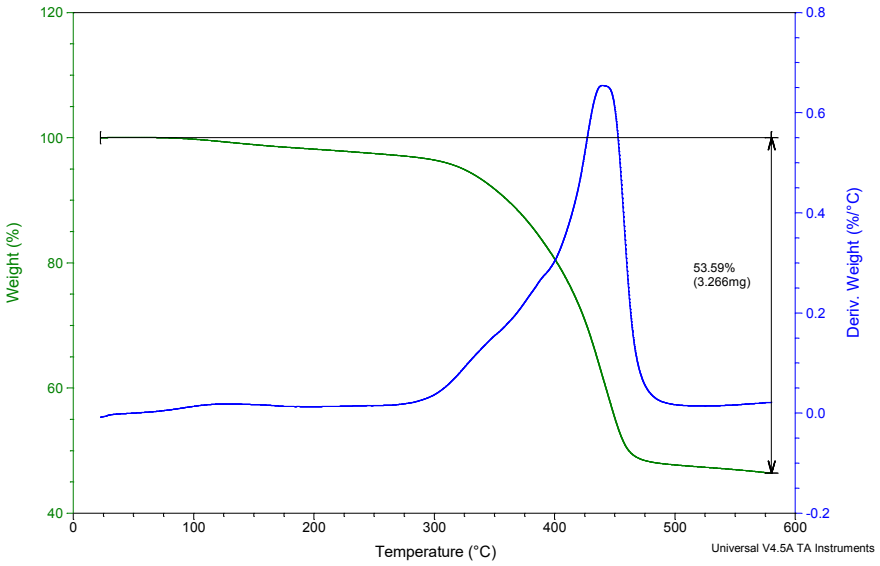

Figure 2.25. TGA data and derivative of zinc phosphide particles synthesized with zinc oleate and grown at 315 ˚C using a ramp rate of 10 °C/min.

2.2.5 Photoresponse Measurements of Particle Films

In order to assess the potential of these particles for photovoltaic applications, their photoresponse was measured. A film of particles was electrodeposited onto a conductive mesoporous *nano*ITO substrate[39] using electrophoretic deposition at 45 V from a toluene/acetonitrile solution of QDs under argon, followed by a one hour anneal under vacuum at 350 °C (Figure 2.26). Controlled potential electrolysis was performed under chopped white light (Figure 2.27) and showed a 100 nA current increase with light irradiation indicating the possibility of using these particles as visible light absorbers.[32]

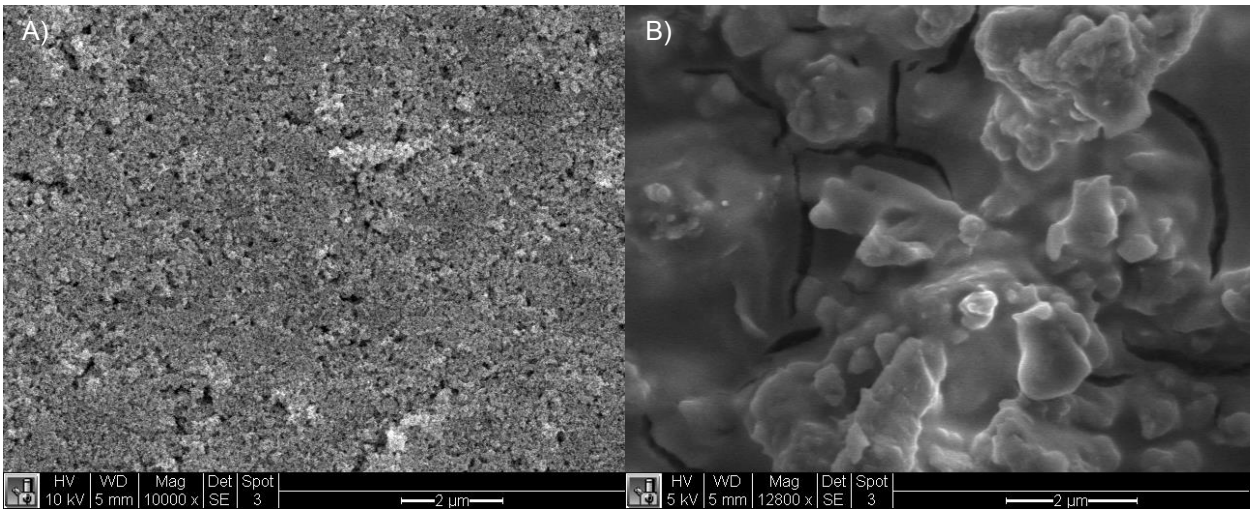

Figure 2.26. SEM images of the (A) bare *nano*ITO substrate and (B) the film of annealed electrodeposited particles on the *nano*ITO substrate.

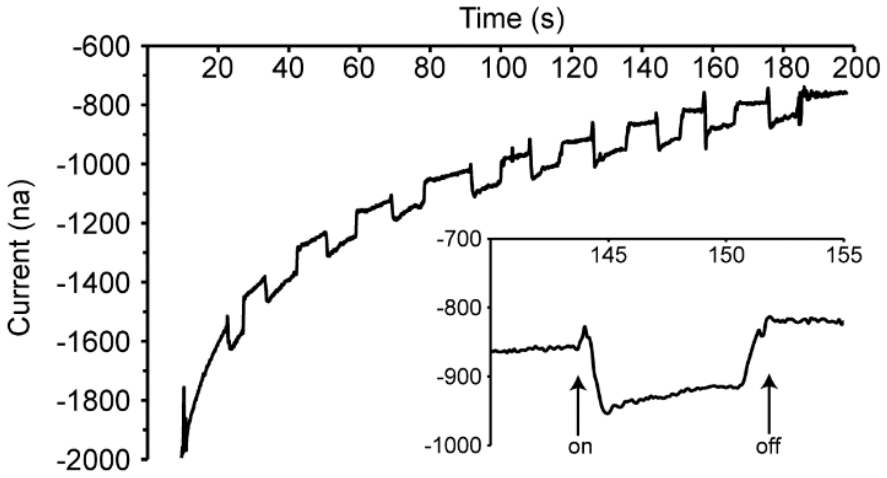

Figure 2.27. Controlled potential electrolysis of Zn_3P_2 nanocrystals on *nano*ITO under chopped white light illumination.

2.3 Conclusion

In conclusion, this work describes a novel three precursor synthesis of colloidal crystalline Zn_3P_2 quantum dots that have clear excitonic absorbance features ranging from 424 to 535 nm, depending on the final growth temperature. NMR experiments revealed a critical molecular transformation that only occurs when $ZnEt_2$, $Zn(O_2CR)_2$, and $P(SiMe_3)_3$ are all present. The observed $(Et_2Zn)P(ZnO_2CR)_2(SiMe_3)$ intermediate was conclusively shown to be a direct precursor to the crystalline zinc phosphide quantum dots obtained in this study. TEM, ICP-OES, TGA, NMR, and XRD experiments showed that the resulting particles were crystalline and confirmed their identity as zinc-rich zinc phosphide QDs that ranged from 2.6 to 2.9 nm in diameter. In contrast to the synthesis of Zn_3P_2 QDs recently reported by Buriak and co-workers which yields 15 ± 2 nm particles from a combination of $ZnMe_2$ and $P(SiMe_3)_3$ with no strongly passivating ligands present, our synthesis yields relatively monodisperse colloidal solutions of small size nanocrystals as a result of carboxylate ligand passivation.[20] The stark contrast between the nanocrystal sizes reported here and by Buriak highlights the critical role of precursor reactivity and ligand binding strength on final particle size, and suggests a strategy for achieving nanocrystals of intermediate size.[40] Initial photoresponse measurements demonstrated the possibility of using these particles as visible light absorbers.

2.4 Experimental

2.4.1 General Considerations

Sodium (dry stick, ACS reagent), potassium (in mineral oil, 98%), red phosphorus (99.999%), myristic acid (≥99), Rhodamine 6G, tetrabutylammonium hexafluorophosphate (for electrochemical analysis, ≥99%), and hexanes (a mixture of isomers, CHROMASOLV) were purchased from Sigma-Aldrich Chemical Company and used without further purification. Omni Trace nitric acid was purchased from EMD Millipore and used without further purification. 18.2 MΩ water was collected from an EMD Millipore water purification system. Acetonitrile was purchased from Burdick and Jackson® (<5ppm low-water brand) and stored in an argon pressurized stainless steel drum plumbed directly into a glove-box. Celite 545 and zinc acetate (99.99%) were purchased from Sigma-Aldrich Chemical Company and heated at 150 °C under vacuum overnight and stored in a nitrogen filled inert glove box prior to use. Oleic acid (90%) was purchased from Sigma-Aldrich Chemical Company and stirred over sieves overnight prior to being freeze-pump-thawed three times and stored in a nitrogen filled inert glove box prior to use. $ZnEt_2$ (95%) was purchased from Strem Chemicals and stored in a -35 °C freezer in a nitrogen filled inert atmosphere glove box. All solvents, including 1-octadecene (≥95%), 1,2-dimethoxyethane (99%), and pentane were purchased from Sigma-Aldrich Chemical Company, dried by stirring overnight with CaH_2, distilled, and stored over 4 Å molecular sieves. C_6D_6 and was purchased from Cambridge Isotope Labs and was similarly dried and stored. ^1H (Field: 300 MHz) and $^{31}P\{H\}$ (Field: 121 MHz) NMR spectra were collected on a 300 MHz Bruker Avance spectrometer. UV-Vis spectra were collected on a Cary 5000 spectrophotometer from Agilent. Fluorescence

measurements were taken on a Horiba FL3-21tau Fluorescence Spectrophotometer. Powder XRD spectra were collected on a Bruker D8 Discover with GADDS 2-D XRD system. ICP-OES was performed using a Perkin Elmer Optima 8300. TEM images were collected on an FEI Tecnai G2 F20 microscope. TEM analysis was performed using manual analysis with the help of the ImageJ software package.[41] HRTEM analysis was performed using the Fei True Image software package. TGA data was collected on a TA Instruments TGA. SEM images were collected on a FEI Sirion SEM. $P(SiMe_3)_3$ was prepared following a literature procedure.[42]

2.4.2 Synthesis of $Zn(O_2C(CH_2)_{12}CH_3)_2$

8.78 grams (38.4 mmol) of myristic acid was added to a 250 mL Schlenk flask and transferred into a nitrogen filled glove box. 100 to 150 mL of pentane was added to the flask to dissolve the acid. The flask was sealed with a septum and was transferred onto a Schlenk line. In the nitrogen filled glove box, 2.25 grams (18.2 mmol) of diethyl zinc was weighed out and mixed with 2 milliliters of pentane and drawn into a syringe outfitted with a needle. The needle was then capped with a septum. *Warning, the next step is very dangerous and should be performed under supervision with extreme care.* The diethyl zinc solution was added drop-wise slowly to the myristic acid solution in an ice bath and under nitrogen. After addition, the solution was removed from the ice bath and left to stir overnight. The solution was transferred into a nitrogen filled glove box and the white solid was collected in a frit. The white solid was washed with copious amounts of pentane to remove any excess myristic acid prior to being dried. The yield was 8.78 grams. The average percent yield was 88% (average of two runs).

2.4.3 Synthesis of $Zn(O_2C(CH_2)_7HC=CH(CH_2)_7CH_3)_2$

8.99 grams (31.8 mmol) of oleic acid was added to a 250 mL Schlenk flask in a nitrogen filled glove box. 100 to 150 mL of pentane was added to the flask. This open port was sealed with a septum. This flask was transferred onto a Schlenk line. In the nitrogen filled glove box, 2.17 grams (17.6 mmol) of diethyl zinc was weighed out and mixed with 10 milliliters of pentane and drawn into a syringe outfitted with a needle. The needle was then capped with a septum. *Warning, the next step is very dangerous and should be performed under supervision with extreme care.* The diethyl zinc solution was added drop-wise slowly to the oleic acid solution over ice and under nitrogen. After addition, the solution was removed from the ice bath and left to stir overnight. The solution was transferred into a nitrogen filled glove box and the white solid was collected in a frit. The white solid was washed with copious amounts of pentane to remove any excess oleic acid prior to being dried. The yield was 7.89 grams. The average percent yield was 80% (average of two runs).

2.4.4 Synthesis of Zinc Phosphide Quantum Dots

0.312 grams (0.6 mmol) of $Zn(MA)_2$ is dispersed in 5 grams of 1-octadecene in a nitrogen filled glove box and pulled into a syringe and stoppered with a septum. The slurry was injected into a 25 mL 3-neck flask outfitted with a reflux condenser, septum, and thermowell under nitrogen. A temperature controller with a probe inside the thermowell was used to control the temperature. The flask was degassed overnight at 100 ºC under vacuum. The flask was put under nitrogen and heated to 101 ºC. In a nitrogen filled glove box, 30.75 µL (0.3 mmol) of diethyl zinc

and 58 μL (0.2 mmol) of $P(SiMe_3)_3$ were added to 3 grams of 1-octadecene and drawn into a syringe and its needle was capped with a septum. In the reaction where there is a delay in $P(SiMe_3)_3$ addition, both reagents were injected into the zinc carboxylate solution in 1.5 grams 1-ODE. The heating was turned off. At 100.2 ºC the temperature controller was turned on to its highest volume setting (>2L) and set at 315 ºC. At 100.0 ºC, the zinc/phosphorus solution was rapidly injected into the flask. The solution was allowed to heat up and run for 60 minutes. Aliquots of 50 μL were taken out and injected into 6 mL of hexanes for UV-Vis monitoring. Alternatively, the desired amount of zinc myristate can be made by degassing the desired amount of myristic acid and injecting diethyl zinc into the flask to provide $Zn(MA)_2$ *in situ*. Additionally, analogous particles can be made with zinc oleate by weighing out the same mmol of zinc oleate into a reaction flask prior to putting the reaction vessel under nitrogen on a Schlenk line. 74.5 mg of particles were collected after work-up when using 0.6 mmol of zinc oleate. Using the TGA model of the mass % coming from the zinc phosphide core (28.46%) the 74.5 mg of particles is an 82% yield.

2.4.5 Zinc Phosphide Quantum Dot Work-up Procedure

All work up was done under nitrogen using dry solvents. To halt particle formation, the reaction flask was removed from the heating mantle and placed in a RT oil bath. The reaction mixture was cannula transferred to a 25 mL Schlenk flask and the solvent was distilled off. The flask was brought into a nitrogen filled glove box and the QDs were dissolved in pentane. The solution was centrifuged to remove any insoluble byproducts. To the pentane solution 15 mL of ethyl acetate and 7 mL of acetonitrile were added to crash out the dots. The heterogeneous solution was centrifuged and the solution was decanted off. This was repeated until mostly solid was

collecting at the bottom (usually 3 to 4 iterations). Next, toluene was used to dissolve the particles and they were crashed out with minimal acetonitrile. This was repeated once or twice. The clean particles could be stored in either pentane or toluene.

2.4.6 NMR Experiments

In a nitrogen filled glove box, 0.0795 grams (0.15 mmol) of $Zn(MA)_2$ was added to a J-Young NMR tube. C_6D_6 was added to the solid. The NMR tube was put in a freezer overnight. While the solvent was still frozen, 14.5 μL (0.05 mmol) of $P(SiMe_3)_3$ was added via syringe. This was put back in the freezer. Next, 7.75 μL (0.075 mmol) of $ZnEt_2$ was added and the tube was sealed. The $^{31}P\{H\}$ NMR data was monitored on a 121 MHz spectrometer taking 256 scans with one minute of shaking in between spectra. This was also performed with 0.0275 (0.15 mmol) grams of $Zn(O_2CCH_3)_2$ instead of $Zn(MA)_2$. For this reaction, $ZnEt_2$ and $P(SiMe_3)_3$ were pre-mixed with C_6D_6. For the monitoring reactions, an internal standard of PPh_3 in Dowtherm® or C_6D_6 within a sealed capillary was used for referencing. If not, the phosphorus spectra were externally calibrated with a H_3PO_4 solution.

2.4.7 Photoresponse Measurements

A FTO coated glass slide (5 × 1 cm) with *nano*ITO deposited on one end (1.5 × 1 cm) was used as a conductive substrate.[39] Electrophoretic deposition was used to deposit oleate capped particles onto the *nano*ITO. Particles were in a toluene/acetonitrile solution. The desired substrate was situated roughly 1 cm from a counter *nano*ITO electrode. A 45 V potential was applied across

the two electrodes with a DC power source and was held for roughly 5 minutes. The film was annealed at 350 ºC for one hour under vacuum. Chopped light controlled potential electrolysis was performed using a BASi Epsilon EC potentiostat. A 3-electrode set-up was used with the quantum dot film was the working electrode, a platinum wire was the auxiliary electrode, and a silver wire was used as the reference electrode. A 0 V bias versus the silver wire was maintained. A 0.1M tetrabutylammonium hexafluorophosphate acetonitrile solution was used as the electrolyte. A white light source was used as the chopped light source. The light was manually blocked and unblocked for ten second increments.

2.4.8 Sample Preparation for Characterization

TEM: A 50/50 solution by volume of pentane and toluene was used as the solvent. A few drops of the QD solution was added to this. The TEM grid (Ultrathin carbon on holey carbon support film, 400 mesh Ted Pella; Graphene support on Lacey Carbon, 300 mesh Ted Pella; Ultra-thin carbon with removable Formvar, 400 mesh Ted Pella) was suspended and 1-2 drops was added and left to dry. The grid was put under vacuum overnight to remove any residual solvent. XRD: Particles were worked-up and dried into a paste. This paste was placed on the center of a silicon <100> single crystal wafer. A syringe was used to draw a square of Apiezon H grease around the sample and a piece of Kapton film was placed down and sealed with the grease. ICP-OES: A small pipette tip of worked up particle solution was crashed out. The solvent was removed. Enough concentrated high purity nitric acid was added to dissolve the particles so the final solution could be diluted with 18.2 MΩ water in a volumetric flask. TGA: worked-up particles were dried

overnight and brought to the instrument room under nitrogen and scraped onto a TGA platinum boat.

2.4.9 Sample Calculation Using the Brus Equation[33]

$$E^* = E_{bulk} + \frac{\hbar^2\pi^2}{2R^2} \times \left(\frac{1}{m_e^*} + \frac{1}{m_h^*}\right) - \frac{1.8e^2}{4\pi\varepsilon_r\varepsilon_0 R}$$

Where E^* is the LEET, E_{bulk} is the band gap of the bulk semiconductor, R is the radius of the particle, m_e^* and m_h^* are the reduced electron and hole masses, e is the charge of an electron, ε_r is the dielectric of the bulk semiconductor, and ε_0 is the permittivity of free space.

$$3.833\times10^{-19} = 2.403\times10^{-19} + \frac{\hbar^2\pi^2}{2R^2} \times \left(\frac{1}{0.2\times9.109\times10^{-31}} + \frac{1}{0.22\times9.109\times10^{-31}}\right) - \frac{1.8e^2}{4\pi(11)\varepsilon_0 R}$$

Mathematica was used to solve for R.

$$R = 1.905\ nm$$
$$D = 3.81\ nm$$

Table 2.1. Summary of Brus analysis results.

m_e^*	m_h^*	255ºC particle diameter (nm)	315ºC particle diameter (nm)
0.128[43]	0.255[44]	3.4	4.2
0.2[45]	0.22[45]	3.0	3.8
0.35[46]	0.45[46]	2.1	2.7
0.2[45]	0.45[46]	2.6	3.2
0.35[46]	0.22[45]	2.6	3.3

2.4.10 Sample Exciton Bohr Radius Calculation[34]

$$a_{ex} = a_H \times \varepsilon_r \times \frac{m_0}{\mu}$$

Where a_H is the Bohr radius is 5.2819*10^{-11} meters, ε_r is the bulk dielectric constant (11), m_0 is the mass of an electron, and μ is:

$$\mu = \frac{1}{m_e^{-1} + m_h^{-1}}$$

Where m_e and m_h are the reduced electron and hole masses.

$$\mu = \frac{1}{\frac{1}{0.128m_0} + \frac{1}{0.255m_0}} = 7.763\times10^{-32}\ kg$$

$$a_H = (5.2819\times10^{-11})\times(11)\times\frac{9.109\times10^{-31}\ kg}{7.763\times10^{-32}\ kg} = 6.84\times10^{-9}\ m = 6.84\ nm$$

Table 2.2. Summary of exciton Bohr radii.

m_e^*	m_h^*	Exciton Bohr radius (nm)
0.128[43]	0.255[44]	6.84
0.2[45]	0.22[45]	5.56
0.35[46]	0.45[46]	2.96
0.2[45]	0.45[46]	4.21
0.35[46]	0.22[45]	4.32

2.4.11 Sample Calculation Using the Scherrer Equation[38]

$$L = \frac{0.9\lambda}{\Delta(2\theta)\cos(\theta_0)}$$

$$D = \frac{4}{3}L$$

Where L is Scherrer or coherence length, λ is the wavelength of the x-ray radiation (0.15418 nm), $\Delta(2\theta)$ is the full-width at half-maximum in radians, θ_0 is the angle of reflection of the peak in radians, and D is the sphere diameter in nm.

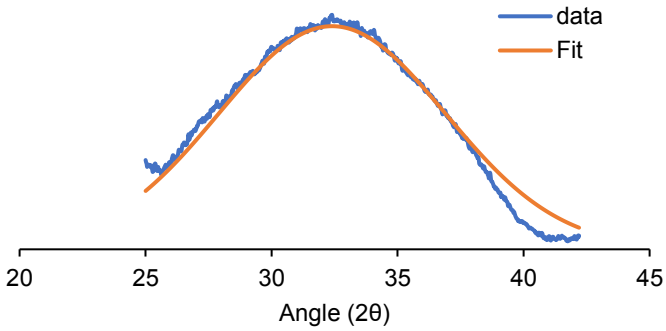

Figure 2.28. 34 degrees (2 Theta) Gaussian fit.

Reflection Angle (radians): 0.283

Δ2θ (radians): 0.18[47]

$$L = \frac{0.9 \times 0.15418}{0.18 \times \cos(0.283)} = 0.80\ nm$$

$$D = \frac{4}{3} \times 0.80\ nm = 1.1\ nm$$

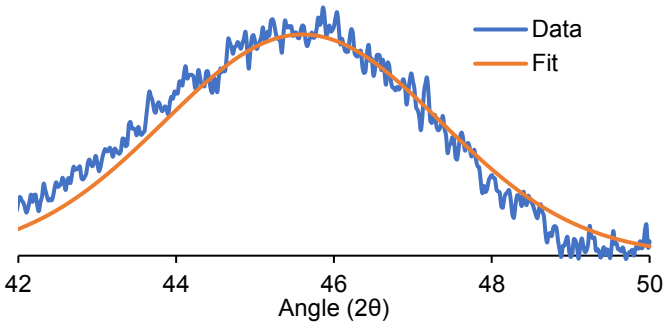

Figure 2.29. 45 degrees (2 Theta) Gaussian fit.

Reflection Angle (radians): 0.397

Δ2θ (radians): 0.07[47]

$$L = \frac{0.9 \times 0.15418}{0.07 \times \cos(0.397)} = 2.09\ nm$$

$$D = \frac{4}{3} \times 2.09\ nm = 2.8\ nm$$

2.4.12 Manually Measuring Particle Diameters

1. Opened TEM image in ImageJ.
2. Set the scale appropriately.
3. Zoomed in on the particles.
4. Used the line tool to draw a line across the particle and measure it.

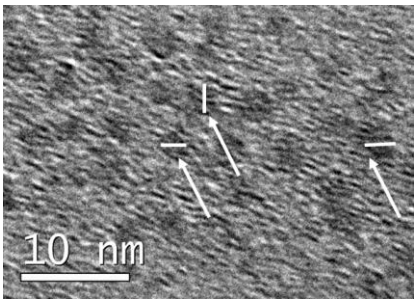

5. Measured 300 unique particles from pictures taken at various magnifications and from different spots on a grid to ensure proper sampling of the particles.

2.5 References

1. Lunt, R. R.; Osedach, T. P.; Brown, P. R.; Rowehl, J. A.; Bulović, V., Practical Roadmap and Limits to Nanostructured Photovoltaics. *Adv. Mater.* **2011,** *23*, 5712-5727.
2. Curtright, A. E.; Morgan, M. G.; Keith, D. W., Expert Assessments of Future Photovoltaic Technologies. *Environ. Sci. Technol.* **2008,** *42*, 9031-9038.
3. Wadia, C.; Alivisatos, A. P.; Kammen, D. M., Materials Availability Expands the Opportunity for Large-Scale Photovoltaics Deployment. *Environ. Sci. Technol.* **2009,** *43*, 2072-2077.
4. Fagen, E. A., Optical properties of Zn3P2. *J. Appl. Phys.* **1979,** *50*, 6505-6515.
5. Bosco, J. P.; Demers, S. B.; Kimball, G. M.; Lewis, N. S.; Atwater, H. A., Band alignment of epitaxial ZnS/Zn3P2 heterojunctions. *J. Appl. Phys.* **2012,** *112*, 093703.
6. Wyeth, N. C.; Catalano, A., Spectral response measurements of minority-carrier diffusion length in Zn3P2. *J. Appl. Phys.* **1979,** *50*, 1403-1407.

7. Suda, T.; Kakishita, K., Epitaxial growth of zinc phosphide. *J. Appl. Phys.* **1992,** *71*, 3039-3041.

8. Bhushan, M.; Catalano, A., Polycrystalline Zn3P2 Schottky barrier solar cells. *Appl. Phys. Lett.* **1981,** *38*, 39-41.

9. Nayar, P. S.; Catalano, A., Zinc phosphide-zinc oxide heterojunction solar cells. *Appl. Phys. Lett.* **1981,** *39*, 105-107.

10. Kimball, G. M.; Lewis, N. S.; Atwater, H. A. In *Mg doping and alloying in Zn3P2 heterojunction solar cells*, Photovoltaic Specialists Conference (PVSC), 2010 35th IEEE, 20-25 June 2010; 2010; pp 001039-001043.

11. Yang, R.; Chueh, Y.-L.; Morber, J. R.; Snyder, R.; Chou, L.-J.; Wang, Z. L., Single-Crystalline Branched Zinc Phosphide Nanostructures: Synthesis, Properties, and Optoelectronic Devices. *Nano Lett.* **2006,** *7*, 269-275.

12. Murray, C. B.; Norris, D. J.; Bawendi, M. G., Synthesis and characterization of nearly monodisperse CdE (E = sulfur, selenium, tellurium) semiconductor nanocrystallites. *J. Am. Chem. Soc.* **1993,** *115*, 8706-8715.

13. Li, L.; Protière, M.; Reiss, P., Economic Synthesis of High Quality InP Nanocrystals Using Calcium Phosphide as the Phosphorus Precursor. *Chem. Mater.* **2008,** *20*, 2621-2623.

14. Weller, H.; Fojtik, A.; Henglein, A., Photochemistry of semiconductor colloids: Properties of extremely small particles of Cd3P2 and Zn3P2. *Chem. Phys. Lett.* **1985,** *117*, 485-488.

15. Buhro, W. E., Metallo-organic routes to phosphide semiconductors. *Polyhedron* **1994,** *13*, 1131-1148.

16. Green, M.; O'Brien, P., A Novel Metalorganic Route to Nanocrystallites of Zinc Phosphide. *Chem. Mater.* **2001,** *13*, 4500-4505.

17. Carenco, S.; Demange, M.; Shi, J.; Boissiere, C.; Sanchez, C.; Le Floch, P.; Mezailles, N., White phosphorus and metal nanoparticles: a versatile route to metal phosphide nanoparticles. *Chem. Commun.* **2010,** *46*, 5578-5580.

18. Miao, S.; Yang, T.; Hickey, S. G.; Lesnyak, V.; Rellinghaus, B.; Xu, J.; Eychmüller, A., Emissive ZnO@Zn3P2 Nanocrystals: Synthesis, Optical, and Optoelectrochemical Properties. *Small* **2013,** *9*, 3415-3422.

19. Luber, E. J.; Mobarok, M. H.; Buriak, J. M., Solution-Processed Zinc Phosphide (α-Zn3P2) Colloidal Semiconducting Nanocrystals for Thin Film Photovoltaic Applications. *ACS Nano* **2013,** *7*, 8136-8146.

20. Mobarok, M. H.; Luber, E. J.; Bernard, G. M.; Peng, L.; Wasylishen, R. E.; Buriak, J. M., Phase-Pure Crystalline Zinc Phosphide Nanoparticles: Synthetic Approaches and Characterization. *Chem. Mater.* **2014,** *26*, 1925-1935.

21. Heath, J. R.; Shiang, J. J., Covalency in semiconductor quantum dots. *Chem. Soc. Rev.* **1998,** *27*, 65-71.

22. Westerhausen, M.; Sapelza, G.; Zabel, M.; Pfitzner, A., (EtZn)4Zn2(PSitBu3)4: a Homometallic Phosphanediide of Zinc with a novel Zn6P4 Cage. *Z. Naturforsch. B* **2004,** *59*, 1548-1550.

23. LEET is determined by fitting the spectra and taking the second-derivative to locate the local minima.

24. Battaglia, D.; Peng, X., Formation of High Quality InP and InAs Nanocrystals in a Noncoordinating Solvent. *Nano Lett.* **2002,** *2*, 1027-1030.

25. Wang, R.; Ratcliffe, C. I.; Wu, X.; Voznyy, O.; Tao, Y.; Yu, K., Magic-Sized Cd3P2 II−V Nanoparticles Exhibiting Bandgap Photoemission. *J. Phys. Chem. C* **2009,** *113*, 17979-17982.

26. LaMer, V. K.; Dinegar, R. H., Theory, Production and Mechanism of Formation of Monodispersed Hydrosols. *J. Am. Chem. Soc.* **1950,** *72*, 4847-4854.

27. Kwon, S. G.; Hyeon, T., Formation Mechanisms of Uniform Nanocrystals via Hot-Injection and Heat-Up Methods. *Small* **2011,** *7*, 2685-2702.

28. Orchard, K. L.; White, A. J. P.; Shaffer, M. S. P.; Williams, C. K., Pentanuclear Complexes for a Series of Alkylzinc Carboxylates. *Organometallics* **2009,** *28*, 5828-5832.

29. Fuhr, O.; Fenske, D., Die ungewöhnliche Umwandlung von P(SnMe3)3 in P4(SnMe2)6. *Z. Anorg. Allg. Chem.* **2004,** *630*, 244-246.

30. Sapelza, G.; Mayer, P.; Westerhausen, M., Synthesis and Characterization of Methylzinc Tri(tert-butyl)silylphosphanide as well as Related Sodium and Potassium Phosphanylzincates. *Z. Anorg. Allg. Chem.* **2005,** *631*, 3087-3091.

31. Schneider, C. A.; Rasband, W. S.; Eliceiri, K. W., NIH Image to ImageJ: 25 years of image analysis. *Nat. Methods* **2012,** *9*, 671-675.

32. See section 2.4 for details.

33. Reid, P. J.; Fujimoto, B.; Gamelin, D. R., A Simple ZnO Nanocrystal Synthesis Illustrating Three-Dimensional Quantum Confinement. *J. Chem. Educ.* **2013,** *91*, 280-282.

34. Kuno, M., *Introductory Nanoscience: Physical and Chemical Concepts*. Garland Science: Taylor & Francis Group: New York, NY, 2012.

35. This larger than average particle gave the most detail during imaging.

36. The discrepancy in expected versus observed peak intensity for the 45 2θ reflection may be the result of a defective lattice and may be an indication of the zinc-rich nature of this sample.

37. Scherrer, P., Bestimmung der Größe und der inneren Struktur von Kolloidteilchen mittels Röntgenstrahlen. *Nachr. Ges. Wiss. Göttingen.* **1918,** *1990*, 98-100.

38. Bawendi, M. G.; Kortan, A. R.; Steigerwald, M. L.; Brus, L. E., X-ray structural characterization of larger CdSe semiconductor clusters. *J. Chem. Phys.* **1989,** *91*, 7282-7290.

39. Hoertz, P. G.; Chen, Z.; Kent, C. A.; Meyer, T. J., Application of High Surface Area Tin-Doped Indium Oxide Nanoparticle Films as Transparent Conducting Electrodes. *Inorg. Chem.* **2010,** *49*, 8179-8181.

40. Mobarok, M. H.; Buriak, J. M., Elucidating the Surface Chemistry of Zinc Phosphide Nanoparticles Through Ligand Exchange. *Chem. Mater.* **2014,** *26*, 4653-4661.

41. Abramoff, M. D., Magalhaes, P. J., Ram, S. J. Biophotonics International 2004, 11, 36-42.

42. Gary, D. C.; Glassy, B. A.; Cossairt, B. M., Investigation of Indium Phosphide Quantum Dot Nucleation and Growth Utilizing Triarylsilylphosphine Precursors. *Chem. Mater.* **2014,** *26*, 1734-1744.

43. Lin-Chung, P. J., Energy band structures of Cd3P2 and Zn3P2. *Phys. Status Solidi B* **1971,** *47*, 33-39.

44. Bosco, J. P.; Scanlon, D. O.; Watson, G. W.; Lewis, N. S.; Atwater, H. A., Energy-band alignment of II-VI/Zn3P2 heterojunctions from x-ray photoemission spectroscopy. *J. Appl. Phys.* **2013,** *113*, 203705.

45. Pawlikowski, J. M., Absorption edge of Zn3P2. *Phys. Rev. B* **1982,** *26*, 4711-4713.

46. Misiewicz, J., Optical and electrical investigations of imperfection levels in Zn3P2. *J. Phys. Chem. Solids* **1989,** *50*, 1013-1022.

47. Instrumental broadening is negligible.

Chapter 3: Resolving the Chemistry of Zinc Phosphide Nanocrystal Growth

3.1 Introduction

Quantum dots (QDs) are an attractive material for a variety of technologies based on the absorption of light including displays, solid-state lighting, photovoltaics, photocatalysis, and biological imaging.[1-4] The use of QDs in these applications is enabled by facile colloidal syntheses that yield crystalline particles with size tunable electronic properties.[5] Size-selective syntheses of high quality II-VI and IV-VI semiconductor QDs may be achieved through control of the precursor conversion kinetics.[6-7] However, precursor-based control of QD nucleation and growth is difficult to achieve for many materials outside the II-VI and IV-VI families.[8]

For phosphide-based QDs, in particular, the presence of kinetically persistent, covalently bonded intermediates has emerged as a key challenge in controlling the nucleation and growth of these colloidal materials. It was recently discovered, for example, that prior to InP QD nucleation in the traditional $P(SiMe_3)_3$ based synthesis, indium and phosphorous first form a kinetically persistent cluster intermediate that builds up in concentration at elevated temperatures.[9-10] It has also been shown that $InMe_3$ reacts with $P(SiMe_3)_3$ to form polycrystalline InP through the initial formation of a molecular dimer, $[Me_2InP(SiMe_3)_2]_2$, and its subsequent decomposition.[11] The realization that InP often arises from observable, kinetically persistent intermediates highlights the importance of understanding the precursor chemistry of other pnictide materials, such as zinc phosphide.

Zinc phosphide has emerged as a potential candidate for scalable thin-film photovoltaic applications due to its direct band gap of 1.5 eV,[12] high extinction coefficient,[13] long minority-

carrier diffusion length,[14] passive grain boundaries,[15] and a high annual electricity potential versus material extraction cost.[16] Several colloidal syntheses of zinc phosphide have emerged in recent years that use differing synthetic methods and yield a wide array of product sizes.[17-21] Buriak and co-workers developed a synthesis of 15 nm particles at 150 °C using $ZnMe_2$ and $P(SiMe_3)_3$ in trioctylphosphine and hypothesized that this transformation proceeded via slow formation of $[MeZn(\mu\text{-}P(SiMe_3)_2)]_2$.[19] Buriak and co-workers also accessed particles between 3 and 8 nm using $ZnMe_2$ and trioctylphosphine at 320-350 ºC via formation of a reduced Zn^0 intermediate.[18-19] Using a similar temperature regime, Arachchige and co-workers were able to access particles that were 3-9 nm in diameter using $ZnEt_2$, $P(SiMe_3)_3$, and hexadecylamine in 1-octadecene (1-ODE) at 230-300 °C.[21] Finally, our group previously reported a synthesis of small 2.5-3 nm zinc phosphide QDs with a tunable excitonic feature in the visible region of the absorption spectrum accessed through a molecular intermediate that is formed *in-situ* from $Zn(O_2CR)_2$, $ZnEt_2$, and $P(SiMe_3)_3$ at 255-315 °C.[20] Little is understood about the role of precursor speciation in the nucleation and growth mechanisms in these differing syntheses. As such, we have set out to develop a set of chemical principles that can be used to design a size tunable synthesis of this intriguing phosphide semiconductor.

Previously, we reported a synthesis of 3 nm Zn-rich Zn_3P_2 QDs by combining 3 equivalents of $Zn(OA)_2$, 1.5 equivalents of $ZnEt_2$, and 1 equivalent of $P(SiMe_3)_3$ in 1-ODE (referred to as Zn-rich seeds in this report). ICP-OES and thermogravimetric analysis indicated these particles had an overall Zn:P ratio of 5:2 where the additional zinc attributed to $Zn(OA)_2$ units bound to the surface. We found that under these conditions the two zinc precurors reacted first to form a known $Zn_5(OA)_6(Et)_4$ cluster, which was found to have dramatically enhanced reactivity with $P(SiMe_3)_3$ compared to either $Zn(OA)_2$ or $ZnEt_2$ alone. This enhanced reactivity led to the buildup and rate-

determining formation of a molecular intermediate with an empirical formula of $(Et_2Zn)P(ZnO_2CR)_2(SiMe_3)$. This intermediate was determined to be responsible for the nucleation and growth of these 3 nm particles. Powder X-ray diffraction (PXRD) analysis of these particles showed a discrepancy in the signal intensity of the major Bragg reflection (versus bulk α-Zn_3P_2), which we hypothesized was due to the small particle size and the complex nature of the zinc phosphide unit cell.[20]

Here we explore growth on these 3 nm Zn-rich Zn_3P_2 seeds using conventional zinc and phosphorus precursors, $Zn(O_2CR)_2$, $ZnEt_2$, and $P(SiMe_3)_3$, at 150 °C. This growth is found to proceed via formation of an intermediate trimer complex $[EtZnP(SiMe_3)_2]_3$.[22] We also explore the chemical and structural evolution that occurs during this post synthetic growth. Using a combination of solution and solid state nuclear magnetic resonance (NMR), PXRD, and transmission electron microscopy (TEM) analysis we have identified three key features of this growth. First, there is a blue shift observed in the optical absorption spectrum of the zinc phosphide seeds that arises on addition of $Zn(O_2CR)_2$. Next, $ZnEt_2$ and $P(SiMe_3)_3$ are simultaneously injected and $[EtZnP(SiMe_3)_2]_3$ forms. Finally, consumption of the trimer is accompanied by particle growth yielding highly crystalline 5 nm particles whose PXRD pattern closely resembles that of bulk α-Zn_3P_2, both in terms of peak position and intensity. This work highlights the variable precursor conversion chemistry that exists in the zinc phosphide system and the critical role of covalently bonded oligomeric intermediates in the nucleation and growth of this material.

3.2 Results and Discussion

3.2.1 Zinc Phosphide Growth on Zn-rich Seeds

Scheme 3.1 shows the optimized growth protocol we have developed using molecular precursors to grow 5 nm particles with a Zn:P ratio of 3.1:2, as determined by ICP analysis, from isolated Zn-rich Zn_3P_2 seeds obtained using our previously published synthetic method.[20] It should be noted that injecting diethyl zinc at a higher temperature or heating the reaction above 150 °C leads to the formation of zinc metal from the thermal decomposition of diethyl zinc (Figure 3.1).[23]

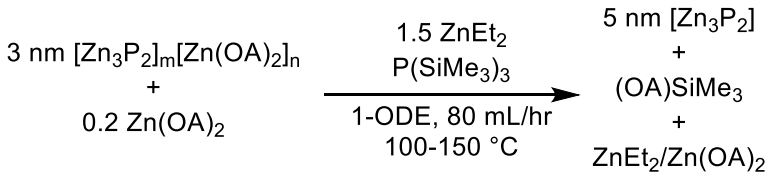

Scheme 3.1. Synthesis of 5 nm α-Zn_3P_2 QDs by adding molecular precursors to Zn-rich Zn_3P_2 seeds ($[Zn_3P_2]_n[Zn(OA)_2]_m$).

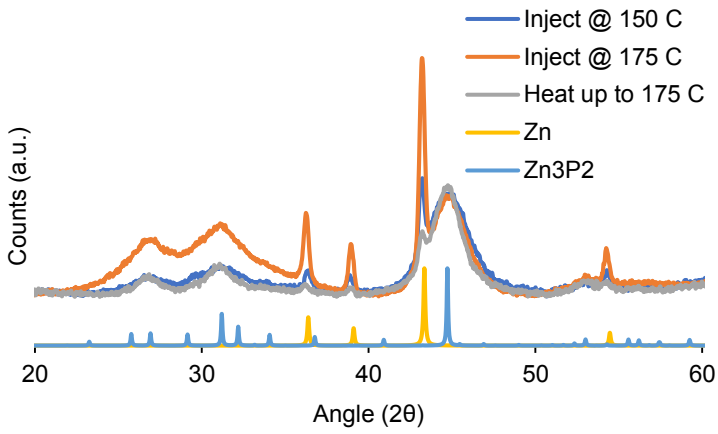

Figure 3.1. PXRD data showing the presence of bulk Zn^0 when $ZnEt_2/P(SiMe_3)_3$ are injected at 150 or 175 °C as well as if the reagents are heated up to 175 °C.

Several key observations were made during this reaction. First, as the colloidal particles were heated to 100 °C in the presence of zinc oleate there was blue shift in the optical absorption of the Zn_3P_2 seeds (Figure 3.2). This blue shift also occurs, albeit at a slower rate, when Zn_3P_2 seeds are heated to 100 °C in the presence of oleylamine or trioctylphosphine (Figures 3.3 and 3.4 respectively).

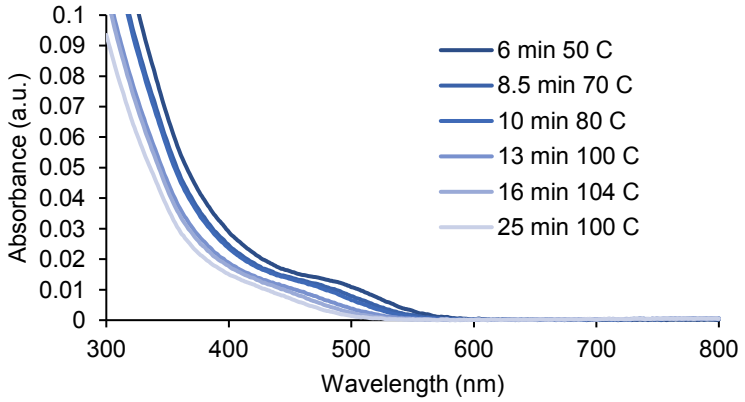

Figure 3.2. Aliquots taken of heating up 3 nm Zn-rich seeds in 1-ODE in the presence of $Zn(OA)_2$ showing the appreciable blue shift of the optical features.

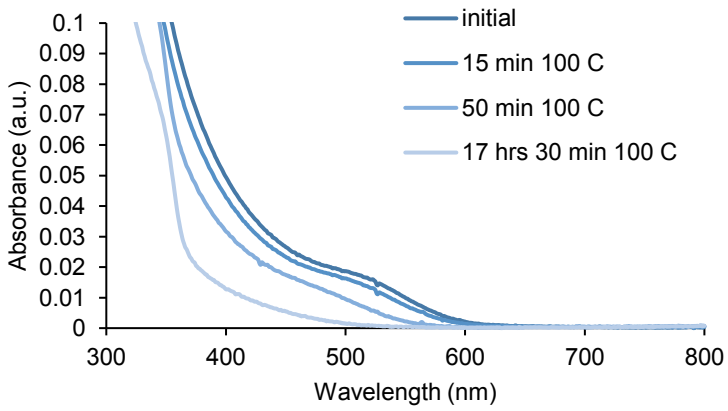

Figure 3.3. Aliquots taken of heating up 3 nm Zn-rich seeds in oleylamine.

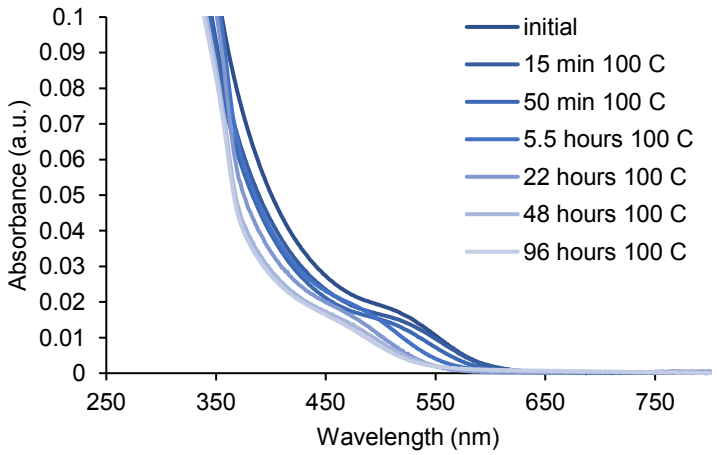

Figure 3.4. Aliquots taken of heating up 3 nm Zn-rich seeds in TOP.

Particles were isolated after being treated with zinc oleate, and TEM analysis indicated that the particles were on average 2.8 ± 0.5 nm in diameter with very similar magic angle spinning (MAS) NMR characteristics and thus indistinguishable in size and structure from the starting Zn_3P_2 seeds (Figure 3.5). This made it difficult to assign the origin of this optical blue shift, however we hypothesize that this dramatic change may result from structural reorganization of the seed particle surface in the presence of Lewis acids or bases, which may alter the exciton confinement properties or electronic structure of this highly confined material.[24-27] The second observation is that during the prolonged heating step following injection of $ZnEt_2$ and $P(SiMe_3)_3$, the larger particles precipitate out of solution as a brown powder.

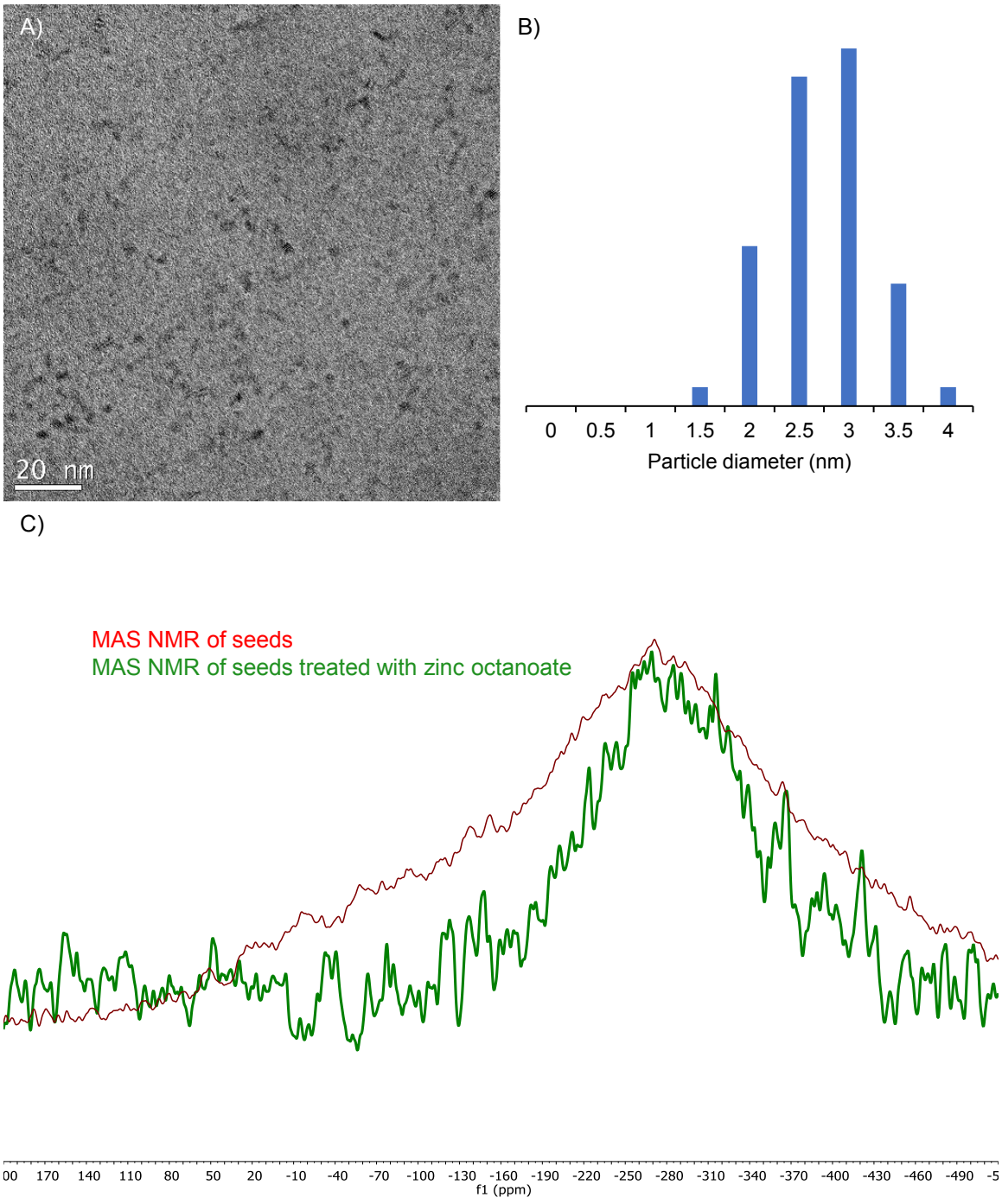

Figure 3.5. (A) TEM and size analysis on particles treated with $Zn(OA)_2$. 219 particles were measured using the Image J software package and the histogram was analyzed using Igor Pro. The average diameter was determined to be 2.8 ± 0.5 nm. (B) MAS NMR spectrum showing the similarity between treated and untreated seeds. 1000 Hz of line broadening was applied.

Structural characterization of these zinc phosphide nanoparticles before and after growth show particles transforming into a more bulk-like structure. The PXRD data of the Zn-rich Zn_3P_2 seeds (Figure 3.6A) has a discrepancy in the intensity of the major reflection at 45 2θ as compared to bulk α-Zn_3P_2.[20] However, these larger particles exhibit a PXRD pattern that better matches that of the bulk (Figure 3.6B). Scherrer analysis of the peak at 45 2θ indicates particles with a diameter of 5 nm, which is in agreement with TEM analysis (Figure 3.7).

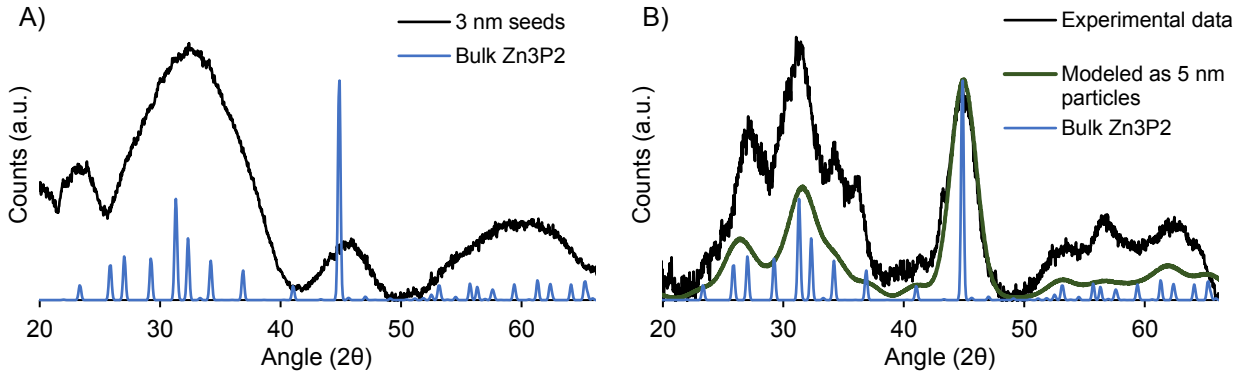

Figure 3.6. PXRD data of (A) Zn-rich Zn_3P_2 seeds and (B) crystalline α-Zn_3P_2 nanocrystals that result from growth. The reference pattern is tetragonal α-Zn_3P_2 (PDF #01-071-6507).

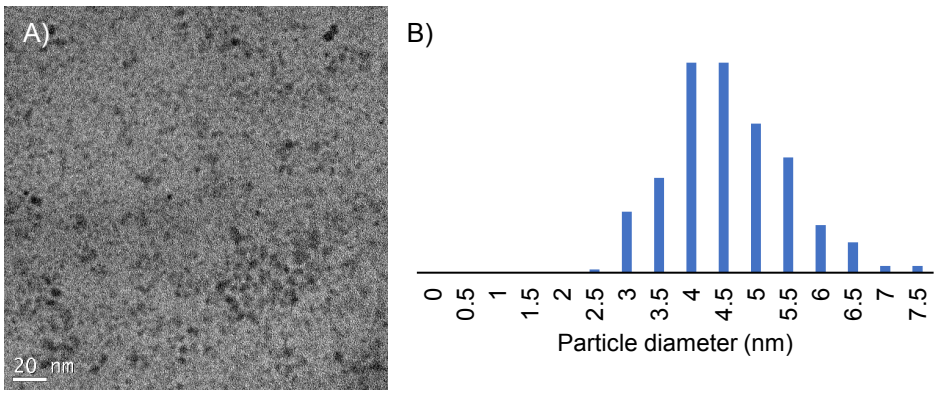

Figure 3.7. TEM and size analysis on particles grown using Scheme 3.1. 276 particles were measured using the Image J software package and the histogram was analyzed using Igor Pro. The average diameter was determined to be 4.4 ± 0.9 nm.

MAS ^{31}P NMR spectroscopy of tetragonal α-Zn_3P_2 shows two peaks at –195 and –228 ppm due to the ordered vacancies in the tetragonal crystal structure (two different resonances overlap in the –228 ppm peak at room temperature).[28] In order to obtain a solid sample for solid-state NMR analysis, the synthesis of both the Zn-rich seeds and the grown particles was scaled up and repeated with zinc octanoate instead of zinc oleate for ease of sample manipulation (see section 3.4.10 further details). Figure 3.8 shows MAS ^{31}P NMR spectra of the initial Zn_3P_2 seeds (bottom), highly crystalline grown particles (top, heated for 24 hours) and grown particles at an intermediate stage of the growth process (middle, heated for 90 minutes). These data show that during growth the phosphorus environments approach those of bulk zinc phosphide, exhibiting a downfield shift that is consistent with crystal growth.[29] The cross polarization data collected showed the presence of minimal oxidized phosphorus species at the particle surface, which dramatically increased upon air exposure of the sample for one week, indicating that the starting particles had a relatively oxide-free surface (Figure 3.9).

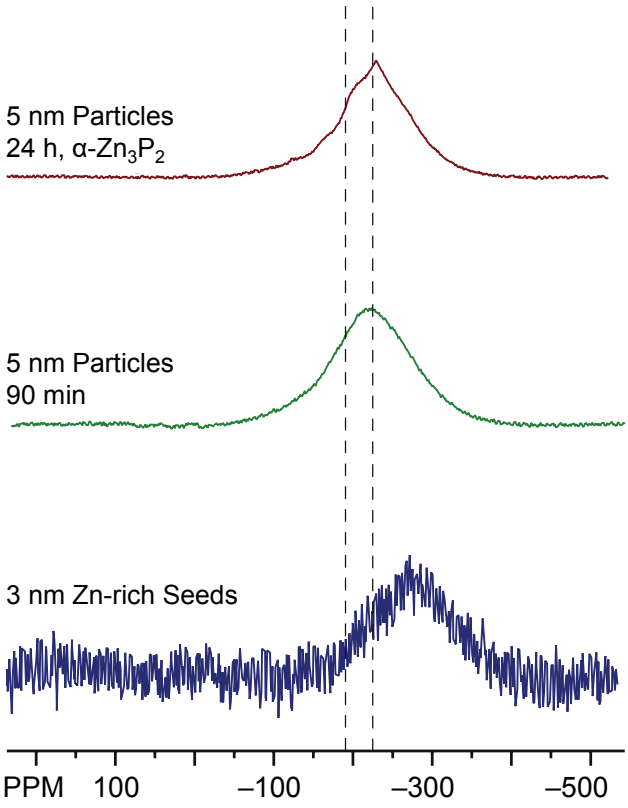

Figure 3.8. Magic-angle spinning ^{31}P NMR (283.34 MHz) data showing the progression from Zn-rich Zn_3P_2 seeds (bottom) to 5 nm crystalline α-Zn_3P_2 (top). The spin rate was 10 kHz and 100 Hz of line broadening was applied to all three samples. The dashed lines show the resonances of bulk α-Zn_3P_2.[28]

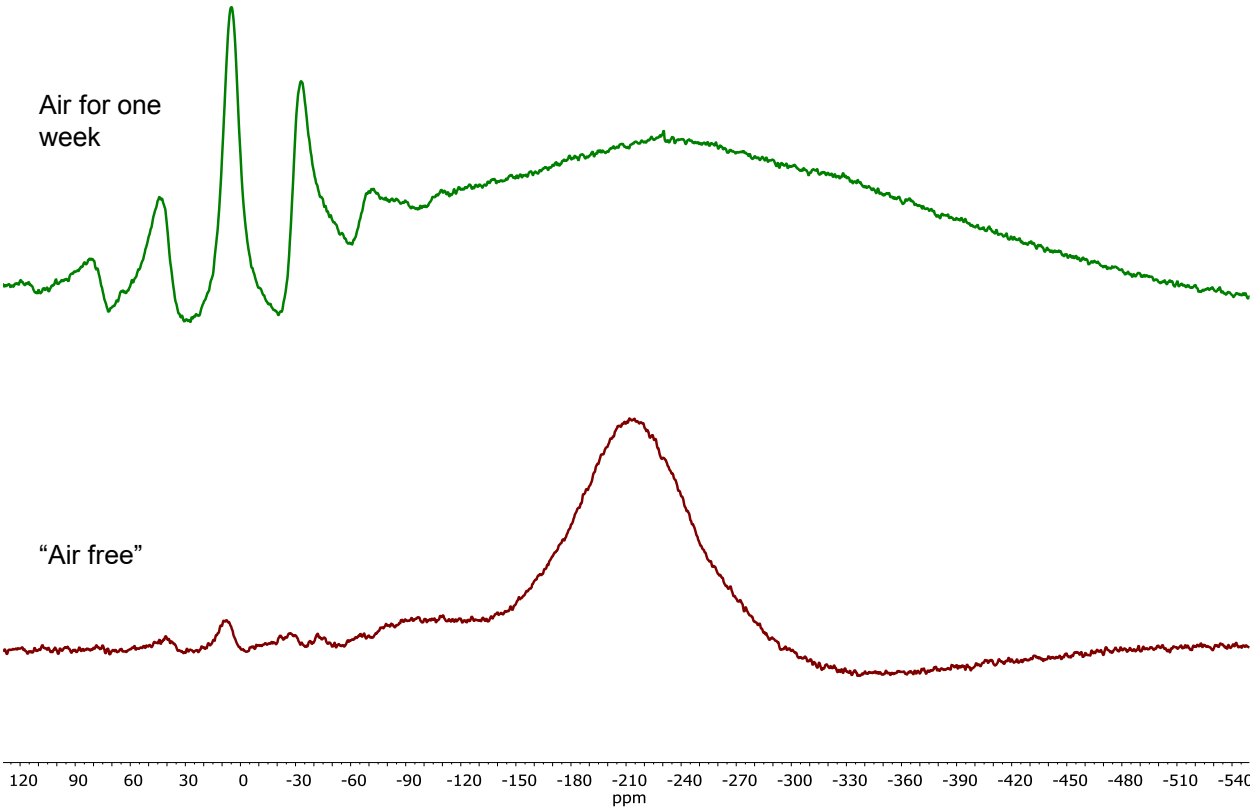

Figure 3.9. Cross polarization solid-state MAS NMR spectra of the sample grown for 24 hours (red) showing a large change in surface oxidation when the sample is left exposed to air for one week (green).

Taken together the PXRD and solid-state NMR data suggest that there is a critical surface-area to volume ratio at which Zn_3P_2 takes on the bulk structure. Given the large unit cell of bulk α-Zn_3P_2, at small sizes the Zn-rich surface may induce significant strain and cause deviations from the bulk structure. Upon growth of the nanocrystals, surface reorganization and crystallization appear to transform the material into the expected structure. It would appear that for our system this transition takes place between 3 and 5 nm in diameter, which corresponds in an approximate decrease in surface area to volume ratio from 2 to 1.2.

3.2.2 Mechanism of Zinc Phosphide Growth

Having verified the composition and structure of the reaction product, we investigated the precursor conversion reaction using solution-phase $^{31}P\{^{1}H\}$ NMR spectroscopy. Figure 3.10 shows the evolution of the phosphorus-containing molecules during the course of this reaction. What these data show is that prior to product precipitation a new molecular intermediate (–247 ppm) is formed and is then consumed in the reaction. A series of control experiments led us to conclude that the addition of zinc carboxylate to the reaction was essential to the building-up of this intermediate (see section 3.4.11). Ultimately the intermediate was identified as $[EtZnP(SiMe_3)_2]_3$ by reaction of 0.2 $Zn(O_2CCH_3)_2$, 1.5 $ZnEt_2$, and 1 $P(SiMe_3)_3$ in C_6D_6 in an oil bath at 130 °C for 30 minutes (Figure 3.11) and independent synthesis of this compound from $P(SiMe_3)_3$, methanol, and $ZnEt_2$ following a literature procedure.[22]

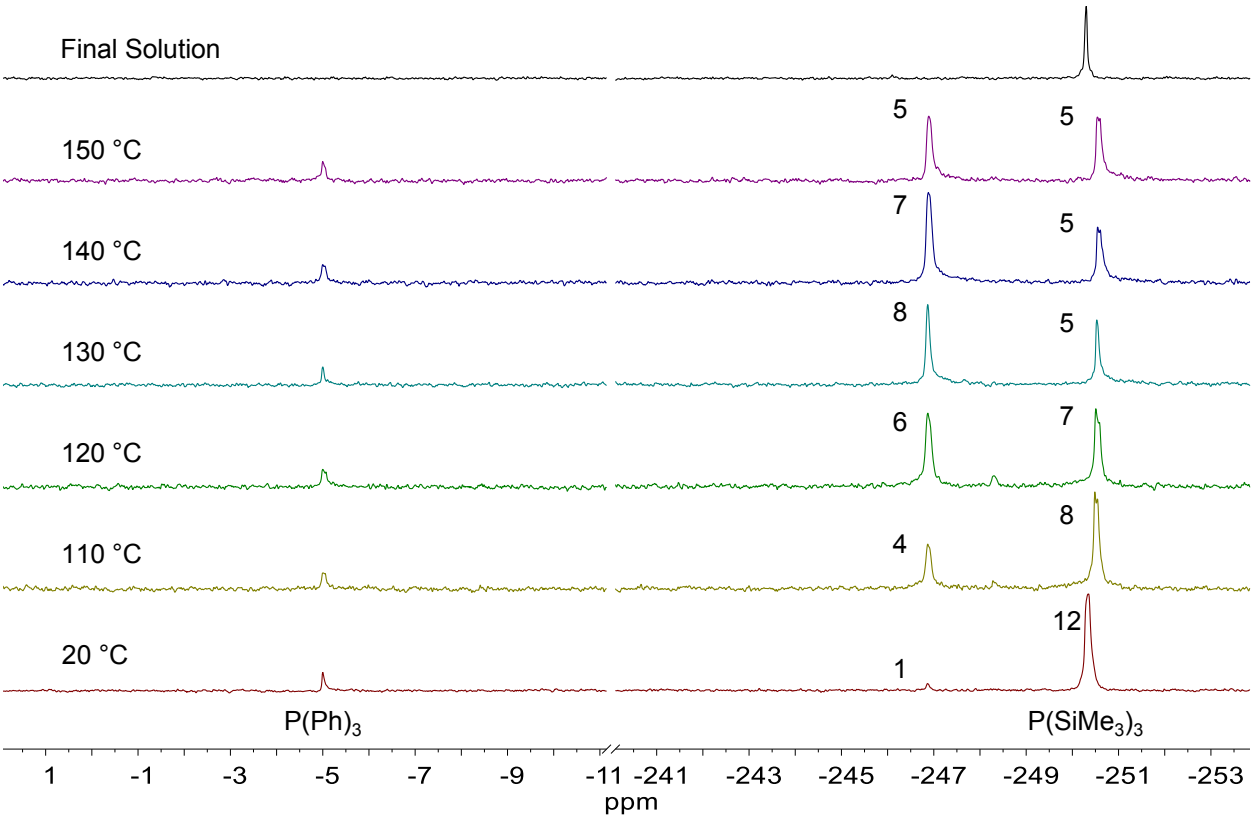

Figure 3.10. Solution-phase $^{31}P\{^{1}H\}$ NMR (121.47 MHz) data showing the precursor conversion of $P(SiMe_3)_3$ (–250.5 ppm) to a molecular intermediate (–247 ppm). The numbers above the peaks correspond to the integrations compared to an internal capillary standard. Data of particles before and after the initial heating step in the presence of $Zn(OA)_2$ showed no molecular phosphorus containing species present (Figure 3.12).

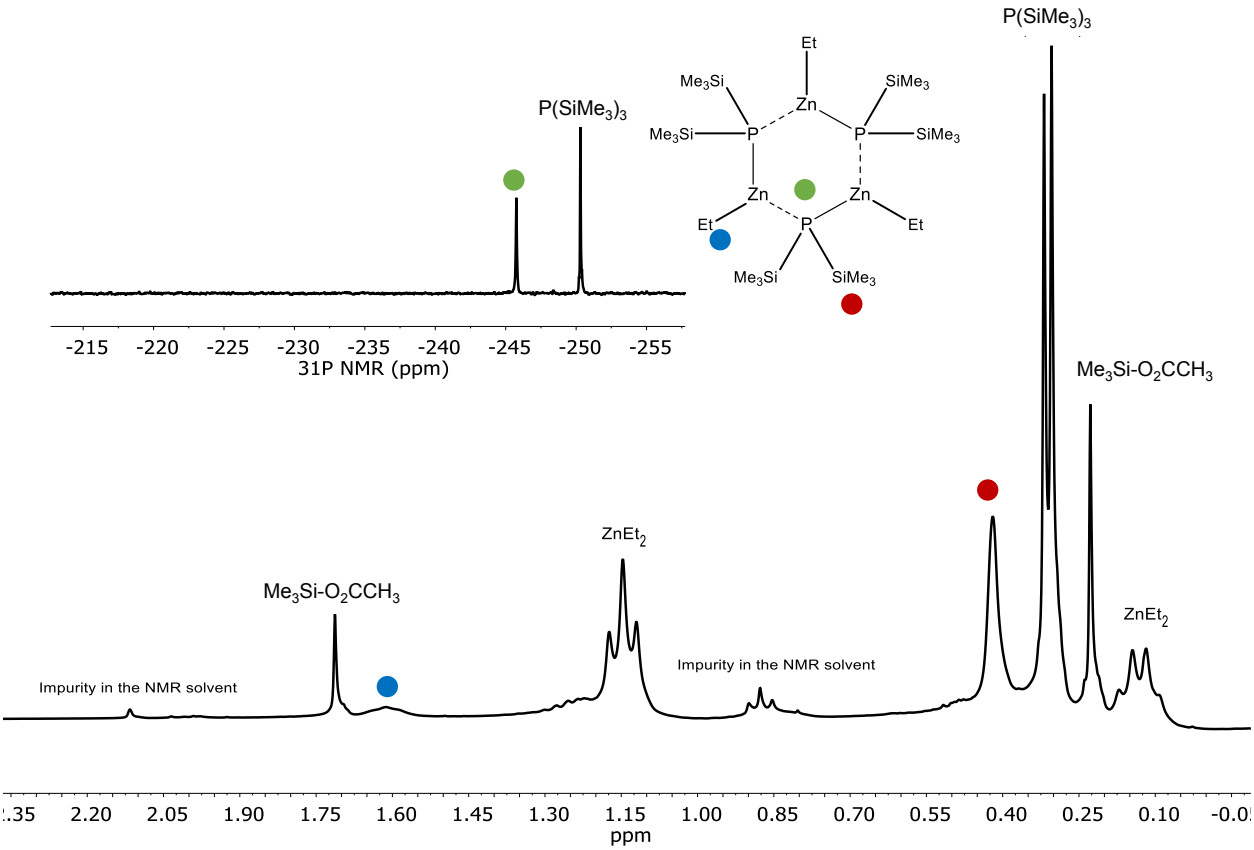

Figure 3.11. $^{31}P\{^{1}H\}$ (inset) and ^{1}H NMR spectra of the reaction between 0.2 $Zn(O_2CCH_3)_2$, 1.5 $ZnEt_2$, and 1 $P(SiMe_3)_3$ identifying the molecular intermediate as $[EtZnP(SiMe_3)_2]_3$.

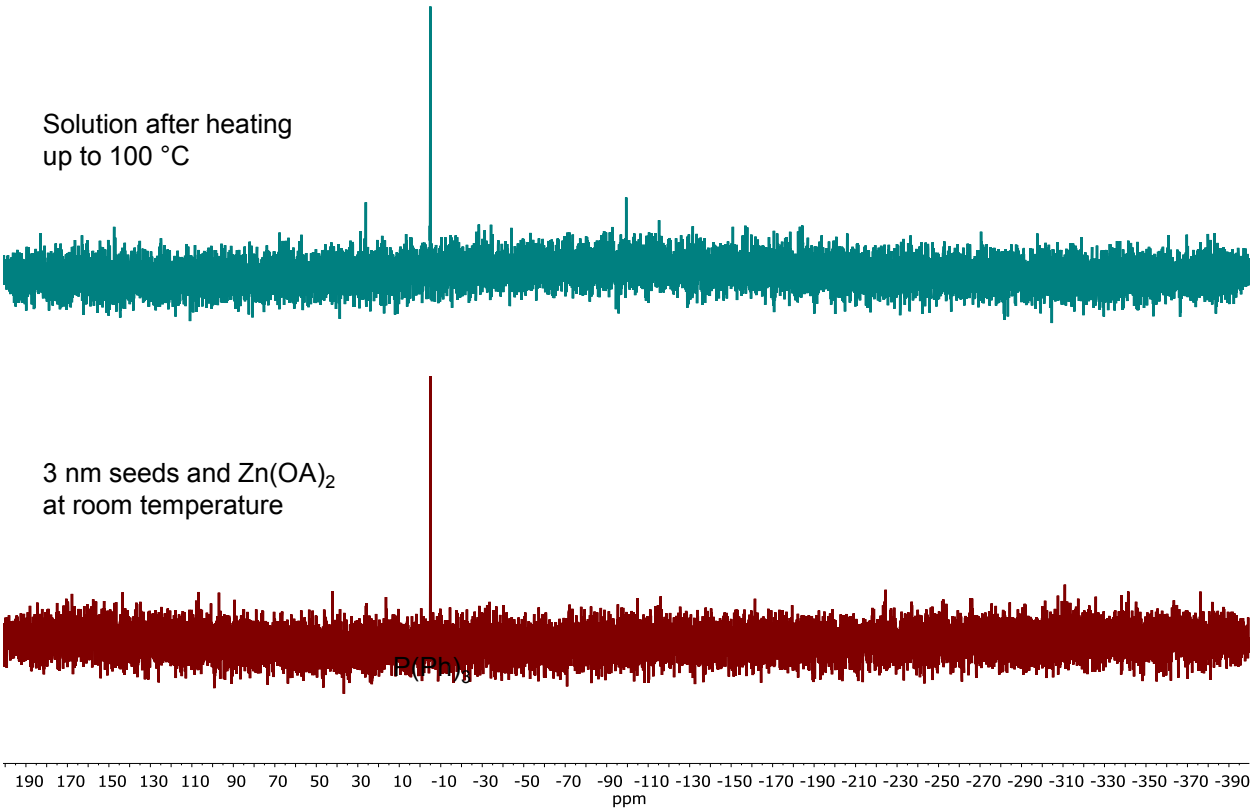

Figure 3.12. $^{31}P\{^{1}H\}$ NMR data showing no molecular species present before and after treating particles with $Zn(OA)_2$.

It is important to note that while $Zn(O_2CR)_2$, $ZnEt_2$, and $P(SiMe_3)_3$ are the same precursors used to generate the phosphorus containing intermediate we previously identified in the synthesis of the Zn-rich Zn_3P_2 seeds, $(Et_2Zn)P(ZnO_2CR)_2(SiMe_3)$, the ratio of $Zn(O_2CR)_2$ to $ZnEt_2$ is very different between the two syntheses.[20] For the growth method developed here, a ratio of 0.2 to 1.5 is being used, instead of 3:1.5. The growth reaction is essentially starved of zinc carboxylate relative to diethyl zinc preventing formation of the pentanuclear zinc cluster. This allows for the initial reaction of $Zn(O_2CR)_2$ with $P(SiMe_3)_3$ followed by reaction with $ZnEt_2$ to preferentially form $[EtZnP(SiMe_3)_2]_3$ as shown in Scheme 3.2. This observation is consistent with the relative

rates of reaction of the various zinc precursors with $P(SiMe_3)_3$, which we previously determined to follow the order $[Zn_5(O_2CR)_6(Et)_4] > Zn(O_2CR)_2 > ZnEt_2$.[20] Control reactions were performed to show that having $[EtZnP(SiMe_3)_2]_3$, $P(SiMe_3)_3$, $ZnEt_2$, and the seeds present led to optimum growth (See section 3.4.12).

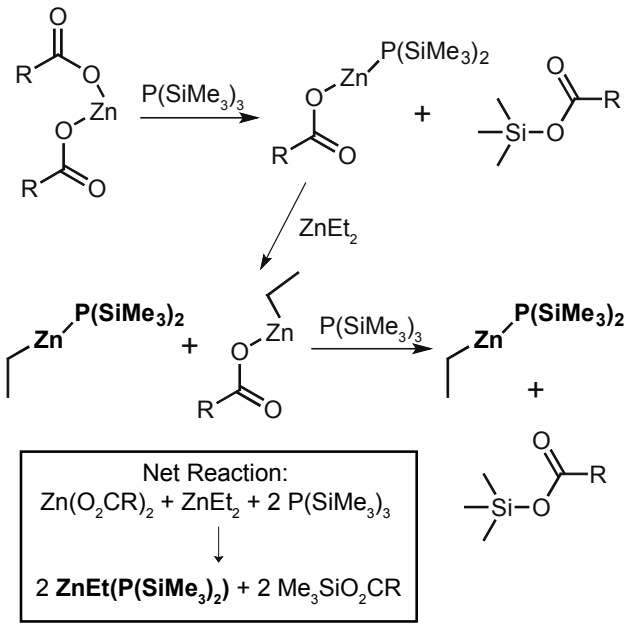

Scheme 3.2. Proposed reaction scheme for the synthesis of the $EtZnP(SiMe_3)_2$ monomer. The monomer is unstable towards oligomerization.

It has been proposed that similar $MeZnP(SiMe_3)_2$ oligomers could be relevant in the synthesis of zinc phosphide nanocrystals in a coordinating solvent, like trioctylphosphine.[19] We set out to test the role of this solvent in our synthesis to see if a coordinating solvent would change the reaction dynamics. We were unable to independently prepare appreciable quantities of $[EtZnP(SiMe_3)_2]_3$ from $ZnEt_2$, MeOH, and $P(SiMe_3)_3$ in the presence of trioctylphosphine, presumably due to the coordinating nature of phosphines (Figure 3.13). Instead, we examined particle growth in the presence of this coordinating base by injecting a solution containing the

trimer, $ZnEt_2$, and $P(SiMe_3)_3$ prepared in 1-ODE into a pot containing zinc phosphide seeds dissolved in trioctylphosphine. A brown precipitate formed in this reaction and its PXRD pattern matched that of the particles formed in 1-ODE alone (Figure 3.14). This would suggest that coordinating solvents interfere with the initial build-up of $RZnP(SiMe_3)_2$ oligomers, but once these species form, their net effect on growth is minimally changed.

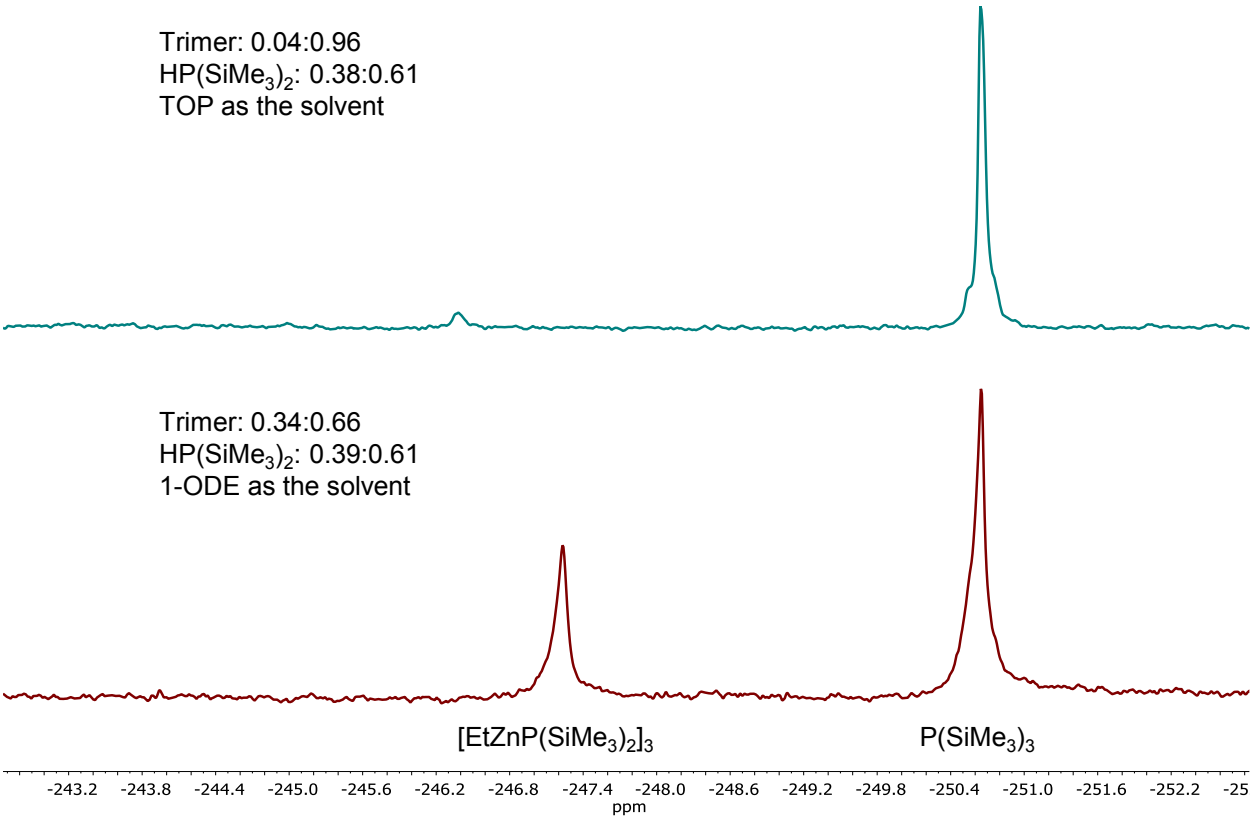

Figure 3.13. $^{31}P\{^1H\}$ NMR data of side by side reactions targeting the synthesis of $[EtZnP(SiMe_3)_2]_3$ in TOP and 1-ODE. The two reactions are identical except for the identity of the solvent.

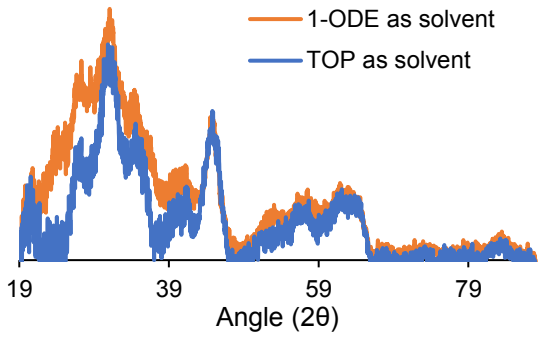

Figure 3.14. PXRD data of the product from the reaction of pre-forming the solution containing $[EtZnP(SiMe_3)_2]_3$ and injecting it into particles in 1-ODE and TOP.

Since we identified a different molecular intermediate responsible for the growth mechanism as compared to what was observed for the Zn-rich seeds, we wanted to better understand the differing nucleation and growth dynamics between $[EtZnP(SiMe_3)_2]_3$ and $(Et_2Zn)P(ZnO_2CR)_2(SiMe_3)$. To study the nucleation and growth dynamics of $[EtZnP(SiMe_3)_2]_3$, our previously reported synthesis was repeated using 0.2 instead of 3 equivalents of $Zn(OA)_2$, which resulted in precipitation of bulk α-Zn_3P_2 and bulk Zn^0 both of which had a domain size of >100 nm as determined by PXRD analysis (Figure 3.15).

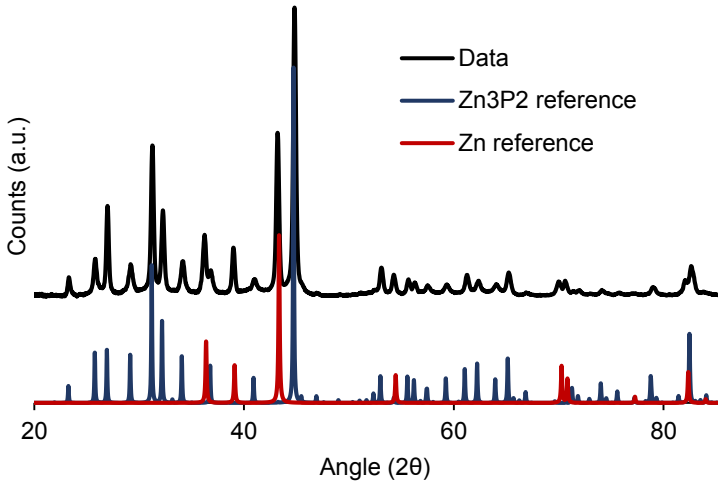

Figure 3.15. PXRD data of the reaction using 0.2 $Zn(OA)_2$, 1.5 $ZnEt_2$, and $P(SiMe_3)_3$ and following our previously reported prep by adding $ZnEt_2$/$P(SiMe_3)_3$ to $Zn(OA)_2$ in 1-ODE at 100 °C and heating up to 315 °C over the course of 60 minutes. The Zn_3P_2 pattern is COD 1010287 and the Zn pattern is COD 9012435.

In order to compensate for the low ligand concentration under these conditions, the reaction was repeated with the oleate deficit made up by Na(OA). Instead of getting 3 nm particles, as was the case for the original synthesis using 3 equivalents of $Zn(O_2CR)_2$, the result of this experiment was colloidally stable 4.7 ± 0.8 nm particles (See Figures 3.16-3.19). These results are summarized in Scheme 3.3.

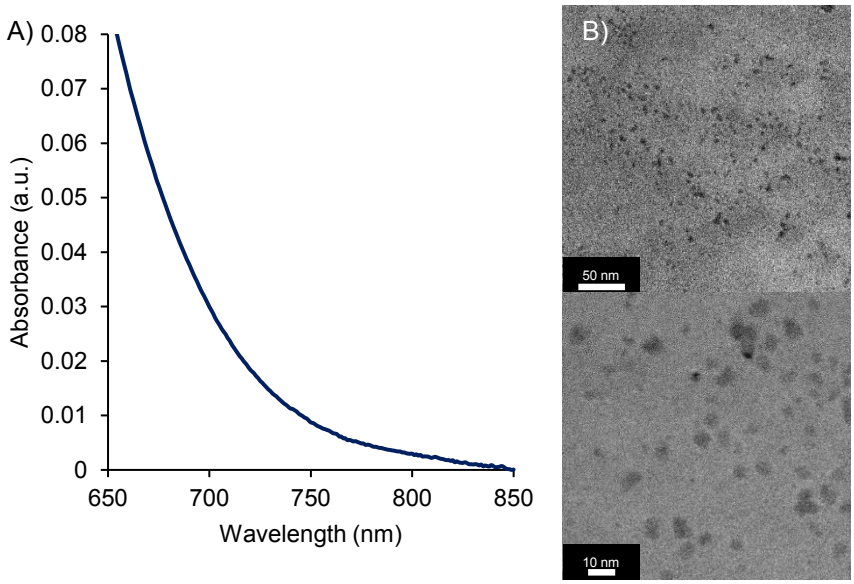

Figure 3.16. (A) UV-Vis spectrum of QDs synthesized with the $[EtZnP(SiMe_3)_2]_3$ as the pertinent precursor and (B) TEM images of these particles showing an average diameter of 4.7 ± 0.8 nm.

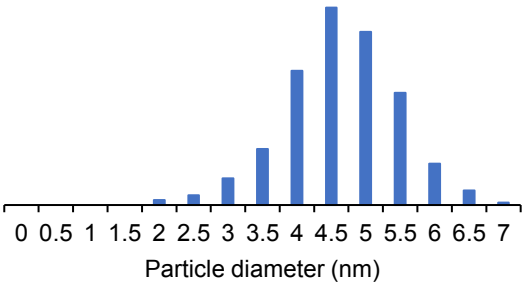

Figure 3.17. TEM particle size histogram of particles grown using NaOA and $[EtZnP(SiMe_3)_2]_3$ as the active intermediate. 317 particles were counted using the Image J software package and the histogram was analyzed using Igor Pro. The average diameter was determined to be 4.7 ± 0.8 nm.

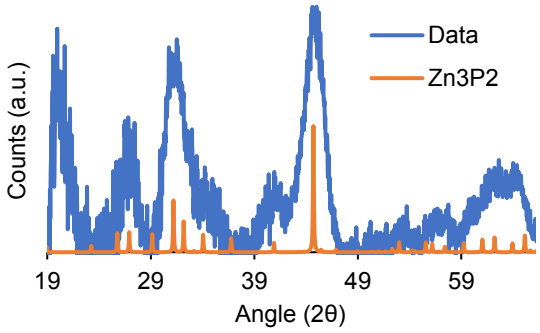

Figure 3.18. PXRD data of the colloidally stable particles grown using NaOA and $[EtZnP(SiMe_3)_2]_3$ as the active intermediate.

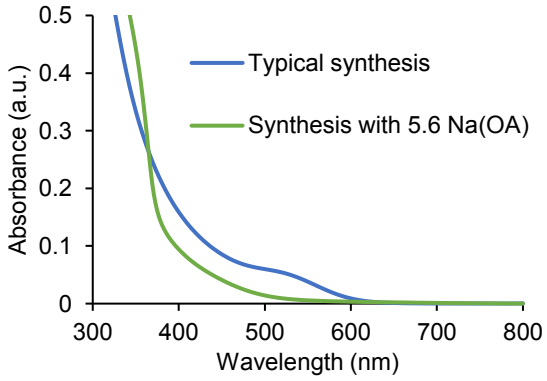

Figure 3.19. UV-Vis spectra comparing the typical synthesis of 3 nm Zn-rich seeds (blue) with a synthesis that includes 5.6 equivalents of Na(OA) (green) showing a reduction the amount of lower energy light absorbed and probable formation of zinc oxide.

Assuming comparable conversion, temporally distinct nucleation and growth, and no Ostwald ripening, the observed 1.7 nm difference in the average particle diameter indicates that an order of magnitude fewer nuclei were formed in the zinc-limited reaction as compared to the zinc-rich conditions. One possibility is that under zinc-limited conditions, conversion to monomer is slower due to the increased stability of $[EtZnP(SiMe_3)_2]_3$, leading to generation of fewer nuclei

than form under zinc-rich conditions where nucleation follows formation of $(Et_2Zn)P(ZnO_2CR)_2(SiMe_3)$.

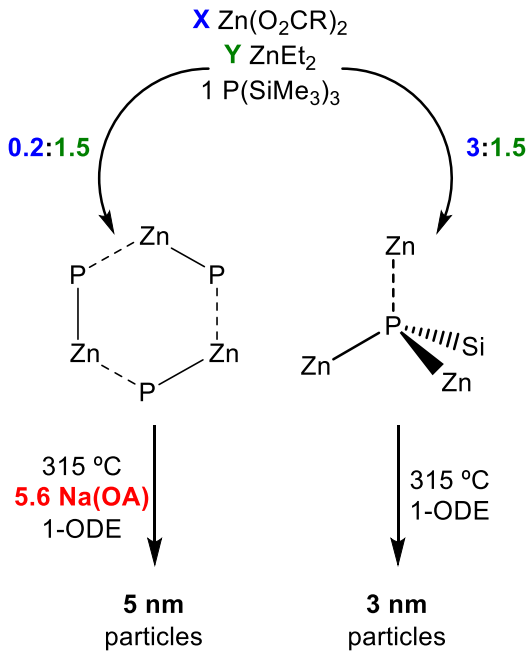

Scheme 3.3. Comparison of product outcomes using two different ratios of $Zn(O_2CR)_2$ to $ZnEt_2$.[20] Truncated structures of the intermediates $[EtZnP(SiMe_3)_2]_3$ (0.2:1.5) and $(Et_2Zn)P(ZnO_2CR)_2(SiMe_3)$ (3:1.5) are shown for simplicity.

3.3 Conclusions

In conclusion, we identified $[EtZnP(SiMe_3)_2]_3$ as an intermediate in the growth of crystalline, stoichiometric 5 nm α-Zn_3P_2 nanocrystals from 3 nm Zn-rich seeds. Solid state MAS NMR and PXRD data suggest that the transformation from 3 nm Zn-rich Zn_3P_2 to 5 nm stoichiometric Zn_3P_2 involves significant structural reorganization to the crystalline α-Zn_3P_2 phase. The observation of $[EtZnP(SiMe_3)_2]_3$ as an intermediate in this growth process stands in contrast to earlier findings where the same precursors, $Zn(O_2CR)_2$, $ZnEt_2$, and $P(SiMe_3)_3$, used in

differing ratios led to the original 3 nm Zn-rich Zn_3P_2 nanocrystals. This result highlights the ability to target different sizes of zinc phosphide nanocrystals depending on the identity of molecular intermediates and their subsequent reaction dynamics leading us to formulate general principles for the synthesis of zinc phosphide. In general, during the synthesis of Zn_3P_2 from $P(SiMe_3)_3$, prior to nucleation, $P(SiMe_3)_3$ undergoes a chemical transformation to a new molecular intermediate containing Zn-P bonds. The structure and composition of this intermediate is dependent on the identity and concentration of the zinc precursor(s) and other ligand additives, and its reactivity governs the nucleation and growth dynamics. In order to have conversion of Zn-P intermediates to monomers as the rate-limiting step, it is important to have a synthesis in which the intermediate is rapidly formed *in situ* or is purposefully synthesized separately and used as a single-source precursor. For Zn_3P_2, two primary growth mechanisms have been explored to date, those involving alkyl zincs (ZnR_2) and those involving zinc carboxylates ($Zn(O_2CR')_2$). For alkyl zinc precursors, rapid formation of the $RZnP(SiMe_3)_2$-based oligomeric intermediates is facilitated by addition of a protic reagent (e.g. water or methanol) or small amounts of metal carboxylate. Addition of zinc carboxylate can tune the rate of the initial reaction with $P(SiMe_3)_3$ via formation of $ZnR(O_2CR')$ clusters, which have enhanced reactivity relative to either independent precursor. In general, the relative rates of reactivity with $P(SiMe_3)_3$ are in the order $[ZnR(O_2CR')] > Zn(O_2CR')_2 > ZnR_2$. Moreover, in the presence of reducing additives or at elevated temperatures, reduction of zinc precursors to zinc metal can further perturb the reaction kinetics and direct reactivity through redox rather than acid-base mechanisms.

3.4 Experimental

3.4.1 General Considerations

All glassware was dried in a 160 ºC oven overnight prior to use. All reactions, unless otherwise noted, were run under an inert atmosphere of nitrogen using a glovebox or standard Schlenk techniques. Hexanes (a mixture of isomers, CHROMASOLV), triphenylphosphine (99%), sodium (dry stick, ACS reagent), potassium (in mineral oil, 98%), red phosphorus (99.999%), and calcium hydride (powder, 0-2 mm, reagent grade, ≥90%, stored in desiccator) were purchased from Sigma-Aldrich and used without further purification. Magnesium sulfate (anhydrous, powder certified) was purchased from Fisher Scientific and used without further purification. Sodium oleate (>97%) was purchased from TCI America and used without further purification. Phosphoric acid (ACS grade) was purchased from Macron Fine Chemicals and used without further purification. Trioctylphosphine (97%), methanol (anhydrous, 99.8%), ethyl acetate (anhydrous, 99.8%), and acetonitrile (anhydrous, 99.8%) were purchased from Sigma-Aldrich and stored in a nitrogen filled glove box over activated 3 Å molecular sieves. Chlorotrimethylsilane (purified by redistillation, ≥99%) was purchased from Sigma-Aldrich and stored under an inert atmosphere. Omni Trace nitric acid was purchased from EMD Millipore and used without further purification. 18.2 MΩ water was collected from an EMD Millipore water purification system. Celite 545 and zinc acetate (99.99%) were purchased from Sigma-Aldrich and heated at 150 °C under vacuum overnight and stored in a nitrogen filled inert glove box prior to use. Oleic acid (90%) was purchased from Sigma-Aldrich and stirred over 3 Å molecular sieves overnight prior to being freeze-pump-thawed three times and stored in a nitrogen filled inert glove box prior to

use. $ZnEt_2$ (95%) was purchased from Strem Chemicals and stored in a -35 °C freezer in a nitrogen filled inert atmosphere glove box. 1-octadecene (90%) 1,2-dimethoxyethane (99%), oleylamine (technical grade, 70%), pentane, heptane, and toluene were purchased from Sigma-Aldrich, dried by stirring overnight with CaH_2, distilled, and stored over activated 3 Å molecular sieves in an inert atmosphere glove box. C_6D_6 was purchased from Cambridge Isotope Labs and was similarly dried and stored. Octanoic acid was purchased from Eastman Chemical Company and dried and distilled from magnesium sulfate and stored over 3 Å molecular sieves in an inert atmosphere glove box. $P(SiMe_3)_3$ was prepared following a literature procedure.[30] Zinc oleate and zinc octanoate were prepared using an adapted literature procedure.[20]

3.4.2 Characterization

Solution ^1H (Field: 300 MHz) and $^{31}P\{^1H\}$ (Field: 121 MHz) NMR spectra were collected on a 300 MHz Bruker Avance spectrometer. Solid-state ^{31}P (Field: 283. 34 MHz) NMR spectra were collected on a 700 MHz Bruker Avance III spectrometer using a cross-polarization pulse program as well as a Hahn echo pulse program with a 120 second relaxation delay, a τ of 300 microseconds, and both at a spin rate of 10 kHz. UV-Vis spectra were collected on an Agilent Cary 5000 spectrophotometer. PXRD diffractograms were collected on a Bruker D8 Discover with a GADDS 2-D XRD system. ICP-OES was performed using a Perkin Elmer Optima 8300. TEM images were collected on a FEI Tecnai G2 F20 microscope. TEM analysis was performed using manual analysis with the help of the ImageJ software package.[31]

3.4.3 Sample Preparation for Characterization

PXRD: Insoluble powders were placed onto a piece of double-sided tape on a silicon <100> single crystal wafer. Solvent was removed from colloidal samples until dry and the paste was spread on a silicon <100> single crystal wafer. ICP-OES: Concentrated, high purity nitric acid was added to dissolve a small amount of the insoluble powders so the final solution could be diluted with 18.2 MΩ water in a volumetric flask to 2%. TEM: Samples were either prepared in toluene or heptane. Insoluble samples were sonicated at room temperature for 5-10 minutes immediately before drop-casting onto a TEM grid (Ultrathin carbon on holey carbon support film, 400 mesh Ted Pella or graphene support on Lacey Carbon, 300 mesh Ted Pella). Samples were placed under vacuum overnight prior to analysis to ensure sample dryness. MAS NMR: Solids were packed into a 3.2 mm zirconia rotor from Bruker inside a nitrogen filled glovebox and were brought out immediately prior to data collection.

3.4.4 Preparation of Stock Solution of 3 nm Zn-rich Seeds

Zn_3P_2 quantum dots were synthesized and purified according to a literature procedure utilizing 1 mmol (290.3 μL) of $P(SiMe_3)_3$ in 20 grams of 1-ODE.[20] Particles were dried overnight under reduced pressure and enough toluene was added to yield a stock solution of 23 mg particles/mL.

3.4.5 Typical Growth Reaction

In a typical reaction, 0.5 mL of the QD stock solution was dried under reduced pressure. 2.5 grams of 1-ODE was then added. 0.0508 grams (0.081 mmol) of $Zn(OA)_2$ was weighed into a 15 mL three-neck flask and transferred onto a Schlenk line. The QD solution was then injected into the flask and heated up to 100 °C over the course of 15 minutes. A solution containing 3.156 grams (4 mL) of 1-ODE, 61.5 μL (0.6 mmol) $ZnEt_2$, and 116.1 μL (0.4 mmol) $P(SiMe_3)_3$ was then syringe-pumped into the flask at a rate of 80 mL/hr (3 minutes). The flask was then heated up to 150 °C and left there for 90 minutes. The flask was then brought into a nitrogen filled glove box and the heterogeneous solution was transferred into a centrifuge tube. The supernatant was discarded and pentane was added to the solid and centrifuged again to remove any trapped 1-ODE. The solid was then transferred to a tared scintillation vial and dried under reduced pressure yielding 30 mg of solid. Note: Longer heating times were observed to result in a small amount of zinc metal via the well-documented decomposition of $ZnEt_2$.[23]

3.4.6 Typical Solution NMR Reactions

In all solution NMR reactions 800 μL of the QD stock solution was used. In a typical reaction, 0.4 grams of 1-ODE was added to the QDs after the toluene was removed under reduced pressure. 8 mg (0.013 mmol) of $Zn(OA)_2$ was added to a J-Young tube. The QD solution in 1-ODE was then added to the J-Young tube and heated up to 100 °C. The NMR tube was then brought back into the glove box and a solution containing 0.51 grams 1-ODE, 9.8 μL (0.096 mmol) $ZnEt_2$, and 18.6 μL (0.064 mmol) $P(SiMe_3)_3$ was added dropwise. The NMR tube was then slowly

heated up to 150 ºC stepwise, taking NMR scans every ten degrees starting at 100 °C. For the NMR control reactions, after adding any combination of $ZnEt_2$ and $P(SiMe_3)_3$ the NMR tubes were heated up to 130 ºC for 30 minutes prior to collecting data.

3.4.7 Pre-forming $[EtZnP(SiMe_3)_2]_3$ Injection Solutions

In a typical synthesis targeting $P(SiMe_3)_3$, $ZnEt_2$, and $[EtZnP(SiMe_3)_2]_3$ to be injected, 116.1 μL (0.4 mmol) $P(SiMe_3)_3$ was added to 2.16 grams 1-ODE. 6.5 μL (0.16 mmol) of methanol was added slowly while stirring. The reaction stirred for 24 hours. Phosphorus NMR spectroscopy was used to confirm that the ratio of $HP(SiMe_3)_2$ to $P(SiMe_3)_3$ was correct. 0.5 grams of 1-ODE was used to thoroughly rinse out the NMR tube to ensure quantitative transfer. 61.5 μL (0.6 mmol) $ZnEt_2$ was then slowly added to the solution while stirring. The reaction stirred for 24 hours. Phosphorus NMR spectroscopy was then used to confirm that the ratio of $[EtZnP(SiMe_3)_2]_3$ to $P(SiMe_3)_3$ was correct. 0.5 grams 1-ODE was used to thoroughly rinse out the NMR tube to ensure quantitative transfer. The solution was then used in reactions. When targeting complete conversion from $P(SiMe_3)_3$ to $[EtZnP(SiMe_3)_2]_3$ it is important that the reaction is run under very concentrated conditions to avoid $H_2P(SiMe_3)$ formation.

3.4.8 Growing on Particles with $[EtZnP(SiMe_3)_2]_3$ Injection Solutions

In a typical synthesis, 0.5 mL of the QD stock solution was dried and dissolved in either 2.5 grams of 1-ODE or 2.63 grams of TOP. The reaction described for typical growth was then repeated using the $[EtZnP(SiMe_3)_2]_3$ injection solution instead of the solution described above.

3.4.9 Growing Particles From $[EtZnP(SiMe_3)_2]_3$ Without Seeds

Our previously reported synthesis was used with 0.025 grams (0.04 mmol) $Zn(OA)_2$ instead of 0.377 grams (0.6 mmol).[20] This was also modified by adding 0.341 grams (1.12 mmol) of sodium oleate to the initial flask containing zinc oleate.

3.4.10 Solid State MAS NMR Sample Preparation

A stock solution of particles synthesized with zinc octanoate was first formed following our previously reported procedure. To synthesize the sample heated for 90 minutes, 45.5 mg of particles were used (assumed same size and ligand coverage as compared to when particles were synthesized with zinc oleate). These particles were dissolved in 12.5 grams of 1-ODE and heated to 100 °C in the presence of 141 mg (0.4 mmol) zinc octanoate. The solubility of zinc octanoate appeared, as expected, to be lower than that of zinc oleate in 1-ODE. To this solution, 15.75 (20 mL) of 1-ODE containing 307.5 μL (3 mmol) $ZnEt_2$ and 580.6 μL (2 mmol) $P(SiMe_3)_3$ was injected at a rate of 200 mL hr^{-1} (which is double the total injection time from the typical synthesis). This solution was then heated to 150 °C for 90 minutes (Figure 3.20).

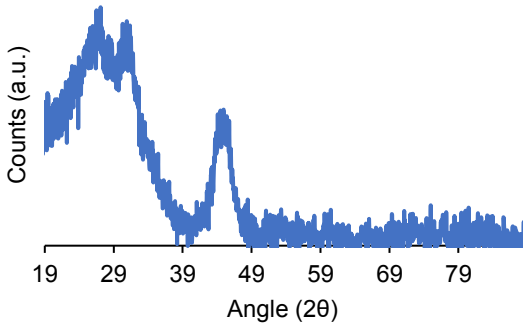

Figure 3.20. PXRD data of sample grown for 90 minutes at 150 °C using zinc octanoate as the zinc carboxylate source.

For the sample heated for 24 hours, 23 mg of zinc octanoate capped particles were used. These were dissolved in 6.25 grams of 1-ODE and added to 71 mg (0.2 mmol) zinc octanoate. This solution was heated to 100 °C. A solution containing 7.89 grams (10 mL) 1-ODE, 153.75 µL (1.5 mmol) $ZnEt_2$, and 290.3 µL (1 mmol) $P(SiMe_3)_3$ were added at a rate of 100 mL hr^{-1} (over the course of 6 minutes, which is double the typical injection time). This was then heated to 150 °C for 24 hours (Figure 3.21).

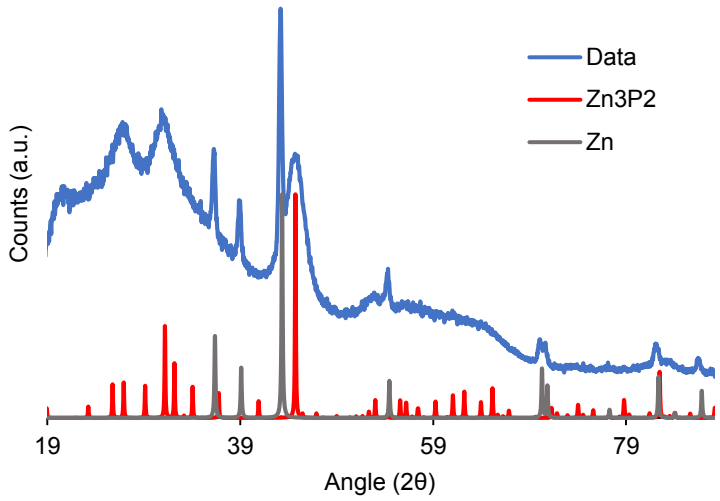

Figure 3.21. PXRD data of the sample heated at 150 °C for 24 hours.

While heating the sample for 24 hours produced a sample with a PXRD pattern that resembled that of our typical synthesis (Figure 3.6), it also showed the presence of Zn^0. We believe this did not play any role in the ^{31}P solid-state NMR and was formed as a side product due to the differing scale and the extended annealing time. This procedure was not optimized.

3.4.11 Control Reactions to Determine What the New Intermediate is as well as How It Forms

Several NMR control reactions were performed in order to determine which reagents were necessary to form $[EtZnP(SiMe_3)_2]_3$. Figure 3.22 shows that when the typical reaction is performed without $ZnEt_2$ the intermediate is not formed. Figure 3.23 shows that if $ZnCl_2$ is used again no intermediate is formed, but it does form when $Zn(O_2CCH_3)_2$ is used. Figure 3.24 shows that the highest concentration of the intermediate is formed when both $Zn(O_2CCH_3)_2$ and $ZnEt_2$ are used.

Na(OA) was also used to see if it was the oleate that was responsible for the formation of this species (Figure 3.25).

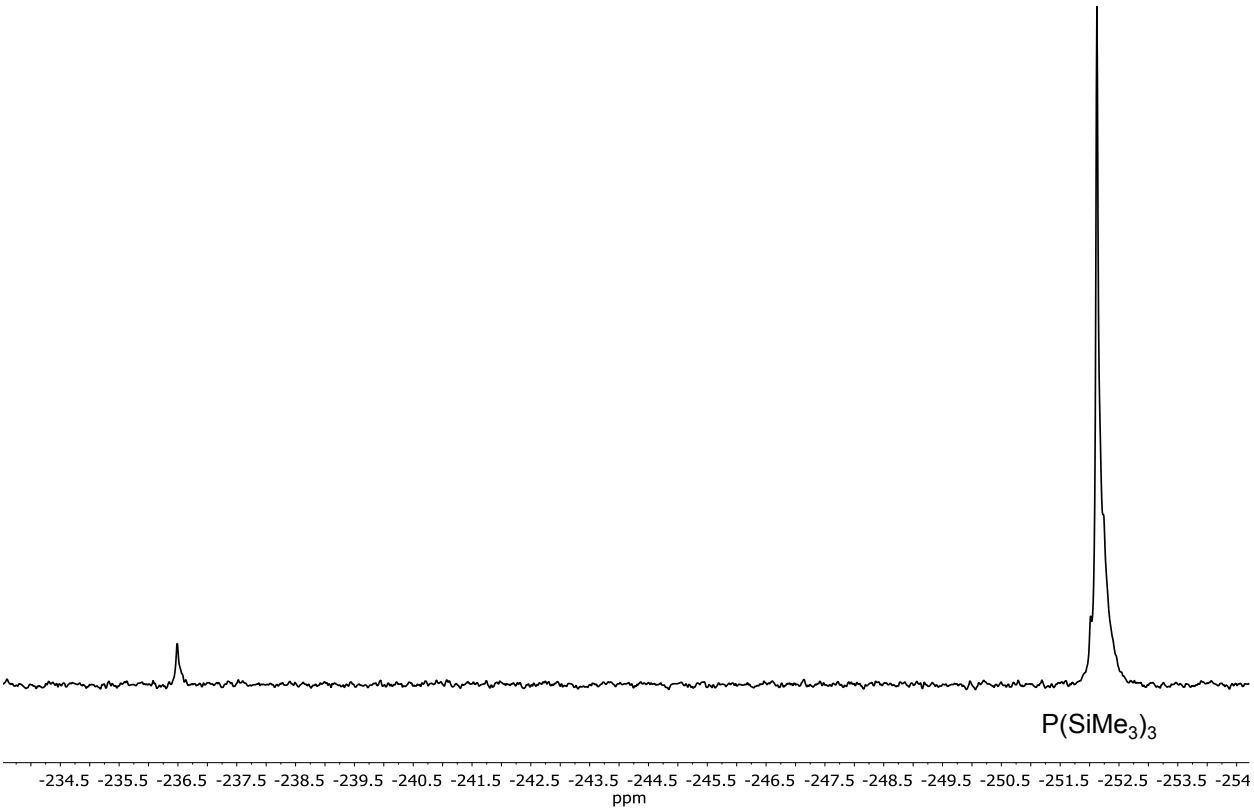

Figure 3.22. $^{31}P\{^{1}H\}$ NMR spectrum of $Zn(OA)_2$-treated particles heated to 130 °C with only $P(SiMe_3)_3$ added, showing that the species at –247 ppm does not form without $ZnEt_2$ present.

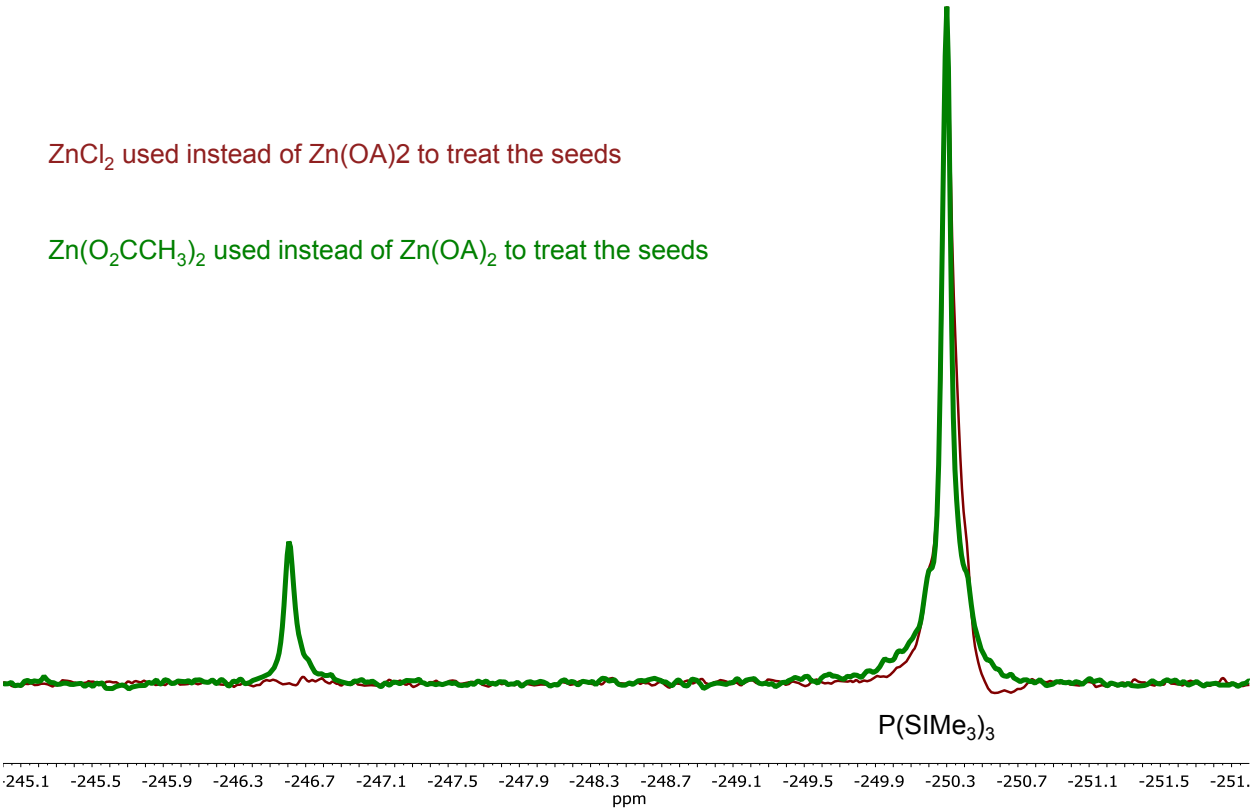

Figure 3.23. $^{31}P\{^{1}H\}$ NMR data of particles treated with $Zn(O_2CCH_3)_2$ (green) or $ZnCl_2$ (red) followed by addition of $ZnEt_2$/$P(SiMe_3)_3$ and heating to 130 °C showing that the species with a chemical shift of –247 ppm can form when $Zn(O_2CCH_3)_2$ is used, but not when $ZnCl_2$ is used.

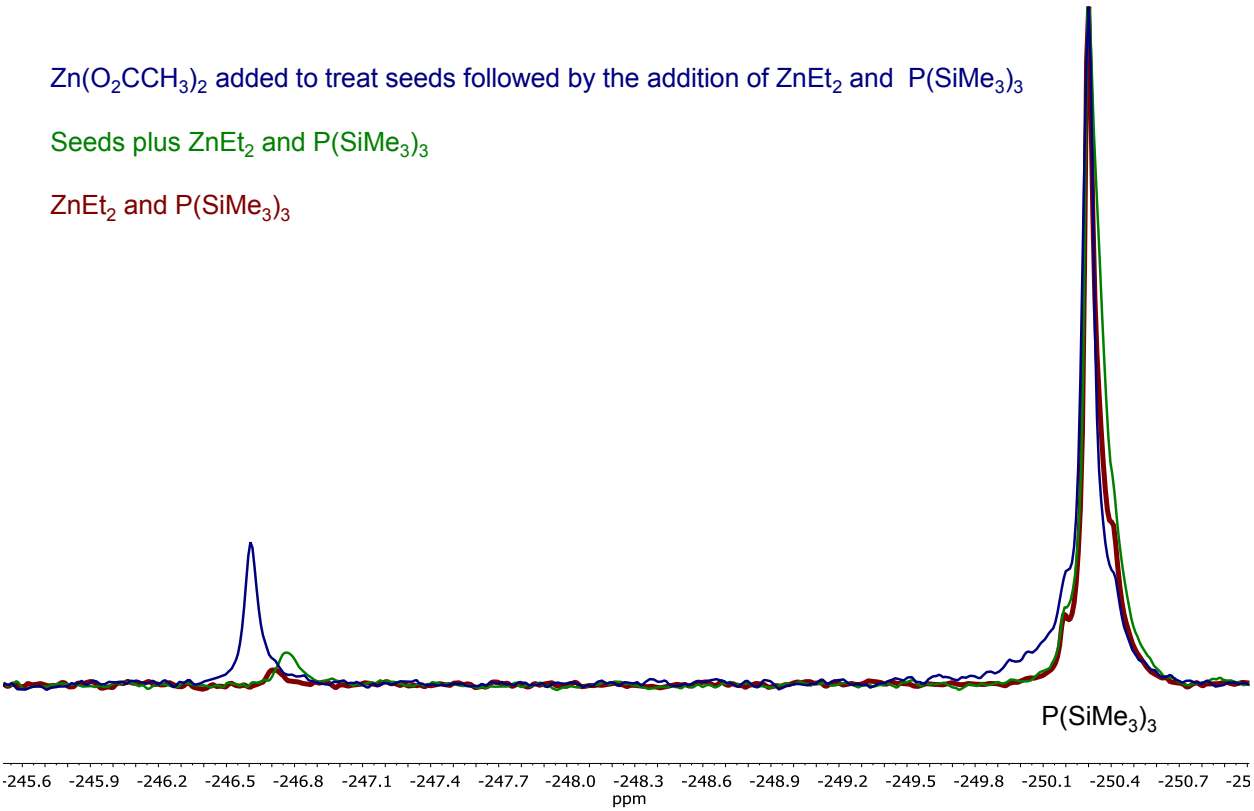

Figure 3.24. $^{31}P\{^{1}H\}$ NMR data of particles treated with $Zn(O_2CCH_3)_2$ (blue) and untreated (green) prior to adding $ZnEt_2/P(SiMe_3)_3$ and heating to 130 °C as well as only $ZnEt_2/P(SiMe_3)_3$ (red) heated to 130 °C showing that the species that comes in at –247 ppm forms in greatest concentration when zinc carboxylate is added to the reaction mixture.

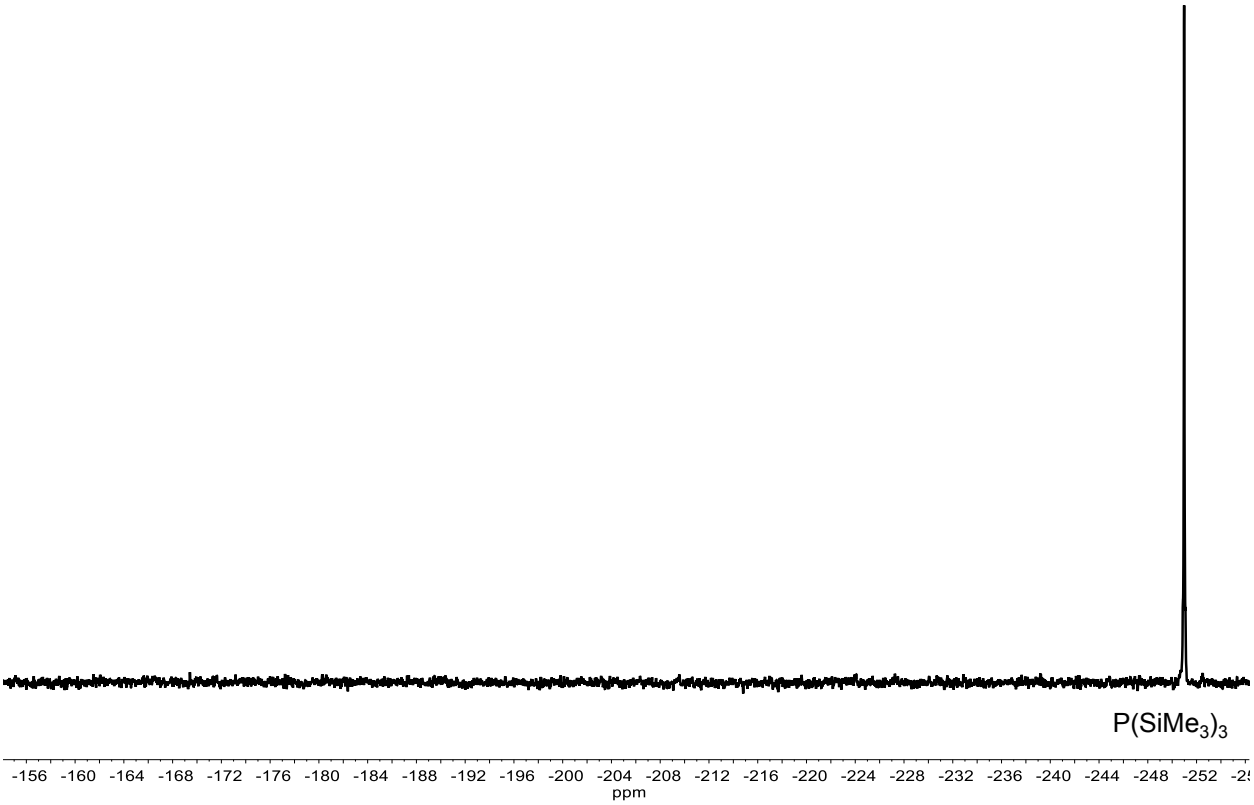

Figure 3.25. $^{31}P\{^{1}H\}$ NMR spectrum of 0.4 Na(OA) + 1.5 $ZnEt_2$ + 1 $P(SiMe_3)_3$ heated to 130 °C for 30 minutes showing no conversion to $[EtZnP(SiMe_3)_2]_3$. This indicates a metal carboxylate is necessary.

Treatment of the 3 nm Zn-rich seeds with $Zn(OA)_2$ generates a soluble and an insoluble reaction component. In order to determine whether the soluble or insoluble component was responsible for the new species, a batch of seeds was treated with $Zn(OA)_2$ and the two components were separated to test this hypothesis (Figure 3.26). Then a mixture of $ZnEt_2$/$P(SiMe_3)_3$ was added to each component separately and showed that the intermediate only forms when added to the insoluble, zinc oleate, portion (Figure 3.27).

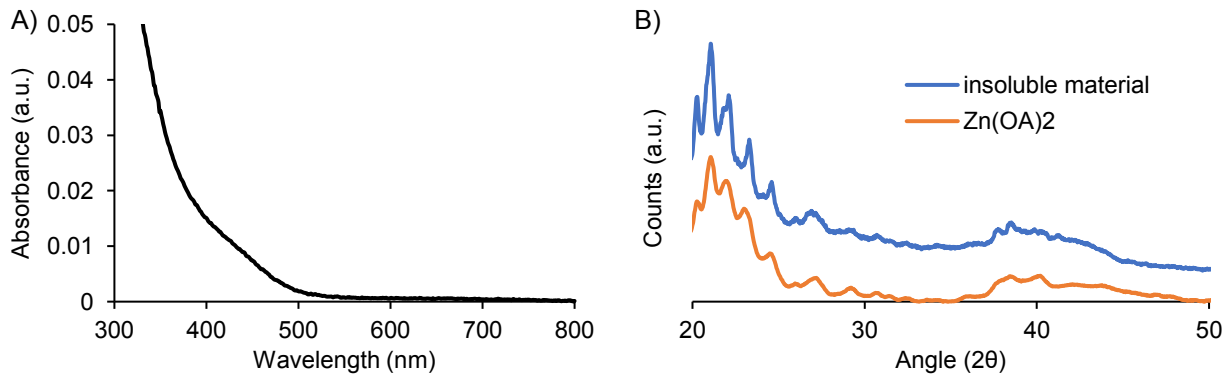

Figure 3.26. UV-vis data (A) of the soluble component following treatment of seeds with $Zn(OA)_2$ and PXRD data (B) of the insoluble material compared to $Zn(OA)_2$.

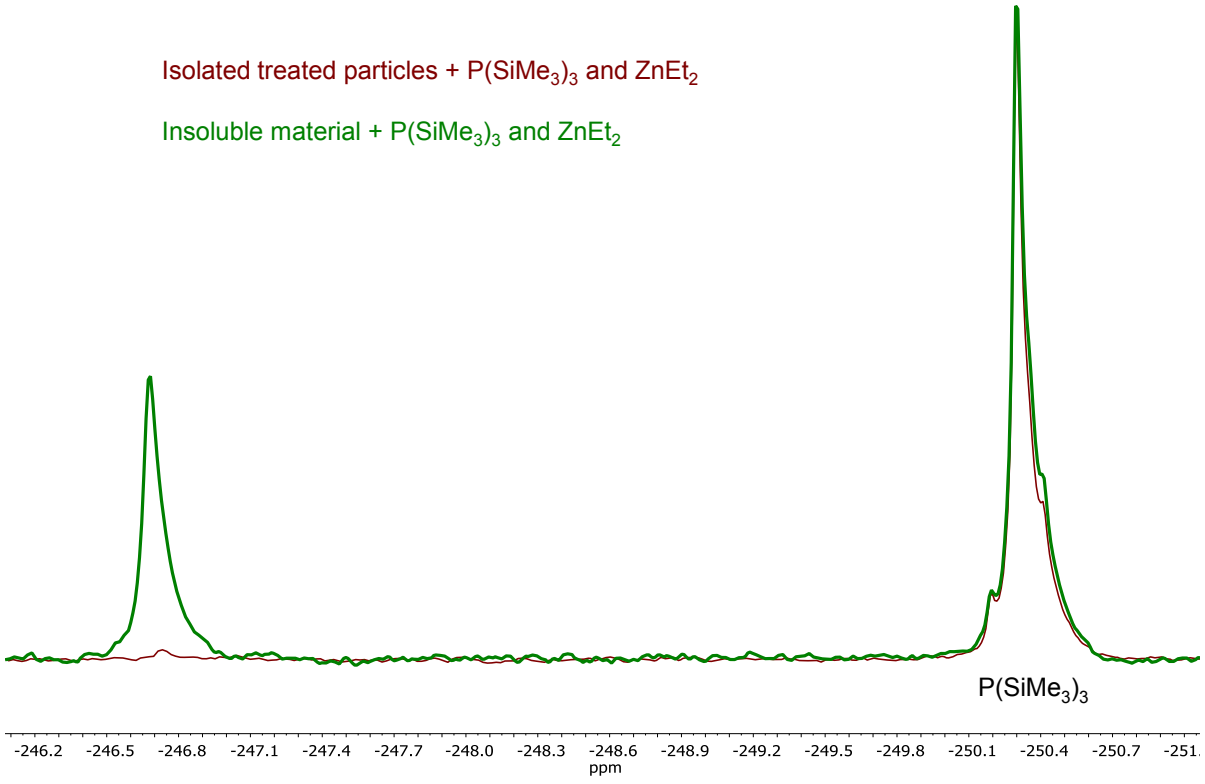

Figure 3.27. $^{31}P\{^{1}H\}$ NMR spectra of a solution containing the soluble component (red) and the insoluble component (green) after adding $ZnEt_2$/$P(SiMe_3)_3$ and heating to 130 °C. These data show that the species that comes in at –247 ppm forms primarily from reaction between the insoluble component ($Zn(O_2CR)_2$), $ZnEt_2$, and $P(SiMe_3)_3$.

Overall it was determined that a metal carboxylate, $ZnEt_2$, and $P(SiMe_3)_3$ were all necessary to form a high yield of the trimer. A small amount of the trimer was observed in the absence of zinc carboxylate, which could be either due to a reaction with $Zn(OA)_2$ in equilibrium with the surface of the particles or through a direct reaction of $P(SiMe_3)_3$ with, or without, a protic impurity followed by reaction with $ZnEt_2$.

3.4.12 Optimization of Growth Conditions

Without the presence of the initial seeds, 67% (20 mg compared to 30 mg) of the yield was collected. The PXRD of this material was poorly resolved indicating the necessity of the seeds being present (Figure 3.28).

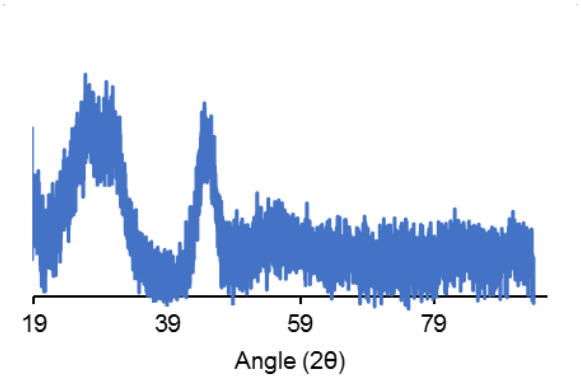

Figure 3.28. PXRD data of heating up $Zn(OA)_2$, $ZnEt_2$, and $P(SiMe_3)_3$ without the presence of the pre-formed seeds.

Both $[EtZnP(SiMe_3)_2]_3$ and additional $ZnEt_2$ and $P(SiMe_3)_3$ were found to be essential for the observed growth on the seeds. When $[EtZnP(SiMe_3)_2]_3$ alone was added to Zn_3P_2 seeds, growth of crystalline Zn_3P_2 was not observed (Figure 3.29).

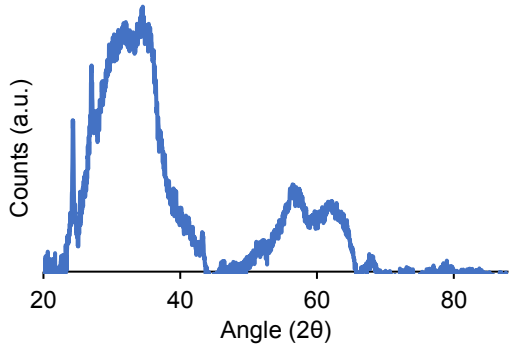

Figure 3.29. PXRD data of the heterogeneous material formed when only $[EtZnP(SiMe_3)_2]_3$ is added to particle seeds.

When 0.6 $P(SiMe_3)_3$ and 1.1 $ZnEt_2$ are added to Zn_3P_2 seeds in the absence of $[EtZnP(SiMe_3)_2]_3$, 33% (10 mg compared to 30 mg) of the yield of Zn_3P_2 was observed (Figure 3.30).

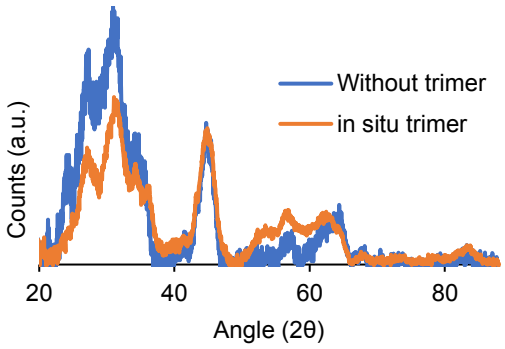

Figure 3.30. PXRD data of the heterogeneous material formed when $P(SiMe_3)_3$ and $ZnEt_2$ are added to particle seeds.

In contrast, addition of a solution containing an appropriate amount of $P(SiMe_3)_3$, $ZnEt_2$, and $[EtZnP(SiMe_3)_2]_3$ to the 3 nm Zn-rich Zn_3P_2 seeds (without addition of $Zn(O_2CR)_2$) resulted

in a brown precipitate, in greater yield (50 mg as compared to 30 mg), that was indistinguishable from the material formed when the trimer was made *in situ* (Figure 3.31).

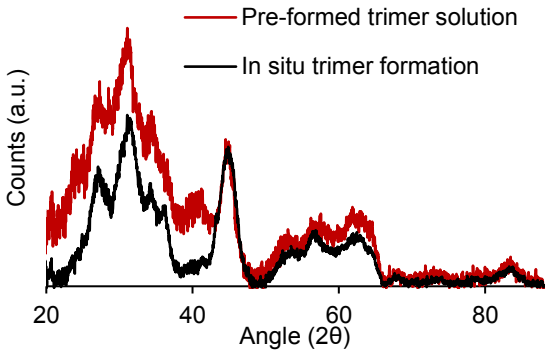

Figure 3.31. PXRD data comparing syntheses where $[EtZnP(SiMe_3)_2]_3$ is formed *in situ* and prior to injection.

3.5 References

1. Nozik, A. J., Quantum dot solar cells. *Physica E* **2002,** *14*, 115-120.
2. McKittrick, J.; Shea-Rohwer, L. E., Review: Down Conversion Materials for Solid-State Lighting. *J. Am. Ceram. Soc.* **2014,** *97*, 1327-1352.
3. Michalet, X.; Pinaud, F. F.; Bentolila, L. A.; Tsay, J. M.; Doose, S.; Li, J. J.; Sundaresan, G.; Wu, A. M.; Gambhir, S. S.; Weiss, S., Quantum Dots for Live Cells, in Vivo Imaging, and Diagnostics. *Science* **2005,** *307*, 538-544.
4. Shirasaki, Y.; Supran, G. J.; Bawendi, M. G.; Bulovic, V., Emergence of colloidal quantum-dot light-emitting technologies. *Nat. Photon.* **2013,** *7*, 13-23.
5. Alivisatos, A. P., Semiconductor clusters, nanocrystals, and quantum dots. *Science* **1996,** *271*, 933-937.

6. Murray, C. B.; Norris, D. J.; Bawendi, M. G., Synthesis and characterization of nearly monodisperse CdE (E = sulfur, selenium, tellurium) semiconductor nanocrystallites. *J. Am. Chem. Soc.* **1993,** *115*, 8706-8715.
7. Hendricks, M. P.; Campos, M. P.; Cleveland, G. T.; Jen-La Plante, I.; Owen, J. S., A tunable library of substituted thiourea precursors to metal sulfide nanocrystals. *Science* **2015,** *348*, 1226-1230.
8. Allen, P. M.; Walker, B. J.; Bawendi, M. G., Mechanistic Insights into the Formation of InP Quantum Dots. *Angew. Chem. Int. Ed.* **2010,** *49*, 760-762.
9. Gary, D. C.; Terban, M. W.; Billinge, S. J. L.; Cossairt, B. M., Two-Step Nucleation and Growth of InP Quantum Dots via Magic-Sized Cluster Intermediates. *Chem. Mater.* **2015,** *27*, 1432-1441.
10. Gary, D. C.; Flowers, S. E.; Kaminsky, W.; Petrone, A.; Li, X.; Cossairt, B. M., Single-Crystal and Electronic Structure of a 1.3 nm Indium Phosphide Nanocluster. *J. Am. Chem. Soc.* **2016,** *138*, 1510-1513.
11. Stuczynski, S. M.; Opila, R. L.; Marsh, P.; Brennan, J. G.; Steigerwald, M. L., Formation of indium phosphide from trimethylindium (In(CH3)3) and tris(trimethylsilyl)phosphine (P(Si(CH3)3)3). *Chem. Mater.* **1991,** *3*, 379-381.
12. Fagen, E. A., Optical properties of Zn3P2. *J. Appl. Phys.* **1979,** *50*, 6505-6515.
13. Bosco, J. P.; Demers, S. B.; Kimball, G. M.; Lewis, N. S.; Atwater, H. A., Band alignment of epitaxial ZnS/Zn3P2 heterojunctions. *J. Appl. Phys.* **2012,** *112*, 093703.
14. Wyeth, N. C.; Catalano, A., Spectral response measurements of minority-carrier diffusion length in Zn3P2. *J. Appl. Phys.* **1979,** *50*, 1403-1407.

15. Bhushan, M.; Catalano, A., Polycrystalline Zn3P2 Schottky barrier solar cells. *Appl. Phys. Lett.* **1981,** *38*, 39-41.

16. Wadia, C.; Alivisatos, A. P.; Kammen, D. M., Materials Availability Expands the Opportunity for Large-Scale Photovoltaics Deployment. *Environ. Sci. Technol.* **2009,** *43*, 2072-2077.

17. Miao, S.; Yang, T.; Hickey, S. G.; Lesnyak, V.; Rellinghaus, B.; Xu, J.; Eychmüller, A., Emissive ZnO@Zn3P2 Nanocrystals: Synthesis, Optical, and Optoelectrochemical Properties. *Small* **2013,** *9*, 3415-3422.

18. Luber, E. J.; Mobarok, M. H.; Buriak, J. M., Solution-Processed Zinc Phosphide (α-Zn3P2) Colloidal Semiconducting Nanocrystals for Thin Film Photovoltaic Applications. *ACS Nano* **2013,** *7*, 8136-8146.

19. Mobarok, M. H.; Luber, E. J.; Bernard, G. M.; Peng, L.; Wasylishen, R. E.; Buriak, J. M., Phase-Pure Crystalline Zinc Phosphide Nanoparticles: Synthetic Approaches and Characterization. *Chem. Mater.* **2014,** *26*, 1925-1935.

20. Glassy, B. A.; Cossairt, B. M., Ternary synthesis of colloidal Zn3P2 quantum dots. *Chem. Commun.* **2015,** *51*, 5283-5286.

21. Ho, M. Q.; Esteves, R. J. A.; Kedarnath, G.; Arachchige, I. U., Size-Dependent Optical Properties of Luminescent Zn3P2 Quantum Dots. *J. Phys. Chem. C* **2015,** *119*, 10576-10584.

22. Rademacher, B.; Schwarz, W.; Westerhausen, M., Heteroleptische Diorganylzink-Verbindungen mit einem Bis (trimethylsilyl) phosphanido-Substituenten. *Z. Anorg. Allg. Chem.* **1995,** *621*, 287-300.

23. Kim, Y. S.; Won, Y. S.; Hagelin-Weaver, H.; Omenetto, N.; Anderson, T., Homogeneous Decomposition Mechanisms of Diethylzinc by Raman Spectroscopy and Quantum Chemical Calculations. *The Journal of Physical Chemistry A* **2008,** *112*, 4246-4253.

24. Stein, J. L.; Mader, E. A.; Cossairt, B. M., Luminescent InP Quantum Dots with Tunable Emission by Post-Synthetic Modification with Lewis Acids. *The Journal of Physical Chemistry Letters* **2016,** *7*, 1315-1320.

25. Frederick, M. T.; Weiss, E. A., Relaxation of Exciton Confinement in CdSe Quantum Dots by Modification with a Conjugated Dithiocarbamate Ligand. *ACS Nano* **2010,** *4*, 3195-3200.

26. Bullen, C.; Mulvaney, P., The Effects of Chemisorption on the Luminescence of CdSe Quantum Dots. *Langmuir* **2006,** *22*, 3007-3013.

27. Talapin, D. V.; Rogach, A. L.; Kornowski, A.; Haase, M.; Weller, H., Highly Luminescent Monodisperse CdSe and CdSe/ZnS Nanocrystals Synthesized in a Hexadecylamine−Trioctylphosphine Oxide−Trioctylphospine Mixture. *Nano Lett.* **2001,** *1*, 207-211.

28. Adolphi, N. L.; Stoddard, R. D.; Goel, S. C.; Buhro, W. E.; Gibbons, P. C.; Conradi, M. S., The 31P NMR spectra of Cd3P2 and Zn3P2. *J. Phys. Chem. Solids* **1992,** *53*, 1275-1278.

29. Tomaselli, M.; Yarger, J. L.; Bruchez, M. J.; Havlin, R. H.; deGraw, D.; Pines, A.; Alivisatos, A. P., NMR study of InP quantum dots: Surface structure and size effects. *J. Chem. Phys.* **1999,** *110*, 8861-8864.

30. Gary, D. C.; Glassy, B. A.; Cossairt, B. M., Investigation of Indium Phosphide Quantum Dot Nucleation and Growth Utilizing Triarylsilylphosphine Precursors. *Chem. Mater.* **2014,** *26*, 1734-1744.

31. Abramoff, M. D., Magalhaes, P. J., Ram, S. J. Biophotonics International 2004, 11, 36-42.

Chapter 4. Synthesis of Zn_3As_2 and $(Cd_yZn_{1-y})_3As_2$ Colloidal Quantum Dots

4.1 Introduction

Quantum dots (QDs) are attractive solution-processable semiconductors for a variety of applications including light harvesting, light emission, and light detection.[1-4] More specifically, QDs that absorb and emit in the infrared (IR) are of interest for telecommunications, *in vivo* imaging, and detecting low energy light.[4-5] Research in this field has primarily focused on III-V (InAs)[6-10] and IV-VI (PbS/PbSe)[11-14] semiconductors. However, II-V materials (Cd_3As_2)[9-10, 15-17] have emerged as attractive candidates for these applications.

The II-V class of semiconductors, specifically Zn_3As_2 and Cd_3As_2, offer several benefits for use in IR optoelectronic technologies. Cd_3As_2 is a semimetal with a band gap of approximately 0 eV, while Zn_3As_2 is a narrow (1 eV) band gap semiconductor, and these two materials can be homogeneously alloyed to achieve a band gap anywhere in that range.[18-19] $(Cd_yZn_{1-y})_3As_2$ is an attractive material to replace $Cd_zHg_{1-z}Te$ given its lower toxicity, wider range of available band gaps, its high compatibility with III-V substrates such as GaAs and InP, and its ability to be tuned between intrinsically n-type (more Cd_3As_2) or p-type (more Zn_3As_2) conductivity.[19-21] Producing such alloys on the nanoscale would allow further tunability of the electronic structure through quantum confinement, and broaden the scope of processing methods for device fabrication. Synthesis of nanoscale $(Cd_yZn_{1-y})_3As_2$ would also provide opportunities to study structure property relationships in this unique class of intrinsically defective materials.[22]

While colloidal Cd_3As_2 nanocrystals were first prepared in 1985,[23] and vapor deposited Zn_3As_2 nanocrystals have been reported,[18, 24-26] there is no literature precedent for the synthesis of colloidal Zn_3As_2 or $(Cd_yZn_{1-y})_3As_2$ QDs.

4.2 Results and Discussion

4.2.1 Synthesis of Zinc Arsenide Quantum Dots

Our approach to access these colloidal materials is to take advantage of the elevated reactivity of mixed zinc alkyl carboxylate oligomeric precursors, which our group has previously developed for the synthesis of zinc phosphide QDs (Scheme 4.1).[27]

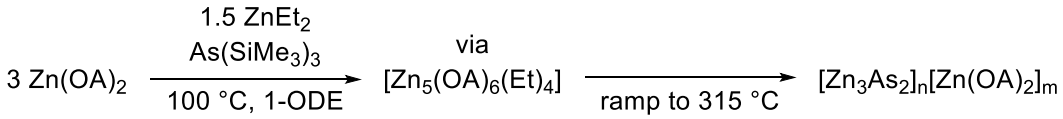

Scheme 4.1. Synthetic scheme for accessing zinc-rich Zn_3As_2 QDs. Where OA: $O_2C(CH_2)_7CH{=}CH(CH_2)_7CH_3$.

Briefly, $Zn(OA)_2$, $ZnEt_2$, and $As(SiMe_3)_3$ are combined at 100 °C and then the temperature is raised to 315 °C. It was found that when immediately ramping the temperature to 315 °C, a brown precipitate containing 5 nm Zn_3As_2 formed (Figure 4.1). When heating up to 315 °C at a rate of approximately 3 °C per minute, the resulting nanocrystals maintained colloidal stability and a resolved lowest energy excitonic transition (LEET) was observed to shift as a function of time and temperature (Figure 4.2A).[28] Further characterization showed that these particles are weakly luminescent (quantum yield < 1%) and have a diameter of 2.8 ± 0.4 nm (Figure 4.2B). Like with

Zn_3P_2, not using $ZnEt_2$ resulted in low quality material without the presence of a LEET (Figure 4.3).[27]

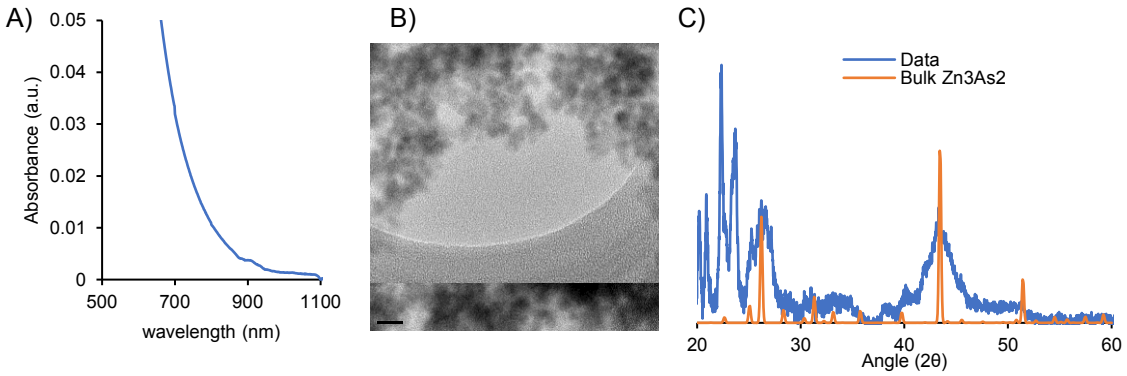

Figure 4.1. (A) UV-Vis spectrum of soluble portion of the reaction after removal of heterogenous material. (B) TEM of heterogenous material with an average size ~4.6 nm. (C) PXRD of heterogeneous portion compared to bulk Zn_3As_2 (PDF 01-089-3431) with Scherrer analysis of the major peak indicating ~4.6 nm particles. The sharp peaks between 20 and 25 2θ could be due to $Zn(OA)_2$ that is still present.[29]

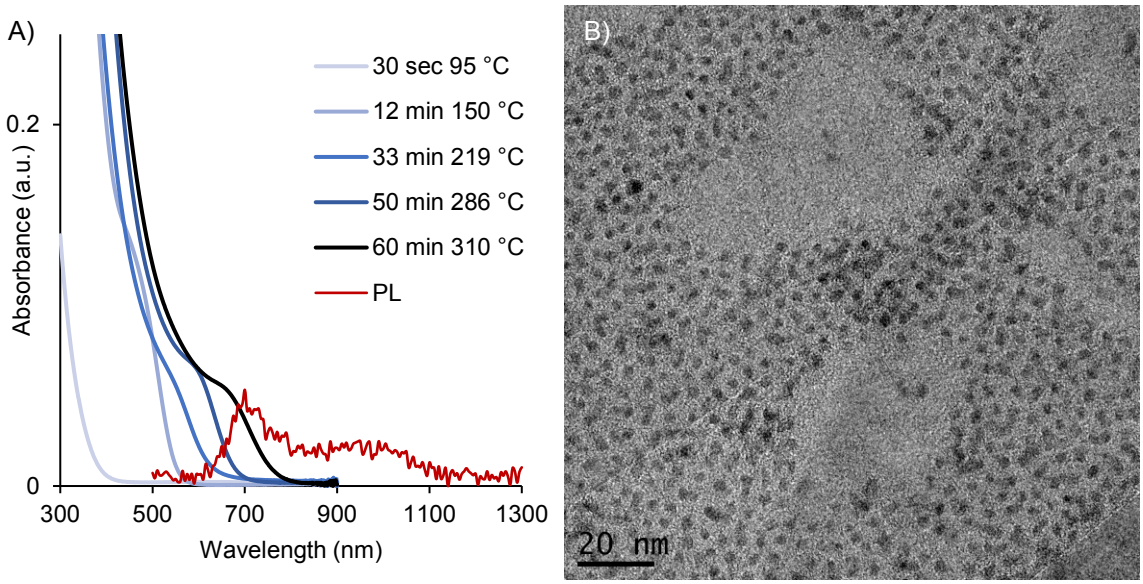

Figure 4.2. (A) UV-Vis data showing the temporal evolution of zinc arsenide quantum dots and the room temperature photoluminescence (PL) spectrum of isolated particles. (B) Transmission electron microscopy image showing spherical particles with an average diameter of 2.8 ± 0.4 nm for 311 particles measured (Figure 4.4).

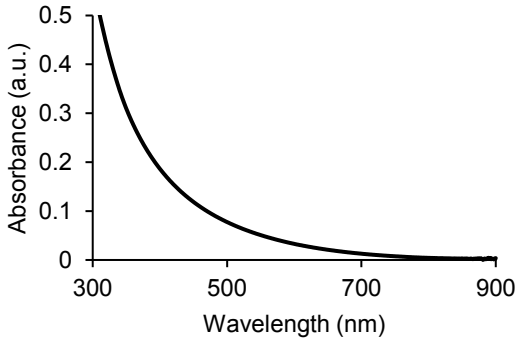

Figure 4.3. UV-Vis data of the resulting material when $ZnEt_2$ is not used in the reaction following Scheme 4.1 with the slower ramp rate.

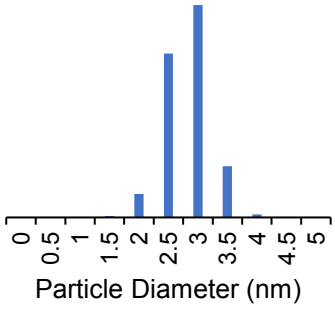

Figure 4.4. Histogram of particle diameters for Zn_3As_2 QDs grown for 60 minutes (315 °C). 311 particles were measured and the average size was determined to be 2.8 ± 0.4 nm.

4.2.2 Importance of Using $Zn(OA)_2$ and $ZnEt_2$ in the Precursor Conversion

Previously our group has shown that the use of both $ZnEt_2$ and $Zn(OA)_2$ is critical to the synthesis of high-quality Zn_3P_2 QDs because during the precursor conversion process, $ZnEt_2$ and $Zn(OA)_2$ react first to form $[Zn_5(OA)_6(Et)_4]$[30], which exhibits markedly enhanced reactivity with $P(SiMe_3)_3$ compared to either $ZnEt_2$ or $Zn(OA)_2$ alone.[27] To highlight the importance of using the two-zinc precursor approach in the synthesis of Zn_3As_2, we probed the precursor conversion chemistry using ^1H nuclear magnetic resonance (NMR) spectroscopy. As was the case with $P(SiMe_3)_3$, no reaction was observed between $As(SiMe_3)_3$ and $ZnEt_2$ at room temperature over the course of seven days (Figure 4.5), and the half-life for the reaction between $As(SiMe_3)_3$ and $Zn(O_2CCH_3)_2$ was estimated to be 14 days at room temperature (Figure 4.6).[28] It is interesting to note that this half-life is more than an order of magnitude longer than the analogous reaction between $P(SiMe_3)_3$ and $Zn(O_2CCH_3)_2$. However, upon pre-forming the $[Zn_5(O_2CCH_3)_6(Et)_4]$ cluster, the half-life for its reaction with $As(SiMe_3)_3$ was observed to be <5 minutes, similar to what was observed for the reaction with $P(SiMe_3)_3$ (Figure 4.7).[28] This result highlights the

dramatic range over which the reactivity of Zn^{2+} with As^{3-} can be tuned. We hypothesize that the enhanced precursor conversion rate that results from using both $ZnEt_2$ and zinc carboxylate leads to an increase in the rate of monomer formation and supersaturation, enabling burst-like nucleation in this system.[31]

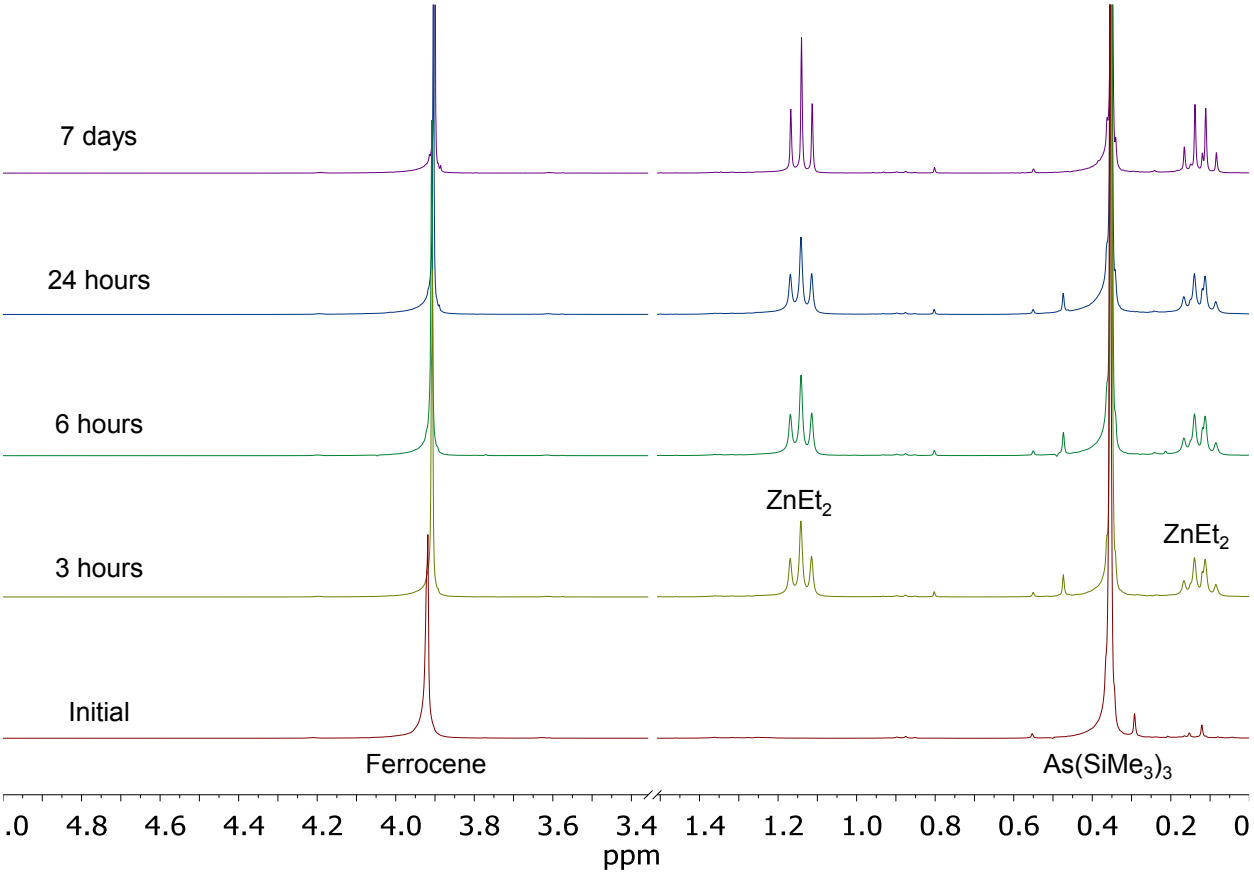

Figure 4.5. Room temperature monitoring of the reaction between 1.5 $ZnEt_2$ and 1 $As(SiMe_3)_3$ with an internal standard of ferrocene. These data show no appreciable reaction between these two reagents at room temperature.

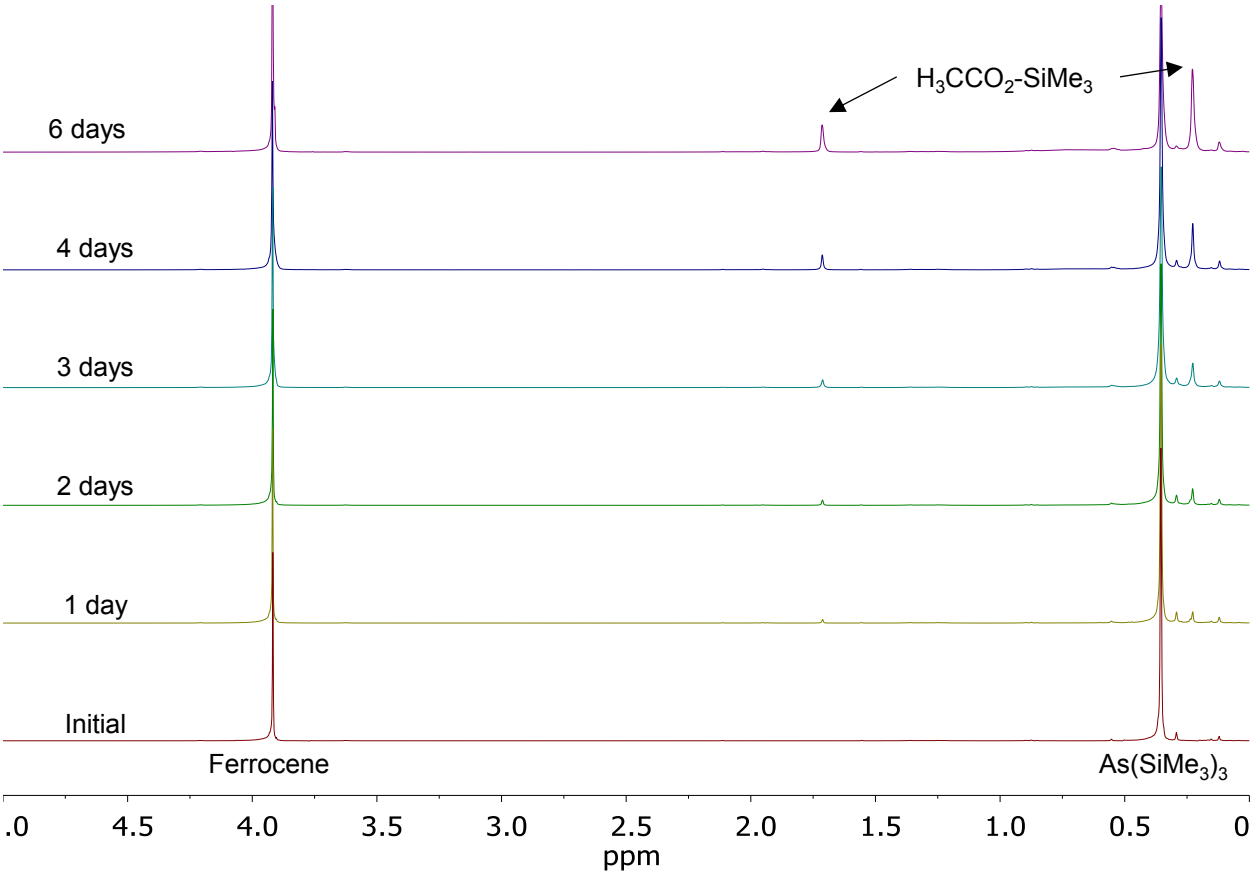

Figure 4.6. Room temperature monitoring of the reaction between 3 $Zn(O_2CCH_3)_2$ and 1 $As(SiMe_3)_3$ with an internal standard of ferrocene. These data show a very slow reaction between these two reagents.

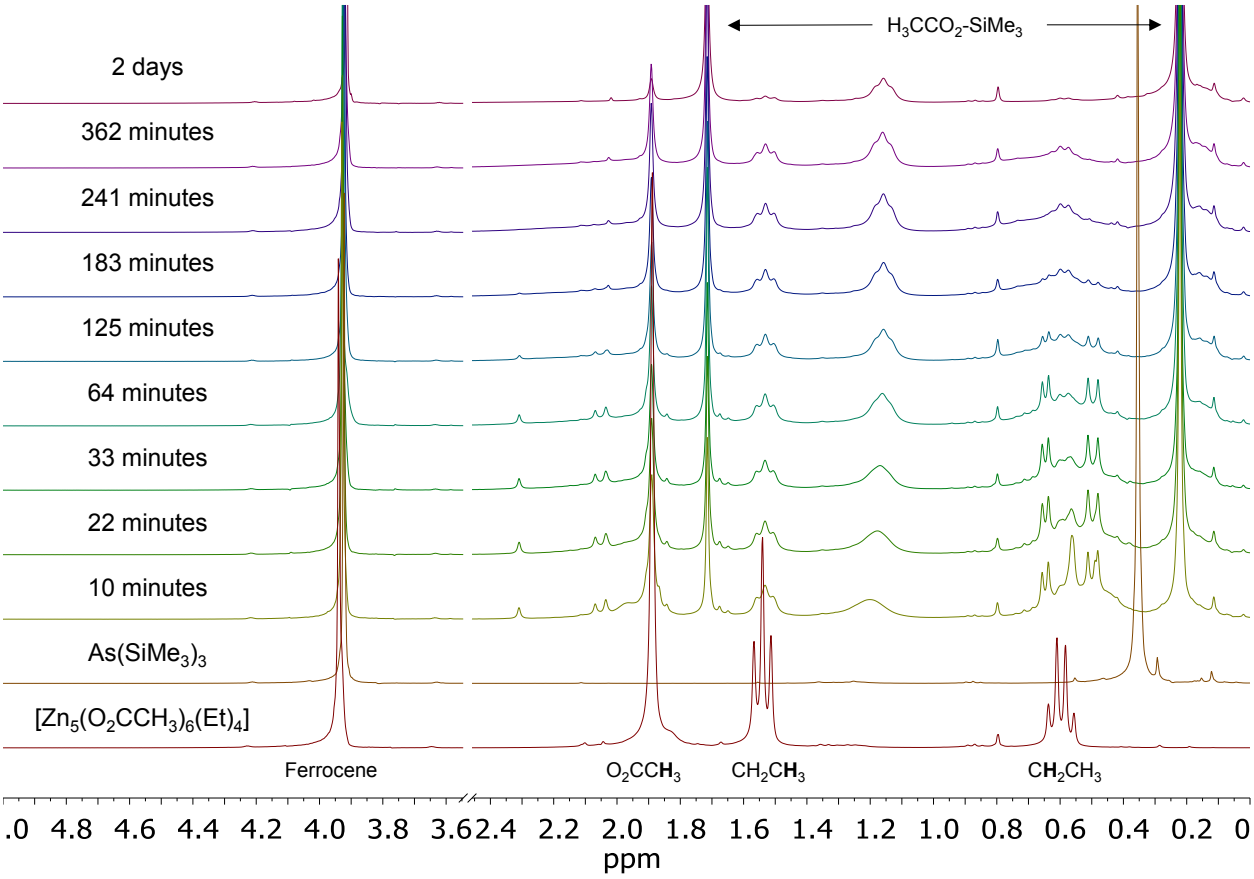

Figure 4.7. Room temperature monitoring of the reaction between $[Zn_5(O_2CCH_3)_6(Et)_4]$ (made from 3 equivalents $Zn(O_2CCH_3)_2$ and 1.5 equivalents $ZnEt_2$) and 1 $As(SiMe_3)_3$ with an internal standard of ferrocene. These data show a very fast reaction between these reagents.

4.2.3 Synthesis of (Cd$_y$Zn1-y)3As2 Colloidal Quantum Dots

To extend the absorption and emission spectra of these II-V QDs into the near-IR we explored the synthesis of a ternary alloy with Cd^{2+} by replacing 0-35% of the $Zn(OA)_2$ in the original synthesis with $Cd(O_2CCH_3)_2$ (Scheme 4.2). In reactions containing Cd^{2+}, it was necessary to maintain the reaction temperature below 250 °C to prevent formation of bulk material (Figure 4.8).

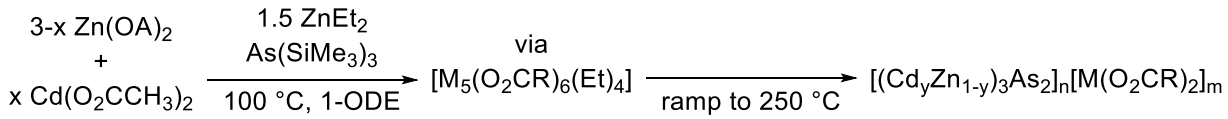

Scheme 4.2. Synthesis of cation-rich $(Cd_yZn_{1-y})_3As_2$ QDs. Where R: CH_3 or $(CH_2)_7CH{=}CH(CH_2)_7CH_3$ and M: Cd or Zn.

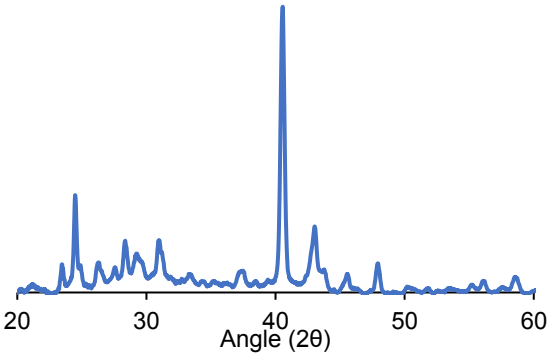

Figure 4.8. PXRD data for a reaction using 15% cadmium acetate and heating up to 315 °C.

Under these conditions the LEET could be varied from 560 nm (2.20 eV, 0% Cd) to 1000 nm (1.24 eV, 35% Cd) (Figure 4.9 for 0, 15, 25, and 35% and Figure 4.10 for 5 and 10%). Replacing additional $Zn(OA)_2$ with either $Cd(O_2CCH_3)_2$ or $Cd(OA)_2$ did not result in material with a smaller band gap (Figure 4.11). Heating up Zn_3As_2 particles in the presence of $Cd(O_2CCH_3)_2$ did not result in stable material.

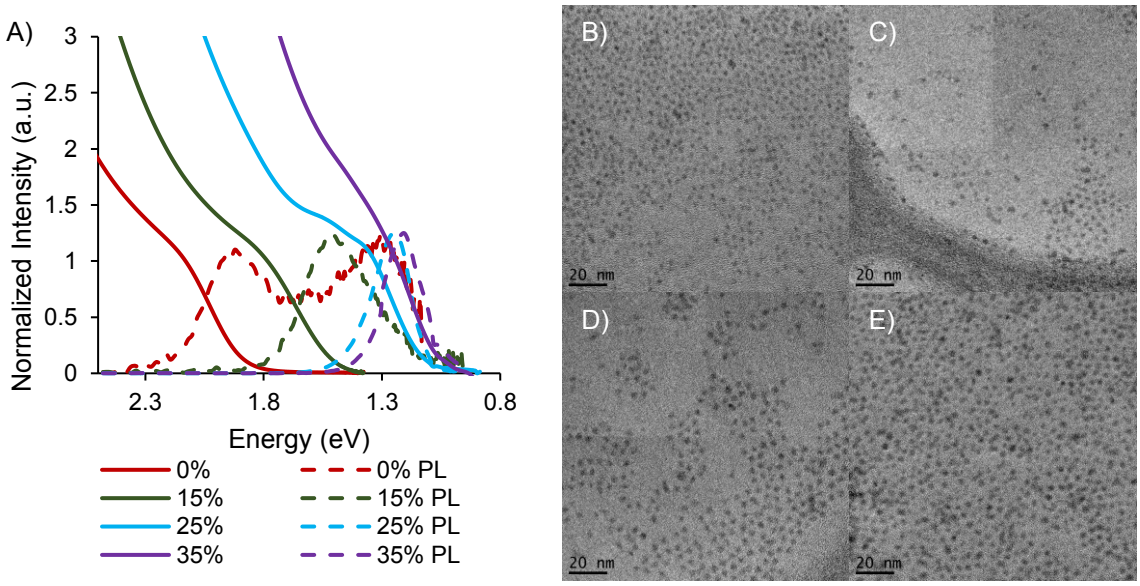

Figure 4.9. (A) UV-Vis data showing the shift to lower energy as more $Cd(O_2CCH_3)_2$ is used in the synthesis. The UV-Vis data for the 35% sample was smoothed to remove noise from the detector changeover (Figure 4.12 for unsmoothed data). All PL intensities were converted using a Jacobian conversion.[32] TEM images of particles prepared using 0% (B), 15% (C), 25% (D), and 35% (E) $Cd(O_2CCH_3)_2$. See Figure 4.13 for the size distributions.

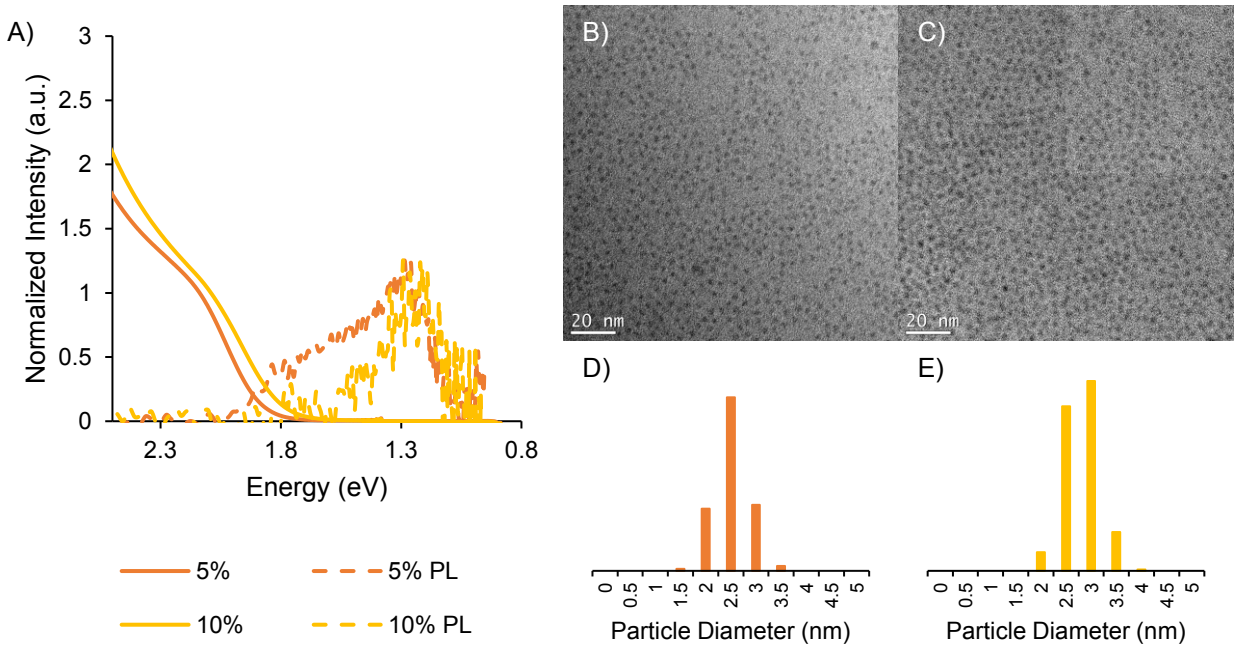

Figure 4.10. (A) UV-Vis (solid) and Fluorescence (dashed) data for samples made with 5 and 10% cadmium. All PL intensities were converted using a Jacobian conversion.[32] (B) TEM of the 5% sample. (C) TEM of the 10% sample. (D) Histogram of diameters for the 5% sample where 308 particles were measured yielding a size of 2.5 ± 0.4 nm. (E) Histogram of diameters for the 10% sample where 309 particles were measured yielding a size of 2.8 ± 0.4 nm.

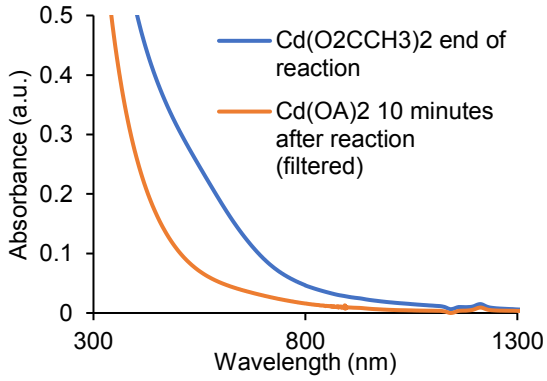

Figure 4.11. UV-Vis data from two reactions where 50% cadmium carboxylate was used. When $Cd(O_2CCH_3)_2$ was used (blue), the reaction did not yield material with a lower band gap. When $Cd(OA)_2$ was used (orange), the reaction turned heterogeneous after ten minutes leaving large band-gap material left in solution.

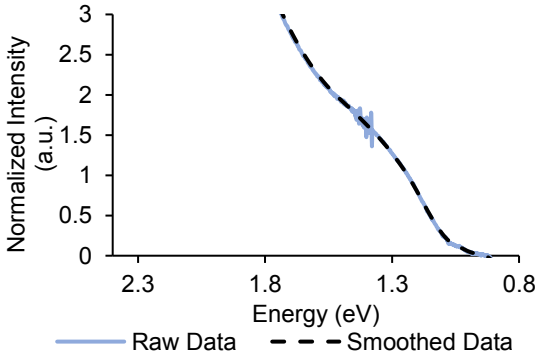

Figure 4.12. Raw and smoothed UV-Vis data for the 35% cadmium sample showing minimal change when smoothed.

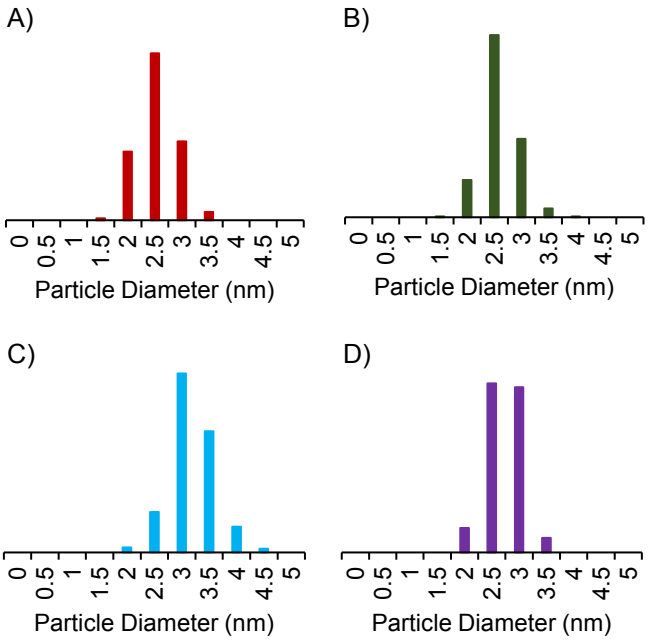

Figure 4.13. (A) Histogram of diameters for the 0% sample where 317 particles were measured yielding a size of 2.5 ± 0.4 nm. (B) Histogram of diameters for the 15% sample where 315 particles were measured yielding a size of 2.6 ± 0.3 nm. (C) Histogram of diameters for the 25% sample where 306 particles were measured yielding a size of 3.2 ± 0.4 nm. (D) Histogram of diameters for the 35% sample where 305 particles were measured yielding a size of 2.7 ± 0.3 nm.

All QDs prepared by this method were luminescent with total quantum yields ranging from <1 to 60% (Figure 4.9A, 4.10, and Table 4.1). The presence of a second, more red-shifted luminescence peak was only observed in the case of 0, 5, and 10% cadmium. As more cadmium was introduced into the lattice, the shift between the LEET and PL maximum decreased from 300 meV to 30 meV. The presence of a highly red shifted peak (Δ>800 meV) is no longer present once more than 10% Cd is used. This, along with the reduction in the red shift from 300 to 30 meV indicates that the number of traps (either on the surface or in the core) decreases as more cadmium is used.

Table 4.1. Photoluminescence quantum yield and emission shifts for all samples.

X% Cadmium	Pl QY	LEET (eV)	PL max (eV)	Δ (meV)	FWHM (meV)
0	1%	2.21	1.93, 1.32	280, 890	294, 365
5	<1%	2.14	1.75, 1.3	390, 840	294, 247
10	<1%	2.09	1.26	830	271
15	4%	1.79	1.51	280	271
25	60%	1.33	1.25	80	165
35	13%	1.24	1.21	30	177

4.2.4 Structural Characterization of Alloyed Quantum Dots

Transmission electron microscopy (TEM) images of these samples show that while the absorption onset is dramatically changing, the particle size stays relatively constant, with average nanocrystal diameters of 2.4 ± 0.4 (0% Cd), 2.5 ± 0.4 (5% Cd), 2.8 ± 0.4 (10% Cd), 2.6 ± 0.3 (15% Cd), 3.2 ± 0.4 (25% Cd), and 2.7 ± 0.3 nm (35% Cd) (Figures 4.9B and 4.10). This suggests that the observed narrowing of the optical band gap on incorporation of Cd indeed results from alloying as opposed to a change in particle size. Furthermore, the relatively constant final nanocrystal size suggests that although the ratio of cadmium to zinc carboxylate is changing, the number of nuclei that form may be similar given that all syntheses are limited by the amount of arsenic present.

Further evidence for alloying can be seen in the powder X-ray diffraction (PXRD) data of these samples (Figure 4.14). It has been shown that the Zn_3As_2-Cd_3As_2 alloy system obeys Vegard's law.[19] The <400> reflection between 40.2 and 44.2 2θ was analyzed giving the percentage of Cd_3As_2 in the nanocrystals at 0%, 33%, 48%, 58%, 69% and 72% when 0, 5, 10, 15, 25 and 35% cadmium acetate was used in the synthesis. Scherrer analysis shows that the particle diameter is not changing significantly (2-3 nm for all samples, Table 4.2), which is in agreement with the TEM data (Figure 4.9 B-E and Figure 4.10 B-C).

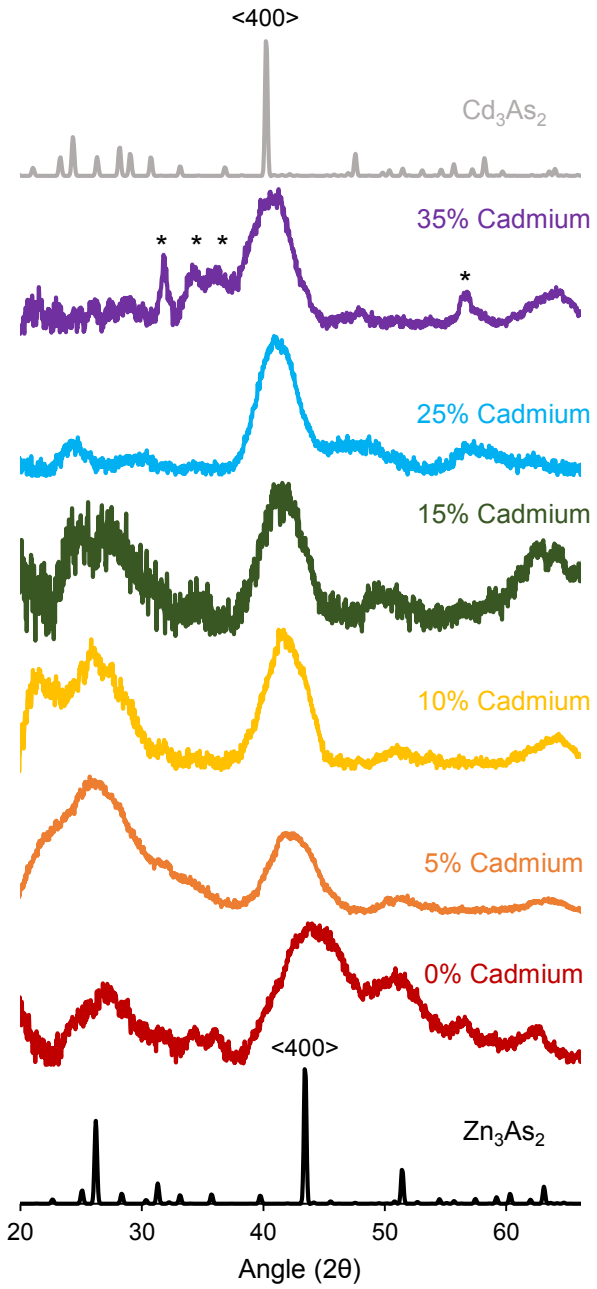

Figure 4.14. PXRD data of the nanocrystals obtained when 0 – 35% percent of the zinc oleate was replaced with cadmium acetate compared to bulk patterns of Zn_3As_2 and Cd_3As_2 (PDF 01-089-3431 and 73-809 respectively). *ZnO impurity (PDF 01-074-0534) arises from decomposition of unreacted zinc carboxylate under these conditions.[33]

Table 4.2. Scherrer analysis of PXRD samples.

X% Cadmium	Scherrer Analysis Diameter (nm)
0	1.8
5	2.6
10	3.2
15	3.0
25	3.0
35	3.0

However, the compositions determined by inductively coupled plasma optical emission spectroscopy (ICP-OES) do not agree with the PXRD analysis when <25% cadmium is used (Table 4.3). While there is still a preference for cadmium incorporation, it is not as drastic as the PXRD data would indicate. As a third way of approximating the percent of cadmium incorporated, Vegard's law was applied to the position of the LEET. 2.2 eV was used as the LEET of 3 nm Zn_3As_2 and 1.22 eV was used as the LEET of 3 nm Cd_3As_2.[15] This analysis ignores the slight bowing in the band gap versus composition that has been observed in bulk II_3V_2 alloys.[26, 34-35]

Table 4.3. Molar ratios of Zn:Cd:As of all samples grown for 45 minutes.

X% Cadmium	Zn	Cd	As
0	6.8	0	2
5	4.4	0.1	2
10	5.9	0.3	2
15	4.0	0.7	2
25	3.5	1.8	2
35*	3.8	2.2	2

*Amount of Zn is artificially high given the presence of a ZnO impurity.

Figure 4.15 compares all three methods for assessing the percent cadmium incorporation. The UV-Vis data appears to match well with the ICP values. This could indicate that using the

position of the <400> reflection and Vegard's law is not a good method for measuring low concentrations of cadmium in this alloy system due to the potential inhomogeneity of cadmium incorporation into the bulk unit cell. This highlights one complication that arises when translating structural parameters from a large, 40 atom, anisotropic unit cell to nanoscale crystallites. Another potential explanation for the difference in composition when <25% cadmium is used is that the resulting particles could be gradient alloys. If the cadmium concentration is highest in the core, this would explain why the apparent cadmium arsenide percentage determined by PXRD is artificially high compared with the other two methods.

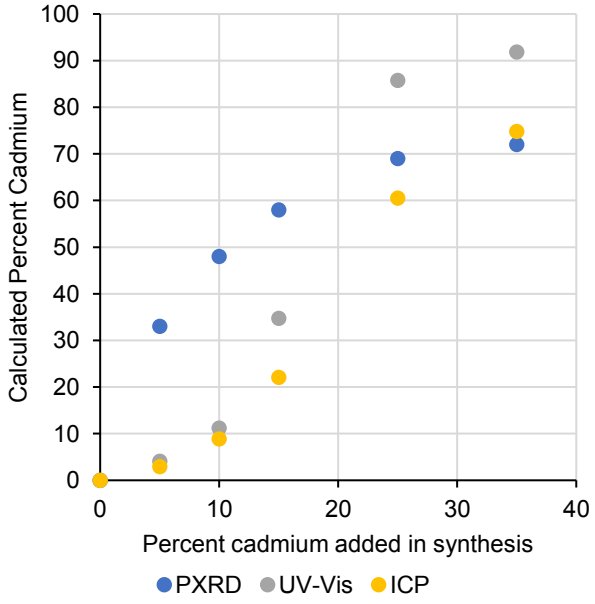

Figure 4.15. Comparison between three methods of calculating the percent cadmium in $(Cd_yZn_{1-y})_3As_2$ QDs compared to the amount used in the synthesis.

4.2.5 Precursor Conversion is Responsible for Enhanced Cadmium Incorporation

Despite differences observed between the methods used to extract composition, all the data suggest that Cd-As bonds are forming faster than Zn-As bonds since the amount of Cd incorporated exceeds the amount introduced into the reaction mixture. Standard thermodynamic values for the bond dissociation energies of Zn-As and Cd-As bonds are not available, however the values for the metal bromides (Zn-Br 33 kcal/mol and Cd-Br 38 kcal/mol) versus the corresponding M-O bond dissociation energies (Zn-O 67 kcal/mol and Cd-O 55 kcal/mol) support these observed kinetics.[36] Further evidence supporting this claim is that the rate of formation of semiconductor units, as measured by the high-energy absorbance intensity, increases as cadmium is introduced into the reaction mixture (Figure 4.16).[37]

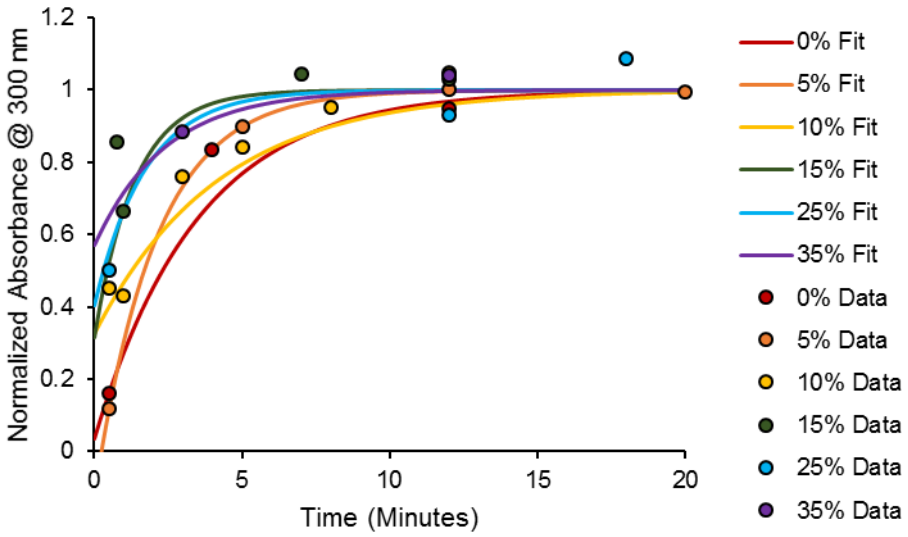

Figure 4.16. Normalized absorbance at 300 nm as a function of time as well as exponential fits for all samples. The 45 minute aliquot was set to 1, except for the 5% data where the max was set to 1.

^{1}H NMR spectroscopy was again employed to probe the reactivity of $Cd(O_2CCH_3)_2$ with the other reagents to account for the preferential incorporation of Cd^{2+} into these nanomaterials. The room temperature half-life of the reaction between $Cd(O_2CCH_3)_2$ and $As(SiMe_3)_3$ was determined to be 1.7 days (Figure 4.17).[28] It was found, however, that $Cd(O_2CCH_3)_2$ reacts with $ZnEt_2$ to form a new species in solution over the course of six hours (Figure 4.18). NMR, ICP, and combustion analysis of the resulting material supports formation of an oligomeric species containing both cadmium and zinc with a single acetate environment (1.86 ppm) and two distinct ethyl environments (1.59 and 1.33 ppm), in analogy with what is observed when $Zn(O_2CCH_3)_2$ and $ZnEt_2$ are combined.

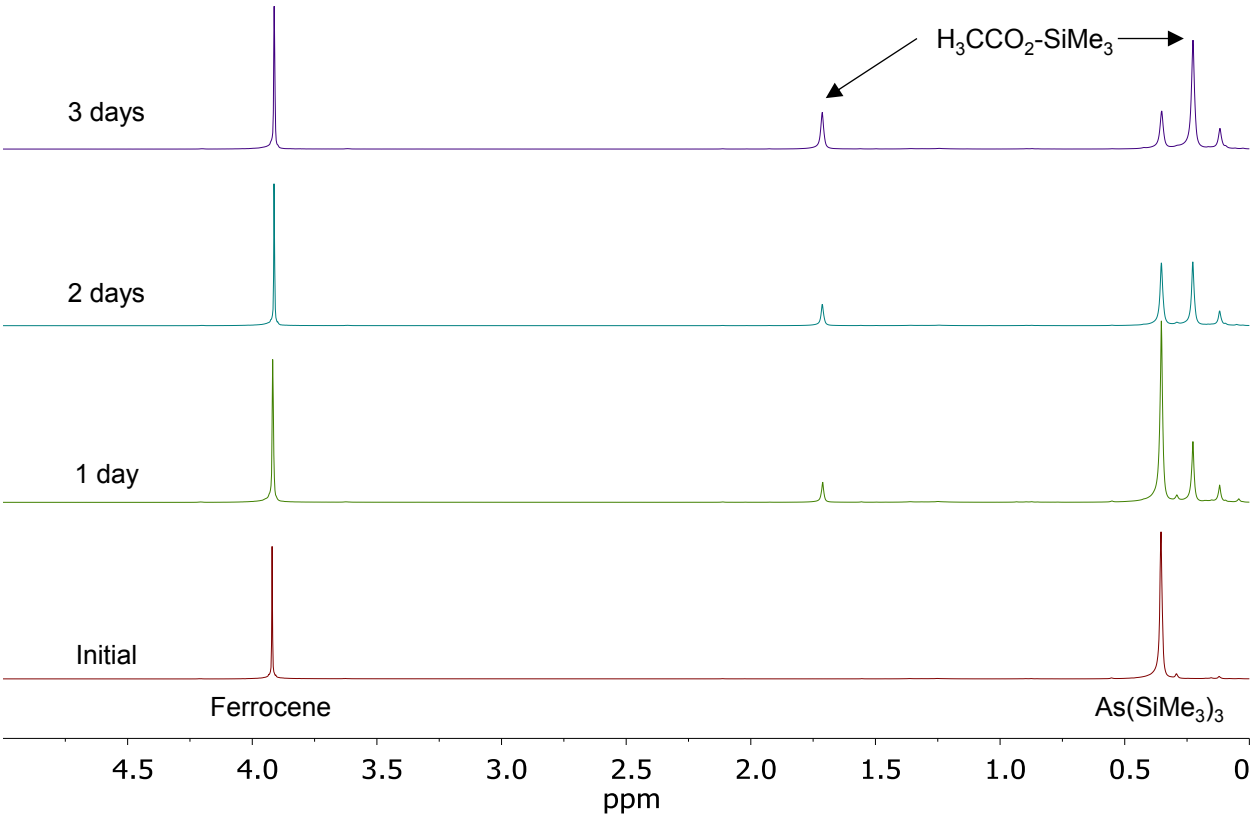

Figure 4.17. Room temperature monitoring of the reaction between 3 $Cd(O_2CCH_3)_2$ and 1 $As(SiMe_3)_3$ with an internal standard of ferrocene. These data show a slow reaction between these two reagents.

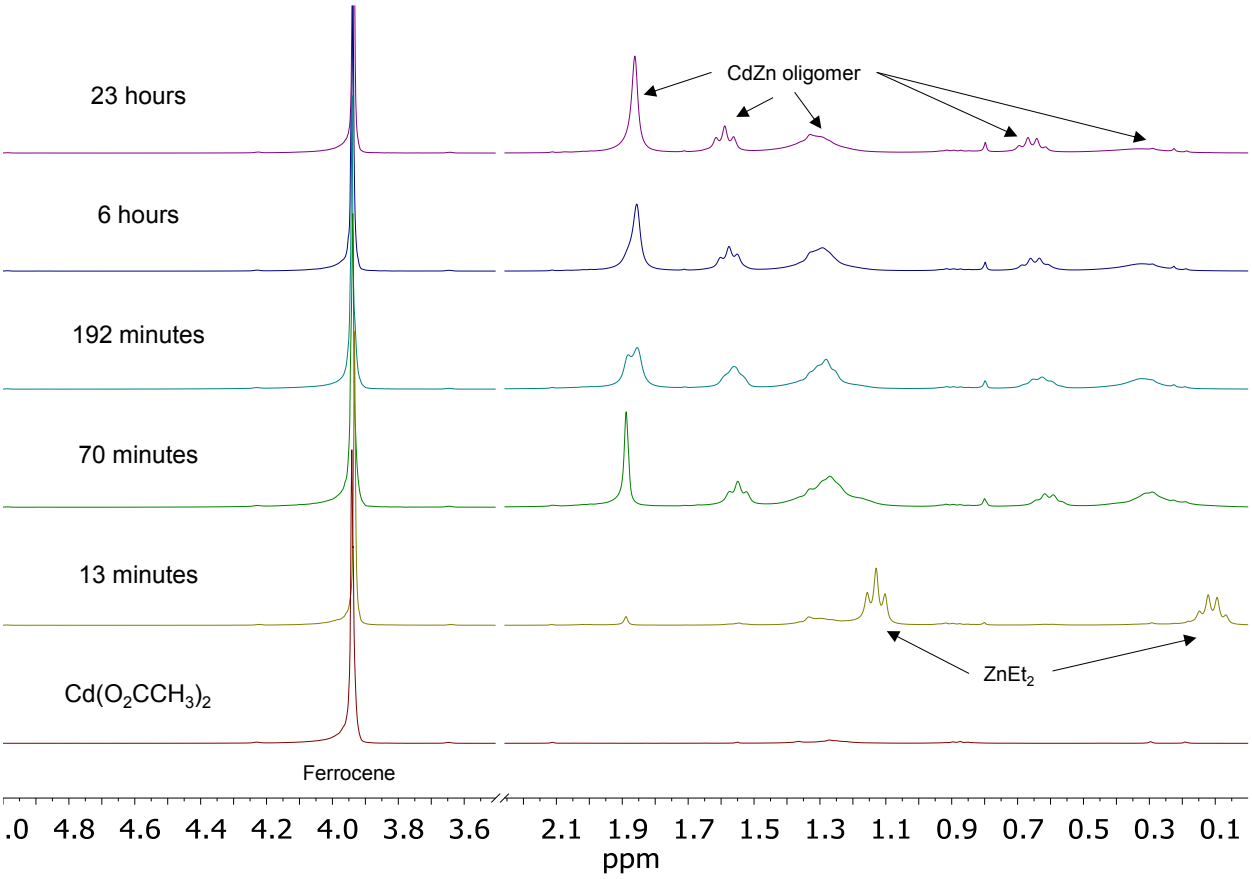

Figure 4.18. Room temperature reaction between 3 $Cd(O_2CCH_3)_2$ and 1.5 $ZnEt_2$ with an internal standard of ferrocene showing the formation of a new cluster similar to that of $[Zn_5(O_2CCH_3)_6(Et)_4]$, but with two different ethyl environments.

The room temperature half-life of the reaction between this new zinc and cadmium containing cluster and $As(SiMe_3)_3$ was found to be <6.5 minutes (Figure 4.19).[28] While the reactivity with $As(SiMe_3)_3$ is enhanced in the presence of $ZnEt_2$, it is also possible that at elevated temperatures $Cd(O_2CCH_3)_2$ could directly react with $As(SiMe_3)_3$. To probe the competition between zinc and cadmium in this reaction, an NMR experiment was set up that used equimolar amounts of zinc and cadmium carboxylate (Figure 4.20). At the reaction endpoint, only unreacted $[Zn_5(O_2CCH_3)_6(Et)_4]$ was observed (Figure 4.21). Additionally, the relative amount of unreacted

$[Zn_5(O_2CCH_3)_6(Et)_4]$ relative to the $Me_3SiO_2CCH_3$ co-product was much greater than when no cadmium acetate was used, suggesting that the acetates of cadmium reacted preferentially with $As(SiMe_3)_3$ (Figure 4.20). This experiment suggests that the Cd-containing clusters react preferentially to pure zinc clusters, supporting the observation of preferential Cd incorporation into the resulting $(Cd_yZn_{1-y})_3As_2$ QDs, which agrees with the high-energy UV-Vis data.

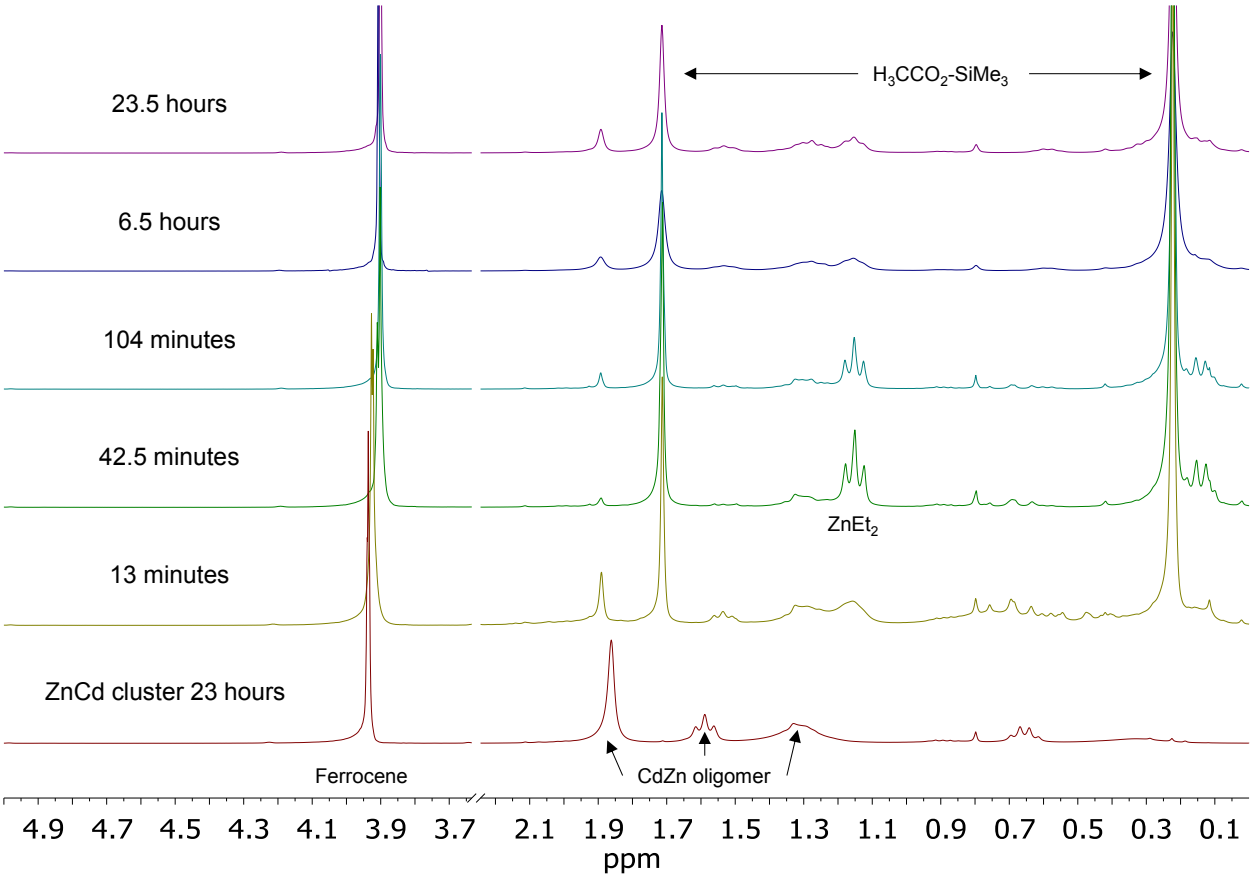

Figure 4.19. Room temperature monitoring of the reaction between a cluster containing Zn and Cd (made from 3 $Cd(O_2CCH_3)_2$ and 1.5 $ZnEt_2$) and 1 $As(SiMe_3)_3$ with an internal standard of ferrocene. These data show a very fast reaction between these reagents.

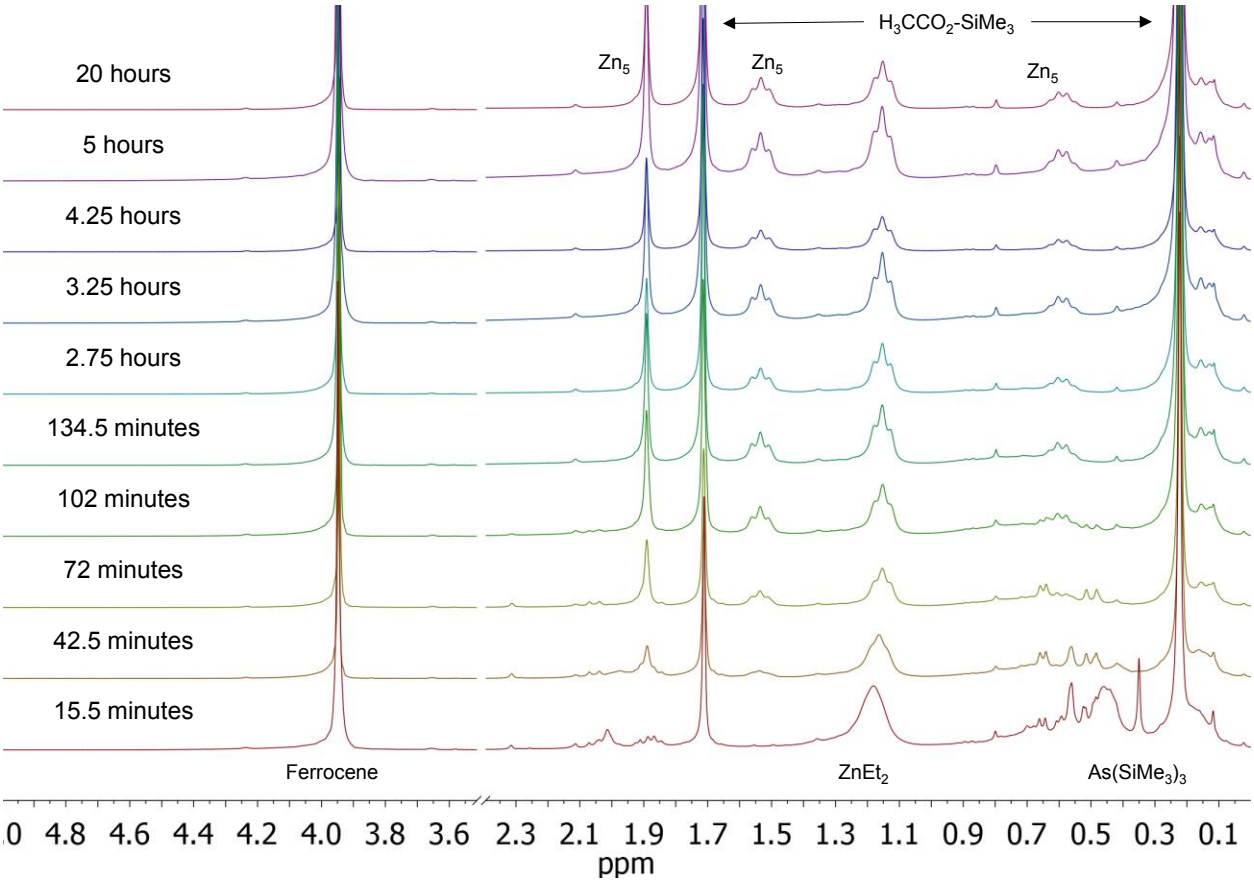

Figure 4.20. Room temperature reaction between 1.5 $Cd(O_2CCH_3)_2$, 1.5 $Zn(O_2CCH_3)_2$, 1.5 $ZnEt_2$, and 1 $As(SiMe_3)_3$ with an internal standard of ferrocene showing the fast consumption of $As(SiMe_3)_3$.

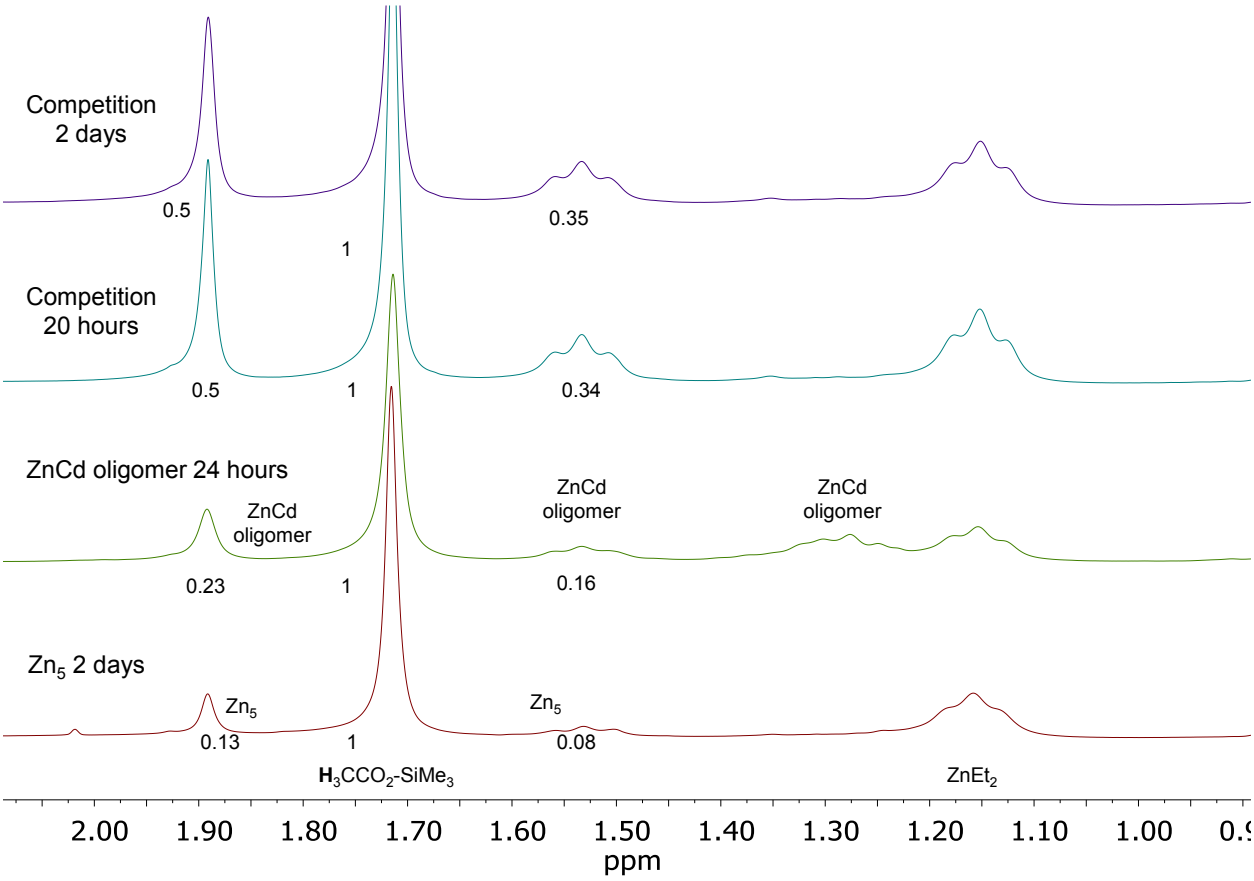

Figure 4.21. Comparison of the final two traces in the competition reaction (using 1.5 $Zn(O_2CCH_3)_2$ and 1.5 $Cd(O_2CCH_3)_2$) compared to the final traces when 3 $Cd(O_2CCH_3)_2$ was used (green) and when 3 $Zn(O_2CCH_3)_2$ was used (red). Peak from H_3CCO_2-$SiMe_3$ set to 1.

4.3 Conclusions

In conclusion, we have demonstrated the synthesis of colloidally stable 3 nm Zn_3As_2 and $(Cd_yZn_{1-y})_3As_2$ nanocrystals with optical band gaps ranging from 2.2 to 1.3 eV. This chemistry relies on the enhanced precursor reactivity provided by using a combination of both $ZnEt_2$ and $M(O_2CR)_2$ (M = Cd, Zn; R = CH_3, $(CH_2)_7CH{=}CH(CH_2)_7CH_3$) in the synthesis, which leads to the formation of oligomeric species containing both zinc and cadmium prior to nucleation. PXRD data

for the resulting $(Cd_yZn_{1-y})_3As_2$ nanocrystals show a shift in all major reflections from those of Zn_3As_2 towards Cd_3As_2, supporting alloy formation. Using three methods to calculate the amount of cadmium we determined that the amount of cadmium incorporated into the QDs was much larger than the amount used in each synthesis. This, along with the ^1H NMR data and the high-energy absorption data, shows that the formation of Cd-As bonds occurs more rapidly than the formation of Zn-As bonds. Moving forward we are optimistic about the prospect of using this synthetic approach for the synthesis of other II-V and related colloidal QDs.

4.4 Experimental

4.4.1 General Considerations

All glassware was dried in a 160 ºC oven overnight prior to use. All reactions, unless otherwise noted, were run under an inert atmosphere of nitrogen using a glovebox or standard Schlenk techniques. Hexanes (a mixture of isomers, CHROMASOLV), triphenylphosphine (99%), sodium (dry stick, ACS reagent), potassium (in mineral oil, 98%), and calcium hydride (powder, 0-2 mm, reagent grade, ≥90%, stored in desiccator) were purchased from Sigma-Aldrich Chemical Company and used without further purification. Phosphoric acid (ACS grade) was purchased from Macron Fine Chemicals and used without further purification. Ethyl acetate (anhydrous, 99.8%), and acetonitrile (anhydrous, 99.8%) were purchased from Sigma-Aldrich and stored in a nitrogen filled glove box over activated 3 Å molecular sieves. Chlorotrimethylsilane (purified by redistillation, ≥99%), arsenic (pieces, 99.999%), oleic acid (≥99%, GC), diethyl zinc, $ZnEt_2$, (≥52 wt. % Zn basis), and ferrocene (98%) were purchased from Sigma Aldrich Chemical

Company and stored under an inert atmosphere. Omni Trace nitric acid was purchased from EMD Millipore and used without further purification. 18.2 MΩ water was collected from an EMD Millipore water purification system. Celite 545 and zinc acetate (99.99%) were purchased from Sigma-Aldrich Chemical Company and heated at 150 °C under vacuum overnight and stored in a nitrogen filled inert glove box prior to use. Oleic acid (90%, technical grade) was purchased from Sigma-Aldrich Chemical Company and stirred over 3 Å molecular sieves overnight prior to being freeze-pump-thawed three times and stored in a nitrogen filled inert glove box prior to use. Dimethyl cadmium, $CdMe_2$, (97%) and cadmium acetate (anhydrous, 99.999%-Cd, PURATREM) were purchased from Strem Chemicals and stored in a nitrogen filled inert atmosphere glove box. 1-octadecene (90%) 1,2-dimethoxyethane (99%), pentane, heptane, and toluene were purchased from Sigma-Aldrich Chemical Company, dried by stirring overnight with CaH_2, distilled, and stored over activated 3 Å molecular sieves in an inert atmosphere glove box. C_6D_6 was purchased from Cambridge Isotope Labs and was similarly dried and stored. Bio Beads S-X1were purchased from Bio-Rad Laboratories and dried under vacuum and stored in an inert atmosphere glove box prior to use. Tristrimethylsilylarsine ($As(SiMe_3)_3$) was prepared by modifying a literature procedure.[38] Zinc oleate ($Zn(OA)_2$) was prepared using an adapted literature procedure with the technical grade oleic acid and stored in a nitrogen filled glove box.[27] Cadmium oleate ($Cd(OA)_2$) was prepared using a modified literature procedure with the ≥99% oleic acid and dimethyl cadmium and stored in a nitrogen filled glove box.[27]

4.4.2 Synthesis of Zinc Arsenide Quantum Dots

0.377 grams (0.6 mmol) of $Zn(OA)_2$ was transferred into a 25 mL 3-neck flask outfitted with a reflux condenser, septum, and thermowell under nitrogen. 6 grams of 1-octadecene was added to this flask. A temperature controller with a thermos-probe were used to monitor and control the reaction temperature. The 1-octadecene and $Zn(OA)_2$ were heated up to 101 °C. In a nitrogen filled glove box, 30.75 µL (0.3 mmol) of $ZnEt_2$ and 59.2 µL (0.2 mmol) of $As(SiMe_3)_3$ were added to 2 grams of 1-octadecene and drawn into a syringe. The heating mantle was turned off and at 100.2 °C was turned back on and set to 315 °C. At 100.0 °C the solution containing $ZnEt_2$ and $As(SiMe_3)_3$ was rapidly injected into the flask. The reaction ran for 60 minutes. This heating profile lead to heterogeneous material. To produce homogeneous particles, the initial set point was set to 150 °C. After 15 minutes the set-point was set to 200 °C, after 30 minutes set to 250 °C, and after 45 minutes set to 315 °C. Particles grown for 60 minutes also formed a ZnO byproduct. This could be eliminated by running the reaction for 45 minutes up to 250 °C.

4.4.3 Synthesis of Cadmium Zinc Arsenide Quantum Dots

X% of the zinc oleate was replaced with cadmium acetate to keep the total number of metal carboxylate mmols constant (0.6 mmol). The cadmium acetate was introduced to the flask the same way the $Zn(OA)_2$ was. Additionally, these reactions were only run for 45 minutes, with a final temperature of 250 °C, using the slow ramping method.

4.4.4 Synthesis of the Cadmium and Zinc Oligomer

0.1366 grams (0.6 mmol) of cadmium acetate was weighed out and stirred in 2 mL of pentane in an inert atmosphere glovebox. 50 μL (0.4 mmol) of diethyl zinc was then added. This mixture was stirred overnight at room temperature. During this reaction, the solution became homogeneous then turned heterogeneous. A crude NMR was taken to compare to the NMR scale reaction. Next all volatiles were removed and the white solid was dissolved in toluene. This mixture was then filtered through a 0.45 μm PTFE filter. The colorless solution was then pumped to dryness to collect elemental analysis (EA) and ICP-OES data. The sample was determined to have 25.1% C and 3.6% H by EA. The ratio of Zn:Cd was determined to be ~3:2 by ICP-OES.

4.4.5 Particle Work-up Procedure

Samples were transferred to Schlenk flask and the 1-octadecene was distilled off. The rest of the work up procedure was done in a nitrogen filled glove box. Particles were suspended in pentane and centrifuged to remove any insoluble material. The particles were then crashed out with a 2:1 mixture of ethyl acetate to acetonitrile. This heterogeneous mixture was then centrifuged. If the particles did not crash out as a solid, the near colorless liquid was decanted off and more ethyl acetate/acetonitrile was added. Once this yielded a mostly solid crash out, this was dissolved in toluene and crashed out with only acetonitrile. This was repeated a few times. Lastly, the particles were dissolved in toluene and centrifuged to remove any insoluble material. For additional purification prior to compositional analysis these samples were purified using gel permeation column chromatography.[39]

4.4.6 NMR Experiments

All NMR experiments were performed with an internal standard of ferrocene in C_6D_6 with a delay time of 30 seconds and set up in an inert atmosphere glove box in a J-Young NMR tube. To test the reactivity of $Zn(O_2CCH_3)_2$ with $As(SiMe_3)_3$, 14.8 µL (0.05 mmol) of $As(SiMe_3)_3$ was added to 0.5 mL C_6D_6. An initial scan was taken prior to the addition of 0.0275 grams (0.15 mmol) of $Zn(O_2CCH_3)_2$. To test the reactivity of $ZnEt_2$ with $As(SiMe_3)_3$, 7.69 µL (0.075 mmol) of $ZnEt_2$ were added to a similar solution of $As(SiMe_3)_3$ in C_6D_6 after an initial scan was taken. To test the reactivity of $[Zn_5(O_2CCH_3)_6(Et)_4]$ with $As(SiMe_3)_3$, 0.0275 grams (0.15 mmol) of $Zn(O_2CCH_3)_2$ and 7.69 µL (0.075 mmol) of $ZnEt_2$ were mixed in 0.5 mL of C_6D_6 and stirred overnight in the J-Young NMR tube. An initial scan was taken to ensure conversion to the zinc cluster. Next, 14.8 µL (0.05 mmol) of $As(SiMe_3)_3$ was added to the NMR tube and monitored. To test the reactivity of $Cd(O_2CCH_3)_2$ and $As(SiMe_3)_3$, 14.8 µL (0.05 mmol) of $As(SiMe_3)_3$ was added to 0.5 mL of C_6D_6 and an initial scan was taken prior to the addition of 0.0342 grams (0.15 mmol) of $Cd(O_2CCH_3)_2$. To test the reactivity of $Cd(O_2CCH_3)_2$ and $ZnEt_2$, 0.5 mL of C_6D_6 was added to 0.0345 grams (0.15 mmol) of $Cd(O_2CCH_3)_2$ and an initial scan was taken prior to the addition of 7.69 µL (0.075 mmol) $ZnEt_2$. To test the reactivity of this product with $As(SiMe_3)_3$, 14.8 µL (0.05 mmol) of $As(SiMe_3)_3$ was added after 23 hours. To test the competition between $Zn(O_2CCH_3)_2$ and $Cd(O_2CCH_3)_2$ reacting with $As(SiMe_3)_3$, a 0.5 mL C_6D_6 solution containing 14.8 µL (0.05 mmol) $As(SiMe_3)_3$ and 7.69 µL (0.075 mmol) $ZnEt_2$ was added to 0.014 grams (0.076 mmol) $Zn(O_2CCH_3)_2$ and 0.0178 grams (0.077 mmol) $Cd(O_2CCH_3)_2$ and monitored.

4.4.7 Characterization

Solution ^{1}H (Field: 300 MHz) NMR spectra were collected on a 300 MHz Bruker Avance spectrometer using a 30 second delay time. UV-Vis spectra were collected on an Agilent Cary 5000 spectrophotometer. Photoluminescence spectra were collected on a home built lock in detected photoluminescence set-up using 500 μm slits, a 450 nm diode chopped at 200 Hz at ~530 mA and 500 pA V^{-1} (for the pre-Amp) for excitation, and collected on a Si:InGaAs detector. PXRD diffractograms were collected on a Bruker D8 Discover with a GADDS 2-D XRD system. ICP-OES was performed using a Perkin Elmer Optima 8300. TEM images were collected on a FEI Tecnai G2 F20 microscope. TEM analysis was performed using manual analysis with the help of the ImageJ software package and Igor Pro.[40]

4.4.8 Sample Preparation for Characterization

PXRD: Solvent was removed from colloidal samples until dry and the paste was spread on a silicon <100> single crystal wafer. ICP-OES: Samples were run through a column made of Bio-Beads multiple times to removed excess ligands prior to acid digestion.[39] Concentrated high purity nitric acid was added to dissolve a small amount of the purified and dried samples so the final solution could be diluted with 18.2 MΩ water in a volumetric flask to 2% nitric acid. TEM: Samples were either prepared in toluene or heptane and drop-casted onto a TEM grid (Ultrathin carbon on holey carbon support film, 400 mesh Ted Pella or graphene support on Lacey Carbon, 300 mesh Ted Pella). Samples were placed under vacuum overnight prior to analysis to ensure sample dryness.

4.4.9 Half-life Calculations

The half-life of the reaction of 3 $Zn(O_2CCH_3)_2$ and 1 $As(SiMe_3)_3$ was determined to be 14 days. This was determined by comparing the relative area of the $As(SiMe_3)_3$ peak to the internal standard (ferrocene). This data was then normalized with the early time points averaged and set to 1. The data over 4 days (Figure 4.22A) was fit and extrapolated to the point when the integral of the $As(SiMe_3)_3$ peak was 0.5. After 4 days, the decomposition rate was enhanced perhaps due to additional decomposition pathways (Figure 4.22B).

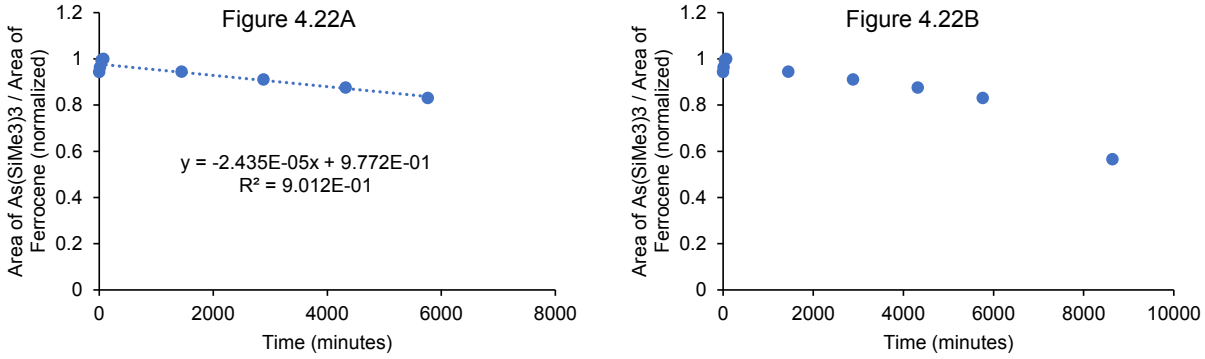

Figure 4.22. Plots showing the loss of the $As(SiMe_3)_3$ NMR signal over time when reacting with $Zn(O_2CCH_3)_2$. (A) ~6000 minutes and (B) ~9000 minutes.

The half-life of the reaction between 1 $As(SiMe_3)_3$ and the cluster pre-formed between 3 $Zn(O_2CCH_3)_2$ and 1.5 $ZnEt_2$ was determined to be <5 minutes due to the fact that there was no $As(SiMe_3)_3$ present during the first spectrum taken after adding $As(SiMe_3)_3$. This was also the case when determining the half-life of the reaction between $As(SiMe_3)_3$ and the cluster pre-formed between 3 $Cd(O_2CCH_3)_2$ and 1.5 $ZnEt_2$ to be <6.5 minutes.

The half-life of the reaction between 3 $Cd(O_2CCH_3)_2$ and 1 $As(SiMe_3)_3$ was determined to be 1.7 days. This was calculated by again comparing the area of the $As(SiMe_3)_3$ peak to that of an

internal standard (ferrocene). The reaction ran past the half-way point so no extrapolation was necessary (Figure 4.23).

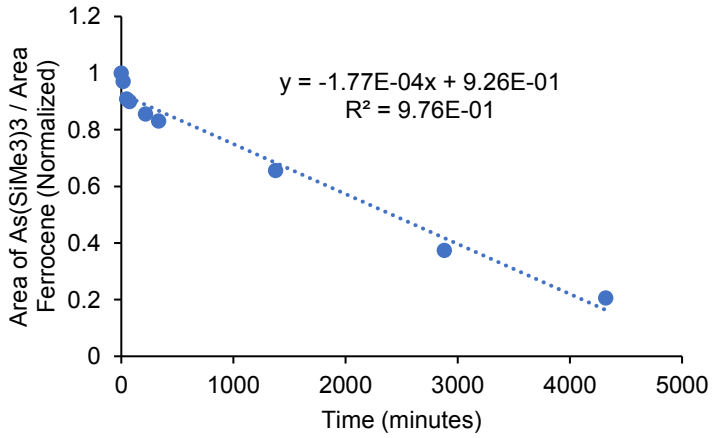

Figure 4.23. Plot showing the loss of the $As(SiMe_3)_3$ NMR signal over time when reacting with $Cd(O_2CCH_3)_2$.

4.5 References

1. Nozik, A. J., Quantum dot solar cells. *Physica E* **2002,** *14*, 115-120.
2. Michalet, X.; Pinaud, F. F.; Bentolila, L. A.; Tsay, J. M.; Doose, S.; Li, J. J.; Sundaresan, G.; Wu, A. M.; Gambhir, S. S.; Weiss, S., Quantum Dots for Live Cells, in Vivo Imaging, and Diagnostics. *Science* **2005,** *307*, 538-544.
3. McKittrick, J.; Shea-Rohwer, L. E., Review: Down Conversion Materials for Solid-State Lighting. *J. Am. Ceram. Soc.* **2014,** *97*, 1327-1352.
4. Konstantatos, G.; Howard, I.; Fischer, A.; Hoogland, S.; Clifford, J.; Klem, E.; Levina, L.; Sargent, E. H., Ultrasensitive solution-cast quantum dot photodetectors. *Nature* **2006,** *442*, 180-183.

5. Taik Lim, Y.; Kim, S.; Nakayama, A.; Stott, N. E.; Bawendi, M. G.; Frangioni, J. V., Selection of Quantum Dot Wavelengths for Biomedical Assays and Imaging. *Mol. Imaging* **2003,** *2*, 50-64.
6. Guzelian, A. A.; Banin, U.; Kadavanich, A. V.; Peng, X.; Alivisatos, A. P., Colloidal chemical synthesis and characterization of InAs nanocrystal quantum dots. *Appl. Phys. Lett.* **1996,** *69*, 1432-1434.
7. Franke, D.; Harris, D. K.; Chen, O.; Bruns, O. T.; Carr, J. A.; Wilson, M. W. B.; Bawendi, M. G., Continuous injection synthesis of indium arsenide quantum dots emissive in the short-wavelength infrared. *Nat. Commun.* **2016,** *7*, 12749.
8. Battaglia, D.; Peng, X., Formation of High Quality InP and InAs Nanocrystals in a Noncoordinating Solvent. *Nano Lett.* **2002,** *2*, 1027-1030.
9. Srivastava, V.; Janke, E. M.; Diroll, B. T.; Schaller, R. D.; Talapin, D. V., Facile, Economic and Size-Tunable Synthesis of Metal Arsenide Nanocrystals. *Chem. Mater.* **2016,** *28*, 6797-6802.
10. Das, A.; Shamirian, A.; Snee, P. T., Arsenic Silylamide: An Effective Precursor for Arsenide Semiconductor Nanocrystal Synthesis. *Chem. Mater.* **2016,** *28*, 4058-4064.
11. Hines, M. A.; Scholes, G. D., Colloidal PbS Nanocrystals with Size-Tunable Near-Infrared Emission: Observation of Post-Synthesis Self-Narrowing of the Particle Size Distribution. *Adv. Mater.* **2003,** *15*, 1844-1849.
12. Yu, W. W.; Falkner, J. C.; Shih, B. S.; Colvin, V. L., Preparation and Characterization of Monodisperse PbSe Semiconductor Nanocrystals in a Noncoordinating Solvent. *Chem. Mater.* **2004,** *16*, 3318-3322.

13. Pietryga, J. M.; Werder, D. J.; Williams, D. J.; Casson, J. L.; Schaller, R. D.; Klimov, V. I.; Hollingsworth, J. A., Utilizing the Lability of Lead Selenide to Produce Heterostructured Nanocrystals with Bright, Stable Infrared Emission. *J. Am. Chem. Soc.* **2008,** *130*, 4879-4885.
14. Hendricks, M. P.; Campos, M. P.; Cleveland, G. T.; Jen-La Plante, I.; Owen, J. S., A tunable library of substituted thiourea precursors to metal sulfide nanocrystals. *Science* **2015,** *348*, 1226-1230.
15. Harris, D. K.; Allen, P. M.; Han, H.-S.; Walker, B. J.; Lee, J.; Bawendi, M. G., Synthesis of Cadmium Arsenide Quantum Dots Luminescent in the Infrared. *J. Am. Chem. Soc.* **2011,** *133*, 4676-4679.
16. Li, D.; Peng, L.; Zhang, Z.; Shi, Z.; Xie, R.; Han, M.-Y.; Yang, W., Large Scale Synthesis of Air Stable Precursors for the Preparation of High Quality Metal Arsenide and Phosphide Nanocrystals as Efficient Emitters Covering the Visible to Near Infrared Region. *Chem. Mater.* **2014,** *26*, 3599-3602.
17. Huang, M.; Hickey, S. G.; Höfer, B.; Ding, F.; He, S.; Schmidt, O. G.; Eychmüller, A.; Miao, S., Band-Emission Evolutions from Magic-sized Clusters to Nanosized Quantum Dots of Cd3As2 in the Hot-Bubbling Synthesis. *J. Phys. Chem. C* **2015,** *119*, 16390-16395.
18. Burgess, T.; Caroff, P.; Wang, Y.; Badada, B. H.; Jackson, H. E.; Smith, L. M.; Guo, Y.; Tan, H. H.; Jagadish, C., Zn3As2 Nanowires and Nanoplatelets: Highly Efficient Infrared Emission and Photodetection by an Earth Abundant Material. *Nano Lett.* **2015,** *15*, 378-385.
19. Castellion, G. A.; Beegle, L. C., The preparation and properties of Cd3As2-Zn3As2 alloys. *J. Phys. Chem. Solids* **1965,** *26*, 767-773.

20. Chelluri, B.; Chang, T. Y.; Ourmazd, A.; Dayem, A. H.; Zyskind, J. L.; Srivastava, A., Molecular beam epitaxial growth of the II-V semiconductor compound Zn3As2. *Appl. Phys. Lett.* **1986,** *49*, 1665-1667.

21. Neethling, J. H.; Scriven, G. J.; Krekels, T., A TEM investigation of Zn3As2 grown on (001) and (111) InP by MOVPE. *J. Mater. Sci.* **2001,** *36*, 3997-4002.

22. Sierański, K.; Szatkowski, J.; Misiewicz, J., Semiempirical Tight-Binding Band Structure of II3V2 Semiconductors: Cd3P2, Zn3P2, Cd3As2, and Zn3As2. *Phys. Rev. B* **1994,** *50*, 7331-7337.

23. Fojtik, A.; Weller, H.; Henglein, A., Photochemistry of semiconductor colloids. Size quantization effects in Q-cadmium arsenide. *Chem. Phys. Lett.* **1985,** *120*, 552-554.

24. Li, J.; Wang, L.-S.; Buchholz, D. B.; Chang, R. P. H., Simultaneous Growth of Pure Hyperbranched Zn3As2 Structures and Long Ga2O3 Nanowires. *Nano Lett.* **2009,** *9*, 1764-1769.

25. Chen, G.; Liu, Z.; Liang, B.; Yu, G.; Xie, Z.; Huang, H.; Liu, B.; Wang, X.; Chen, D.; Zhu, M.-Q.; Shen, G., Single-Crystalline p-Type Zn3As2 Nanowires for Field-Effect Transistors and Visible-Light Photodetectors on Rigid and Flexible Substrates. *Adv. Funct. Mater.* **2013,** *23*, 2681-2690.

26. Im, H. S.; Park, K.; Jang, D. M.; Jung, C. S.; Park, J.; Yoo, S. J.; Kim, J.-G., Zn3P2–Zn3As2 Solid Solution Nanowires. *Nano Lett.* **2015,** *15*, 990-997.

27. Glassy, B. A.; Cossairt, B. M., Ternary synthesis of colloidal Zn3P2 quantum dots. *Chem. Commun.* **2015,** *51*, 5283-5286.

28. See section 4.4.9 for half-life calculations.

29. Glassy, B. A.; Cossairt, B. M., Resolving the Chemistry of Zn3P2 Nanocrystal Growth. *Chem. Mater.* **2016,** *28*, 6374-6380.

30. Orchard, K. L.; White, A. J. P.; Shaffer, M. S. P.; Williams, C. K., Pentanuclear Complexes for a Series of Alkylzinc Carboxylates. *Organometallics* **2009,** *28*, 5828-5832.

31. LaMer, V. K.; Dinegar, R. H., Theory, Production and Mechanism of Formation of Monodispersed Hydrosols. *J. Am. Chem. Soc.* **1950,** *72*, 4847-4854.

32. Mooney, J.; Kambhampati, P., Get the Basics Right: Jacobian Conversion of Wavelength and Energy Scales for Quantitative Analysis of Emission Spectra. *The Journal of Physical Chemistry Letters* **2013,** *4*, 3316-3318.

33. Zhao, X.; Zheng, B.; Li, C.; Gu, H., Acetate-derived ZnO ultrafine particles synthesized by spray pyrolysis. *Powder Technol.* **1998,** *100*, 20-23.

34. Wagner, R.; Palik, E.; Swiggard, E., Interband Magnetoabsorption in CdxZn3-xAs2 and Cd3AsxP2-x. *J. Phys. Chem. Solids, Suppl* **1971,** *1*, 471.

35. Pawlikowski, J. M., Optical band gap of Cd3P2-Zn3P2 semiconductor solid solutions. *J. Phys. C Solid State* **1985,** *18*, 5605-5616.

36. Luo, Y.-R., *Comprehensive Handbook of Chemical Bond Energies*. CRC Press: 2007.

37. Talapin, D. V.; Gaponik, N.; Borchert, H.; Rogach, A. L.; Haase, M.; Weller, H., Etching of Colloidal InP Nanocrystals with Fluorides: Photochemical Nature of the Process Resulting in High Photoluminescence Efficiency. *J. Phys. Chem. B* **2002,** *106*, 12659-12663.

38. Gary, D. C.; Glassy, B. A.; Cossairt, B. M., Investigation of Indium Phosphide Quantum Dot Nucleation and Growth Utilizing Triarylsilylphosphine Precursors. *Chem. Mater.* **2014,** *26*, 1734-1744.

39. Shen, Y.; Roberge, A.; Tan, R.; Gee, M. Y.; Gary, D. C.; Huang, Y.; Blom, D. A.; Benicewicz, B. C.; Cossairt, B. M.; Greytak, A. B., Gel permeation chromatography as a multifunctional processor for nanocrystal purification and on-column ligand exchange chemistry. *Chemical Science* **2016,** *7*, 5671-5679.

40. Abramoff, M. D., Magalhaes, P. J., Ram, S. J. Biophotonics International 2004, 11, 36-42.

Glossary

1-ODE	1-octadecene
Ac	acetate
CP	cross polarization
ICP-OES	inductively coupled plasma optical emission spectrometry
IR	infrared
LEET	lowest energy electronic transition
MAS	magic angle spinning
NMR	nuclear magnetic resonance
OA	oleate ($O_2C(CH_2)_7CH=CH(CH_2)_7CH_3$)
PL	photoluminescence
PXRD	powder X-ray diffraction
QDs	quantum dots
QY	quantum yield
TEM	transmission electron microscopy
TOP	trioctylphosphine
UV-Vis	ultra violet visible

Bibliography

Abramoff, M. D., Magalhaes, P. J., Ram, S. J. Biophotonics International 2004, 11, 36-42.

Adolphi, N. L.; Stoddard, R. D.; Goel, S. C.; Buhro, W. E.; Gibbons, P. C.; Conradi, M. S., The 31P NMR spectra of Cd3P2 and Zn3P2. *J. Phys. Chem. Solids* **1992,** *53*, 1275-1278.

Aldakov, D.; Lefrancois, A.; Reiss, P., Ternary and quaternary metal chalcogenide nanocrystals: synthesis, properties and applications. *Journal of Materials Chemistry C* **2013,** *1*, 3756-3776.

Ali, M. N.; Gibson, Q.; Jeon, S.; Zhou, B. B.; Yazdani, A.; Cava, R. J., The Crystal and Electronic Structures of Cd3As2, the Three-Dimensional Electronic Analogue of Graphene. *Inorg. Chem.* **2014,** *53*, 4062-4067.

Alivisatos, A. P., Semiconductor clusters, nanocrystals, and quantum dots. *Science* **1996,** *271*, 933-937.

Allen, P. M.; Walker, B. J.; Bawendi, M. G., Mechanistic Insights into the Formation of InP Quantum Dots. *Angew. Chem. Int. Ed.* **2010,** *49*, 760-762.

Aubin, M. J.; Caron, L. G.; Jay-Gerin, J. P., Band structure of cadmium arsenide at room temperature. *Phys. Rev. B* **1977,** *15*, 3872-3878.

Battaglia, D.; Peng, X., Formation of High Quality InP and InAs Nanocrystals in a Noncoordinating Solvent. *Nano Lett.* **2002,** *2*, 1027-1030.

Bawendi, M. G.; Kortan, A. R.; Steigerwald, M. L.; Brus, L. E., X‐ray structural characterization of larger CdSe semiconductor clusters. *J. Chem. Phys.* **1989,** *91*, 7282-7290.

Beberwyck, B. J.; Alivisatos, A. P., Ion Exchange Synthesis of III–V Nanocrystals. *J. Am. Chem. Soc.* **2012,** *134*, 19977-19980.

Becker, G.; Schmidt, H.; Uhl, G.; Uhl, W.; Regitz, M.; Rösch, W.; Vogelbacher, U. J., Tris (Trimethylsilyl) Phosphine and Lithium Bis (Trimethylsilyl) Phosphide. Bis‐(Tetrahydrofuran). *Inorg. Synth.* **1990,** *27*, 243-249.

Benkeser, R. A.; Riel, F. J., The reactions of some triarylsilanes with methyllithium and phenylisopropylpotassium. *J. Am. Chem. Soc.* **1951,** *73*, 3472-3474.

Bhushan, M.; Catalano, A., Polycrystalline Zn3P2 Schottky barrier solar cells. *Appl. Phys. Lett.* **1981,** *38*, 39-41.

Bosco, J. P.; Demers, S. B.; Kimball, G. M.; Lewis, N. S.; Atwater, H. A., Band alignment of epitaxial ZnS/Zn3P2 heterojunctions. *J. Appl. Phys.* **2012,** *112*, 093703.

Bosco, J. P.; Scanlon, D. O.; Watson, G. W.; Lewis, N. S.; Atwater, H. A., Energy-band alignment of II-VI/Zn3P2 heterojunctions from x-ray photoemission spectroscopy. *J. Appl. Phys.* **2013,** *113*, 203705.

Brown, A. C.; Carpino, L. A., Magnesium in methanol: substitute for sodium amalgam in desulfonylation reactions. *J. Org. Chem.* **1985,** *50*, 1749-1750.

Buhro, W. E., Metallo-organic routes to phosphide semiconductors. *Polyhedron* **1994,** *13*, 1131-1148.

Bullen, C.; Mulvaney, P., The Effects of Chemisorption on the Luminescence of CdSe Quantum Dots. *Langmuir* **2006,** *22*, 3007-3013.

Burgess, T.; Caroff, P.; Wang, Y.; Badada, B. H.; Jackson, H. E.; Smith, L. M.; Guo, Y.; Tan, H. H.; Jagadish, C., Zn3As2 Nanowires and Nanoplatelets: Highly Efficient Infrared Emission and Photodetection by an Earth Abundant Material. *Nano Lett.* **2015,** *15*, 378-385.

Carenco, S.; Demange, M.; Shi, J.; Boissiere, C.; Sanchez, C.; Le Floch, P.; Mezailles, N., White phosphorus and metal nanoparticles: a versatile route to metal phosphide nanoparticles. *Chem. Commun.* **2010,** *46*, 5578-5580.

Castellion, G. A.; Beegle, L. C., The preparation and properties of Cd3As2-Zn3As2 alloys. *J. Phys. Chem. Solids* **1965,** *26*, 767-773.

Chelluri, B.; Chang, T. Y.; Ourmazd, A.; Dayem, A. H.; Zyskind, J. L.; Srivastava, A., Molecular beam epitaxial growth of the II‐V semiconductor compound Zn3As2. *Appl. Phys. Lett.* **1986,** *49*, 1665-1667.

Chen, G.; Liu, Z.; Liang, B.; Yu, G.; Xie, Z.; Huang, H.; Liu, B.; Wang, X.; Chen, D.; Zhu, M.-Q.; Shen, G., Single-Crystalline p-Type Zn3As2 Nanowires for Field-Effect Transistors and Visible-Light Photodetectors on Rigid and Flexible Substrates. *Adv. Funct. Mater.* **2013,** *23*, 2681-2690.

Cossairt, B. M., Shining Light on Indium Phosphide Quantum Dots: Understanding the Interplay among Precursor Conversion, Nucleation, and Growth. *Chem. Mater.* **2016,** *28*, 7181-7189.

Curtright, A. E.; Morgan, M. G.; Keith, D. W., Expert Assessments of Future Photovoltaic Technologies. *Environ. Sci. Technol.* **2008,** *42*, 9031-9038.

Das, A.; Shamirian, A.; Snee, P. T., Arsenic Silylamide: An Effective Precursor for Arsenide Semiconductor Nanocrystal Synthesis. *Chem. Mater.* **2016,** *28*, 4058-4064.

Ding, L.; He, S.; Chen, D.; Huang, M.; Xu, J.; Hickey, S. G.; Eychmuller, A.; Yu, S.-H.; Miao, S., Encapsulated Cd3P2 quantum dots emitting from the visible to the near infrared for bio-labelling applications. *CrystEngComm* **2014,** *16*, 9622-9630.

Dowgiałło-Plenkiewicz, B.; Plenkiewicz, P., Inverted band structure of Cd3As2. *Phys. Status Solidi B* **1979,** *94*, K57-K60.

Dowgiałło-Plenkiewicz, B.; Plenkiewicz, P., Spin–Orbit and Crystal Field Splittings of the Valence Band in II3V2 Semiconducting Compounds. *Phys. Status Solidi B* **1978,** *87*, 309-315.

Fagen, E. A., Optical properties of Zn3P2. *J. Appl. Phys.* **1979,** *50*, 6505-6515.

Fojtik, A.; Weller, H.; Henglein, A., Photochemistry of semiconductor colloids. Size quantization effects in Q-cadmium arsenide. *Chem. Phys. Lett.* **1985,** *120*, 552-554.

Franke, D.; Harris, D. K.; Chen, O.; Bruns, O. T.; Carr, J. A.; Wilson, M. W. B.; Bawendi, M. G., Continuous injection synthesis of indium arsenide quantum dots emissive in the short-wavelength infrared. *Nat. Commun.* **2016,** *7*, 12749.

Frederick, M. T.; Weiss, E. A., Relaxation of Exciton Confinement in CdSe Quantum Dots by Modification with a Conjugated Dithiocarbamate Ligand. *ACS Nano* **2010,** *4*, 3195-3200.

Friedfeld, M. R.; Stein, J. L.; Cossairt, B. M., Main-Group-Semiconductor Cluster Molecules as Synthetic Intermediates to Nanostructures. *Inorg. Chem.* **2017**.

Fuhr, O.; Fenske, D., Die ungewöhnliche Umwandlung von P(SnMe3)3 in P4(SnMe2)6. *Z. Anorg. Allg. Chem.* **2004,** *630*, 244-246.

García-Rodríguez, R.; Hendricks, M. P.; Cossairt, B. M.; Liu, H.; Owen, J. S., Conversion Reactions of Cadmium Chalcogenide Nanocrystal Precursors. *Chem. Mater.* **2013,** *25*, 1233-1249.

Gary, D. C.; Flowers, S. E.; Kaminsky, W.; Petrone, A.; Li, X.; Cossairt, B. M., Single-Crystal and Electronic Structure of a 1.3 nm Indium Phosphide Nanocluster. *J. Am. Chem. Soc.* **2016,** *138*, 1510-1513.

Gary, D. C.; Glassy, B. A.; Cossairt, B. M., Investigation of Indium Phosphide Quantum Dot Nucleation and Growth Utilizing Triarylsilylphosphine Precursors. *Chem. Mater.* **2014,** *26*, 1734-1744.

Gary, D. C.; Terban, M. W.; Billinge, S. J. L.; Cossairt, B. M., Two-Step Nucleation and Growth of InP Quantum Dots via Magic-Sized Cluster Intermediates. *Chem. Mater.* **2015,** *27*, 1432-1441.

Glassy, B. A.; Cossairt, B. M., Resolving the Chemistry of Zn3P2 Nanocrystal Growth. *Chem. Mater.* **2016,** *28*, 6374-6380.

Glassy, B. A.; Cossairt, B. M., Ternary synthesis of colloidal Zn3P2 quantum dots. *Chem. Commun.* **2015,** *51*, 5283-5286.

Glassy, B. A.; Lai, N. L.; Cossairt, B. M., Synthesis of Zn3As2 and (CdyZn1-y)3As2 colloidal quantum dots. *Submitted.* **2017**.

Goel, S. C.; Chiang, M. Y.; Buhro, W. E., Synthesis of homoleptic silylphosphido complexes (M[P(SiMe3)2][.mu.-P(SiMe3)2])2, where M = zinc and cadmium, and their use in metalloorganic routes to Cd3P2 and MGeP2. *J. Am. Chem. Soc.* **1990,** *112*, 5636-5637.

Green, M.; O'Brien, P., A Novel Metalorganic Route to Nanocrystallites of Zinc Phosphide. *Chem. Mater.* **2001,** *13*, 4500-4505.

Green, M.; O'Brien, P., A Novel Synthesis of Cadmium Phosphide Nanoparticles Using the Single-Source Precursor [MeCdPtBu2]3. *Adv. Mater.* **1998,** *10*, 527-528.

Green, M.; O'Brien, P., The synthesis of cadmium phosphide nanoparticles using cadmium diorganophosphide precursors. *J. Mater. Chem.* **1999,** *9*, 243-247.

Guzelian, A. A.; Banin, U.; Kadavanich, A. V.; Peng, X.; Alivisatos, A. P., Colloidal chemical synthesis and characterization of InAs nanocrystal quantum dots. *Appl. Phys. Lett.* **1996,** *69*, 1432-1434.

Haacke, G.; Castellion, G. A., Preparation and Semiconducting Properties of Cd3P2. *J. Appl. Phys.* **1964,** *35*, 2484-2487.

Harris, D. K.; Allen, P. M.; Han, H.-S.; Walker, B. J.; Lee, J.; Bawendi, M. G., Synthesis of Cadmium Arsenide Quantum Dots Luminescent in the Infrared. *J. Am. Chem. Soc.* **2011,** *133*, 4676-4679.

Hassler, K., Darstellung und Charakterisierung der Trisilylphosphane (Ph 3 Si) n P (SiMe 3) 3− n, n= 1, 2, 3. *Monatsh. Chem.* **1982,** *113*, 421-425.

Heath, J. R.; Shiang, J. J., Covalency in semiconductor quantum dots. *Chem. Soc. Rev.* **1998,** *27*, 65-71.

Hendricks, M. P.; Campos, M. P.; Cleveland, G. T.; Jen-La Plante, I.; Owen, J. S., A tunable library of substituted thiourea precursors to metal sulfide nanocrystals. *Science* **2015,** *348*, 1226-1230.

Hines, M. A.; Scholes, G. D., Colloidal PbS Nanocrystals with Size-Tunable Near-Infrared Emission: Observation of Post-Synthesis Self-Narrowing of the Particle Size Distribution. *Adv. Mater.* **2003,** *15*, 1844-1849.

Ho, M. Q.; Esteves, R. J. A.; Kedarnath, G.; Arachchige, I. U., Size-Dependent Optical Properties of Luminescent Zn3P2 Quantum Dots. *J. Phys. Chem. C* **2015,** *119*, 10576-10584.

Hoertz, P. G.; Chen, Z.; Kent, C. A.; Meyer, T. J., Application of High Surface Area Tin-Doped Indium Oxide Nanoparticle Films as Transparent Conducting Electrodes. *Inorg. Chem.* **2010,** *49*, 8179-8181.

Huang, M.; Hickey, S. G.; Höfer, B.; Ding, F.; He, S.; Schmidt, O. G.; Eychmüller, A.; Miao, S., Band-Emission Evolutions from Magic-sized Clusters to Nanosized Quantum Dots of Cd3As2 in the Hot-Bubbling Synthesis. *J. Phys. Chem. C* **2015,** *119*, 16390-16395.

Hupfer, A.; Hirsch, D.; Schulze, S., Photoemission on A 3IIB 2V semiconductor material. Cd3As2, Zn3As2, Cd3P2, Zn3P2 crystals and thin films. *Phys. Status Solidi B* **1989,** *152*, 505-517.

Im, H. S.; Park, K.; Jang, D. M.; Jung, C. S.; Park, J.; Yoo, S. J.; Kim, J.-G., Zn3P2–Zn3As2 Solid Solution Nanowires. *Nano Lett.* **2015,** *15*, 990-997.

Khanna, P. K.; Singh, N.; More, P., Synthesis and band-gap photoluminescence from cadmium phosphide nano-particles. *Current Applied Physics* **2010,** *10*, 84-88.

Kietzmann, R.; Willig, F.; Weller, H.; Vogel, R.; Nath, D. N.; Eichberger, R.; Liska, P.; Lehnert, J., Picosecond Time Resolved Electron Injection from Excited Cresyl Violet Monomers and Cd3P2 Quantum Dots into TiO2. *Molecular Crystals and Liquid Crystals* **1991,** *194*, 169-180.

Kim, Y. S.; Won, Y. S.; Hagelin-Weaver, H.; Omenetto, N.; Anderson, T., Homogeneous Decomposition Mechanisms of Diethylzinc by Raman Spectroscopy and Quantum Chemical Calculations. *The Journal of Physical Chemistry A* **2008,** *112*, 4246-4253.

Kimball, G. M.; Lewis, N. S.; Atwater, H. A. In *Mg doping and alloying in Zn3P2 heterojunction solar cells*, Photovoltaic Specialists Conference (PVSC), 2010 35th IEEE, 20-25 June 2010; 2010; pp 001039-001043.

Konstantatos, G.; Howard, I.; Fischer, A.; Hoogland, S.; Clifford, J.; Klem, E.; Levina, L.; Sargent, E. H., Ultrasensitive solution-cast quantum dot photodetectors. *Nature* **2006,** *442*, 180-183.

Kornowski, A.; Eichberger, R.; Giersig, M.; Weller, H.; Eychmüller, A., Preparation and Photophysics of Strongly Luminescing Cd3P2 Quantum Dots. *The Journal of Physical Chemistry* **1996,** *100*, 12467-12471.

Kuno, M., *Introductory Nanoscience: Physical and Chemical Concepts*. Garland Science: Taylor & Francis Group: New York, NY, 2012.

Kwon, S. G.; Hyeon, T., Formation Mechanisms of Uniform Nanocrystals via Hot-Injection and Heat-Up Methods. *Small* **2011,** *7*, 2685-2702.

LaMer, V. K.; Dinegar, R. H., Theory, Production and Mechanism of Formation of Monodispersed Hydrosols. *J. Am. Chem. Soc.* **1950,** *72*, 4847-4854.

Li, D.; Peng, L.; Zhang, Z.; Shi, Z.; Xie, R.; Han, M.-Y.; Yang, W., Large Scale Synthesis of Air Stable Precursors for the Preparation of High Quality Metal Arsenide and Phosphide Nanocrystals as Efficient Emitters Covering the Visible to Near Infrared Region. *Chem. Mater.* **2014,** *26*, 3599-3602.

Li, J.; Wang, L.-S.; Buchholz, D. B.; Chang, R. P. H., Simultaneous Growth of Pure Hyperbranched Zn3As2 Structures and Long Ga2O3 Nanowires. *Nano Lett.* **2009,** *9*, 1764-1769.

Li, L.; Protière, M.; Reiss, P., Economic Synthesis of High Quality InP Nanocrystals Using Calcium Phosphide as the Phosphorus Precursor. *Chem. Mater.* **2008,** *20*, 2621-2623.

Lim, T. H.; Teh, G. B.; Tilley, R. D. In *Synthesis and Characterization of Highly Crystalline Zinc Phosphide Nanoparticles*, Key Eng. Mater., Trans Tech Publ: 2016; pp 3-7.

Lin-Chung, P. J., Energy band structures of Cd3P2 and Zn3P2. *Phys. Status Solidi B* **1971,** *47*, 33-39.

Luber, E. J.; Mobarok, M. H.; Buriak, J. M., Solution-Processed Zinc Phosphide (α-Zn3P2) Colloidal Semiconducting Nanocrystals for Thin Film Photovoltaic Applications. *ACS Nano* **2013,** *7*, 8136-8146.

Lunt, R. R.; Osedach, T. P.; Brown, P. R.; Rowehl, J. A.; Bulović, V., Practical Roadmap and Limits to Nanostructured Photovoltaics. *Adv. Mater.* **2011,** *23*, 5712-5727.

Luo, Y.-R., *Comprehensive Handbook of Chemical Bond Energies*. CRC Press: 2007.

Matchett, M. A.; Viano, A. M.; Adolphi, N. L.; Stoddard, R. D.; Buhro, W. E.; Conradi, M. S.; Gibbons, P. C., Sol-gel-like route to crystalline cadmium phosphide nanoclusters. *Chem. Mater.* **1992,** *4*, 508-511.

McKittrick, J.; Shea‐Rohwer, L. E., Review: Down Conversion Materials for Solid‐State Lighting. *J. Am. Ceram. Soc.* **2014,** *97*, 1327-1352.

Miao, S.; Chen, D.; Madani, A.; Jorgensen, M. R.; Bolaños Quiñones, V. A.; Ma, L.; Hickey, S. G.; Eychmüller, A.; Schmidt, O. G., Optofluidic Sensor: Evaporation Kinetics Detection of Solvents Dissolved with Cd3P2 Colloidal Quantum Dots in a Rolled-Up Microtube. *Advanced Optical Materials* **2015,** *3*, 187-193.

Miao, S.; Eychmüller, A.; Hickey, S. G., "Artificial Supermolecule": Progress in the Study of II–V Colloidal Semiconductor Nanocrystals. In *Molecules at Work*, Wiley-VCH Verlag GmbH & Co. KGaA: 2012; pp 121-153.

Miao, S.; Hickey, S. G.; Rellinghaus, B.; Waurisch, C.; Eychmüller, A., Synthesis and Characterization of Cadmium Phosphide Quantum Dots Emitting in the Visible Red to Near-Infrared. *J. Am. Chem. Soc.* **2010,** *132*, 5613-5615.

Miao, S.; Hickey, S. G.; Waurisch, C.; Lesnyak, V.; Otto, T.; Rellinghaus, B.; Eychmüller, A., Synthesis of Monodisperse Cadmium Phosphide Nanoparticles Using ex-Situ Produced Phosphine. *ACS Nano* **2012,** *6*, 7059-7065.

Miao, S.; Yang, T.; Hickey, S. G.; Lesnyak, V.; Rellinghaus, B.; Xu, J.; Eychmüller, A., Emissive ZnO@Zn3P2 Nanocrystals: Synthesis, Optical, and Optoelectrochemical Properties. *Small* **2013,** *9*, 3415-3422.

Michalet, X.; Pinaud, F. F.; Bentolila, L. A.; Tsay, J. M.; Doose, S.; Li, J. J.; Sundaresan, G.; Wu, A. M.; Gambhir, S. S.; Weiss, S., Quantum Dots for Live Cells, in Vivo Imaging, and Diagnostics. *Science* **2005,** *307*, 538-544.

Misiewicz, J., Optical and electrical investigations of imperfection levels in Zn3P2. *J. Phys. Chem. Solids* **1989,** *50*, 1013-1022.

Misiewicz, J.; Pawlikowski, J. M., Optical band-gap of Zn3As2. *Solid State Commun.* **1979,** *32*, 687-690.

Misiewicz, J.; Wróbel, J. M.; Jezierski, K., Interband transitions in Zn3As2. *Solid State Commun.* **1993,** *86*, 509-511.

Mobarok, M. H.; Buriak, J. M., Elucidating the Surface Chemistry of Zinc Phosphide Nanoparticles Through Ligand Exchange. *Chem. Mater.* **2014,** *26*, 4653-4661.

Mobarok, M. H.; Luber, E. J.; Bernard, G. M.; Peng, L.; Wasylishen, R. E.; Buriak, J. M., Phase-Pure Crystalline Zinc Phosphide Nanoparticles: Synthetic Approaches and Characterization. *Chem. Mater.* **2014,** *26*, 1925-1935.

Mooney, J.; Kambhampati, P., Get the Basics Right: Jacobian Conversion of Wavelength and Energy Scales for Quantitative Analysis of Emission Spectra. *The Journal of Physical Chemistry Letters* **2013,** *4*, 3316-3318.

Murray, C. B.; Norris, D. J.; Bawendi, M. G., Synthesis and characterization of nearly monodisperse CdE (E = sulfur, selenium, tellurium) semiconductor nanocrystallites. *J. Am. Chem. Soc.* **1993,** *115*, 8706-8715.

Nayar, P. S.; Catalano, A., Zinc phosphide‐zinc oxide heterojunction solar cells. *Appl. Phys. Lett.* **1981,** *39*, 105-107.

Neethling, J. H.; Scriven, G. J.; Krekels, T., A TEM investigation of Zn3As2 grown on (001) and (111) InP by MOVPE. *J. Mater. Sci.* **2001,** *36*, 3997-4002.

Nozik, A. J., Quantum dot solar cells. *Physica E* **2002,** *14*, 115-120.

Ojo, W.-S.; Xu, S.; Delpech, F.; Nayral, C.; Chaudret, B., Room-Temperature Synthesis of Air-Stable and Size-Tunable Luminescent ZnS-Coated Cd3P2 Nanocrystals with High Quantum Yields. *Angew. Chem. Int. Ed.* **2012,** *51*, 738-741.

Orchard, K. L.; White, A. J. P.; Shaffer, M. S. P.; Williams, C. K., Pentanuclear Complexes for a Series of Alkylzinc Carboxylates. *Organometallics* **2009,** *28*, 5828-5832.

Pawlikowski, J. M., Absorption edge of Zn3P2. *Phys. Rev. B* **1982,** *26*, 4711-4713.

Pawlikowski, J. M., Band structure and properties of Zn3P2— promising new infrared material∗. *Infrared Physics* **1981,** *21*, 181-187.

Pawlikowski, J. M., Comments on Zn3P2 band structure. *J. Appl. Phys.* **1982,** *53*, 3639-3642.

Pawlikowski, J. M., Optical band gap of Cd3P2-Zn3P2 semiconductor solid solutions. *J. Phys. C Solid State* **1985,** *18*, 5605-5616.

Pietryga, J. M.; Werder, D. J.; Williams, D. J.; Casson, J. L.; Schaller, R. D.; Klimov, V. I.; Hollingsworth, J. A., Utilizing the Lability of Lead Selenide to Produce Heterostructured Nanocrystals with Bright, Stable Infrared Emission. *J. Am. Chem. Soc.* **2008,** *130*, 4879-4885.

Plenkiewicz, P.; Dowgiałło-Plenkiewicz, B., Energy band structure of Cd3P2 for real D 4h15 symmetry I. Energy bands. *Phys. Status Solidi B* **1979,** *92*, 379-387.

Pongkittiphan, V.; Theodorakis, E.; Chavasiri, W., Hexachloroethane: a highly efficient reagent for the synthesis of chlorosilanes from hydrosilanes. *Tetrahedron Lett.* **2009,** *50*, 5080-5082.

Prince, P.; Bearpark, M.; McGrady, G.; Steed, J., Hypervalent hydridosilicates: synthesis, structure and hydride bridging. *Dalton Trans.* **2008**, 271-282.

Rademacher, B.; Schwarz, W.; Westerhausen, M., Heteroleptische Diorganylzink‐Verbindungen mit einem Bis (trimethylsilyl) phosphanido‐Substituenten. *Z. Anorg. Allg. Chem.* **1995,** *621*, 287-300.

Reid, P. J.; Fujimoto, B.; Gamelin, D. R., A Simple ZnO Nanocrystal Synthesis Illustrating Three-Dimensional Quantum Confinement. *J. Chem. Educ.* **2013,** *91*, 280-282.

Rogach, A. L.; Eychmüller, A.; Hickey, S. G.; Kershaw, S. V., Infrared-Emitting Colloidal Nanocrystals: Synthesis, Assembly, Spectroscopy, and Applications. *Small* **2007,** *3*, 536-557.

Sapelza, G.; Mayer, P.; Westerhausen, M., Synthesis and Characterization of Methylzinc Tri(tert-butyl)silylphosphanide as well as Related Sodium and Potassium Phosphanylzincates. *Z. Anorg. Allg. Chem.* **2005,** *631*, 3087-3091.

Savela, R.; Zawartka, W.; Leino, R., Iron-catalyzed chlorination of silanes. *Organometallics* **2012,** *31*, 3199-3206.

Scherrer, P., Bestimmung der Größe und der inneren Struktur von Kolloidteilchen mittels Röntgenstrahlen. *Nachr. Ges. Wiss. Göttingen.* **1918,** *1990*, 98-100.

Schneider, C. A.; Rasband, W. S.; Eliceiri, K. W., NIH Image to ImageJ: 25 years of image analysis. *Nat. Methods* **2012,** *9*, 671-675.

Shen, Y.; Roberge, A.; Tan, R.; Gee, M. Y.; Gary, D. C.; Huang, Y.; Blom, D. A.; Benicewicz, B. C.; Cossairt, B. M.; Greytak, A. B., Gel permeation chromatography as a multifunctional processor for nanocrystal purification and on-column ligand exchange chemistry. *Chemical Science* **2016,** *7*, 5671-5679.

Shirasaki, Y.; Supran, G. J.; Bawendi, M. G.; Bulovic, V., Emergence of colloidal quantum-dot light-emitting technologies. *Nat Photon* **2013,** *7*, 13-23.

Sierański, K.; Szatkowski, J.; Misiewicz, J., Semiempirical Tight-Binding Band Structure of II3V2 Semiconductors: Cd3P2, Zn3P2, Cd3As2, and Zn3As2. *Phys. Rev. B* **1994,** *50*, 7331-7337.

Silvey, G. A., Zn3As2, A Semiconducting Intermetallic Compound. *J. Appl. Phys.* **1958,** *29*, 226-227.

Srivastava, V.; Janke, E. M.; Diroll, B. T.; Schaller, R. D.; Talapin, D. V., Facile, Economic and Size-Tunable Synthesis of Metal Arsenide Nanocrystals. *Chem. Mater.* **2016,** *28*, 6797-6802.

Stein, J. L.; Mader, E. A.; Cossairt, B. M., Luminescent InP Quantum Dots with Tunable Emission by Post-Synthetic Modification with Lewis Acids. *The Journal of Physical Chemistry Letters* **2016,** *7*, 1315-1320.

Stein, J. L.; Steimle, M. I.; Terban, M. W.; Petrone, A.; Billinge, S. J. L.; Li, X.; Cossairt, B. M., Cation exchange induced transformation of InP magic-sized custers. *Submitted.* **2017**.

Stuczynski, S. M.; Opila, R. L.; Marsh, P.; Brennan, J. G.; Steigerwald, M. L., Formation of indium phosphide from trimethylindium (In(CH3)3) and tris(trimethylsilyl)phosphine (P(Si(CH3)3)3). *Chem. Mater.* **1991,** *3*, 379-381.

Suda, T.; Kakishita, K., Epitaxial growth of zinc phosphide. *J. Appl. Phys.* **1992,** *71*, 3039-3041.

Sujak-Cyrul, B.; Kolodka, B.; Misiewicz, J.; Pawlikowski, J. M., Intraband and interband optical transitions in Zn3AS2. *J. Phys. Chem. Solids* **1982,** *43*, 1045-1051.

Taik Lim, Y.; Kim, S.; Nakayama, A.; Stott, N. E.; Bawendi, M. G.; Frangioni, J. V., Selection of Quantum Dot Wavelengths for Biomedical Assays and Imaging. *Mol. Imaging* **2003,** *2*, 50-64.

Talapin, D. V.; Gaponik, N.; Borchert, H.; Rogach, A. L.; Haase, M.; Weller, H., Etching of Colloidal InP Nanocrystals with Fluorides: Photochemical Nature of the Process Resulting in High Photoluminescence Efficiency. *J. Phys. Chem. B* **2002,** *106*, 12659-12663.

Talapin, D. V.; Rogach, A. L.; Kornowski, A.; Haase, M.; Weller, H., Highly Luminescent Monodisperse CdSe and CdSe/ZnS Nanocrystals Synthesized in a Hexadecylamine−Trioctylphosphine Oxide−Trioctylphospine Mixture. *Nano Lett.* **2001,** *1*, 207-211.

Tamang, S.; Lincheneau, C.; Hermans, Y.; Jeong, S.; Reiss, P., Chemistry of InP Nanocrystal Syntheses. *Chem. Mater.* **2016,** *28*, 2491-2506.

Tomaselli, M.; Yarger, J. L.; Bruchez, M. J.; Havlin, R. H.; deGraw, D.; Pines, A.; Alivisatos, A. P., NMR study of InP quantum dots: Surface structure and size effects. *J. Chem. Phys.* **1999,** *110*, 8861-8864.

Wadia, C.; Alivisatos, A. P.; Kammen, D. M., Materials Availability Expands the Opportunity for Large-Scale Photovoltaics Deployment. *Environ. Sci. Technol.* **2009,** *43*, 2072-2077.

Wagner, R.; Palik, E.; Swiggard, E., Interband Magnetoabsorption in CdxZn3-xAs2 and Cd3AsxP2-x. *J. Phys. Chem. Solids, Suppl* **1971,** *1*, 471.

Wang, R.; Ratcliffe, C. I.; Wu, X.; Voznyy, O.; Tao, Y.; Yu, K., Magic-Sized Cd3P2 II−V Nanoparticles Exhibiting Bandgap Photoemission. *J. Phys. Chem. C* **2009,** *113*, 17979-17982.

Wang, R.; Ratcliffe, C. I.; Wu, X.; Voznyy, O.; Tao, Y.; Yu, K., Magic-Sized Cd3P2 II−V Nanoparticles Exhibiting Bandgap Photoemission. *J. Phys. Chem. C* **2009,** *113*, 17979-17982.

Weller, H.; Fojtik, A.; Henglein, A., Photochemistry of semiconductor colloids: Properties of extremely small particles of Cd3P2 and Zn3P2. *Chem. Phys. Lett.* **1985,** *117*, 485-488.

Westerhausen, M.; Sapelza, G.; Zabel, M.; Pfitzner, A., (EtZn)4Zn2(PSitBu3)4: a Homometallic Phosphanediide of Zinc with a novel Zn6P4 Cage. *Z. Naturforsch. B* **2004,** *59*, 1548-1550.

Wyeth, N. C.; Catalano, A., Spectral response measurements of minority-carrier diffusion length in Zn3P2. *J. Appl. Phys.* **1979,** *50*, 1403-1407.

Xie, R.; Zhang, J.; Zhao, F.; Yang, W.; Peng, X., Synthesis of Monodisperse, Highly Emissive, and Size-Tunable Cd3P2 Nanocrystals. *Chem. Mater.* **2010,** *22*, 3820-3822.

Yang, R.; Chueh, Y.-L.; Morber, J. R.; Snyder, R.; Chou, L.-J.; Wang, Z. L., Single-Crystalline Branched Zinc Phosphide Nanostructures: Synthesis, Properties, and Optoelectronic Devices. *Nano Lett.* **2006,** *7*, 269-275.

Yu, W. W.; Falkner, J. C.; Shih, B. S.; Colvin, V. L., Preparation and Characterization of Monodisperse PbSe Semiconductor Nanocrystals in a Noncoordinating Solvent. *Chem. Mater.* **2004,** *16*, 3318-3322.

Żdanowicz, W.; Wojakowski, A., Preparation and Semiconducting Properties of Cadmium Phosphide (Cd3P2). *Phys. Status Solidi B* **1965,** *8*, 569-575.

Zhao, X.; Zheng, B.; Li, C.; Gu, H., Acetate-derived ZnO ultrafine particles synthesized by spray pyrolysis. *Powder Technol.* **1998,** *100*, 20-23.

Zhao, X.-G.; Shi, J.-L.; Hu, B.; Zhang, L.-X.; Hua, Z.-L., Confinement of Cd3P2 nanoparticles inside ordered pore channels in mesoporous silica. *J. Mater. Chem.* **2003,** *13*, 399-403.

Appendix A: Model of Zn_3P_2 QD surface based on TGA and ICP-OES Data

Assumptions:

- Particles have a diameter of 2.9 nm
- Zn:P ratio is 2.5:1
- Possible zinc oxide shell thickness 0.116 nm (less than a monolayer)
- Surface ligands are $Zn(OA)_2$
- $Zn(OA)_2$ converts to ZnO upon thermal decomposition

Inorganic core mass:

$$mass = density \times volume = density \times \frac{4}{3}\pi r^3$$

$$mass = (4.55\ g\ cm^{-3}) \times \left(\frac{4}{3}\pi\left(\left(\frac{2.9}{2} - 0.116\right) \times 10^{-7}\right)^3\right) = 4.524 \times 10^{-20}\ grams$$

Moles of zinc and phosphorus

$$moles\ of\ zinc: 3 \times \frac{4.524 \times 10^{-20}\ grams}{258.12\ gram\ mol^{-1}} = 5.259 \times 10^{-22}\ moles$$

$$moles\ of\ phosphorus: 2 \times \frac{4.524 \times 10^{-20}\ grams}{258.12\ gram\ mol^{-1}} = 3.506 \times 10^{-22}\ moles$$

ZnO layer

$$volume\ of\ layer = \frac{4}{3}\pi r^3 - Zn_3P_2\ volume$$

$$volume = \frac{4}{3}\pi\left(\frac{2.9}{2}\right)^3 - \frac{4}{3}\pi\left(\frac{2.9}{2} - 0.116\right)^3 = 2.826\ nm^3 = 2.826 \times 10^{-21}\ cm^3$$

$$mass\ of\ layer = density \times volume$$

$$mass\ of\ layer = (5.61\ g\ cm^{-1}) \times (2.826 \times 10^{-21}\ cm^3) = 1.585 \times 10^{-20}\ grams$$

$$moles\ ZnO = moles\ Zn = \frac{mass}{MW} = \frac{1.585 \times 10^{-20}\ grams}{81.41\ grams\ mol^{-1}} = 1.948 \times 10^{-22}\ moles$$

Surface

The total moles of zinc can be determined using the Zn:P ratio

$$total\ moles\ of\ zinc = moles\ P \times 2.5 = 3.506 \times 10^{-22} \times 2.5 = 8.764 \times 10^{-22}\ moles$$

$$remaining\ moles\ of\ zinc = 8.764 \times 10^{-22} - 1.948 \times 10^{-22} - 5.259 \times 10^{-22}$$

$$remaining\ moles\ of\ zinc = 1.558 \times 10^{-22}\ moles$$

$$mass\ of\ surface = moles \times MW$$

$$mass\ of\ surface = (1.558 \times 10^{-22}\ moles) \times (628.3\ grams\ mol^{-1}) = 9.790 \times 10^{-20}\ grams$$

$$mass\ of\ surface\ ZnO\ post\ heating = surface\ zinc\ moles \times MW_{ZnO}$$

$$Surface\ ZnO = (1.558 \times 10^{-22}\ moles) \times (81.41\ grams\ mol^{-1}) = 1.268 \times 10^{-20}\ grams$$

Inorganic mass %

$$Total\ mass = core\ mass + ZnO\ layer\ mass + surface\ mass$$

$$Total\ mass = 4.524\times10^{-20}\ grams + 1.585\times10^{-20}\ grams + 9.790\times10^{-20}\ grams$$

$$Total\ mass = 1.590\times10^{-19}\ grams$$

$$Inorganic\ mass = core\ mass + ZnO\ layer\ mass + surface\ ZnO\ mass$$

$$Inorganic\ mass = 4.524\times10^{-20}\ grams + 1.585\times10^{-20}\ grams + 1.268\times10^{-20}\ grams$$

$$Inorganic\ mass = 7.378\times10^{-20}\ grams$$

$$Inorganic\ mass\ \% = 46.4\%$$

This is in line with the TGA data collected for this particles (Figure 2.25).

Appendix B: Synthesis of Para-substituted Tris(triarylsilyl)phosphines

B.1 General Considerations

Sodium (dry stick, ACS reagent), potassium (in mineral oil, 98%), red phosphorus (99.999%), trichlorosilane (99%), palladium dichloride (99%), hexachloroethane (99%), magnesium sulfate (anhydrous, ≥99.5%), 4-bromotoluene (98%), 1-bromo-4-chlorobenzene (99%), 4-bromobenzotrifluoride (99%), iodine (chips, ≥99%), chlorotriphenylsilane (96%), chlorotrimethylsilane (≥99%), magnesium turnings (98%), and Celite 545 were purchased from Sigma-Aldrich Chemical Company and used without further purification. All solvents, including 1,2-dimethoxyethane (99%), toluene, hexanes, diethyl ether, and tetrahydrofuran were purchased from Sigma-Aldrich Chemical Company, dried by stirring overnight with CaH_2, distilled, and stored over 4 Å molecular sieves. C_6D_6 and $CDCl_3$ were purchased from Cambridge Isotope Labs and were dried similarly. Concentrated hydrochloric acid was purchased from Fisher Scientific. Magnesium turnings were activated following literature procedures prior to use.[1] ^{1}H, ^{31}P, ^{13}C, and ^{19}F NMR spectra were collected on 300 and 500 MHz Bruker Avance spectrometers.

B.2 Synthesis of Para-substituted Triarylsilanes

B.2.1 Synthesis of (p-$MeC_6H_4)_3SiH$

This synthesis was adapted from a literature procedure.[2] In a 250 mL 3-neck flask 100 mL diethyl ether, 2.67 grams (110 mmol) activated magnesium, and one iodine chip were added under

N_2. Then 16.83 grams (98.4 mmol) of p-bromotoluene were added. The reaction mixture was refluxed and briefly heated with a heat gun. After about 6 minutes the solution became cloudy and darkened to an orange color. After 4.5 hours, the solution was cannula transferred to a 250 mL 3-neck flask set up with a pressure equalizing dropping funnel, septum, and a Schlenk flow adapter that had been purged with N_2. 10 mL of diethyl ether was added to the dropping funnel. 3.4 mL (33.7 mmol) of trichlorosilane was added via syringe under N_2. The diethyl ether/silane solution was added drop-wise at a rate around one drop per second. Once added, the solution was left to stir for 30 minutes. The solution was then quenched with a 0.5-1 M HCl solution. The aqueous layer was washed three times with 20 mL of diethyl ether. The organic layers were combined and dried with magnesium sulfate. The solution was filtered through a paper filter. The diethyl ether was removed under reduced pressure, resulting in a yellow oil. The oil was dissolved in hexanes and put in the freezer at −30 °C. The resulting solids were collected. These solids were further purified by stirring in hot methanol (60 °C) for two hours and collected on a frit. The yield for this reaction was 1.7 grams. The average percent yield was 30% (7 runs). ^{1}H NMR (301 MHz): $CDCl_3$, (d, 7.47, 6H), (d, 7.19, 6H), (s, 5.42, 1H), (s, 2.37, 9H).

B.2.2 Synthesis of (p-$ClC_6H_4)_3SiH$

This synthesis was adapted from a literature procedure.[3] 4.5 grams (185 mmol) of activated magnesium was added to 30 mL of diethyl ether and a chip of iodine in a 250 mL 3-neck flask under N_2. A saturated diethyl ether solution containing 31.61 grams (165 mmol) of 1-bromo-4-chlorobenzene was added to the flask. The solution started refluxing on its own after fifteen

minutes and turned brown. *Warning, the next step is very exothermic and should be done in an ice bath.* After 40 minutes, 5.45 mL (54 mmol) of trichlorosilane was added via syringe under N_2. The reaction mixture was refluxed in an oil bath for 4 hours. The reaction was quenched by pouring into a 600 mL beaker with an ice/5% HCl mixture. The aqueous layer was washed with three 20 mL portions of diethyl ether. The diethyl ether layers were combined and dried with magnesium sulfate. The solution was filtered through a paper filter. The diethyl ether was removed under reduced pressure yielding an oil. Upon the addition of pentane, a white precipitate formed. The solution was put in the freezer at −30 °C to encourage further precipitation. The white solids were collected and recrystallized in ethanol. The yield was 6.9 grams. The average % yield was 46% (2 runs). ^{1}H NMR (300 MHz): $CDCl_3$, (d, 7.46, 6H), (d, 7.36, 6H), (s, 5.42, 1H).

B.2.3 Synthesis of (p-$CF_3C_6H_4)_3SiH$

This synthesis was adapted from literature procedure.[3] In a typical synthesis targeting 10 grams of the desired product, 3 grams (123 mmol) of activated magnesium was added to 100 mL of diethyl ether in a 3-neck 250 mL flask under N_2. Next, 9 mL (64 mmol) of 4-bromobenzotrifluoride and one chip of iodine were added to the flask. The reaction mixture was refluxed for 2 hours and then cooled to room temperature. Another 3-neck 250 mL flask was set up with a pressure equalizing dropping funnel and a septum under N_2. The reaction mixture was cannula transferred into the second 3-neck flask. To the dropping funnel, 50 mL of diethyl ether as well as 2.2 mL (21.8 mmol) of trichlorosilane were added under N_2. This solution was added drop-wise and the reaction mixture was cooled over ice during the addition. The solution was brought to reflux in an oil bath and left overnight. The solution was then cooled to room temperature and

quenched over an ice/5% HCl solution in a 600 mL beaker. The aqueous layer was washed with three 20 mL portions of ether. The ether layers were collected and dried with magnesium sulfate. This solution was filtered through a paper filter and the solvent was removed by vacuum. The resulting yellow solid was recrystallized twice from pentane. The yield was 3.7 grams. The average % yield was 48% (3 runs). ^{1}H NMR (300 MHz): $CDCl_3$, (m, 7.69, 12H), (s, 5.60, 1H); ^{19}F (282 MHz): –64.06.

B.3 Synthesis of Chlorotriarylsilanes

B.3.1 Synthesis of (p-$MeC_6H_4)_3SiCl$

The synthesis was modified from a literature procedures,[4-5] and was performed in an inert atmosphere glove box. In a typical synthesis, 0.0198 grams (0.1 mmol) of palladium dichloride and 0.594 grams (2.5 mmol) of hexachloroethane were measured into a 100 mL round bottom flask. Then 2.93 grams (9.7 mmol) of (p-$MeC_6H_4)_3SiH$ was added. Next, 2.22 grams of tetrahydrofuran was added. Upon addition of the solvent, the solution turned black and started giving off gas. The reaction flask was loosely stoppered and the reaction was stirred at room temperature overnight. The reaction mixture was analyzed by ^{1}H NMR spectroscopy prior to working up to ensure the reaction went to completion. The THF was removed under reduced pressure and re-dissolved in copious amounts of pentane. The solution was filtered through Celite. The pentane was removed under reduced pressure yielding a white solid that did not require further purification. The yield was 1.23 g. The average % yield was 63% (5 runs). ^{1}H NMR (300 MHz): $CDCl_3$, (d, 7.53, 6H), (d, 7.22, 6H), (s, 2.38, 9H).

B.3.2 Synthesis of (p-$ClC_6H_4)_3SiCl$

This synthesis was performed in an inert atmosphere glove box. In a typical synthesis, 0.130 grams (0.7 mmol) palladium dichloride and 0.866 grams (3.7 mmol) of hexachloroethane were weighed out into a 100 mL round bottom flask. 5.253 grams (14.4 mmol) of (p-$ClC_6H_4)_3SiH$ was added. 3.17 grams of THF was then added. A septum used to loosely stopper the reaction flask and the reaction was stirred at room temperature overnight. Again, the extent of the reaction was monitored by ^1H NMR spectroscopy and was determined to be complete prior to workup. The THF was removed under reduced pressure and the solid was re-dissolved in pentane. This mixture was filtered through Celite. The pentane was removed by vacuum leaving sticky oil. The oil was re-dissolved in pentane and put in the freezer. The next day a white solid had precipitated and was collected by filtration. The yield was 4.46 g. The average % yield was 54% (4 runs). ^1H NMR (300 MHz): $CDCl_3$, (d, 7.52, 6H), (d, 7.41, 6H).

B.3.3 Synthesis of (p-$CF_3C_6H_4)_3SiCl$

A 100 mL Schlenk flask was brought into an inert atmosphere glove box. The following reagents were then added: 0.2043 grams (1.2 mmol) of palladium dichloride, 1.2292 grams (5.2 mmol) of hexachloroethane, and 9.6462 grams (20.8 mmol) of (p-$ClC_6H_4)_3SiH$. 4.6302 grams of THF were then added. The Schlenk flask was stoppered, removed from the glove box, and put under nitrogen on a Schlenk line. The reaction was left to stir and the progress was monitored by ^1H NMR. After five days, the reaction had gone to completion. The reaction vessel was brought into the box and the THF was removed under reduced pressure. The solid was then dissolved in

pentane and filtered through Celite. The pentane was removed under reduced pressure yielding a pale yellow solid that did not require further purification. The yield was 9.44 g, 91%. ^{1}H NMR (300 MHz): $CDCl_3$, (m, 7.73, 12H); ^{19}F (282 MHz): $CDCl_3$, -64.17.

B.4 Synthesis of Tris(triarylsilyl)phosphines

B.4.1 Synthesis of $P(SiPh_3)_3$

This synthesis was adapted from literature procedures.[6-7] *Warning: This reaction uses Na/K alloy, which is highly pyrophoric and should be handled with absolute exclusion of both oxygen and water. Certain byproducts and unreacted starting materials remaining at the end of this reaction may be pyrophoric and should be quenched as described below.* In a typical synthesis Na/K alloy was prepared by measuring out 0.479 grams (20.8 mmol) of sodium and 0.629 grams (16.1 mmol) of potassium with fresh surfaces exposed in an inert atmosphere glove box. These were mixed in a 3-neck 250 mL flask until the eutectic liquid was obtained. Next, 100 mL of 1,2-dimethoxyethane (DME) was added to the flask. The flask was closed with two Teflon stoppers and a Schlenk gas flow adapter. *Warning: The following operation requires extreme care.* The apparatus was removed from the box and transferred onto a nitrogen gas line by first performing three nitrogen/vacuum back-fill cycles. The Na/K solution was refluxed for two hours. The solution was cooled to room temperature. While cooling, 0.392 grams (12.6 mmol) of red phosphorus was weighed out in an inert atmosphere glove box and placed in a solid addition funnel and capped in a 100 mL round bottom flask. This apparatus was brought out of the glove box and once the Na/K solution was cooled the solid addition funnel was transferred under a counter flow

of N_2 into the side neck and the red phosphorus was added. This solution was then brought back to reflux for 24 hours. Over the duration, the solution turned pitch black, indicating formation of $(Na/K)_3P$. After 24 hours, the solution was cooled to room temperature. A pressure equalizing dropping funnel was exchanged for the reflux condenser under a counter low of N_2. 10.919 grams (37 mmol) of chlorotriphenylsilane was dissolved in 50 mL DME in an inert atmosphere glove box and added to a Schlenk flask. This solution was cannula transferred into the addition funnel under nitrogen. This solution was then added drop-wise to the phosphide suspension. The solution was brought back to reflux for 24 hours following the addition. The reaction mixture was then brought into an inert atmosphere glove box and stirred with 100 mL of toluene overnight. This solution was filtered through Celite and the solvent was removed under reduced pressure. The resulting white solid was re-crystalized from 1,2-dimethoxyethane. The yield was 2.9 g. The average % yield was 25% (5 runs). To quench the byproducts and unreacted metal remaining at the end of the reaction, all the solid waste generated upon filtration were put into a 3-neck flask in the glovebox and transferred to a Schlenk line under nitrogen. 1,2-Dimethoxyethane, followed by isopropanol, and finally water were injected through a septum to safely quench these materials. ^{1}H NMR (500 MHz): C_6D_6, (d, 7.47, 18H), (t, 7.03, 9H), (t, 6.92, 18H); $^{31}P\{^1H\}$ NMR (121.5 MHz): C_6D_6, (s, –262.3); ^{13}C NMR (125.7 MHz): C_6D_6, (d, 137.06), (d, 135.74), (s, 129.33), (s, 127.73).

B.4.2 Synthesis of $P(Si(p\text{-}MeC_6H_4)_3)_3$

This reaction was carried out and the product isolated by adaptation of the above synthesis for $P(SiPh_3)_3$ using 7.65 grams of $ClSi(p\text{-}MeC_6H_4)_3$. The yield was 1.83 grams, 26%. ^{1}H NMR

(300 MHz): C_6D_6, (d, 7.63, 18H), (d, 6.82, 18H), (s, 2.06, 27H); $^{31}P\{^1H\}$ (121.5 MHz): C_6D_6, –259.47; ^{13}C (125.7 MHz): C_6D_6, (s, 138.67), (d, 127.29), (d, 132.99), (s, 128.37), (s, 21.45).

B.4.3 Synthesis of $P(Si(p\text{-}ClC_6H_4)_3)_3$

This reaction was carried out and the product isolated by adaptation of the above synthesis for $P(SiPh_3)_3$ using 10.9380 grams of $ClSi(p\text{-}ClC_6H_4)_3$. The yield was 1.89 g, 20%. ^1H NMR (300 MHz): C_6D_6, (d, 7.09, 18H), (d, 6.91, 18H); $^{31}P\{^1H\}$ (121.5 MHz): C_6D_6, –257; ^{13}C (125.7 MHz): C_6D_6, (d, 137.70), (s, 137.28), (d, 131.93), (s, 128.36).

B.4.4 Synthesis of $P(Si(p\text{-}CF_3C_6H_4)_3)_3$

This reaction was carried out and the product isolated by adaptation of the above synthesis for $P(SiPh_3)_3$ using 9.43 grams of $ClSi(p\text{-}CF_3C_6H_4)_3$. The yield was 0.85 grams 10%. ^1H NMR (500 MHz): $CDCl_3$, (m, 7.33, 36H); $^{31}P\{^1H\}$ (202.4 MHz): $CDCl_3$, –261.32; ^{13}C (125.7 MHz): $CDCl_3$, 123.4 (complex q, $^1J_{CF}$ = 274 Hz), 124.6 (m), 132.6 (complex q, $^2J_{CF}$ = 33 Hz), 135.7 (m), 136.8 (m).

B.5 References

1. Brown, A. C.; Carpino, L. A., Magnesium in methanol: substitute for sodium amalgam in desulfonylation reactions. *J. Org. Chem.* **1985,** *50*, 1749-1750.

2. Prince, P.; Bearpark, M.; McGrady, G.; Steed, J., Hypervalent hydridosilicates: synthesis, structure and hydride bridging. *Dalton Trans.* **2008**, 271-282.
3. Benkeser, R. A.; Riel, F. J., The reactions of some triarylsilanes with methyllithium and phenylisopropylpotassium. *J. Am. Chem. Soc.* **1951,** *73*, 3472-3474.
4. Pongkittiphan, V.; Theodorakis, E.; Chavasiri, W., Hexachloroethane: a highly efficient reagent for the synthesis of chlorosilanes from hydrosilanes. *Tetrahedron Lett.* **2009,** *50*, 5080-5082.
5. Savela, R.; Zawartka, W.; Leino, R., Iron-catalyzed chlorination of silanes. *Organometallics* **2012,** *31*, 3199-3206.
6. Hassler, K., Darstellung und Charakterisierung der Trisilylphosphane (Ph 3 Si) n P (SiMe 3) 3− n, n= 1, 2, 3. *Monatsh. Chem.* **1982,** *113*, 421-425.
7. Becker, G.; Schmidt, H.; Uhl, G.; Uhl, W.; Regitz, M.; Rösch, W.; Vogelbacher, U. J., Tris (Trimethylsilyl) Phosphine and Lithium Bis (Trimethylsilyl) Phosphide. Bis-(Tetrahydrofuran). *Inorg. Synth.* **1990,** *27*, 243-249.

Vita

Benjamin Andrew Glassy was born in 1990 to parents Jeremy and Danette Glassy. He grew up on Mercer Island, WA where he graduated high school at Mercer Island High School in 2009. He attended the Robert D. Clark Honors College at the University of Oregon in Eugene, OR, where he graduated *magna cum laude* with a Bachelor of Science degree in chemistry in 2012. At UO, Benjamin worked in the research laboratory of Professor Catherine J. Page on several different projects with an emphasis on characterizing inorganic materials for a sustainable future. Benjamin then attended graduate school at the University of Washington in Seattle, WA. There, he worked with Assistant Professor Brandi M. Cossairt on the synthesis of zinc pnictide QDs for light harvesting applications. He married Anita Kasina in 2015. He obtained a Doctor of Philosophy degree in inorganic chemistry in 2017.